



Swansea University  
Prifysgol Abertawe



## Swansea University E-Theses

---

# High-dimensional glyph-based visualization and interactive techniques.

Chung, David H. S

### How to cite:

---

Chung, David H. S (2014) *High-dimensional glyph-based visualization and interactive techniques..* thesis, Swansea University.

<http://cronfa.swan.ac.uk/Record/cronfa42276>

### Use policy:

---

This item is brought to you by Swansea University. Any person downloading material is agreeing to abide by the terms of the repository licence: copies of full text items may be used or reproduced in any format or medium, without prior permission for personal research or study, educational or non-commercial purposes only. The copyright for any work remains with the original author unless otherwise specified. The full-text must not be sold in any format or medium without the formal permission of the copyright holder. Permission for multiple reproductions should be obtained from the original author.

Authors are personally responsible for adhering to copyright and publisher restrictions when uploading content to the repository.

Please link to the metadata record in the Swansea University repository, Cronfa (link given in the citation reference above.)

<http://www.swansea.ac.uk/library/researchsupport/ris-support/>

# **High-dimensional Glyph-based Visualization and Interactive Techniques**

David H. S. Chung

Submitted to Swansea University in fulfilment  
of the requirements for the Degree of Doctor of Philosophy.



**Swansea University**  
**Prifysgol Abertawe**

Department of Computer Science  
Swansea University

2014

ProQuest Number: 10797984

All rights reserved

INFORMATION TO ALL USERS

The quality of this reproduction is dependent upon the quality of the copy submitted.

In the unlikely event that the author did not send a complete manuscript and there are missing pages, these will be noted. Also, if material had to be removed, a note will indicate the deletion.



ProQuest 10797984

Published by ProQuest LLC (2018). Copyright of the Dissertation is held by the Author.

All rights reserved.

This work is protected against unauthorized copying under Title 17, United States Code  
Microform Edition © ProQuest LLC.

ProQuest LLC.  
789 East Eisenhower Parkway  
P.O. Box 1346  
Ann Arbor, MI 48106 – 1346



## Declaration

This work has not previously been accepted in substance for any degree and is not concurrently submitted in candidature for any degree.

Signed ..... (candidate)

Date 10/04/2015.....

## Statement 1

This thesis is the result of my own independent work/investigation, except where otherwise stated.

Signed ..... (candidate)

Date 10/04/2015.....

## Statement 2

I hereby give consent for my thesis, if accepted, to be available for photocopying and for inter-library loan, and for the title and summary to be made available to outside organisations.

Signed .. ..... (candidate)

Date 10/04/2015.....



---

# Abstract

---

The advancement of modern technology and scientific measurements has led to datasets growing in both size and complexity, exposing the need for more efficient and effective ways of visualizing and analysing data. Despite the amount of progress in visualization methods, high-dimensional data still poses a number of significant challenges in terms of the technical ability of realising such a mapping, and how accurate they are actually interpreted. The different data sources and characteristics which arise from a wide range of scientific domains as well as specific design requirements constantly create new special challenges for visualization research.

This thesis presents several contributions to the field of glyph-based visualization. Glyphs are parametrised objects which encode one or more data values to its appearance (also referred to as visual channels [Ber83]) such as their size, colour, shape, and position. They have been widely used to convey information visually, and are especially well suited for displaying complex, multi-faceted datasets. Its major strength is the ability to depict patterns of data in the context of a spatial relationship, where multi-dimensional trends can often be perceived more easily. Our research is set in the broad scope of multi-dimensional visualization, addressing several aspects of glyph-based techniques, including visual design, perception, placement, interaction, and applications. In particular, this thesis presents a comprehensive study on one interaction technique, namely sorting, for supporting various analytical tasks. We have outlined the concepts of glyph-based sorting, identified a set of design criteria for sorting interactions, designed and prototyped a user interface for sorting multivariate glyphs, developed a visual analytics technique to support sorting, conducted an empirical study on perceptual orderability of visual channels used in glyph design, and applied glyph-based sorting to event visualization in sports applications.

The content of this thesis is organised into two parts. Part I provides an overview of the basic concepts of glyph-based visualization, before describing the state-of-the-art in this field. We then present a collection of novel glyph-based approaches to address challenges created from real-world applications. These are detailed in Part II. Our first approach involves designing glyphs to depict the composition of multiple error-sensitivity fields. This work addresses the problem of single camera positioning, using both 2D and

---

3D methods to support camera configuration based on various constraints in the context of a real-world environment. Our second approach present glyphs to visualize actions and events “*at a glance*”. We discuss the relative merits of using metaphoric glyphs in comparison to other types of glyph designs to the particular problem of real-time sports analysis. As a result of this research, we delivered a visualization software, *MatchPad*, on a tablet computer. It successfully helped coaching staff and team analysts to examine actions and events in detail whilst maintaining a clear overview of the match, and assisted in their decision making during the matches.

Next, we introduce a novel glyph-based sorting framework. The framework focuses on sorting and ordering glyphs as part of an interactive process in visualization. We examine several technical aspects of glyph sorting and provide design principles for developing effective visually sortable glyphs. Glyphs that are visually sortable provide two key benefits: 1) performing comparative analysis of multiple attributes between glyphs, and 2) to support multi-dimensional visual search. We also describe a system that incorporates focus+context glyphs to control high-dimensional sorting in a visually intuitive manner, and demonstrate its usefulness to a case study of rugby event analysis. We extend the usability of glyph-based sorting through the development of a visual analytic approach. The method incorporates a knowledge-assisted ranking framework to convert a user’s knowledge on ranking using regression modelling. This enables users to analyse and sort multi-dimensional events in a more flexible manner. We apply this approach in the context of sport event data for re-organising key match videos.

In order to investigate the benefits of sorting in glyph-based visual design, we present an empirical study that focus on the perception of orderability for different visual channels. We find that some visual channels (for example, value) are perceived to be more ordered than others (for example, hue) than the actual order measured in the data. As a result, some visual channels are more sensitive to noise than others. Two additional studies are presented to investigate its affect on two types of visualization tasks, namely: visual search, and categorical perception. We find that visual channels that tend to be perceived as ordered, improve the accuracy of min and max judgements. On the other hand, visual channels that appear more discrete i.e., those that tend to be perceived as less ordered, improve the accuracy of identifying element pairs. Finally, we provide concluding remarks in this part, and discuss possible directions for future work.

---

## Acknowledgements

---

Firstly, I would like to give special thanks to my supervisors Bob Laramée and Min Chen for their tireless guidance, support, patience, and encouragement during the course of my PhD. I am truly grateful to have had the experience of working under their supervision, and the invaluable knowledge I have learnt from them which I will carry with me for the rest of my career. I would like to extend my thanks to Iwan Griffiths and Adrian Morris for their involvement, and giving me the fantastic opportunity to work in the SportsViz research team. Without this project and the collaborative links to industrial partners, this work would not have been possible. I must also thank the Welsh Government and the Research Institute of Visual Computing (RIVIC) for funding this research.

This thesis would not be finished without the support of a number of people that I wish to sincerely thank. To start with, I want to thank Phil Legg and Matt Parry who have been incredible teammates and a joy to work with both as fellow researchers, and as close friends. I will remember my time at SportsViz as one of my fondest because of you two. I want to thank the great research colleagues that I have had the privilege in working with, in particular to Rita Borgo, Daniel Archambault, and Johannes Kehler. Special thanks go to Concepta Graphic Design for their artwork, Karl Proctor for his feedback on the user-study design, and Helen Purchase for her help on data analysis. I would also like to thank my peers and friends within the Department of Computer Science who all understand the mixed emotions and difficulties that a PhD has to offer.

Finally, I would like to thank my family. You have always been behind me in everything I did, and without your constant love and support, I would not be able to achieve my goals such as this thesis. And for that, I will always be grateful. So to Sau, Lucy, Mum, and Dad - *this is for you.*





---

## Publications

---

The work contained in this thesis is based on the following publications:

- Rita Borgo, Johannes Kehrer, David H. S. Chung, Eamonn Maguire, Robert S. Laramee, Helwig Hauser, Matthew Ward and Min Chen. **Glyph-based Visualization: Foundations, Design Guidelines, Techniques and Applications.** In *Eurographics State of the Art Reports*, pp. 39-63, Girona, 2013.
- David H. S. Chung, Robert S. Laramee, Johannes Kehrer, Helwig Hauser, and Min Chen. **Glyph-based Multi-field Visualization.** Book Chapter in C. Hansen, M. Chen, H. Hagen, C. Johnson, A. Kaufman (eds.), *Scientific Visualization*, Springer, 2014.
- David H. S. Chung, Matthew L. Parry, Philip A. Legg, Iwan W. Griffiths, Robert S. Laramee and Min Chen. **Visualizing Multiple Error-Sensitivity Fields for Single Camera Positioning.** In *Computing and Visualization in Science*, Vol. 15, No. 6, pp. 303-317, 2012.
- Philip A. Legg, David H. S. Chung, Matthew L. Parry, Mark W. Jones, Rhys Long, Iwan W. Griffiths and Min Chen. **MatchPad: Interactive Glyph-Based Visualization for Real-Time Sports Performance Analysis.** In *Computer Graphics Forum*, Vol. 31, Issue 3pt4, pp. 1255-1264, 2012.
- David H. S. Chung, Philip A. Legg, Matthew L. Parry, Rhodri Bown, Iwan W. Griffiths, Robert S. Laramee and Min Chen. **Glyph Sorting: Interactive Visualization for Multi-dimensional Data.** In *Information Visualization*, Vol. 1, No. 1, pp. 76-90, 2015.
- David H. S. Chung, Philip A. Legg, Matthew L. Parry, Rhodri Bown, Iwan W. Griffiths, Robert S. Laramee and Min Chen. **Knowledge-Assisted Ranking: A Visual Analytic Application for Sport Event Data.** In *IEEE Computer Graphics & Applications*, forthcoming, 2015.

- 
- David H. S. Chung, Daniel Archambault, Rita Borgo, Darren J. Edwards, Robert S. Laramée and Min Chen. **How Ordered is it? On Perceptual Orderability of Visual Channels.** *Technical Report*, Department of Computer Science, Swansea University, UK, 2014. (Under review)

**Note on joint works:** The work in Chapter 2 based on [BKC\*13], is a piece of collaborative work by a team of researchers from five different institutions: Dr. Rita Borgo and my PhD supervisor Dr. Robert S. Laramée from Swansea University, Dr. Johannes Kehrer at the time worked under University of Bergen and Vienna University of Technology, Eamonn Maguire and my PhD co-supervisor Prof. Min Chen from Oxford University, Prof. Helwig Hauser from University of Bergen, and Matthew Ward from Worcester Polytechnic Institute. This work presents a state-of-the-art report on glyph-based visualization, where my contributions involved creating the taxonomy, surveying glyph-based visualization papers in a range of application domains, and classifying the literature according to the taxonomy.

Chapter 4 is the outcome of a research project done together with two Research Assistants, Dr. Philip Legg and Matthew Parry, my project supervisor Dr. Iwan Griffiths, and PhD co-supervisor Prof. Min Chen as part of the SportsViz research group. This research involved collaborating with an industrial partner, namely, Rhys Long - the head of performance analyst at the Welsh Rugby Union to develop a novel, glyph-based visualization for visualizing sport events [LCP\*12]. A senior lecturer in Computer Science at Swansea University, Dr. Mark Jones was also involved in this work. I was the principal researcher concerning the different aspects of glyph-design and the algorithm for interactive glyph positioning, while Dr. Philip Legg did mainly the implementation of the software on a tablet device.

I was the principal researcher with respect to the work described in Chapter 3, Chapter 5, and Chapter 6. This work was done in collaboration with my supervisor Dr. Robert S. Laramée and the SportsViz team (same as Chapter 4). And finally, I was also the principal researcher with respect to the work in Chapter 7. This research is a inter-department work between Dr. Rita Borgo and Dr. Daniel Archambault from Computer Science, and Dr. Darren J. Edwards from Psychology at Swansea University, in addition to my two supervisors Dr. Robert S. Laramée and Prof. Min Chen.

Supplementary material can be found at: <http://www.cs.swan.ac.uk/~cschung/thesis/>

---

# Contents

---

|          |   |           |
|----------|---|-----------|
| <b>I</b> | <b>Background and Motivation</b>  | <b>1</b>  |
| <b>1</b> | <b>Introduction</b>   | <b>3</b>  |
| 1.1      | Glyph-based Visualization . . . . .   | 4         |
| 1.1.1    | A brief history of the study of signs . . . . .                                 | 5         |
| 1.1.2    | Terminology . . . . .   | 7         |
| 1.1.3    | High-dimensional Glyph Representation . . . . .                                 | 8         |
| 1.1.4    | Challenges . . . . .  | 10        |
| 1.2      | Contribution . . . . .  | 11        |
| 1.3      | Thesis Structure . . . . .  | 13        |
| <b>2</b> | <b>A Survey on Glyph-based Visualization</b>                                    | <b>15</b> |
| 2.1      | Introduction . . . . .  | 16        |
| 2.1.1    | Contributions . . . . .   | 16        |
| 2.1.2    | Scope and Methodology . . . . .   | 17        |
| 2.2      | Classification and Overview . . . . .   | 17        |
| 2.2.1    | Design Aspects for Glyphs . . . . .   | 19        |
| 2.2.2    | Glyph Placement . . . . .   | 26        |
| 2.2.3    | Interaction . . . . .   | 26        |
| 2.3      | Glyph-based Multivariate Visualization . . . . .                                | 27        |
| 2.3.1    | Glyph-based Techniques for Event-based Data . . . . .                           | 27        |
| 2.3.2    | Glyph-based Techniques for Geo-spatial Data . . . . .                           | 30        |
| 2.3.3    | Glyph-based Techniques for High-dimensional Data . . . . .                      | 31        |
| 2.4      | Glyph-based Multi-field Visualization . . . . .                                 | 32        |
| 2.4.1    | Glyph-based Techniques for Multiple Scalar Data . . . . .                       | 32        |
| 2.4.2    | Glyph-based Techniques for Flow Data . . . . .                                  | 34        |
| 2.4.3    | Glyph-based Techniques for Tensor Data . . . . .                                | 38        |
| 2.4.4    | Glyph-based Techniques for High-dimensional, Physical Simulation Data . . . . . | 42        |
| 2.5      | Visual Analysis of Multi-dimensional data . . . . .                             | 44        |
| 2.6      | Discussion . . . . .  | 45        |

---

|           |  |           |
|-----------|--|-----------|
| 2.7       | Summary . . . . .  | 46        |
| <b>II</b> | <b>Research Development</b>  | <b>49</b> |
| <b>3</b>  | <b>Designing High dimensional Glyphs for Visualizing Multiple Error-Sensitivity Fields</b> | <b>51</b> |
| 3.1       | Introduction . . . . .   | 51        |
| 3.2       | System Overview . . . . .  | 54        |
| 3.3       | Camera Sensitivity and Error Derivation . . . . .  | 55        |
| 3.3.1     | Snooker Reconstruction . . . . .   | 57        |
| 3.3.2     | Homography Sensitivity Analysis . . . . .  | 58        |
| 3.4       | Error Sensitivity Visualization . . . . .  | 59        |
| 3.4.1     | General Design Principles . . . . .  | 60        |
| 3.4.2     | Visual Mapping of Multiple Error Sensitivity . . . . .                                     | 61        |
| 3.4.3     | Sample points in 3D visualization . . . . .  | 63        |
| 3.4.4     | Spherical Mapping . . . . .  | 63        |
| 3.5       | User Consultation - 2D . . . . .   | 65        |
| 3.6       | User Consultation - 3D . . . . .   | 70        |
| 3.7       | Discussion . . . . .   | 73        |
| 3.8       | Summary . . . . .  | 74        |
| <b>4</b>  | <b>Interactive Glyph-Based Visualization for Real-Time Sports Performance Analysis</b>     | <b>75</b> |
| 4.1       | Introduction . . . . .   | 75        |
| 4.2       | Requirements Analysis . . . . .  | 77        |
| 4.2.1     | Rugby Union . . . . .  | 77        |
| 4.2.2     | Rugby Performance Analysis . . . . .   | 77        |
| 4.3       | <i>MatchPad</i> Pipeline . . . . .   | 79        |
| 4.4       | Glyph-based Visual Mapping . . . . .   | 80        |
| 4.4.1     | Data Space . . . . .   | 80        |
| 4.4.2     | Design Options . . . . .   | 82        |
| 4.4.3     | Resultant Design for <i>MatchPad</i> . . . . .   | 83        |
| 4.5       | Visualization Interaction . . . . .  | 85        |
| 4.5.1     | Interactive Visualization . . . . .  | 85        |
| 4.5.2     | Scale-Adaptive Layout . . . . .  | 86        |
| 4.6       | Case Study: Welsh Rugby Union . . . . .  | 87        |
| 4.7       | Discussion . . . . .   | 88        |
| 4.8       | Summary . . . . .  | 90        |

---

|          |  |            |
|----------|--|------------|
| <b>5</b> | <b>Glyph Sorting: Interactive Visualization for Multi-dimensional Data</b> | <b>93</b>  |
| 5.1      | Introduction . . . . .   | 93         |
| 5.2      | Sorting: Entities and Sort Keys . . . . .                                  | 96         |
| 5.3      | Design Principles of Sortable Glyphs . . . . .                             | 97         |
| 5.4      | Interactive Glyph-based Visual System . . . . .                            | 100        |
| 5.4.1    | Focus and Context Glyph-based Interface . . . . .                          | 100        |
| 5.4.2    | Interactive, Multi-dimensional Glyph Plot . . . . .                        | 102        |
| 5.4.3    | Hierarchical Axis Binning . . . . .  | 102        |
| 5.5      | Case Study: Sports Event Analysis . . . . .                                | 105        |
| 5.5.1    | Visual Mapping of Sort Keys . . . . .                                      | 105        |
| 5.5.2    | Visual Comparison of Two Matches . . . . .                                 | 107        |
| 5.5.3    | Domain Expert Review . . . . .   | 111        |
| 5.6      | Discussion . . . . .   | 112        |
| 5.7      | Summary . . . . .  | 113        |
| <b>6</b> | <b>Glyph Sorting: A Visual Analytic Approach</b>                           | <b>115</b> |
| 6.1      | Introduction . . . . .   | 115        |
| 6.2      | Problem Specification . . . . .  | 117        |
| 6.3      | Visual Analytics for Multivariate Sorting . . . . .                        | 118        |
| 6.3.1    | System Overview . . . . .  | 118        |
| 6.3.2    | Knowledge-Assisted Ranking Framework . . . . .                             | 120        |
| 6.3.3    | Model Visualization . . . . .  | 124        |
| 6.3.4    | Glyph-based Visualization . . . . .  | 125        |
| 6.3.5    | Sorted Event Replay . . . . .  | 126        |
| 6.4      | Case Study: “What is a successful strategy to score?” . . . . .            | 128        |
| 6.5      | Discussion . . . . .   | 129        |
| 6.6      | Summary . . . . .  | 130        |
| <b>7</b> | <b>Glyph Sorting: Perceptual Orderability</b>                              | <b>131</b> |
| 7.1      | Introduction . . . . .   | 132        |
| 7.2      | Orderability of Visual Channels . . . . .                                  | 133        |
| 7.2.1    | Data generation . . . . .  | 134        |
| 7.2.2    | Noise Function . . . . .   | 134        |
| 7.2.3    | Visual Mapping of Elements . . . . .                                       | 135        |
| 7.2.4    | Just Noticeable Difference . . . . .                                       | 136        |
| 7.3      | Experimental Overview . . . . .  | 138        |
| 7.3.1    | Interface . . . . .  | 139        |
| 7.3.2    | Pilot Studies . . . . .  | 140        |
| 7.3.3    | Crowdsource Consistency . . . . .  | 141        |
| 7.4      | Experiment 1: How ordered is it? . . . . .                                 | 142        |
| 7.4.1    | Results . . . . .  | 143        |
| 7.4.2    | Discussion . . . . .   | 145        |

---

|          |   |            |
|----------|---|------------|
| 7.5      | Experiment 2: Which is smallest? Which is largest? . . . . .  | 148        |
| 7.5.1    | Results . . . . .   | 149        |
| 7.5.2    | Discussion . . . . .  | 150        |
| 7.6      | Experiment 3: How many pairs? . . . . .   | 151        |
| 7.6.1    | Results . . . . .   | 152        |
| 7.6.2    | Discussion . . . . .  | 154        |
| 7.7      | Limitations . . . . .   | 154        |
| 7.8      | General Discussion and Summary . . . . .  | 155        |
| <b>8</b> | <b>Conclusion</b>   | <b>159</b> |
| 8.1      | Future Work . . . . .   | 163        |
|          | <b>Bibliography</b>   | <b>167</b> |
|          | <b>Appendix A Designing High-dimensional Glyphs for Visualizing Multiple Error-Sensitivity Fields</b> | <b>185</b> |
| A.1      | User Consultation: Questionnaire . . . . .  | 185        |
|          | <b>Appendix B Glyph Sorting: A Visual Analytic Approach</b>   | <b>187</b> |
| B.1      | Empirical Study on Formal Rankings . . . . .  | 187        |
|          | <b>Appendix C Glyph Sorting: Perceptual Orderability</b>  | <b>189</b> |
| C.1      | Experimental Stimuli: How ordered is it? . . . . .  | 189        |
| C.2      | Experimental Stimuli: Which is smallest? Which is largest? . . . . .                                  | 193        |
| C.3      | Experimental Stimuli: How many pairs? . . . . .   | 207        |

---

# List of Figures

---

- 1.1 In philosophy, language studies and psychology, signs may take one of the three forms: icon, index, and symbol. In many other contexts, terms such as visual metaphor, ideogram, and pictogram are also used to describe subclasses of signs [BKC\*13]. . . . . 5
- 1.2 Codes provide a framework within which signs assume a meaning. A symbol, for example (+), can have different interpretations depending on the coding convention such as the symbol for 'first aid' in medicine, or the arithmetic symbol for 'addition'. . . . . 5
- 1.3 The Pioneer plaque on board the 1972 Pioneer 10 Spacecraft [NAS]. The pictorial message displayed information about the origin of the spacecraft in case the Pioneer 10 is intercepted by extraterrestrial life. . . . . 6
- 1.4 Examples of glyph-based visualizations: (left) visualization of Magnetic Resonance Spectroscopy (MRS) data using superquadrics [FLKI09], (middle) 2D arrows showing the wind direction and magnitude over Australia [TB96], and (right) 3D arrows to depict the flow on the surface of a ring [LWSH04]. Glyphs vary in appearance from one application to another depending on the underlying data. . . . . 8
- 1.5 Examples of glyph-based visualizations: (left) glyph-based visualization of 3D data [LKH09], (middle) network activity glyphs [PR08], and (right) 3D fish glyphs for exploring biomedical multi-modal data [MgDN06]. . . . . 9
- 2.1 Examples of visual channels applied to point symbols. [MRO\*12] . . . . 22
- 2.2 Gestalt principles of perceptual organisation. A theoretical framework that describe the self-organising tendencies in human perception when several visual channels are combined or structured in some form [War08b]. 23



---

|      |   |    |
|------|---|----|
| 2.3  | Bar chart glyphs showing the monetary exchange rates of 10 U.S. countries over 3 years [War08a]. Each glyph represents a month within a year (i.e., each row), with the exchange rate of each U.S. country mapped to the height of the individual bars. The dimensions (i.e., each bar) on the glyph can be ordered to improve the overall effectiveness of the visualization. Two methods are compared: (left) bars in random ordering, and (right) bars that are sorted based on the first record. Gradual changes and anomalies are much easier to perceive when the dimensions are ordered. | 24 |
| 2.4  | Examples of different glyph placement strategies: <b>Data-driven</b> positions glyphs along some attribute axis or an underlying grid for data with spatial information such as map visualization. <b>Structure-driven</b> arranges glyphs to show an ordering, hierarchical, or other relationship of the data variables. <b>Feature-driven</b> places glyphs at local features such as iso-surfaces. <b>User-driven</b> allows users to incorporate their knowledge by interactively placing glyphs at specific regions in the domain.  | 26 |
| 2.5  | Visualizing monthly health data consisting of multiple time-dependent variables using (left) 3D pencil icons, and (right) 3D helix glyphs. The glyphs are placed over a map to show the temporal characteristics of different diseases [TSWS05].  | 28 |
| 2.6  | Glyph-based visualization of sounds. Symbolic icons are used to convey the semantic information of sound in movies such as birds chirping, chimes, and the creaking of doors. The icons are positioned along a timeline of the movie [JBMC10].  | 29 |
| 2.7  | Visualization of water-vapor mixing ratio, illustrating the progression of uncertainty by the use of spaghetti plots and uncertainty glyphs [SZD*10].   | 30 |
| 2.8  | Parallel glyphs for visualizing large, high-dimensional data. Each glyph represents a single high-dimensional object which are arranged along a pivot axis. Polylines are rendered to connect each glyph in order to compare changes in attribute values [FCI05].   | 32 |
| 2.9  | Visualization of a magnetohydrodynamics simulation dataset displaying vortex tubes with positive vorticity (cuboids and ellipsoid glyphs) and negative vorticity (stars) [SEK*98].  | 33 |
| 2.10 | The visualization of vector field clustering of flow around an engine. A combination of $ v $ -range and $\theta$ -range glyph is used for depicting the range of vector magnitude and direction in each vector cluster [PGL*12].   | 36 |
| 2.11 | Shearing barbell glyphs to depict the uncertainty of different integrators and step-sizes between a pair of streamlines [LPSW96].   | 37 |
| 2.12 | Glyph-based visualization for the diagnosis of coronary artery disease using a supertorus glyph [MSSD*08]. Data attributes are encoded into its colour, opacity, size, and roundness.   | 40 |

---

|      |   |    |
|------|---|----|
| 2.13 | Visualization of geometry tensors by augmenting superquadric glyphs with concave shapes to show eigenvalue sign differences and colouring to show their quadratic forms [SK10]. . . . .   | 42 |
| 2.14 | Close up visualization of turbulent flow past a cylinder. Kirby and Laidlaw [KML99] composite multiple visualization layers using a variety of techniques such as glyph-based, colour-mapping, and texture-based encodings. The example shown here depicts two scalar fields, two vector fields, and a tensor field in the same image. . . . .  | 43 |
| 3.1  | Constraint maps of a sample snooker room wall (Left) and a construction scene (Center) with dynamic constraints (Right). The green region highlights valid camera mounting positions with invalid positions mapped to red. The construction scene images correspond to the right wall of the camera surveillance scene in Figure 3.7. The focus region must be fully in view of the camera for a position to be considered as valid. . . . .  | 52 |
| 3.2  | An overview of the combined visualization pipeline for depicting error sensitivity in single camera positioning. There are three main stages: Extracting the error sensitivity data from sample camera positions, generating the 2D error map and generating the 3D environment visualization. . . . .  | 54 |
| 3.3  | A 3D reconstruction of the camera environment in the snooker scene. A set of sampled camera positions are shown using grey spherical markers around the region of interest. . . . .   | 55 |
| 3.4  | (Top) Reconstruction pipeline for extracting ball positions in a snooker scene using a single camera. The 3D reconstruction is based on a 2D homography. (Bottom) Camera sensitivity analysis of the projective transform. Error sensitivity fields (or vector fields) are derived to quantify the impact of image distortion from inaccurate feature correspondence. . . . .   | 56 |
| 3.5  | Example camera positions around the (First row) snooker table scene and (Third row) security scene. Below each image is the associated inverse transformation of the camera position to obtain a projected top-down view. It can be seen that the quality of the inverse transformation is greatly influenced by the camera position. . . . .   | 57 |
| 3.6  | Development of the 2D error visualization using different approaches is shown. (a) presents a stacked vector glyph design, where magnitude is mapped to the length of the vector. This is extended in (b) to a Co-Planar Star glyph which normalises the vectors and uses a heat map to depict the resultant error. (c) incorporates stacked ribbons (center) and streamlines (right) into the error visualization. Streamline thickness is mapped to vector magnitude. (d) generates a closed Beziér curve based on the vector field. The glyph size is mapped to the resultant error. . . . . | 62 |

---

|      |   |    |
|------|---|----|
| 3.7  | Visualization of the 3D camera positioning around the snooker scene (Top row) and security scene (Bottom row). The cameras are modelled using spheres, and colour mapped to its error magnitude. The sample points are then projected onto a spherical surface centred at the focus region, giving users an overview of the statistical error. (Left) shows a glyph-based approach for depicting the average vector error and (Right) uses a colour-mapped sphere for illustrating the overall error magnitude. | 64 |
| 3.8  | Comparative evaluation of error visualization designs. (a) uses stacked vector glyphs. (b) co-planar star glyphs. (c) weighted streamlines. (d) stacked stream ribbons and (e) colour-coded Bézier glyphs. . . . .  | 68 |
| 3.9  | Comparison of error sensitivity between camera positions B (left) and position C (right) from Figure 3.11 using colour-coded Bézier glyphs. . . . .   | 69 |
| 3.10 | Graph showing the result of users ranking the visual designs from worst-to-best as a measure from 1-5. . . . .  | 70 |
| 3.11 | 3D visualization showing the 3 candidate camera positions labelled A, B and C, after filtering. These camera positions are highlighted using opacity. . . . .   | 71 |
| 3.12 | 3D visualization showing the 3 candidate camera positions in the surveillance scene labelled D, E and F after filtering. These camera positions are highlighted using opacity. . . . .  | 72 |
| 4.1  | The pipeline used to compute the <i>MatchPad</i> visualization. There are four key stages: XML processing, event visual mapping, graphical composition, and the combined video, visualization and information pane of the <i>MatchPad</i> . . . . .   | 79 |
| 4.2  | Some designs of metaphoric pictograms. In (a), initial stickmen designs were produced to prompt an artist. The artist produced several different designs: (b) a refined stickman design, (c) a contemporary design, (d) a posterized colour design and (e) a silhouette design. In (f) the scrum is depicted using the silhouette design (cf. (a) and (b)). . . . .   | 83 |
| 4.3  | Components and visual channels of the glyphs. . . . .   | 84 |
| 4.4  | Scale-adaptive layout for key events. In (a), the key events are shown at a scale where no overlap occurs. As the user condenses the visualization timeline for an overview, the algorithm determines the most suited layout for each glyph. In (b), the glyph are stacked horizontally. In (c), the glyph are scaled based on their duration. In (d), the glyph are stacked vertical. Finally, (e) combines two (or more) events to generate a new macro glyph that is used in place. . . . .                  | 86 |
| 4.5  | Pseudo-code for the scale-adaptive layout. . . . .  | 88 |
| 4.6  | MatchPad being used by the Welsh Rugby Union. . . . .   | 89 |

---

|     |  |     |
|-----|--|-----|
| 4.7 | Screenshots of the <i>MatchPad</i> . <b>Top:</b> Overview of a 17 minutes period from a match using the <i>MatchPad</i> . Match and Team events are depicted using metaphoric pictograms that are instantly recognizable. Home team events are shown in red, above the centre line, and away team events are shown in blue below the centre line. The user can also choose whether to show critical match events such as scoring events and referee decisions on the centre line due to their high importance. <b>Bottom:</b> Zoomed-in view on a region of the visualization. Phase ball actions are shown using coloured regions sized dependent on duration and phase count. Outcome indicators for positive or negative results are shown using green and amber circles respectively when the information is available. Ball in Play events are shown by the pale green background on the timeline. The information pane at the bottom of the screen provides more in-depth detail for a particular event when selected by the user. . . . . | 91  |
| 5.1 | Visual representation of two example multi-dimensional glyphs, namely (a) Star glyphs and (b) Bar chart glyphs when glyphs on the left are unordered, in comparison to glyphs on the right which are ordered to two sorting parameters. . . . .  | 94  |
| 5.2 | Variations of glyph design in accordance with the design principles of sortable glyphs (a)-(h). For each principle, the top row depicts a glyph with greater emphasis and the bottom row depicts a glyph with less emphasis. . . . .   | 96  |
| 5.3 | A graphical pipeline illustrating the glyph sorting framework. It consists of four key steps: 1) visual mapping of data to glyphs. We propose general design guidelines for creating visually sortable glyphs to support interactive sorting and multivariate analysis. Alternatively, a default glyph (e.g., Star glyph) is used. 2) integrating a focus and context glyph control panel for selecting multiple sort keys, 3) constructing the glyph sorting tool which enables users to perform high-dimensional sorting and interactively adjust various display options and 4) visual representation of sorted results on an Interactive, Multi-dimensional glyph plot. . . . .  | 101 |
| 5.4 | A focus and context glyph-based user interface for selecting sort keys. Clicking on a visual component of the glyph highlights that particular sort key in focus. . . . .  | 102 |
| 5.5 | Diagram illustrating hierarchical axis binning along one sorting axis. Intervals (or sub-regions) at each level of sorting can be sub-divided by different attributes where additional sort functions can be mapped. We note that the axis mapping can be applied along multiple axes. . . . .   | 103 |

---

|     |   |     |
|-----|---|-----|
| 5.6 | A snapshot of the glyph-based sorting system. The software consists of three main interfaces: 1) a glyph control panel for controlling sort keys in a visual manner, 2) an IMG-plot for displaying the sorted results, and 3) an option panel to support interactive exploration. Additional statistical information and a glyph-based legend is displayed through tabbed viewing panels. . . . .   | 104 |
| 5.7 | Components and visual channels of the glyph. . . . .  | 107 |
| 5.8 | Swatch chart illustrating the visual sort key parameter space and legends using focus and context glyphs. Continuous attributes are indicated by ( $\rightarrow$ ) and discrete attributes are labelled with their corresponding values. . . . .  | 108 |
| 5.9 | Visual comparison of two rugby matches using the IMG plot. Top: Match 1 ( <b>M1</b> ). Bottom: Match 2 ( <b>M2</b> ). For each match, the glyphs are ordered using three sort keys: Gain versus Start Event and Tortuosity. Mean bars are also displayed as a user-option to provide additional statistical information. . . . .  | 110 |
| 6.1 | The user interface contains four main views. The glyph-based visualization shows the sorted events of a match, and allows a user to select and import events to the system. Once events are imported, the ranking input view is used to specify a sorting requirement. The model visualization view allows the user to analyse how the current model parameters and accuracy correspond to their ranking input. The ranking model can then be exported to one of the primary axes in the glyph-based visualization for viewing the sorted results. The axes can also be modified by clicking on a component in the glyph control panel. . . . . | 119 |
| 6.2 | A knowledge-assisted ranking framework. It consists of five steps: the user's <b>ranking</b> input as an example to the system, a <b>knowledge discovery</b> process to predict a set of sortable attributes combined into a function, <b>knowledge externalization</b> to convey the analytical model through visualization, <b>model validation</b> based on ranking analysis, and finally, using the model to interactively analyse, rank and replay match videos ( <b>knowledge application</b> ). . . . .  | 120 |
| 6.3 | Visual comparison of the ranking models using (a) Linear, (b) Polynomial and (c) Logistic regression in parallel co-ordinates. The contribution of each attribute is depicted using gauges that correspond along each axis. In order to convey the model's overall accuracy, the ranking model is plotted as an additional axis gauge which encodes the ranking confidence $\tau$ . Note that each regression model may discover a different set of key performance indicators. . . . .   | 123 |

---

|     |  |     |
|-----|--|-----|
| 6.4 | Refining the model parameters. Users can adjust the contribution of each attribute $w_j$ in the ranking model by scaling the axis widths using sliders in the ranking preferences. This example shows how modifying the weights (highlighted in the red circle) can result to an improved model as shown by the larger ranking gauge (see right most axis). . . . .  | 124 |
| 6.5 | Brushing glyphs in the glyph-based canvas (a) renders the glyph in focus, while non-selected glyphs are drawn as red markers to indicate their position. Non-selected glyphs can also be interactively scaled by the user (b) in order to reduce the amount of visual occlusion. . . . .   | 125 |
| 6.6 | Video playback of sorted events. We integrate four different broadcasting feeds that recorded the event. . . . .   | 126 |
| 6.7 | Visual comparison of two matches. The events are sorted according to successful traits that resulted in points scored as defined by the model shown in Figure 6.4, and tortuosity. The analyst observed a group of events highlighted in the green circle (a) where a high percentage of points are scored, which is significantly less in the second match (b). . . | 127 |
| 7.1 | Visualizing an unordered sequence using value and size. . . . .  | 133 |
| 7.2 | The visual stimuli used in our experiments. Each 1D plot is mapped using the visual channels taken from semiology of graphics [Ber83]. . .   | 135 |
| 7.3 | Comparing shape similarity between a given shape, and its predecessor, to measure the distinctiveness as the number of spikes (star-shape) and edges (elementary-shape) increases. . . . .   | 138 |
| 7.4 | A screenshot of the visual interface for Experiment 1: How ordered is it? Shape is tested in this example. . . . .   | 143 |
| 7.5 | Comparing the effects of visual channel against perceived orderedness (top) and response time (bottom) in Experiment 1. Significant differences are listed above each bar, with (mean, median) values indicated below. Error bars show 95% confidence intervals. Bars are colour-coded using ColorBrewer [HB11]. . . . .   | 144 |
| 7.6 | Comparison of measured orderedness (or correlation coefficient) versus perceived orderedness. Points depict the perceived orderedness for each visual channel, organised by power scale of measured orderedness. The average is plotted (dashed line) against visual channels (coloured lines) using a line of best fit. . . . .                                     | 146 |
| 7.7 | A screenshot of the visual interface for Experiment 2: Which is smallest? Which is largest? . . . . .  | 149 |
| 7.8 | Comparing the effects of visual channel against error rate (top) and response time (bottom) in Experiment 2. Significant differences are listed above each bar, with (mean, median) values indicated below. Error bars show 95% confidence intervals. . . . .  | 150 |
| 7.9 | A screenshot of the visual interface for Experiment 3: How many pairs? . . . . .   | 152 |

---

|      |  |     |
|------|--|-----|
| 7.10 | Comparing the effects of visual channel against error rate (top) and response time (bottom) in Experiment 3. Significant differences are listed above each bar, with (mean,median) values indicated below. Error bars show 95% confidence intervals. . . . .   | 153 |
| 7.11 | Visual channel ranking for Experiment 1 and Experiment 2 based on performance (top) and response time (bottom). We also compare this to participants' <i>perceived</i> ranking collected from our qualitative survey data. The ranking is from worst (7th) to best (1st). . . . .  | 156 |
| 7.12 | A performance summary of each visual channel in all three experiments. The ranking in <b>How ordered is it?</b> is based on mean orderedness, while the ranking in the other two experiments ( <b>Which is smallest? Which is largest?</b> and <b>How many pairs?</b> ) is based on mean error. . . . .  | 157 |
| B.1  | Table showing the empirical study results for sorting rugby events. Each sub-row within a task corresponds to five participants along with their optional meta-answer (see Appendix for details). For task 1 and 2, their ranking is shown from the 12 possible events $e_i$ , and are ranked from worst-to-best with 1-5 and 1-10 respectively. A colour-map is applied to emphasise the worst and best events. . . . . | 188 |

---

## List of Tables

---

|     |   |     |
|-----|---|-----|
| 2.1 | A classification of glyph-based techniques for multi-field and multi-variate data. Each technique is grouped by application domain along the rows, and the type of visual channels used to construct the glyph along the columns. Entries are ordered in chronological order within each application group. The colours show the visualization challenge which each paper address: perception and design challenge, glyph placement challenge, and big data challenge as outlined in Section 1.1.4. . . . . . | 18  |
| 2.2 | A taxonomy of visual channels [CF13]. Each visual channel is classified into four categories: geometric, optical, topological and relational, and semantic channels. Glyphs are created by mapping data attributes to one or many visual channels. . . . .  | 21  |
| 3.1 | Comparison of visual mappings shown in Figure 3.8. Each design is assessed against a number of set criteria which ideally should be achieved. An asterisk in the table indicates the design satisfies that particular criteria. . . . .   | 66  |
| 4.1 | A range of events are to be mapped in the visualization. Each event is augmented with levels of association (i.e., the match, team or player), and additional attributes (i.e., outcome and numerical and enumerative values). We also illustrate four possible glyph designs: metaphoric pictogram, abstract icon, shape, and colour. We choose to use metaphoric pictogram to represent events in <i>MatchPad</i> . . . . .   | 81  |
| 5.1 | Table illustrating the set of sort keys in rugby event analysis. Each attribute is classified based on typedness, and the visual channel mapped to the glyph. Data attributes are ranked in order of importance from top to bottom. . . . .   | 106 |
| 7.1 | Qualitative survey participants filled after each experiment. . . . .   | 140 |



---

|      |   |     |
|------|---|-----|
| 7.2  | Experiment 1 results. Reporting $p$ -values of post-hoc results analysing the effects of noise level on perceived orderedness under different visual channels. Significant differences are highlighted in red using a Bonferoni corrected $\alpha = 0.01$ . . . . . | 147 |
| C.1  | The visual stimuli for value (visual channel) under five different noise levels (measured orderedness) used in Experiment 1: How ordered is it?   | 189 |
| C.2  | The visual stimuli for size (visual channel) under five different noise levels (measured orderedness) used in Experiment 1: How ordered is it?  | 190 |
| C.3  | The visual stimuli for hue (visual channel) under five different noise levels (measured orderedness) used in Experiment 1: How ordered is it?   | 190 |
| C.4  | The visual stimuli for texture (visual channel) under five different noise levels (measured orderedness) used in Experiment 1: How ordered is it?   | 191 |
| C.5  | The visual stimuli for orientation (visual channel) under five different noise levels (measured orderedness) used in Experiment 1: How ordered is it? . . . . .   | 191 |
| C.6  | The visual stimuli for shape (visual channel) under five different noise levels (measured orderedness) used in Experiment 1: How ordered is it?   | 192 |
| C.7  | The visual stimuli for numeric (visual channel) under five different noise levels (measured orderedness) used in Experiment 1: How ordered is it?   | 192 |
| C.8  | The visual stimuli for value (visual channel) under noise levels $N_1, N_2, N_3$ , and $N_4$ (measured orderedness) used in Experiment 2: Which is smallest? Which is largest? . . . . .  | 193 |
| C.9  | The visual stimuli for value (visual channel) under noise levels $N_5, N_6, N_7$ , and $N_8$ (measured orderedness) used in Experiment 2: Which is smallest? Which is largest? . . . . .  | 194 |
| C.10 | The visual stimuli for size (visual channel) under noise levels $N_1, N_2, N_3$ , and $N_4$ (measured orderedness) used in Experiment 2: Which is smallest? Which is largest? . . . . .   | 195 |
| C.11 | The visual stimuli for size (visual channel) under noise levels $N_5, N_6, N_7$ , and $N_8$ (measured orderedness) used in Experiment 2: Which is smallest? Which is largest? . . . . .   | 196 |
| C.12 | The visual stimuli for hue (visual channel) under noise levels $N_1, N_2, N_3$ , and $N_4$ (measured orderedness) used in Experiment 2: Which is smallest? Which is largest? . . . . .  | 197 |
| C.13 | The visual stimuli for hue (visual channel) under noise levels $N_5, N_6, N_7$ , and $N_8$ (measured orderedness) used in Experiment 2: Which is smallest? Which is largest? . . . . .  | 198 |
| C.14 | The visual stimuli for texture (visual channel) under noise levels $N_1, N_2, N_3$ , and $N_4$ (measured orderedness) used in Experiment 2: Which is smallest? Which is largest? . . . . .  | 199 |

LIST OF TABLES

---

C.15 The visual stimuli for texture (visual channel) under noise levels  $N_5, N_6, N_7$ , and  $N_8$  (measured orderedness) used in Experiment 2: Which is smallest? Which is largest? . . . . . 200

C.16 The visual stimuli for orientation (visual channel) under noise levels  $N_1, N_2, N_3$ , and  $N_4$  (measured orderedness) used in Experiment 2: Which is smallest? Which is largest? . . . . . 201

C.17 The visual stimuli for orientation (visual channel) under noise levels  $N_5, N_6, N_7$ , and  $N_8$  (measured orderedness) used in Experiment 2: Which is smallest? Which is largest? . . . . . 202

C.18 The visual stimuli for shape (visual channel) under noise levels  $N_1, N_2, N_3$ , and  $N_4$  (measured orderedness) used in Experiment 2: Which is smallest? Which is largest? . . . . . 203

C.19 The visual stimuli for shape (visual channel) under noise levels  $N_5, N_6, N_7$ , and  $N_8$  (measured orderedness) used in Experiment 2: Which is smallest? Which is largest? . . . . . 204

C.20 The visual stimuli for numeric (visual channel) under noise levels  $N_1, N_2, N_3$ , and  $N_4$  (measured orderedness) used in Experiment 2: Which is smallest? Which is largest? . . . . . 205

C.21 The visual stimuli for numeric (visual channel) under noise levels  $N_5, N_6, N_7$ , and  $N_8$  (measured orderedness) used in Experiment 2: Which is smallest? Which is largest? . . . . . 206

C.22 The visual stimuli for value (visual channel) under three different noise levels (measured orderedness) used in Experiment 3: How many pairs? . 207

C.23 The visual stimuli for size (visual channel) under three different noise levels (measured orderedness) used in Experiment 3: How many pairs? . 208

C.24 The visual stimuli for hue (visual channel) under three different noise levels (measured orderedness) used in Experiment 3: How many pairs? . 209

C.25 The visual stimuli for texture (visual channel) under three different noise levels (measured orderedness) used in Experiment 3: How many pairs? . 210

C.26 The visual stimuli for orientation (visual channel) under three different noise levels (measured orderedness) used in Experiment 3: How many pairs? . . . . . 211

C.27 The visual stimuli for shape (visual channel) under three different noise levels (measured orderedness) used in Experiment 3: How many pairs? . 212

C.28 The visual stimuli for value (visual channel) under three different noise levels (measured orderedness) used in Experiment 3: How many pairs? . 213



## **Part I**

# **Background and Motivation**



# CHAPTER 1

---

## Introduction

---

### Contents

---

|       |   |    |
|-------|---|----|
| 1.1   | Glyph-based Visualization . . . . .             | 4  |
| 1.1.1 | A brief history of the study of signs . . . . . | 5  |
| 1.1.2 | Terminology . . . . .                           | 7  |
| 1.1.3 | High-dimensional Glyph Representation . . . . . | 8  |
| 1.1.4 | Challenges . . . . .                            | 10 |
| 1.2   | Contribution . . . . .                          | 11 |
| 1.3   | Thesis Structure . . . . .                      | 13 |

---

**I**T is well known today that we are experiencing an overwhelming surge in the volume and complexity of data to which we have ready access. Advance simulations, scientific measurements, business transactions, and even social media are just a few activities which contribute to this growing mass, and our ability to effectively analyse data has become more challenging. Much of this data is multi-dimensional in nature, whether it be from tables, spreadsheets, video multimedia, or complex computations. Each record (or data entity) may contain anywhere between two attributes to several thousand attributes, and with the increasing size of records, the more difficult it is to detect, classify, and extract any meaningful relationships. For example in genetics, scientists are accustomed to studying millions of DNA sequences and their molecular structures in order to understand the behaviour of specific genotypes.

Visualization has emerged as a powerful tool for the exploration of such large and complex datasets. The visualization of data is the process of conveying data using graphical representations. While algorithmic analysis can be used to quickly and accurately process data to identify trends and outliers, it is dependent on having a computational model of the underlying phenomena. The problem is that one may often not know what

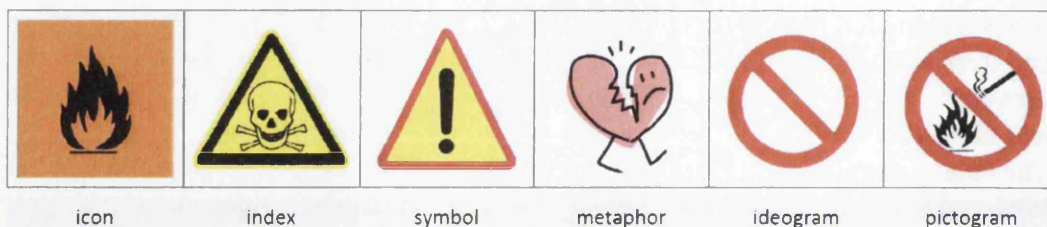
one is looking for, and may not have the required knowledge to define model parameters and threshold values to effectively guide the analysis. Visualization, on the other hand, uses the remarkable abilities and reasoning of a human to process visual information and extract meaning from the data such as structural patterns, trends, and anomalies. The famous expression “*I Know It When I See It*” (IKIWISI) by Potter Stewart [Gew96] implies the notion that we often cannot make sense out of data by solely observing their raw values, but instead rely on our visual pattern recognition system to help us gain knowledge of the data. Overall, there are three main goals of visualization: 1) *Visual exploration*. To allow users to investigate unknown data characteristics more effectively, 2) *Visual analysis*. To confirm the existence of data features and stimulate new hypotheses, and finally 3) *Presentation*. To disseminate information or findings to others, for example, domain experts, colleagues, and the general audience.

A visualization can be realised in many ways. Technically, the type of visualization approach depends highly on the properties of data that need to be presented. These techniques can be classified into two general sub-fields: information visualization, and scientific visualization [PNE02]. Information visualization involves the visual representation of abstract data. In most cases, abstract data do not have an inherent spatial domain, leading to a host of common techniques such as bar charts, pie charts and line graphs, as well as more advanced techniques such as parallel coordinates, histograms, and tree maps [War08a]. Scientific visualization deals with the numerical solution resulting from computational simulations or modelling, and is studied in various disciplines, for example, medicine, weather ensembles, and flow simulations. Such data consists of fields of values (e.g., scalars and vectors) that are coupled with a spatial domain. Examples of techniques used to depict scientific data include colour maps, streamlines, glyphs, and volume rendering [PNE02].

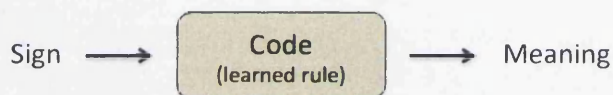
## 1.1 Glyph-based Visualization

Glyph-based visualization is a popular approach for conveying information visually, where a data set is depicted by a collection of small visual objects referred to as *glyphs*. Individual dimensions/attributes of a data point are encoded to various visual features of a glyph (i.e., a shape or symbol) such as its size, colour, and orientation. Since a large number of data dimensions can be incorporated into properties of a single glyph, this makes it a highly suitable technique for communicating and supporting multi-dimensional analysis. Glyphs can be placed and viewed either independently from others, or in some cases, glyphs can be spatially connected to convey the topological relationships between data points or the geometric continuity of the underlying data space.

While glyphs are a form of illustrative graphics in visualization, fundamentally they are dictionary-based encoding schemes. A broader interpretation by Borgo *et. al* [BKC\*13] describe glyphs as a type of *visual sign* that can make use of characteristics from other types of signs such as *icons*, *indices*, and *symbols* (see Figure 1.1).



**Figure 1.1:** In philosophy, language studies and psychology, signs may take one of the three forms: icon, index, and symbol. In many other contexts, terms such as visual metaphor, ideogram, and pictogram are also used to describe subclasses of signs [BKC\* 13].



**Figure 1.2:** Codes provide a framework within which signs assume a meaning. A symbol, for example (+), can have different interpretations depending on the coding convention such as the symbol for ‘first aid’ in medicine, or the arithmetic symbol for ‘addition’.

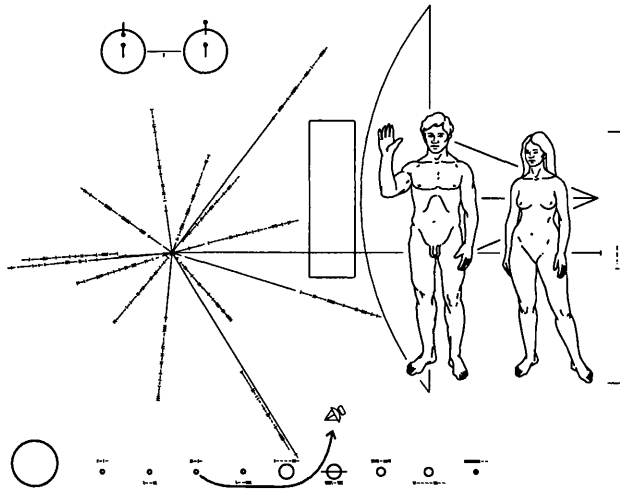
We encounter many of these today, for example, traffic signs, map symbols, and icons to navigate through computer system menus. Although the use of glyphs in the context of multi-dimensional visualization and graphical symbols may seem rather different, they share many interesting attributes, such as being “small”, being “visual”, having “meaning”, requiring “learning”, and often being “metaphoric”. Historically, the use of visual signs dates back to almost 40,000 years ago, and has had a significant role in the invention of current icons and glyphs. It is thus interesting to study briefly their related history and concepts.

### 1.1.1 A brief history of the study of signs

Symbolism has played an important part in the development of human culture, especially as a form of communication. Since the 16th century, its uses in English have been mostly associated with etymology, archaeology, topography and graphonomics as a way to express thoughts, ideas, and concepts. The Paleolithic Age (18,000 BC) present hundreds of examples in the form of cave paintings. It was not until the Neolithic Age where the first forms of pre-writing symbols were introduced for communication: the Petroglyphs. These are images created with rock engravings, where *petra* (meaning “stone”), and *glÿphein* (meaning “to carve”). Even in current times, tribal societies continue to use this form of symbolic writing.

An interesting aspect of petroglyphs is their similarity across different continents;





**Figure 1.3:** *The Pioneer plaque on board the 1972 Pioneer 10 Spacecraft [NAS]. The pictorial message displayed information about the origin of the spacecraft in case the Pioneer 10 is intercepted by extraterrestrial life.*

the commonality of styles strengthen the hypothesis that the human conceptual system is symbolic in nature as investigated by Jungian psychology and early works from Mircea Eliade [EM91]. Psychophysical studies have demonstrated that re-occurring visual patterns in petroglyphs and cave paintings are “hard-wired” into the human brain, which allows us to decipher diagrams and images more efficiently. As such, petroglyphs is a unit of knowledge representation. Over the years, petroglyphs have evolved into graphical symbols known as ideograms that are more illustrative of the signs we see today. The main goal of ideograms is to represent an “idea”, and is sometimes comprehensible only by familiarity, or with prior knowledge. For example, the ideogram shown in Figure 1.1 represents “not allowed” in many countries, but this is highly dependant on *how* it is interpreted. Such ideograms must rely on a conventional rule (or coding) in order to derive meaning from its signs (see Figure 1.2). However, once a coding is established, this can lead to an efficient form of visual communication. Contemporary examples of ideograms can be found in wayfinding signage, as well as technical notations such as arabic numerals, mathematical notations or binary systems which maintain the same meaning despite the difference in language or environment. Some ideograms however, convey their idea through pictorial resemblance of a physical object, and are referred to as pictograms (see Figure 1.1). One interesting example is the Pioneer plaque on board the 1972 Pioneer 10 spacecraft as shown in Figure 1.3, which features a pictorial message designed to provide information about the origin of the spacecraft.

The use of glyphs and signs as a means of communication has traversed human generations due to their cross-cultural expressive power. A prime example can be seen in written languages. Ideograms and pictograms form the base of early written symbols

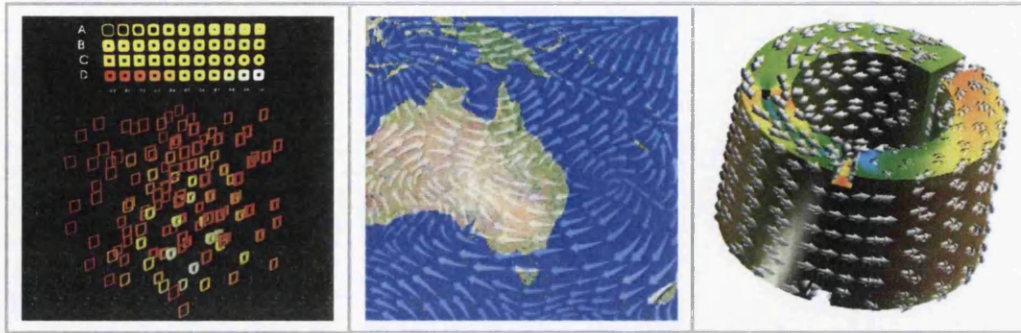
such as cuneiforms and hieroglyphs, to sophisticated logographic writing system such as the ones developed in Chinese and Eastern cultures. For example, Chinese characters are derived directly from individual pictograms, or combinations of pictograms and phonetic signs that represent logograms (i.e., a word, or a morpheme) in the writing of Chinese, Japanese, and Korean. Glyphs for information display and writing systems are therefore similar to some extent in the way they are formed. Fundamentally, both consist of smaller individual components (or visual mappings) that can be combined to represent a piece of information, word, or a sign. It makes sense to consider glyphs as a type of visual language. And as with many languages, they can be learned, or even memorised to which processing can become effortless, making glyphs a potentially effective approach for communicating data quickly.

With the advent of the computer era, icons have become one of the most popular means of conveying messages. In the early 1980s, the CHI community [BSG89, Bly82, Gay89] investigated the use of distinctive sounds to represent specific events or other information, creating a new type of multi-sensory icon known as "earcon". Since then, icons now appear in most media platforms, and incorporate more sophisticated features such as animation and interactive shading. As highlighted by Marcus [Mar03], specialised communities such as health and medicine, finance, transportation, education and training already possess a well-established visual sign system. The expressive power inherent to such visual sign systems is appealing to media, technology and information visualization alike. The major challenge lies in the development of well-designed sign systems.

### 1.1.2 Terminology

The definition of the term *glyph* may have various interpretations across the visualization community. Telea [Tel07] describe glyphs as a "*sign*" for "associating discrete visual signs with individual attributes". Ward *et al.* [WGK10] define a glyph as "a visual representation of a piece of data or information where a graphical entity and its attributes are controlled by one or more data attributes". More generally, we consider a *glyph* (or sometimes also an icon) to be a parameterised visualization object such that its' appearance e.g., shape, colour, size, orientation, texture, etc., encodes the data values which the glyph should represent. It also makes sense to consider *composite glyphs* as another form of glyph. Composite glyphs are constructed either in 3D by combining basic geometric shapes such as spheres, boxes, and cylinders that map to data values (for example, the glyphs in [KE01]), or in 2D by composing regions (i.e., *main body*, *exterior*, and *interior* [MPRSDC12]) that use different visual properties such as pictograms, colour, and text to display the data.

A glyph-based visualization is then created by arranging a certain number of these glyphs across the domain of reference (these could be just a few, or just one, or many, even so many that they merge into a dense visualization) such that every glyph becomes a visualization of the data at (or nearby) the location where the glyph is placed. Examples



**Figure 1.4:** Examples of glyph-based visualizations: (left) visualization of Magnetic Resonance Spectroscopy (MRS) data using superquadrics [FLKI09], (middle) 2D arrows showing the wind direction and magnitude over Australia [TB96], and (right) 3D arrows to depict the flow on the surface of a ring [LWSH04]. Glyphs vary in appearance from one application to another depending on the underlying data.

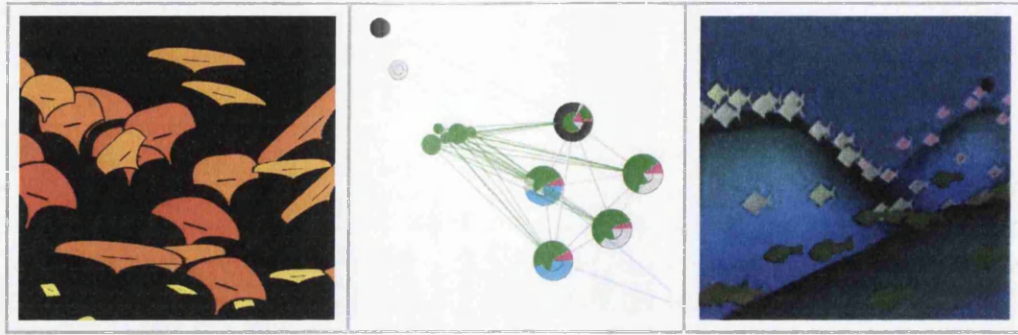
of glyph-based visualizations are shown in Figure 1.4 and Figure 1.5.

A property of all glyph-based visualization approaches is that a discrete visualization is created (instead of a continuous representation like a colour map). Only at certain locations across the domain are individual glyphs displayed to represent the data. This means that this approach is only suitable, when it is possible to assume a certain minimal degree of continuity of the data such that a mental reconstruction of the data, in particular the space between the glyphs, is at least principally possible. In data visualization, this is often possible, making glyph-based visualization particularly interesting for this particular field of application. Alternatively, a glyph-based visualization also makes sense for discrete data, if a one-to-one relation between every instance of the data and the glyphs is established.

### 1.1.3 High-dimensional Glyph Representation

Multiple dimensions are hard to think in, and sometimes impossible to visualize due to the large number of possible values associated with each dimension. Our research focuses primarily on addressing the problem of **high-dimensional data** using glyphs. A dataset is typically called high-dimensional if the dataset contains three or more attribute dimensions. The definition: *multi-dimensional*, is more broadly used to describe the property of such datasets with high-dimensionality already in mind. For attributes less than three, the terms *univariate* and *bivariate* are frequently used instead to describe datasets that contain only one and two dimensions respectively.

High-dimensional data is particularly challenging when coupled with the constraints of glyph-based visual design, for example, the relative size of a glyph may limit the amount of information they can visually display. Not only that, but the underlying data



**Figure 1.5:** Examples of glyph-based visualizations: (left) glyph-based visualization of 3D data [LKH09], (middle) network activity glyphs [PR08], and (right) 3D fish glyphs for exploring biomedical multi-modal data [MgDN06].

type and their specific domain context can also heavily influence the way data is encoded in a glyph-based approach. There are two types of multi-dimensional visualization challenges which we consider in this thesis. First, there is **multi-field visualization** which studies the visualization of data that are given as fields of numerical values. Each field of data co-exist within the same spatial domain, and is depicted using a set of sample data which are given at specified points along the domain to reveal the underlying features. This type of data is commonly found in the domain of scientific visualization, and is the product of complex simulation or modelling. For example, the modelling of engines in Computational Fluid Dynamics (CFD) consists of a vector-field which describe its flow behaviour, in addition to other fields of data such as pressure, temperature and stress (e.g., scalar fields) in the resulting simulation [KML99]. Scientists need to examine the multiple fields simultaneously in order to fully understand the physical phenomena, and the close interactions that occur between fields.

The second type is **multivariate visualization**. Previous works [FLKI09, FH09] have often used the term “*multivariate*” interchangeably to describe the characteristics of multi-field data. In our work, we make a clear distinction between the two. Fundamentally, data attributes within a multivariate dataset may or may not have any inherent spatial structure. The data is typically given in the form of a table, where each column represents an attribute, and each row is a single entity. These attributes may be categorical or numerical in nature, presenting a different kind of challenge for visualization research. Mixed data types are mostly found in the domain of information visualization such as surveillance, stock markets, and geo-spatial visualization. Multivariate datasets also differ in the fact that they can include attributes from a variety of other data sources (e.g., a video). The integration of different data sources allows data analysts to investigate trends in greater detail, for example in activity recognition, security officers will analyse how an event (e.g., a fight) affects the pattern of pedestrian movement [BBS\*08].

The problem of finding an effective representation for a high-dimensional entity is

a hard problem to solve. With the underlying data being very different, the visualization of multi-field and multivariate data using glyphs has led to a wide variety of visual representations. Figure 1.4 (Multi-field glyphs) and Figure 1.5 (Multivariate glyphs) present a few examples illustrating some of these differences. As the dimensionality of a high-dimensional dataset increases, so does the complexity of finding an effective visual representation that promotes insight into such data. In particular, finding a mapping that enables a large number of parameters to be encoded into a glyph, while still be readily perceived remains a significant challenge. Thus, this thesis aims to address several aspects towards the following primary research goal:

**Research goal:** *“How many variables can we effectively encode using a glyph?”*

The answer to this problem is non-trivial, and is heavily influenced by various considerations in glyph-based visual design such as its size (e.g., the amount of visual space the glyph occupies), or the type of information the glyph is trying to represent. The next section will discuss some of these potential challenges.

### 1.1.4 Challenges

Glyph-based approaches share common problems in general when visualizing multiple data attributes. We outline the most important challenges in detail below:

- **Perception and Design.** One of the major challenges in glyph-based visualization is how to create a visualization mapping that can reveal multiple fields of data and their correlations at a time. Encoding multi-faceted data can be non-trivial, since each data variable may contain various types of information (e.g., categorical and ratio data) and additional derived quantities (e.g., statistical measurements). Hence, glyphs must carefully be designed in order to convey the relationships between these fields effectively. On the other hand, there is also the perceptual challenge of how easy it is to understand and correctly interpret such a visualization. Simply encoding data to different visual features of a glyph does not necessarily lead to a good design, and at worse, may confuse viewers or lead to misinterpretations. The design of glyphs is also constrained by their size in comparison with an entire visualization (e.g., smaller glyphs versus larger glyphs), which restricts the number of variables that can be physically encoded and displayed on a screen without loss of information.
- **Glyph Placement and Interaction.** The placement or layout of glyphs on a display can communicate significant information regarding the data values themselves, as well as the relationships between data points. Methods range from using data dimensions as positional attributes, to placing glyphs across a surface of a physical structure such as an engine. In simulation and modelling, the spatial structure is usually pre-determined, and therefore a sampling method needs

to be carefully chosen in order to convey the underlying features. Too dense of a sampling will lead to visual clutter, while a sparser placement may not capture the feature at all. An important part to placement strategies and glyph-based visualization is the effective use of interaction. We find that interactive visualization techniques such as spatial relaxation, brushing, and filtering is often required to support visual exploration, for example, by highlighting areas of interest, which enables users to interrogate and extract information about the data more efficiently.

- **Big Data.** A major technical issue arises from the sheer volume of data that may be generated from complex simulations and scientific measurements. When combined with high dimensional data, not only do such datasets become difficult to analyse and explore, but they also expose a fundamental problem in modern computing and their capacity to process and render large numbers of high-dimensional glyphs. In particular, visualizing large datasets has a significant impact to the interactivity of glyph-based visualization. Therefore, glyph-based algorithms must be able to handle large datasets and present results at close to interactive frame rates in order to increase its usability.

This thesis addresses several aspects within the first two challenges on perception, visual design, placement, and interaction. While the datasets we work with are large and high-dimensional, they may not necessarily be considered as ‘big’, since the term *big data* often concerns datasets involving millions of records (e.g., in particle simulation). The scalability of high-dimensional glyph-based visualization to big data is an important research challenge, and we consider some of these as future work (Chapter 8).

## 1.2 Contribution

The main contributions of this thesis are as follows:

- An overview of the current state-of-the-art glyph-based literature for depicting multivariate or multi-field data [BKC\*13]. The survey draws links between fundamental concepts from semiotics, perception and cognition to understand why glyph-based representations work, and how to design such representations for optimal display given a specific design criterion. Examples of effective glyphs used in various applications such as medical, flow, and sports visualization are described.
- The development of a novel collection of glyph-based visualizations to depict the composition of multiple error-sensitivity fields for single camera positioning [CPL\*12]. In many data acquisition tasks, the placement of a real camera can vary in complexity from one scene to another due to real-world practicalities that cannot be easily encoded into an algorithm. We use 2D and 3D visualization methods to effectively support such a process based on error-sensitivity of

reconstruction and other physical and financial constraints. This enables a user to make dynamic decisions without the need for extensive manual configuration through trial and error. We demonstrate our approach on two real-world applications, namely, snooker analysis and camera surveillance.

- A design study to visualize actions and events “at a glance” using glyphs. Our approach addresses the current problem in real-time sports performance analysis [LCP\*12], where coaching staff and analysts need to examine actions and events in detail whilst maintaining a clear overview of a match. We discuss the relative merits of metaphoric glyphs in comparison with other types of glyph designs in this particular application, and describe an algorithm to manage the glyph layout at different spatial scales in interactive visualization. As a result of this research, we developed a visualization software, MatchPad, on a tablet computer which was used by the Welsh Rugby Union during the Rugby World Cup 2011. The system allows coaches to convey crucial information back to the players in a visually-engaging manner to help improve their performance.
- The introduction and development of high-dimensional, focus and context glyphs that are visually sortable to support sorting of multivariate data [CLP\*15a]. Glyphs that are visually sortable provide two key benefits: 1) performing comparative analysis of multiple attributes between glyphs, and 2) to support multi-dimensional visual search. We describe a novel glyph-based, interactive system for controlling high-dimensional sorting and viewing sorted results. The system incorporates a hierarchical axis binning method to encode multiple dimensions onto a single axis. This effectively reduces visual clutter by relaxing the positioning of glyphs. We demonstrate the usability of glyph sorting in rugby event analysis for comparing and analysing trends within matches.
- A knowledge-assisted, visual analytic application to support the ranking and analysis of multivariate events [CLP\*15b]. In the context of sport event data, coaches and analysts heavily rely on browsing key events for analysing team and player performance. We introduce a novel approach that allows domain experts to effectively search and re-organise a set of events in a flexible manner by converting a user’s knowledge on ranking using regression analysis. We provide details of our system that integrates both glyph-based and information visualization techniques to facilitate the discovery and application of knowledge at different stages of a visual analytic process.
- An empirical evaluation on the perceptual orderability of visual channels [CAB\*14]. The design of effective glyphs for visualization often involves a number of different visual encodings or “channels” (e.g., size, shape, and hue). Since spatial positioning is usually specified in advance, we must rely on other visual channels to convey additional relationships for multivariate analysis. One

such relationship is the apparent order present in the data. This work builds upon our previous research on sorting glyphs [CLP\*15a]. We found evidence that certain visual channels are perceived as more ordered (for example, value) while others are perceived as less ordered (for example, hue) than the measured order present in the data. As a result, certain visual channels are more/less sensitive to noise. We also find visual channels that tend to be perceived as ordered, improve the accuracy of min and max judgements of elements in a sequence.

### **1.3 Thesis Structure**

The remainder of the thesis is structured as follows: In Chapter 2 we discuss the state-of-the-art in glyph-based visualization. A detailed overview of foundations, design guidelines and techniques is presented. In Chapter 3, we describe several novel approaches for visualizing multiple error-sensitivity fields for single camera positioning. Chapter 4 presents a design study comparing metaphoric glyphs and other glyph-based designs for visualizing events and actions “*at a glance*”. A conceptual framework is then introduced in Chapter 5 to design visually sortable glyphs for interactive sorting of multi-dimensional data. Chapter 6 extends this work, developing a knowledge-assisted, visual analytic application for ranking multivariate events. An empirical study on the perceptual orderability of different visual channels is detailed in Chapter 7. Finally, in Chapter 8 we draw our concluding remarks of the thesis, and discuss potential future research based on this work.





---

## A Survey on Glyph-based Visualization

---

### Contents

---

|       |  |    |
|-------|--|----|
| 2.1   | Introduction . . . . .   | 16 |
| 2.1.1 | Contributions . . . . .  | 16 |
| 2.1.2 | Scope and Methodology . . . . .  | 17 |
| 2.2   | Classification and Overview . . . . .  | 17 |
| 2.2.1 | Design Aspects for Glyphs . . . . .  | 19 |
| 2.2.2 | Glyph Placement . . . . .  | 26 |
| 2.2.3 | Interaction . . . . .  | 26 |
| 2.3   | Glyph-based Multivariate Visualization . . . . .                                   | 27 |
| 2.3.1 | Glyph-based Techniques for Event-based Data . . . . .                              | 27 |
| 2.3.2 | Glyph-based Techniques for Geo-spatial Data . . . . .                              | 30 |
| 2.3.3 | Glyph-based Techniques for High-dimensional Data . . . . .                         | 31 |
| 2.4   | Glyph-based Multi-field Visualization . . . . .                                    | 32 |
| 2.4.1 | Glyph-based Techniques for Multiple Scalar Data . . . . .                          | 32 |
| 2.4.2 | Glyph-based Techniques for Flow Data . . . . .                                     | 34 |
| 2.4.3 | Glyph-based Techniques for Tensor Data . . . . .                                   | 38 |
| 2.4.4 | Glyph-based Techniques for High-dimensional, Physical<br>Simulation Data . . . . . | 42 |
| 2.5   | Visual Analysis of Multi-dimensional data . . . . .                                | 44 |
| 2.6   | Discussion . . . . .   | 45 |
| 2.7   | Summary . . . . .  | 46 |

---

**T**HE visualization of data that are given as either fields of values or multiple data dimensions is a classical topic in visualization research. A substantial amount of relevant work has been done in the past decade, introducing a rich collection of well-proven techniques for depicting and revealing insight into multi-dimensional analysis. Glyph-based visualization is one possible approach to realise such a visualization. Its major strength is the ability to present patterns of multi-dimensional data in the context of a spatial relationship where such patterns can be more readily perceived. Other visualization techniques such as direct volume rendering find it difficult to depict multivariate or multi-field data, whereas techniques such as parallel co-ordinates do not convey the spatial relationship inherent in the data as effectively. In the era of data deluge, this provides strong motivation to investigate the cost-effectiveness of using glyph-based visualization. This chapter is the result of a piece of collaborative research from leading groups in the field, where I made significant contributions in creating the taxonomy, surveying important glyph-based literature in a range of applications, and classifying these work according to this taxonomy. An extension is made for this thesis by focusing the scope of the survey to high-dimensional glyphs, and updating the taxonomy to classify related work based on the glyph-based visualization challenge they address, and the visual encoding required to achieve this solution.

### 2.1.1 Contributions

In light of these challenges, the main contributions of this chapter are:

- The classification of multi-field and multivariate glyph-based techniques into three main challenges: perception and design, glyph placement, and the technical challenge associated with visualizing big datasets. We sub-group this further based on their visual encoding in order to investigate common similarities between glyph-based approaches, and to highlight visual encodings where current research have not yet fully explored.
- A review of recent theories developed in semiotics, perception and cognition; and identifying their relevance to glyph-based visual design.
- Surveying a large collection of applications in two contrasting visualizing communities where glyph-based visualization has already made an impact.

The content of this chapter is organised as follows: In Section 2.2, we describe our classification method based on concepts in visual semiotics, and provide an overview of state-of-the-art work using this classification. Section 2.3 presents a survey of multivariate glyphs used within applications of information visualization. We then review examples of multi-field glyphs used within applications of scientific visualization in

Section 2.4. Section 2.5 gives an overview of related literature in visual analytics—an important research field to high-dimensional glyph-based visualization. Section 2.6 provides a discussion of the survey. We draw our concluding remarks in Section 2.7.

### 2.1.2 Scope and Methodology

In this chapter, we review important visualization papers in the past decade that utilise glyph-based techniques for depicting high-dimensional data. The visualization of multiple dimensions can be classified into two general sub-fields: **multivariate visualization** and **multi-field visualization**. In practice, they describe the type of data we are dealing with, i.e., abstract data or scientific data as described in Section 1.1.3.

The broad aim of this survey is to compare the differences in the design and application of multi-field and multivariate glyphs. We present this through real examples of successful glyph-based work in various application domains of information and scientific visualization. Since our focus is on glyph-based solutions for high-dimensional data, we only consider techniques that use glyphs which encode three or more parameters. As a result, we do not include visualization papers in chemistry and physics as these glyphs only encode a small number of attributes. Similarly, literature that utilises popular multi-dimensional graphs such as scatter plot matrices [VMCJ10] are beyond the scope of this survey, as the points themselves are of low dimensionality.

## 2.2 Classification and Overview

The classification of glyph-based visualization for high-dimensional data is non-trivial given the many visualization applications, the diverse domain-specific knowledge required, and the variety of glyph-based techniques that has been developed to address these problems.

We follow a perceptual approach in order to classify glyph-based techniques using fundamental links drawn from semiology. Important to semiotics and visualization is that all glyphs share a common processing step, whereby data attributes are encoded into different visual features of a glyph. Such a mapping is referred to as *visual channel* [War08b]. The taxonomy by Chen and Floridi [CF13] organises a rich collection of visual channels into four main categories: geometric, optical, topological, and semantic channel. Glyphs are created by mapping data attributes to one or many of these channels. For instance, some approaches may use more visual channels from only one type of category, while others may use fewer number of visual channels, but from several different categories. Visual channels provides a framework in which glyph-based approaches can be effectively classified, and we make use of this in order to structure the papers surveyed in this chapter.

Our top level classification groups the literature according to the number of different visual channel categories explored in the resulting glyph-based design (i.e., using one,

| Application domain  | Author/Technique |           | Visual Channel Taxonomy |                 |                                    |                  |
|---|------------------|-----------|-------------------------|-----------------|------------------------------------|------------------|
|   |                  |           | Geometric channel       | Optical channel | Topological and Relational channel | Semantic channel |
| Glyph-based Multivariate Visualization:<br><i>Event-based, Geo-spatial, High-dimensional</i>        | [SFGF72]         | [Che73]   | ✓                       |                 |                                    |                  |
|   | [Pan01]          |           |                         | ✓               |                                    |                  |
|   | [MBP98]          | [PLC*11]  |                         | ✓               | ✓                                  |                  |
|   | [HE99]           |           |                         |                 |                                    |                  |
|   | [FS04]           | [FW10]    | ✓                       | ✓               |                                    |                  |
|   | [SSOG08]         | [SZD*10]  |                         |                 |                                    |                  |
|   | [BBS*08]         |           |                         | ✓               |                                    | ✓                |
| [PR08]  | [FCI05]          | ✓         | ✓                       | ✓               |                                    |                  |
| [KE01]  | [TSWS05]         | ✓         | ✓                       |                 | ✓                                  |                  |
| [PRdJ07]  |                  | ✓         | ✓                       | ✓               | ✓                                  |                  |
| Glyph-based Multi-field Visualization:<br><i>Multiple Scalar, Flow, Tensor, Physical Simulation</i> | [Bar81]          | [Kin04]   |                         |                 |                                    |                  |
|   | [Hab90]          | [RE05]    |                         |                 |                                    |                  |
|   | [TWBW99]         | [OHG*08]  | ✓                       |                 |                                    |                  |
|   | [CM92]           | [MSM*08]  |                         |                 |                                    |                  |
|   | [WPL96]          | [SK10]    |                         |                 |                                    |                  |
|   | [CWD*02]         | [JKLS10]  |                         |                 |                                    |                  |
|   | [HYW03]          |           |                         |                 |                                    |                  |
|   | [CA91]           | [KW06]    |                         |                 |                                    |                  |
|   | [PWL96]          | [RP08]    |                         |                 |                                    |                  |
|   | [LPSW96]         | [MSSD*08] |                         |                 |                                    |                  |
|   | [SEK*98]         | [PPvA*09] | ✓                       | ✓               |                                    |                  |
|   | [WEL*00]         | [SK10]    |                         |                 |                                    |                  |
|   | [CR00]           | [CPL*11]  |                         |                 |                                    |                  |
|   | [WMM*02]         | [HLNW11]  |                         |                 |                                    |                  |
|   | [KMH03]          | [ROP11]   |                         |                 |                                    |                  |
|   | [KYHR05]         | [MRO*12]  |                         |                 |                                    |                  |
|   | [dLvW93]         |           | ✓                       |                 | ✓                                  |                  |
|   | [LAK*98]         | [CM93]    |                         | ✓               | ✓                                  |                  |
|   | [RWG*12]         |           | ✓                       |                 |                                    | ✓                |
| [PGL*12]  |                  | ✓         | ✓                       | ✓               |                                    |                  |
| [KML99]   |                  | ✓         | ✓                       | ✓               |                                    |                  |

**Table 2.1:** A classification of glyph-based techniques for multi-field and multivariate data. Each technique is grouped by application domain along the rows, and the type of visual channels used to construct the glyph along the columns. Entries are ordered in chronological order within each application group. The colours show the visualization challenge which each paper address: *perception and design* challenge, *glyph placement* challenge, and *big data* challenge as outlined in Section 1.1.4.

two, three, or all four types of visual channels). We then sub-divide the work depending on whether they are multivariate glyphs (e.g., an application of information visualization), or multi-field glyphs (e.g., an application of scientific visualization). Papers are then colour-coded according to the three main challenges in glyph-based visualization:

perception and design, glyph placement, and big data as outlined previously in Section 1.1.4. If a paper addresses more than one challenge, we choose the main challenge addressed by the paper. And lastly, those papers belonging to a sub-class appear in chronological order (see Table 2.1).

Classifying the papers in this way facilitates the comparison of similar papers with one another. The classification provides three major aims: (1) to provide a quick but comprehensive overview of recent glyph-based solutions for high-dimensional data, and a summary of the main contributions of each paper, (2) to compare and contrast the difference between multivariate and multi-field glyph-based design from two very different communities, and (3) to highlight unaddressed areas for future research.

In the visualization literature, there have been several major surveys related to glyph-based visualization. The survey by Ward [War08a] provides a technical framework for glyph-based visualization, covering aspects on visual mapping and placement strategies, as well as addressing important issues such as bias in mapping and interpretation. Ropinski *et al.* [RP08, ROP11] present a taxonomy of glyph-based techniques for spatial medical data. Because glyphs are commonly used in vector field visualization, they have been discussed and compared with other forms of visualization in a collection of surveys on flow visualization [LWSH04, MLP\*10]. Separate surveys also exist for multivariate and multi-field research. Fuchs and Hauser [FH09] describe a general visualization pipeline for depicting multi-field data, and classify techniques according to the point at which the multi-field nature of the data is being tackled. The surveys by Wong and Burgeon [WB97a], and more recently Liu [Liu11] give a comprehensive overview of techniques for multivariate data. However, there is a need to build on these surveys by taking a holistic overview of glyph-based visualization in terms of fundamental concepts in visual design, techniques, and applications. We give a brief overview of a theoretical framework for designing glyphs before analysing examples of glyphs and their application to real-world problems in more detail.

### **2.2.1 Design Aspects for Glyphs**

Glyph-based visualization approaches span across a spectrum of visual designs from, for example, dense arrangements of relatively simple shapes (e.g., stick figures) to individual instances of complex glyphs that reveal a lot of information (but only for few, selected places) – the local flow probe [dLvW93] would be an example for this type of glyph-based visualization. Additionally, we can differentiate visualization solutions according to which form aspects are varied according to the data, and how many different values a glyph eventually represents (usually this number is not too large, often 2 to 4, but then also examples exist where dozens of values are represented). Glyphs also vary with respect to whether they are constructed in a 2D or 3D visualization space. It would also make sense to consider glyph-based visualization approaches which are based on the placement of glyphs on surfaces within 3D (often referred to as 2.5D [LWSH04, MLP\*10]). All of these design requirements are usually taken into

consideration when designing new glyphs, and depending on the variability and complexity of each aspect, different glyph-based designs may be more suitable than others.

A number of design guidelines such as Tufte's principles [Tuf83] have been proposed to help describe what a good visualization should achieve. Such principles include:

- showing the data.
- avoid distorting what the data have to say.
- make large datasets coherent.
- encourage the eye to compare different pieces of data.
- reveal the data at several levels of detail, from a broad overview to the fine structure.
- serve a reasonably clear purpose: description, exploration, tabulation, or decoration.

While these visualization goals are useful to glyph-based visualization, they do not provide much insight towards understanding which glyph-based design is more appropriate for a given task. In the following sections, we provide an overview of the technical aspects of designing glyph-based visualization which we use to classify each paper.

### 2.2.1.1 Visual Channels

At the fundamental level, the perception of glyphs can be decomposed to a set of visual properties such as its size, shape, colour, and orientation which encode different values of a data variable. Such properties is often referred to as *visual channels*, and thus a glyph may make use of one or many of these channels for information display. Other terms have also been used within the literature, for instance, Bertin called them *retinal variables* [Ber83], while Ware referred to them as *visual encoding variables* as well as *visual channels* [War04, War08b]. The concept was first introduced in visual semiotics: a theoretical framework that encapsulates the mechanisms through which graphical representations can signify information. Semiotics is the study of signs, and while it has mainly been explored in cartography for designing maps [Mac95], its usefulness and relevance to data visualization [MRO\*12] and glyphs [MPRSDC12] is gaining wider recognition.

One of the first and probably most unique attempt at developing a syntax of visual signs based on formal rules was proposed by Bertin [Ber83]. He identified six basic visual channels, namely: value, size, texture, hue, shape, and orientation which are the fundamental units of constructing any graphics sign. Since then, researchers have suggested adding more visual channels such as colour saturation and arrangement [Mor74], as well

| Geometric Channels  | Optical Channels   | Topological and Relational Channels  | Semantic Channels  |
|---|--|--|--|
| <ul style="list-style-type: none"> <li>• size / length / width / depth / area / volume</li> <li>• orientation / slope</li> <li>• angle</li> <li>• shape</li> <li>• curvature</li> <li>• smoothness</li> </ul> | <ul style="list-style-type: none"> <li>• intensity / brightness</li> <li>• colour / hue / saturation</li> <li>• opacity / transparency</li> <li>• texture (partly geometric)</li> <li>• line styles (partly geometric)</li> <li>• focus / blur / fading</li> <li>• shading and lighting effects</li> <li>• shadow</li> <li>• depth (implicit / explicit cues)</li> <li>• implicit motion / motion blur</li> <li>• explicit motion / animation / flicker</li> </ul> | <ul style="list-style-type: none"> <li>• spatial location</li> <li>• connection</li> <li>• node / internal node / terminator</li> <li>• intersection / overlap</li> <li>• depth ordering / partial occlusion</li> <li>• closure / containment</li> <li>• distance / density</li> </ul> | <ul style="list-style-type: none"> <li>• number</li> <li>• text</li> <li>• symbol / ideogram</li> <li>• sign / icon / logo / glyph / pictogram</li> <li>• isotype</li> </ul> |

**Table 2.2:** A taxonomy of visual channels [CF13]. Each visual channel is classified into four categories: geometric, optical, topological and relational, and semantic channels. Glyphs are created by mapping data attributes to one or many visual channels.

as fuzziness, resolution, and clarity [Mac95, MRO\*12] as shown in Figure 2.1. Cleveland and McGill made the first attempt at ranking several visual channels (e.g., position, length, and colour) based on how effective they encode different data types for data visualization [CM84]. This exercise was later extended to 13 visual channels [Mac86]. In addition, perceptual studies have been carried out to evaluate the effectiveness of some visual channels, relating to special visual properties in which certain visual channels are perceived [Wil67, QH87, ROP11]. For example, the *pop-out effects* on some visual channels (e.g., colour) is stronger than others (e.g., shape), which can be taken advantage of to draw a viewer’s attention to important features in a visualization. A comprehensive review of visual properties for glyph-based design is presented in the taxonomy by Maguire *et al.* [MPRSDC12].

Our classification is based on the recent framework by Chen and Floridi [CF13], who organise over 30 visual channels into a simple taxonomy consisting of four categories: geometric, optical, topological, and semantic channels. The categorisation is the first research of its kind to facilitate the vast amount of techniques proposed in the visualization



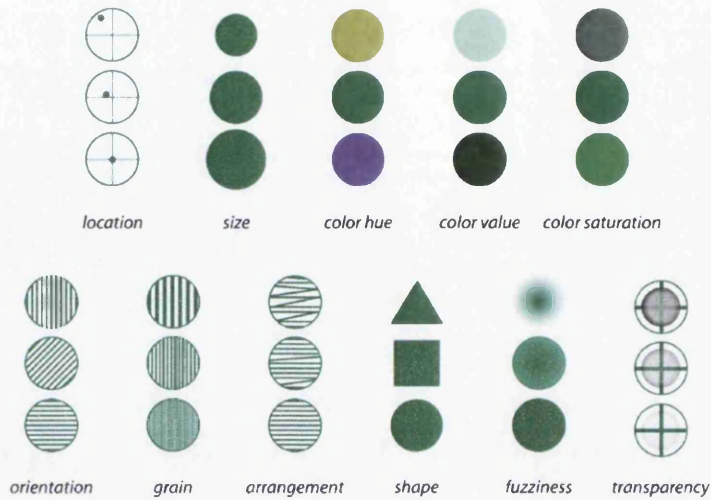


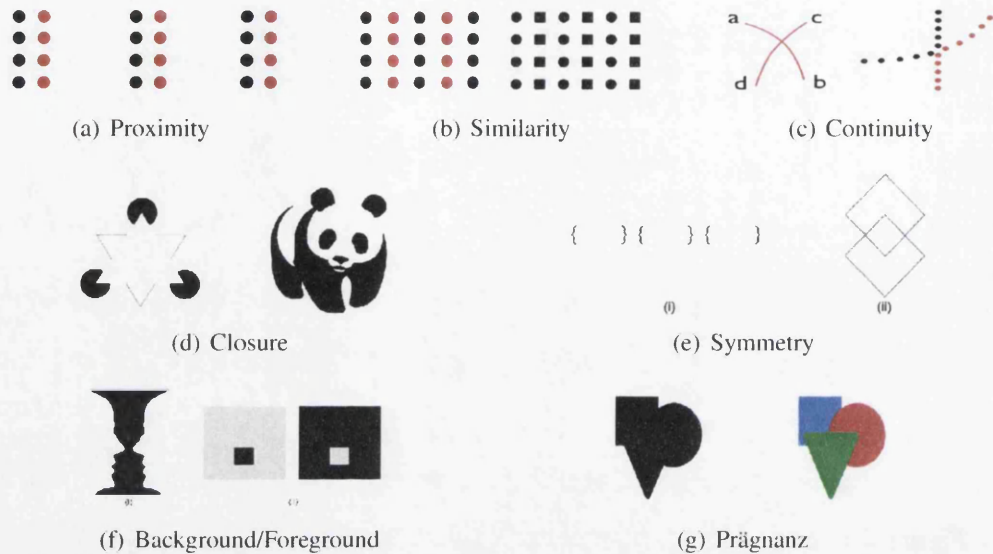
Figure 2.1: Examples of visual channels applied to point symbols. [MRO\* 12]

literature. Following this approach, a rich collection of visual channels is summarised in Table 2.2. Most of these visual channels can be of potential use in glyph-based design, though only a small number of channels have been utilised. This suggests that the design space for glyphs is far from being fully explored.

### 2.2.1.2 Perceptual Organisation

Designing glyphs usually involves several design considerations. Apart from encoding variables to a visual channel, the way in which different channels are organised can create various visual effects to the information being conveyed. The first major attempt to understand pattern perception was undertaken by Gestalt psychologists who outline a set of fundamental and universal rules of perceptual organisation known as “*Gestalt Laws*”. The word “*gestalt*” simply means “pattern” in German. These laws describe the way we see patterns in visual displays, which can easily be generalised to a set of design principles for creating glyphs. Eight Gestalt laws are discussed here: proximity, similarity, continuity, closure, symmetry, background/foreground, and prägnanz.

**Proximity.** The spatial proximity is a powerful perceptual organising principle and one of the most useful in design. The proximity principle states that objects that are closer to one another are perceived to be more related than those that are spaced farther apart. Figure 2.2(a) shows three arrays of dots that illustrate this phenomena. The existence of three groups (or clusters) is perceptually inescapable, even though there are two sets of identifiable colours.



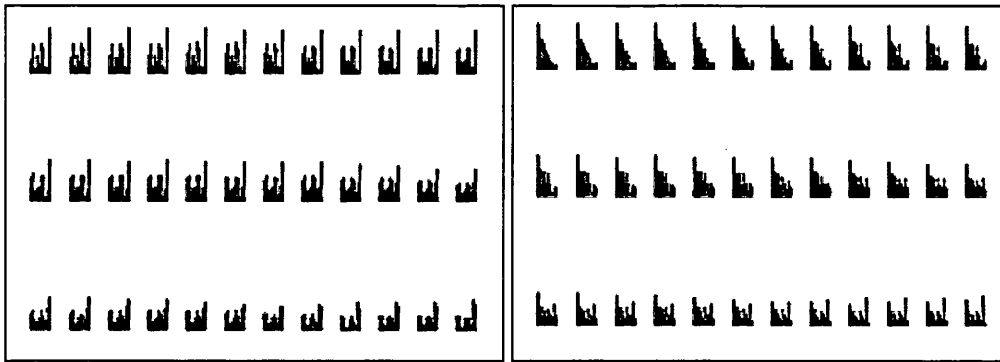
**Figure 2.2:** Gestalt principles of perceptual organisation. A theoretical framework that describe the self-organising tendencies in human perception when several visual channels are combined or structured in some form [War08b].

**Similarity.** The visual characteristics of individual elements can also determine how they are grouped. The similarity principle states that similar elements tend to be grouped together. In Figure 2.2(b) we demonstrate two different ways of visually separating the column information, namely by colour (e.g., black circles vs. red circles), and shape (e.g., circles vs. squares).

**Continuity.** The continuity principle states that we are more likely to construct visual entities out of elements that are arranged on a line or curve, rather than those that contain abrupt changes in direction. A common application of this principle is in node-link diagrams. When elements are positioned smoothly, this can be stronger than similarity of colour as shown in Figure 2.2(c).

**Closure.** In some complex arrangements, elements can often be grouped into a single, recognisable pattern. Figure 2.2(d) gives two examples showing the closure principle, where there is a perceptual tendency to perceive closed contours that have gaps in them. Closed contours are widely used to visualize set concepts in Venn-Euler diagrams. In glyph-based design, this may lead to the perception of fairly complex structures.

**Symmetry.** The symmetry principle can provide a powerful organising effect, whereby symmetrical shapes are formed around their centre. In Figure 2.2(e) (i), the



**Figure 2.3:** Bar chart glyphs showing the monetary exchange rates of 10 U.S. countries over 3 years [War08a]. Each glyph represents a month within a year (i.e., each row), with the exchange rate of each U.S. country mapped to the height of the individual bars. The dimensions (i.e., each bar) on the glyph can be ordered to improve the overall effectiveness of the visualization. Two methods are compared: (left) bars in random ordering, and (right) bars that are sorted based on the first record. Gradual changes and anomalies are much easier to perceive when the dimensions are ordered.

perceived picture is usually three sets of opening and closing brackets while in Figure 2.2(e) (ii) the dominant picture would be two overlapping diamonds. One possible application of symmetry is in tasks in which data analysts are looking for similarities between two different sets of time-dependant data. It is often easier to compare if these time series are positioned symmetrically [LLCD11].

**Figure and Ground.** The figure/ground effect suggest that elements are perceived as either figure (element of focus) or ground (background or surrounding area). In this principle, several factors play an important role: surroundness, size (or area), symmetry, parallelism, and external edges. Each of these five properties can determine which parts of a figure are classified as foreground or as background (see Figure 2.2(f) for example).

**Pragänz.** The pragänz principle states that when a viewer is confronted with an ambiguous or complex representation, the simplest and most stable interpretation is always favoured. For example in Figure 2.2(g), even without colour information, we tend to perceive the complex shape as a composition of basic primitives (e.g., a square, circle, and triangle) that are joined together.

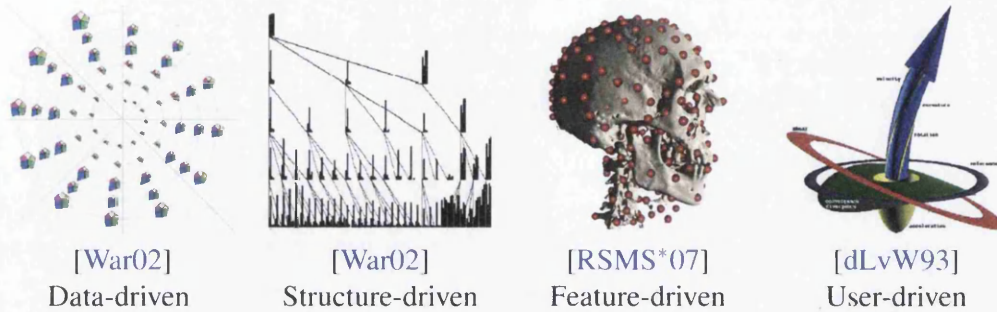
### 2.2.1.3 Data Mapping Order

The order in which dimensions are displayed on the glyph can have a significant impact to the effectiveness of the overall visualization. By modifying the order of dimensions

while preserving the type of mapping, as many as  $N!$  alternate views can be generated. An important issue in using glyphs is to ascertain which ordering(s) will be most supportive of the task at hand. Several possibilities exist beyond random ordering or the order in which the attributes are originally stored. One example is presented by Ward [War08a] as shown in Figure 2.3. Sorting the exchange rates of 10 countries in the U.S. by their relative values in the first year of the time series exposes a number of interesting trends, anomalies, and periods of relative stability and instability. Ward [War08a] describes four possible strategies for ordering:

- **Correlation-driven.** Many researchers have proposed using correlation and other similarity measures to order dimensions for improved visualization [Ber83, ABK98, FK03, BS92]. These orderings help reveal clusters of similar variables, outlier records, and gradual shifts in relationships between variables.
- **Complexity and Symmetry-driven.** Gestalt principles indicate we have a preference for simple shapes, and we are good at seeing and remembering symmetry. In [PWR04] the shapes of star glyphs resulting from using different dimension orders were evaluated for two attributes: monotonicity (the direction of change is constant) and symmetry (similar ray lengths on opposite sides of the glyph). The ordering that maximised the number of simple and symmetric shapes was chosen as the best. User studies showed improved performance with complexity and symmetry optimised orderings.
- **Data-driven.** Another option is to base the order of the dimensions on the values of a single record (base), using an ascending or descending sort of the values to specify the global dimension order. This can allow users to see similarities and differences between the base record and all other records.
- **User-driven.** As a final strategy, we can allow users to apply knowledge of the data set to order and group dimensions by many aspects, including derivative relations, semantic similarity, and importance. Derivative relations mean that the user is aware that one or more dimensions may simply be derived through combinations of other dimensions. Semantic similarity indicates dimensions that have related meanings within the domain.

Alternatively, we can order the dimensions on a glyph based on its visual appearance. Some attribute dimensions are likely to have more importance than others for a given task, and thus ordering or assigning such dimensions to more visually prominent features (e.g., colour) of the glyph will likely have a positive impact on task performance. In order to optimally represent a data variable using a visual channel of the glyph, the corresponding data range should be normalised, for instance, to the unit interval [War02, LKH09, ROP11]. The remapped data attributes parametrize the visual appearance of a glyph. Ropinski *et al.* [RP08], for example, use an interface similar to a



**Figure 2.4:** Examples of different glyph placement strategies: **Data-driven** positions glyphs along some attribute axis or an underlying grid for data with spatial information such as map visualization. **Structure-driven** arranges glyphs to show an ordering, hierarchical, or other relationship of the data variables. **Feature-driven** places glyphs at local features such as iso-surfaces. **User-driven** allows users to incorporate their knowledge by interactively placing glyphs at specific regions in the domain.

transfer function editor for mapping a data attribute to a visual channel of a glyph. In addition, the semantics of the data variable should also be considered, and is an important guideline for selecting the appropriate mapping [War02, ROP11].

## 2.2.2 Glyph Placement

The placement of glyphs is a prominent visual stimulus and can be used to convey information about the data as shown in Figure 2.4. In the context of information visualization, Ward [War02] categorises placement strategies into *data-* and *structure-driven* placement. The former is directly based on individual variables or spatial dimensions of the data, or on derived information such as principal components analysis (PCA) [WG11] or multi-dimensional scaling (MDS) [WB97b]. Examples of data-driven strategies are placing the glyphs in a 2D scatter plot, or aligning them with the underlying data grid (in case of spatial data). Structure-driven placement, on the other hand, is based on the ordering, hierarchical or other relationship of the data variables. According to Ropinski *et al.* [ROP11], such strategies are not directly applicable to medical data. Therefore, they suggest *feature-driven* placement as an additional category, where glyphs are placed on local data features such as iso-surfaces [RSMS\*07, MSSD\*08]. We consider it useful to also consider *user-driven* placement, where glyphs are manually placed to investigate the data at a certain location [dLvW93, Tre00].

## 2.2.3 Interaction

Interactive visualization looks at the ability to navigate and interrogate datasets through interaction to improve understanding. The literature in this field is vast, and for a com-

prehensive coverage of techniques, readers may consult the state-of-the-art survey by Zudilova [ZSAcL08]. However, as in many multi-dimensional approaches, the interaction of glyph-based visualization is an important aspect for visual exploration of complex datasets. Yi *et al.* [YKSJ07] identify seven key areas for the use of interaction in visualization: select, explore, reconfigure, encode, abstract/elaborate, filter, and connect. For the exploration of data, Cockburn *et al.* [CKB09] investigate different interface schemes for studying the overview and detail of datasets. Chittaro [Chi06] also investigates the use of interactive visualization, however focuses primarily on small-screen mobile devices. While many interactive methods can be generally applied to a host of visualization techniques, some are tailored to the specific case of glyph-based approaches. Such an example is described by Ebert *et al.* [ESZM96], who incorporate two-handed interaction and stereoscopic viewing for the exploration of 3D glyph-based visualization. Shaw *et al.* [SHB\*99] investigate new techniques for using an interactive lens to explore a 3D glyph-based visualization. And the work by Yang *et al.* [YHW\*07] propose a *Value and Relation* display that is designed for interactive exploration of large datasets.

## **2.3 Glyph-based Multivariate Visualization**

All of the papers in this section use glyph-based approaches to visualize multivariate data. However, some of these techniques can also be applied in the scientific domain as demonstrated in [SFGF72, Che73], and therefore may be classified in either group. The research here is divided according to the data's characteristics which makes them fundamentally different. In particular, we investigate three types of data: event-based, geo-spatial, and high-dimensional.

### **2.3.1 Glyph-based Techniques for Event-based Data**

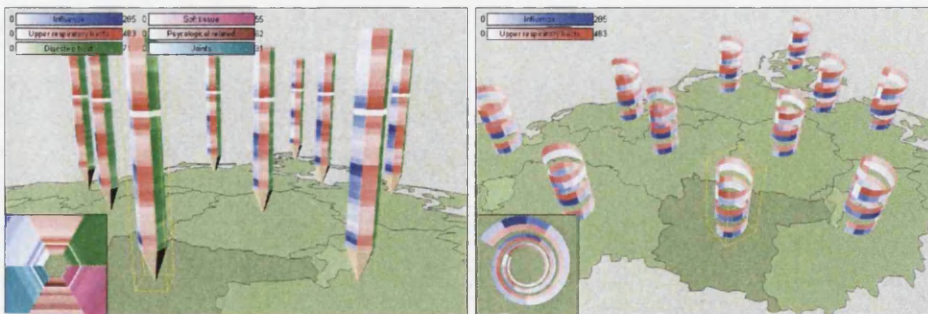
Events usually describe happenings of interest that occur at a given time or location. A popular and classic approach that combines the visualization of space and time is the space-time cube concept developed by Hägerstrand in 1989 [H89], where the actual events are visualized by placing glyphs at those positions where events are located in time and space. The work by Tominski *et al.* [TSWS05] presents such an example using helix and pencil icons to visualize spatial-temporal data on maps. The dimension of time is mapped by extending the length/height of the icons in 3D space. Pencil icons is a useful visual metaphor due to their familiarity, and it allows time-dependent attributes to be effectively encoded using colour intensity along the faces (or sides) of the pencil. The pencil icons are used to analyse linear patterns that may occur in spatial-temporal data. The helix icon, on the other hand, is used to emphasise the cyclic characteristics of temporal dependencies based on their geometric shape. In order to create a helix icon, a ribbon is formed for each time-dependent variable. The authors demonstrate their work

on visualizing monthly health data on a map monitoring the behaviour of six diseases (see Figure 2.5).

Forlines and Wittenburg [FW10] introduce *Wakame* glyphs to depict multi-dimensional sensor readings. They demonstrate their approach to display a building's environmental sensor information containing 40 dimensions, and over 50K samples. *Wakame* glyphs extend 2D radar charts to 3D using time, and connects each instance with a polygonal surface to create a visualization object. A colour is then assigned to each vertex that corresponds to the different dimensions. The glyphs are positioned over a 2D building plan to compare sensor information between different regions.

Botchen *et al.* [BBS\*08] describe the VideoPerpetuoGram (VPG), a dynamic technique for visualizing activity recognition found in video streams. This involves stacking temporally spaced intervals of key video frames and using colour filled glyphs to represent geometric information (e.g., object identifier, position, size), semantic information (e.g., action type and inter-object relation) and statistical information (the certainty and error margins of the analytical results). They demonstrate their technique on surveillance video footage for summarising the motion of people and actions.

An alternative glyph-based approach for mapping temporal data is to encode the time dimension directly onto the glyph as shown by Pearlman and Rheingans [PR08]. The authors introduce compound glyphs for visualizing network security events. The compound glyph representation is a pie chart in which the size and colour of each segment is mapped to the amount of activity and the type of service. One of the motivations of using a simple pie chart design, is its ability to extend to the temporal domain by slicing the glyph as concentric layers for depicting information at different time instances. Each glyph indicates a node on the network in which connectivity lines in the visualization represent the communication between nodes. They successfully demonstrate their method on a simulated network consisting of a small set of client users. Suntinger *et al.* [SSOG08] also use glyph-based event visualization to create an *Event Tunnel* for business analysis and incident exploration. Events here are depicted using spherical



**Figure 2.5:** Visualizing monthly health data consisting of multiple time-dependent variables using (left) 3D pencil icons, and (right) 3D helix glyphs. The glyphs are placed over a map to show the temporal characteristics of different diseases [TSWS05].



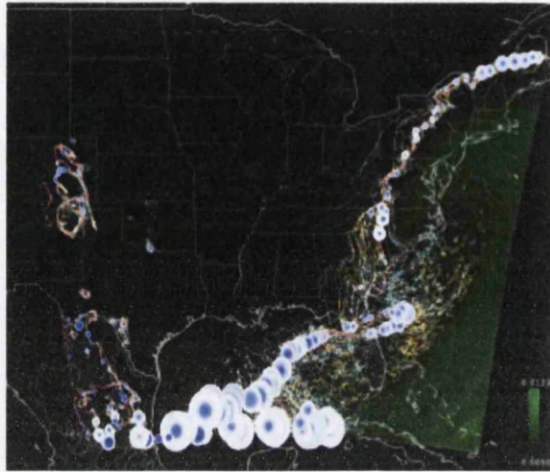
**Figure 2.6:** Glyph-based visualization of sounds. Symbolic icons are used to convey the semantic information of sound in movies such as birds chirping, chimes, and the creaking of doors. The icons are positioned along a timeline of the movie [JBMCI0].

event glyphs which are then sub-divided into colour-coded regions or by using size to map several attributes.

The work by Jänicke *et al.* [JBMCI0] describes *SoundRiver*, a visualization system that conveys the semantic information of sound in movies through visual feedback to enhance the experience of hearing-impaired viewers. The system automatically extracts sound features (e.g., music, speech, rain, etc.) from movies, and maps them to a collection of programmable visual metaphors. Symbolic icons are used to effectively show different sound effects such as “aircraft flying by”, and “chimes” that are otherwise difficult visualize. The size and colour of the icon are then mapped to volume and atmosphere of the sound, resulting in an overall expressive glyph design. Each glyph is placed along a timeline, combining other visualization features such as an envelope representing the music strand, and additional icons representing speech events (see Figure 2.6).

Parry *et al.* [PLC\*11] introduce a novel event selection concept for summarising video storyboards. A video storyboard is a form of video visualization, used to summarise the major events in a video using illustrative visualization. There are three main technical challenges in creating a video storyboard, (a) event classification, (b) event selection and (c) event illustration. This paper focuses on challenges (b) and (c) which they demonstrate using a case study on Snooker video visualization. For event illustration, the authors explore a collection of iconic glyphs which convey some metaphors in addition to data values for event labelling. These include ball objects that vary in size, opacity and colour for representing ball trajectory and semantic information (e.g., ball type, event importance), textured circle glyphs and numbered icons for depicting the sequences of shots, and a pie chart icon to represent scoring and video timing information.





**Figure 2.7:** Visualization of water-vapor mixing ratio, illustrating the progression of uncertainty by the use of spaghetti plots and uncertainty glyphs [SZD\*10].

### 2.3.2 Glyph-based Techniques for Geo-spatial Data

Geo-spatial analysis is a well-established field which involves analysing data with a geographical or geo-spatial aspect. Cartographic research contributes to a large proportion of this work, with icons and symbols playing a central role to many of its applications. However, we often find that geo-spatial visualization may incorporate inter-disciplinary techniques from other domains, and thus can be classified under more than one category. MacEachren *et. al* [MBP98] is such an example where the authors present a novel approach to visualize reliability in mortality maps using a bi-variate mapping. Given a base geographical map (United States), the technique involves using colour filled regions to represent the data and texture overlay to represent the reliability.

Healey and Enns introduce a different approach [HE99] using multi-colored perceptual texture elements known as *pexels* for visualizing multi-dimensional datasets across a height field. The pexels appearance is determined by encoding attribute values into three texture dimensions: height, density and regularity. Pexels incorporate pre-attentive features (e.g., height) to improve the accuracy of visual search-based tasks. To assess its effectiveness, the authors apply their technique on a typhoon data set where wind speed, pressure and precipitation is mapped to the pexel properties.

Pang [Pan01] provides an overview of various geo-spatial uncertainty metrics and identifies two methods for integrating this data into a geo-spatial representation: (a) mapping uncertainty information to graphic attributes (e.g., hue, opacity) or by using (b) animation to convey uncertainty. By treating uncertainty fields as an additional layer of information in cartography, techniques such as uncertainty glyphs can be visualized independently and overlaid on top of an existing geo-spatial visualization.

Fuchs and Schumann [FS04] describe a method for integrating high-dimensional,

complex visualizations onto maps. Rather than designing new icons, they use current methods such as ThemeRiver icons and TimeWheel icons. These are referred to as *visugrams*; created by taking existing visualization techniques and reducing them in size so they form an icon, which can then be positioned spatially over a map. The focus of this paper discusses a general strategy for positioning such icons on maps using an adaptive labelling method that incorporates focus+context techniques.

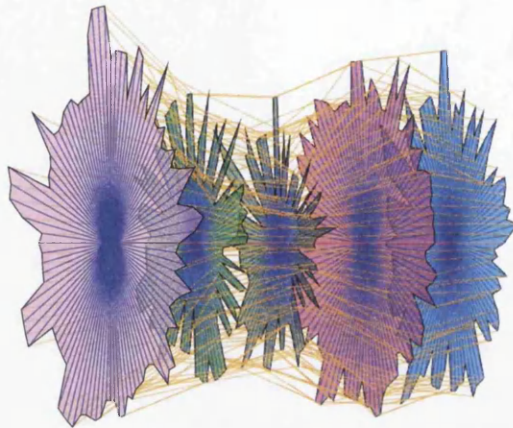
The work of Sanyal *et al.* [SZD\*10] introduce *Noodles*: an interactive tool for visualizing ensemble uncertainty in numerical weather models. The software incorporates glyphs, ribbons and spaghetti plots that use a variety of encodings such as colour and size as shown in Figure 2.7. They demonstrate their work on the 1933 Superstorm simulation, where the visual mappings illustrate the statistical errors (e.g., mean, standard deviation, interquartile range and 95% confidence intervals) in the data.

### **2.3.3 Glyph-based Techniques for High-dimensional Data**

Generic glyphs for high-dimensional data is a desirable tool due to their applicability to a diverse range of fields. One of the most popular used approach is star glyphs, which was first introduced by Siegel *et al.* [SFGF72]. Star glyphs map multiple dimensions to axes that radiate evenly from its centre, and the length of each axis represent the data value. A line is then drawn joining each axis to form a shape. The glyphs are typically placed in a 2D arrangement defined by two attribute axes, or in a uniform grid. What makes star glyphs so effective is its ability to compare similarities between multi-dimensional entities holistically based on its geometric properties. It has been used to depict a variety of datasets which include: myocardial infarction data [SFGF72], coal data [PWR04], and animal datasets [LBR03].

An extension to the this work by Fanea *et al.* [FCI05] combine star glyphs with another multi-dimensional technique: parallel coordinates, to create a new type of glyph called *Parallel Glyphs*. Their approach overcomes the problem of overlapping polylines in parallel coordinates, and the difficulties of comparing two star glyphs (because they are spatially separated). Parallel glyphs are constructed by extending parallel coordinates into the third dimension, and connecting them as star glyphs. Colour-scales are applied to support comparison and selection task in 3D. They demonstrate their work on a plant dataset consisting of 100 generations of different bushes, each having five attributes.

Chernoff [Che73] introduce a novel, and interesting glyph called *Chernoff Faces* which displays data using cartoon faces by mapping data to different facial features, such as its eyes, eye brows, mouth, and head shape. The glyph was developed using the idea that since they use the perceptual characteristics of real faces, they may be particularly easy for people to use given our heightened sensitivity to facial structure and expression. The author demonstrate their approach to a fossil and geological dataset containing over 70 different specimens, in which each face encoded 8 variables. It was shown that chernoff faces are able to help in cluster analysis, discrimination analysis,



**Figure 2.8:** *Parallel glyphs for visualizing large, high-dimensional data. Each glyph represents a single high-dimensional object which are arranged along a pivot axis. Polylines are rendered to connect each glyph in order to compare changes in attribute values [FC105].*

and detect substantial changes in time series.

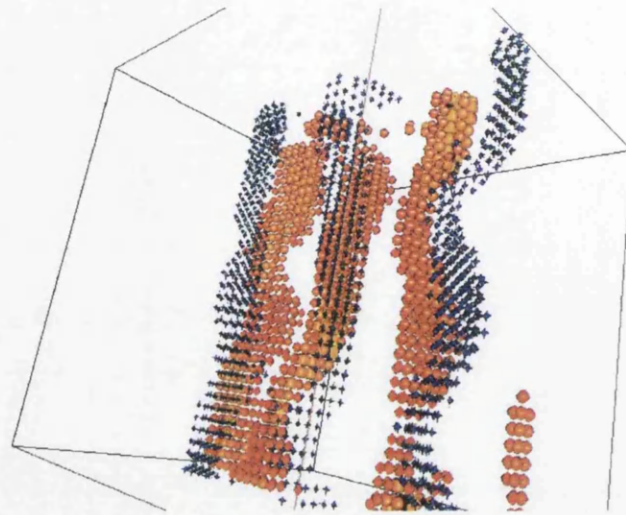
Kraus and Ertl [KE01] present a visualization system using customised glyphs for interactive data exploration in 3D. The primary goal is to provide tools that allow users to interactively customise the definition of glyphs according to the dataset they are trying to visualize. Composite glyphs are created by combining basic geometric objects such as spheres, boxes, cones, cylinders, and text that map each variable in the dataset. Each glyph can also incorporate an extra dimension using colour. They describe an application to a car development project, visualizing the results of computer simulations.

## 2.4 Glyph-based Multi-field Visualization

This section describe glyph-based techniques that have been used in multi-field visualization. Data is usually obtained from simulation and modelling or from sophisticated scanning technology in various scientific domains, resulting to several fields of data that have either a scalar, vector, or tensor property [Tel07]. Multi-field data concerns with one or many of such fields. We also consider physical simulation data as a separate data type (e.g., [GRE09]), since they often involve the modelling of multi-attribute entities that are not characterised by the previous data types.

### 2.4.1 Glyph-based Techniques for Multiple Scalar Data

Due to its multivariate characteristics, geometric shapes are often used to represent multiple data attributes. The work by Barr [Bar81] presents such an approach by introducing



**Figure 2.9:** Visualization of a magnetohydrodynamics simulation dataset displaying vortex tubes with positive vorticity (cuboids and ellipsoid glyphs) and negative vorticity (stars) [SEK\*98].

geometric shapes (superquadrics) used for creating and simulating three-dimensional scenes. The author defines a mathematical framework used to explicitly define a family of geometric primitives from which their position, size, and surface curvature can be altered by modifying a family of different parameters. Example glyphs include: a torus, star-shape, ellipsoid, hyperboloid, toroid. Furthermore, the author describes angle-preserving shape transformations that can be applied to primitives to create geometric effects such as bending or twisting.

Using the set of superquadrics defined by Barr [Bar81], Shaw *et. al* [SEK\*98] describe an interactive glyph-based framework for visualizing multi-dimensional data. As opposed to the analytical focus in the previous work, the authors describe a method for mapping data attributes appropriately to shape properties such that visual cues effectively convey data dimensionality without depreciating the cognition of global data patterns. They map values in decreasing order of data importance to location, size, colour and shape (of which two dimensions are encoded by shape). Using superellipsoids, they apply their framework to the "thematic" document similarities [SEK\*98] and magnetohydrodynamics simulation of the solar wind in the distant heliosphere (see Figure 2.9) [E\*00, ES01].

An alternative approach for representing multi-field data is to overlay multiple visualizations onto a single image. The report by Taylor [Tay02] provides an overview of some of these techniques for visualizing multiple scalar fields on a 2D manifold. Taylor initially hypothesise that the largest number of data sets can be displayed by mapping each field to the following: (1) a unique surface characteristic, (2) a different visualization technique for each field or (3) by using textures/glyphs whose features depend on

the data sets. One such technique is introduced by Weigle *et al.* [WEL\*00], who describe the use of *oriented slivers*. The authors depict each field as texture slivers oriented at different degrees, and where luminance is mapped to their relative scalar values. In the final step, each scalar representation is fused into a single image for simultaneous viewing. The authors demonstrate their work on a scanning electron microscope (SEM) data set containing 8 different scalar fields. An alternative approach is developed by Bokinsky [Bok03] using *data-driven spots* (DDS). Here, multiple scalar fields is mapped to textured spots containing a single type of sparse, distinct glyphs of a specific size, colour and motion to produce visually separable fields.

Layering methods can also be extended to surfaces on 3D objects. Crawfis and Allison [CA91] introduce such a method using texture mapping and raster operations. The interactive programming framework enables users to overlay different data sets by defining raster functions/operations. Such a function may include glyph textures for mapping data attributes (e.g., vector data). Using a generated synthetic dataset, they present a method for reducing the visual clutter by mapping colour to a height field and using a bump map to represent the vector and contour plots. The final texture is mapped onto a 3D surface.

Feng *et al.* [FLKI09] introduce Scaled Data-Driven Spheres (SDDS) to visualize multi-dimensional volume datasets and evaluate their work against superquadric glyphs [E\*00, Kin04]. SDDS extends the work by Bokinsky [Bok03] of 2D coloured spots, into 3D using coloured spheres. For SDDS, the field type and magnitude is mapped to colour and sphere radius as oppose to superquadric glyphs, where each scalar parameter is encoded into four glyph properties: thickness, overall roundness, cross-section roundness and colour. The authors demonstrate their technique to visualize a combination of Magnetic Resonance Spectroscopy (MRS) and Magnetic Resonance Imaging (MRI) data to scan brain tumours and determine tumour boundaries.

## 2.4.2 Glyph-based Techniques for Flow Data

Flow visualization has been a very attractive field within visualization research for a long time already, leading to a number of surveys [LWSH04, PL09, MLP\*10] that cover various aspects such as techniques, seeding and placement strategies, and feature extraction methods. Flow data consist of a vector field (2D or 3D) that describe the behaviour of the flow, as well as other fields (e.g., pressure, heat, etc.) and derived attributes that may also impact its behaviour. Most visualization research has pre-dominantly been conducted on simulation data resulting from *Computational Fluid Dynamics* (CFD). In general, such simulation data and experimental data is characterised by a certain level of *uncertainty* due to inaccuracies in the mathematical models and parameters. Integrating the presentation of data with uncertainty fields increases the complexity of the task significantly, and has since grown to become a field of research of its own [PWL96]. We therefore sub-group the following work according to these two specific application domains.

### 2.4.2.1 Computational Fluid Dynamics

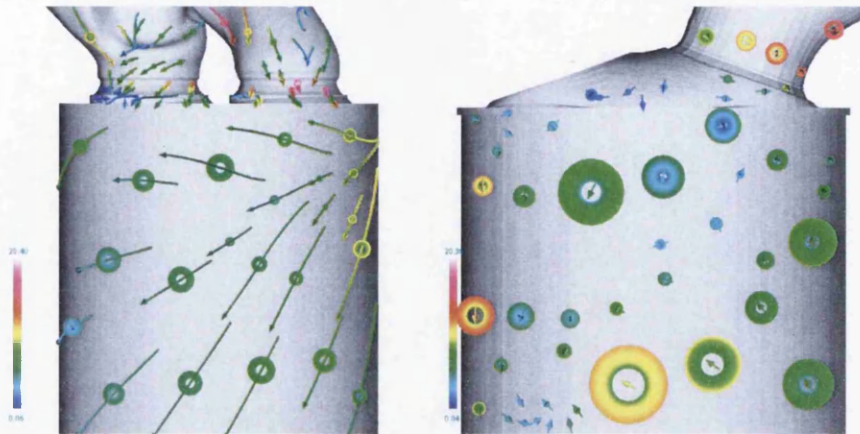
Glyph-based methods in the flow visualization community typically involves smaller glyphs that are densely positioned along the domain to reveal features of the flow [LWSH04]. This approach often results to fewer number of fields being depicted. De Leeuw and Van Wijk [dLvW93] instead introduce a larger, interactive probe-glyph for visualizing multiple flow characteristics in a small region. Such probe-glyphs is placed interactively (and sparsely) along a streamline to show local features in more detail. One focus of this paper is the visualization of six components: velocity, curvature, shear, acceleration, torsion and convergence. In order to facilitate such a mapping, the authors incorporate a larger glyph design. The core components of the glyph consist of the following: 1) a curved vector arrow where the length and direction represents the velocity and the curvedness is mapped to the curvature, 2) a membrane perpendicular to the flow where its displacement to the centre is mapped to acceleration, 3) candy stripes on the surface of the velocity arrow illustrates the amount of torsion, 4) a ring describes the plane perpendicular to the flow over time (shear-plane), and finally 5) the convergence and divergence of the flow is mapped to a *lens* or osculating paraboloid.

Crawfis and Max [CM93] describe textured splats in volume rendering for visualizing 3D scalar and vector field data. The aims of this approach is to enhance the performance speed of rendering glyphs in large, 3D datasets. Inspired by the work of Westover [Wes90], they integrate vector field representation in volume rendering using tiny vector particles or scratch marks in the splatting texture. The authors demonstrate their algorithm to a several datasets, including: climate data, tornado simulation, and airflow through an aerogel substrate.

Urness *et al.* [UIL\*06] introduce novel techniques for visualizing two co-located 2D vector fields. Based on combining and overlaying two flow representations (e.g., glyph, line integral convolution, or streamlines), the authors describe two techniques for enhancing the visual clarity of each vector field. The first approach uses different luminance intensities to allow certain fields to visually stand-out. The second approach utilises an embossing effect to visually separate the fields. The authors demonstrate their work on three data sets: particle image velocimetry (PIV), magnetohydrodynamic light supersonic jets and fluid dynamics.

In the context of weather simulation, Martin *et al.* [MSM\*08] present a study to validate the effectiveness of traditional 2D hurricane visualizations by observing the users ability to mentally integrate the magnitude and direction of flow in a vector field. In particular, the authors focus on evaluating 2D glyphs (or wind barb) - a technique commonly used for depicting wind magnitude and direction in weather visualizations. For both magnitude and direction, users had to estimate the value at a given point and estimate the average value over a rectangular region. The authors use a real hurricane simulation data set in their study.

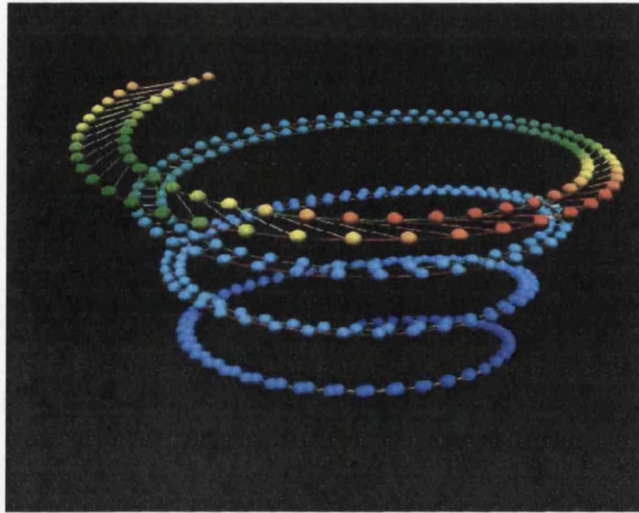
The visualization of time-dependent, unsteady flow is still highly regarded as one of the most difficult challenges today due to the dynamic nature of the data [MLP\*10]. The



**Figure 2.10:** The visualization of vector field clustering of flow around an engine. A combination of  $|v|$ -range and  $\theta$ -range glyph is used for depicting the range of vector magnitude and direction in each vector cluster [PGL\*12].

work by Hlawatsch *et al.* [HLNW11] address this problem using *flow-radar* glyphs to visualize unsteady flow with static images. The flow-radar is constructed by transforming time-dependant vector attributes into polar co-ordinates, whereby vector direction is mapped to angle, and the time to radius. In addition, the velocity magnitude is encoded using colour. The radar glyphs provides a visual summary of the flow over multiple time steps. A method for visualizing flow uncertainty is described using a single arc that represents the angular variation at given seed point. The authors demonstrate their work on two CFD simulation data sets.

Peng *et al.* [PGL\*12] describe an automatic vector field clustering algorithm and techniques that incorporate statistical-based multi-field glyphs for cluster visualization. The algorithm incorporates several properties such as the mesh resolution, velocity magnitude, velocity direction, and the euclidean distance to cluster regions of similar flow in image space. Glyphs are then sampled at the centre of each cluster. A collection of clustering glyph-based visualizations are introduced, such as  $|v|$ -range glyph or “disc” (see Figure 2.10 for example) that depicts the local minimum and maximum vector. The inner and outer radius of the disc is mapped to the vector magnitudes. The  $\theta$ -range glyph combines a vector glyph that illustrates the average velocity direction and magnitude, and a semi-transparent cone that shows the variance of vector field direction. Other visualizations include streamlets that are traced from the cluster centre, and colour coding with mean velocity. The authors demonstrate their clustering results on a series of synthetic and real-world CFD meshes.



*Figure 2.11: Shearing barbell glyphs to depict the uncertainty of different integrators and step-sizes between a pair of streamlines [LPSW96].*

#### **2.4.2.2 Uncertainty Visualization**

A number of approaches have been used to quantify and visualize uncertainty simultaneously with the underlying data. Glyphs is especially well suited for this particular task as detailed by the work of Wittenbrink *et al.* [WPL96]. Where traditional vector visualization methods such as wind barbs [MSM\*08] and arrow glyphs [LWSH04] simply ignore uncertainty information, the authors develop glyphs that depict several uncertainty metrics derived from simulation of winds and ocean currents (e.g., direction, magnitude, as well as mean direction and length) using a variety of commonly mapped glyph attributes (e.g., length, area, colour and/or angles). This method shows the uncertainty in the exact manner which the decision-maker wants to see it, combined with the data. Other methods described by Pang *et al.* [PWL96] and Wittenbrink *et al.* [WPL95] are to add geometry or to animate the geometry. In order to emphasise areas of high uncertainty, they use glyphs that are scaled to magnitude. However, this will result in unnecessary attention to areas with low certainty.

One similar approach introduced by MacEachren [Mac92] is to encode uncertainty into the glyphs by blurring them. In visualization the areas with high certainty will have glyphs that are clear, while areas with high uncertainty will have glyphs that are more unclear. This technique involves the use of predefined glyphs of two clarity levels and is unable to display a variable degree of uncertainty.

Lodha *et al.* [LPSW96] present a system (UFLOW) for visualizing uncertainties in fluid flow resulting from different integrators and step-sizes for computing streamlines. A pair of streamlines are interactively seeded by the user using different integration or step-size. Their differences are then visualized using several approaches that encode the



uncertainty through their shape, size and colour. Examples approaches include uncertainty ribbons and rakes, in addition to uncertainty glyphs such as line segment glyphs, shearing barbell glyphs, and twirling batons (see Figure 2.11 for example).

Further approaches for uncertainty visualization utilise 2D layering techniques, for example, Cedilnik and Rheingans [CR00] introduce procedural annotations which are deformed to show uncertainty information. The aim is to present the data and uncertainty with minimal visual distraction. Since meshes and grids are already present within a vector field representation, they exploit this area to prevent unwanted distraction from the data. A procedural grid-like texture is blended with the image and deformed accordingly to indicate regions of uncertainty. In addition, they also apply their technique as a way to deform glyphs to show their uncertainty values.

Ribicic *et al.* [RWG\*12] describe an interactive sketch-based visualization system for investigating simulation models, and to assess the uncertainty associated with changing different model parameters. The authors demonstrate their approach on flood management simulation as a means of risk assessment. Such an approach provides an intuitive mechanism for transforming sketches into boundary conditions of a simulation and to deliver visual feedback to end-users. A set of glyphs and icons are used to depict various simulation attributes. These include vector glyphs for illustrating the force field on a water flow and ensemble handle glyphs for representing uncertainty values.

The idea of uncertainty is also widely used in the field of Geographic Information Systems (GIS), and provides relevant work to the design of uncertainty glyphs. Such an example is presented by MacEachren *et al.* [MRO\*12], who evaluate the performance of visualizing three types of uncertainty (e.g., accuracy, precision, and trustworthiness) using point symbols. More specifically, they investigate how different visual channels and iconicity of point symbols affect *intuitiveness* for representing different categories of uncertainty, and the *effectiveness* for a typical map use task: assessing and comparing the aggregate uncertainty in two map regions. The results show that some visual channels (for example, fuzziness and location) are more effective at encoding different uncertainties than others (for example, orientation and saturation).

### 2.4.3 Glyph-based Techniques for Tensor Data

Tensor attributes are high-dimensional generalisations of scalars, vectors and matrices [Tel07]. Just as a scalar is described by a single number, and a vector is described by an array of one dimension, any tensor with respect to a basis is described by a multi-dimensional array. Tensor fields are commonly found in applications such as medicine and material science. In this subsection, we mainly discuss examples of glyph-based work in these two areas.

### 2.4.3.1 Medical Visualization

In medical visualization, glyphs are often used to portray the characteristics of diffusion tensor magnetic imaging (DT-MRI or DTI) [HJ05]. The work of Laidlaw *et al.* [LAK\*98] presents two novel methods for such an approach. The first method uses normalised ellipsoids, where the principal axes and radii are mapped to the tensor eigen vectors and eigen values respectively. Glyph normalisation reduces the visual clutter and enables full depiction of the data set. The second method incorporates concepts from oil painting to represent seven tensor data attributes as multiple layers of varying brush strokes which is composited into a single visualization. The authors demonstrate their technique on DTIs of healthy and diseased mouse spinal cords.

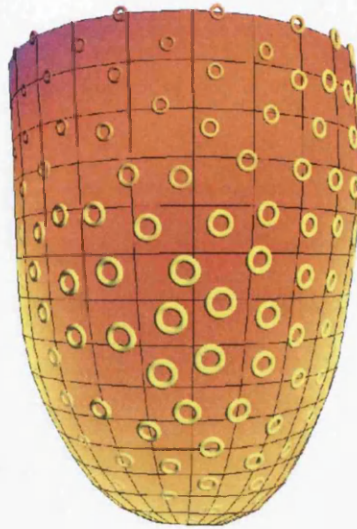
Tuch *et al.* [TWBW99] discuss the use of higher angular resolution sampling to help reveal diffusion phenomena that are not present in standard tensor imaging. These include anisotropic and non-Gaussian diffusion regions in human brain white matter containing heterogeneous fibre orientations. The authors make use of orbital glyphs to depict the diffusion value defined by a function of angle and minimum diffusion value for each voxel.

Westin *et al.* [WMM\*02] introduce a novel analytical solution to the Stejskal-Tanner diffusion equation system to produce a set of parameters that describe the shape of a tensor. This approach effectively reduces the number of tensor attributes that need to be encoded for DTI visualization compared to previous solutions using eigenvalue and eigenvector decomposition. The analytical solution derives three shape metrics:  $c_l$ ,  $c_p$ , and  $c_s$  to indicate the linear, planar and spherical properties of a tensor. Each shape metric is then mapped to a composite tensor glyph built from a sphere, disc and rod. In addition, the composite tensor glyphs is colour-coded according to shape such that blue is mapped to linear case, yellow to planarity and red for spherical case. The aim of this approach is to reduce the ambiguity caused by traditional ellipsoid representations.

Building upon previous research by Barr [Bar81] and Westin *et al.* [WMM\*02], Kindlmann [Kin04] describe a novel approach of visualizing tensor fields using superquadric glyphs. The motivation of superquadric tensor glyphs addresses the problem of asymmetry and ambiguity prone in previous techniques (e.g. cuboids and ellipsoids). An explicit and implicit parameterisation of superquadric primitives is presented, along with geometric anisotropy metrics  $c_l, c_p, c_s$  [WMM\*02] and user-controlled edge sharpness parameter  $\gamma$ , to create a barycentric triangular domain of shapes that change in shape, flatness and orientation under different parameter values. A subset of the family of superquadrics is chosen and applied towards visualizing a DT-MRI tensor field which is then compared against an equivalent ellipsoid visualization.

Kindlmann extends this work further using glyph-packing [KW06]: a novel glyph placement strategy. The goal of this work is to improve upon the discrete nature of glyph-based visualization using regular grid sampling, to a more continuous character such as texture-based methods by *packing* the glyphs into the field. A tensor-based potential energy is defined to derive the placement of a system of particles whose final

**Figure 2.12:** Glyph-based visualization for the diagnosis of coronary artery disease using a supertorus glyph [MSSD\*08]. Data attributes are encoded into its colour, opacity, size, and roundness.



positions is used to place the glyphs. However, this placement strategy can be computationally expensive. The work by Hlawitschka *et al.* [HSH07] presents an alternative glyph packing method using Delaunay triangulation which successfully reduces the computation cost.

Oeltze *et al.* [OHG\*08] incorporate 3D glyphs for visualizing perfusion parameters in conjunction with their ventricular anatomical context. They propose two glyph designs: (a) 3D Bull's Eye Plot (BEP) Segment and (b) 3D Time-Intensity Curve (TIC) Miniatures for depicting four perfusion parameters: *Peak Enhancement (PE)*, *Time To Peak (TTP)*, *Integral* and *Up-slope* which describe the myocardial contractility and viability. The 3D BEP segments are ring-shaped glyphs which extend the previous work [CWD\*02] from 2D to 3D space. An improved glyph (TIC miniatures) enables intuitive mapping of all important parameters in cardiac diagnosis as a result of encoding TIC semantic metaphors (glyph shape) that is familiar to domain experts. They apply their technique on three datasets from a clinical study.

The work by Meyer-Spradow *et al.* [MSSD\*08] present an interactive 3D glyph-based approach for the visualization of SPECT-based myocardial perfusion data. They utilise a supertorus prototype glyph which characterises SPECT data based on its colour, opacity, size and roundness. In addition, the visualization combines the glyphs with a colour-map of the myocardium in order to depict the state of the underlying tissue. A novel placement strategy is used to position the glyphs along the 3D surface (i.e., the myocardium) according to random distributions with relaxation. One motivation of such a placement strategy is to provide a more even-distribution of glyphs. This addresses the problem of unbalanced placement that can occur from regular grid sampling in complex and non-uniform meshes.

Peeters *et al.* [PPvA\*09] present a novel technique for fast, detailed and accurate rendering of high angular resolution diffusion imaging (HARDI) data. HARDI glyphs

are built by deforming a large number of points along a spherical surface according to the orientation distribution function (ODF). Previous work on geometry-based HARDI glyphs often compromise the detail (reduce the number of polygons) in order to achieve feasible interaction. The authors make use of GPU-accelerated glyph rendering to preserve glyph detail, whilst maintaining an interactive performance for HARDI data exploration.

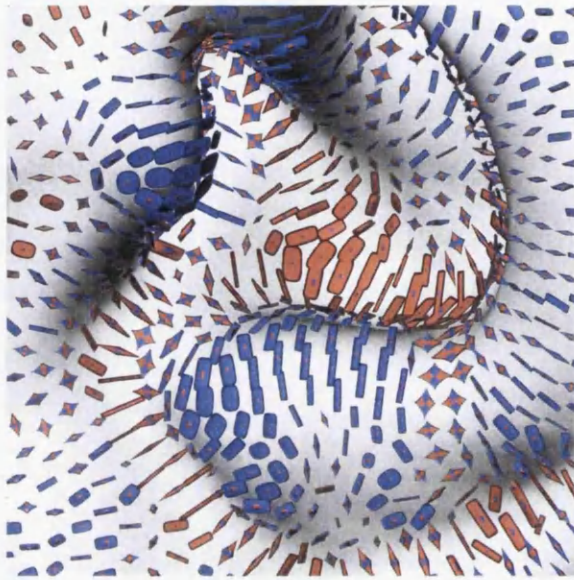
### **2.4.3.2 Material Science**

Many physical quantities of interest are described by tensor fields. Examples of such phenomena include deformation, stress, and electric field, and is commonly visualized using tensor glyphs. The work by Kriz *et al.* [KYHR05] provide a review of such techniques on second-order tensors which include: Lamé's stress ellipsoids, Haber glyphs [Hab90], Reynolds tensor glyph [HYW03], and hyper streamtubes [DH93]. Furthermore, the authors introduce a Principal, Normal and Shear (PNS) glyph for visualizing stress tensors and their gradients. The method extends the stress ellipsoids by mapping the shearing and stress component to the surface colour of the ellipsoid.

Schultz and Kindlmann [SK10] describe an approach to visualize general symmetric second order tensors that could be non-positive-definite by augmenting superquadric glyphs with concave shapes. The work extends previous methods (e.g., [Kin04], [WMM\*02]) which concentrate only on tensors with strictly positive eigenvalues such as diffusion tensors to the general case by mapping the glyph shape to show eigenvalue sign differences. The shape between two eigenvectors is convex if the corresponding eigenvalues have the same sign, and concave if they are different. They then use colour to indicate the tensor's quadratic form as shown in Figure 2.13.

Kelly *et al.* [JKLS10] evaluate the perceptual effectiveness of four existing tensor glyph-based techniques: box glyphs [SKH95], cylinder glyphs [AWB01], ellipsoids [FWZ01] and super-quadrics [JKM06] for encoding three tensor variables: the director (orientation), uniaxiality and biaxiality in nematic liquid crystal visualization. More precisely, the work focuses on how accurate a single glyph represents the tensor data characteristics. The experiment consist of showing several test glyph cases with various parameter values to users. Data recorded include four error metrics that correspond with each tensor parameter and total error along with the response time for users to select their answer from a multiple choice option. The results of the study show that super-quadric glyphs performed better over the other glyph-based techniques tested.

More recently, Chen *et al.* [CPL\*11] describe a visualization method to convey asymmetric eigenvalue and eigenvector topology within fluid flows and solid deformations. They describe a hybrid visualization technique in which hyperstreamlines and elliptical glyphs are applied to a real-world dataset. This enables a more faithful representation of flow behaviours inside complex domains. In addition, tensor magnitude, which is an important quantity in tensor field analysis is mapped to the density of hyperstreamlines and sizes of glyphs, allowing colour to be used to encode other tensor



**Figure 2.13:** Visualization of geometry tensors by augmenting superquadric glyphs with concave shapes to show eigenvalue sign differences and colouring to show their quadratic forms [SK10].

quantities. To facilitate quick visual exploration of the data from different viewpoints and at different resolutions, the authors propose an image-space approach in which hyperstreamlines and glyphs are generated quickly in the image plane. The combination of these techniques leads to an efficient tensor field visualization system for domain scientists. They demonstrate the effectiveness of their visualization technique through applications of complex simulated engine fluid flow and earthquake deformation data.

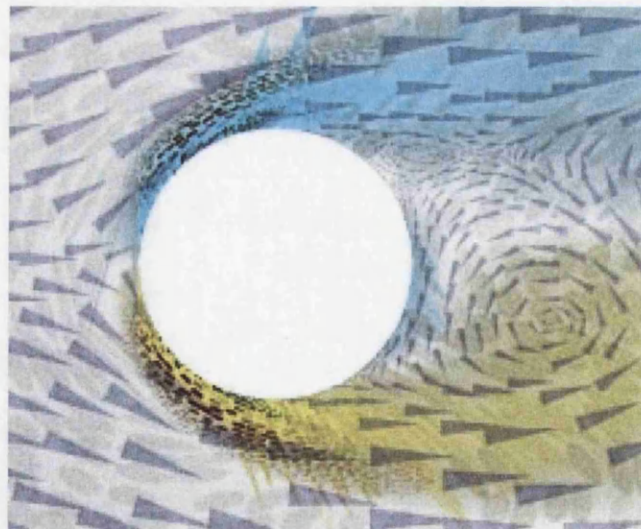
#### 2.4.4 Glyph-based Techniques for High-dimensional, Physical Simulation Data

The study of high-dimensional, physical simulation data is often of special interest due to its multiple facets. The inter-relationship of different types of field is particularly interesting for visualization researchers and domain experts [Tay02], especially when combined in the context of their spatial relationship. One of the most successful 2D multi-field visualization technique is developed by Kirby and Laidlaw [KML99] who stochastically arrange multiple visualization layers to minimise perceptual overlap (see Figure 2.14). This paper extends the work by Laidlaw *et. al* [LAK\*98] by applying visualization concepts from oil painting, art and design, to the problems in fluid mechanics. Given a permutation of layers, a user-specified importance value is attached to each visualization of increasing weights in order to provide greater emphasis to higher layers. Visual cues such as colour and opacity indicate regions and layers of importance (e.g.,

rate of strain tensor example emphasise the velocity more by using black arrows). This method enables the simultaneous depiction of 6-9 data attributes, in which the authors apply to a simulated 2D flow field past a cylinder at different reynolds number. The example shows the visualization of velocity, vorticity, rate of strain tensor, turbulent charge and turbulent current using a series of visualization techniques such as tensor ellipses, vector arrows and colour mapping.

Konyha *et al.* [KMH03] introduce an interactive 3D glyph-based visualization for rigid body simulation data and propose a set of glyphs for depicting vector and angular quantities. These include *coloured disks* which are colour-coded to force magnitude, *glyph arrows* for visualizing vector quantities, sector and *spiral* glyphs for mapping multiple angular properties. The authors demonstrate their technique for visualizing a chain and belt driven timing drives in engines.

Other types of simulation data involve modelling high-dimensional, physical entities such as particles, and complex molecules. These simulations typically result in very large datasets, and can be simply challenging due to the sheer number of glyphs that need to be rendered. With the increasing power of modern graphics hardware, many approaches have therefore exploited GPU-accelerated techniques in combination with glyphs in order to improve performance and rendering capacity. For example, the work by Reina and Ertl [RE05] introduce glyphs for visualizing molecular simulation data in thermodynamics. The dipole glyphs consist of several parts: two spherical components that represent the molecular radii, a cylindrical magnet that connects the spheres and a



**Figure 2.14:** Close up visualization of turbulent flow past a cylinder. Kirby and Laidlaw [KML99] composite multiple visualization layers using a variety of techniques such as glyph-based, colour-mapping, and texture-based encodings. The example shown here depicts two scalar fields, two vector fields, and a tensor field in the same image.

colour mapping index for visual identification. The authors parameterise each molecular type as a series of geometric variables which are sent to the GPU for efficient rendering.

Grottel *et al.* [GRE09] introduce a benchmarking tool for evaluating the performance of different CPU/GPU combinations to address the challenge of fast rendering for time-dependant point-based molecular visualization. A comprehensive review of different uploading strategies in OpenGL is given. In particular, the work looks at the use of compound glyphs which integrate colour-coded cylinders and spheres for representing molecular data, and optimising the process of transferring large number of data to the graphics card for rendering GPU glyphs.

## 2.5 Visual Analysis of Multi-dimensional data

The previous sections discuss examples of high-dimensional glyph-based techniques across a range of application domains. In these approaches, the goal is to use glyphs to directly encode each attribute of the data. However, in the visualization and analysis of big data such as social networking data and other multi-modal streams, the sheer volume of attributes and data points means it is often not feasible to use such a direct approach due to the amount of visual clutter when visualizing a large number of glyphs. This problem significantly limits the effectiveness of glyph-based visualization and our ability to interrogate complex datasets. Hence, the analysis of high-dimensional data requires more sophisticated methods [DEK\*12].

An important research field that addresses this topic is visual analytics. The goal of visual analytics is to facilitate analytical reasoning through interactive visual interfaces [DEK\*12]. Analytic reasoning techniques such as machine learning, dimension reduction, and predictive analytics [Fod02] help overcome the problem of high-dimensionality by reducing the number of dimensions that need to be analysed [DEK\*12]. There are two general approaches to the reduction of variables. The first approach involves combining two or more similar dimensions together using, for example, principal components analysis or multi-dimensional scaling [Fod02]. The other approach uses mathematical models to extract and derive new statistical features from the data which captures the underlying relationship. Such features usually consists of a smaller number of variables, allowing for more effective and expressive visualizations to be produced. Since automated analysis only work reliably with well-defined problems, the idea is to support such approaches using interactive visualization. Visualization can then, for example, support the user in adjusting parameters at different stages of a data mining algorithm [HNH\*12], as well as presenting these results [TC05].

One common characteristic of visual analytic applications is their use of multiple linked views that make use of both information and scientific visualization techniques to support the visual analysis of large datasets. Coordinated views are useful because they combine the strengths of various techniques that may be better suited for different parts of the analysis process. Concepts and techniques of glyph-based visualiza-

tion is particularly well-suited for such a task as shown in a variety of domains which include: sports analytics [PSBS12, PVF13], text collections [DYW\*13], and climate research [KMDH11]. For example, Kehrer *et al.* [KMDH11] adopt glyphs to visualize heterogeneous datasets in climate research to help analysts work with different constituents simultaneously from multiple simulations. They propose glyphs to depict the median temperature, interquartile range and distance metrics using colour, size and the upper/lower shape of the glyph respectively. Other approaches may use glyph-based methods to aggregate between levels of data. The work by Mistelbauer *et al.* [MKB\*12] for instance, introduces Smart Super Views for the analysis of different datasets in medical visualization. The system maps the relevance of different views to a super-elliptical shape, allowing scientists to analyse multiple regions of interest of different modalities simultaneously. Glyphs have also been used as part of a focus+context view for emphasising interesting features in the domain as shown by Straka *et al.* [SCC\*04]. The vast amount of literature in visual analytics has resulted in several major surveys such as in [KAF\*08, MSS12, DEK\*12], and is fast becoming a research area for the utility of novel glyph-based visualization.

## 2.6 Discussion

In order to understand the foundations of glyph-based design and to classify different glyph-based approaches, we made a connection between the perceptual studies of visual channels and glyphs with a focus on high-dimensional representation. We also examined several methods for glyph placement and supporting glyph-based interactions. Noticeably, we found that several factors may influence the design of glyphs, for example, data dimensionality (both spatial and temporal), as well as the number of attributes and their data types.

While this survey has confirmed that glyph-based visualization is an important technique in the field of visualization, we have also observed some doubts in the community about the encoding capability of glyphs primarily due to their size, limited capacity of individual visual channels and cognitive demand for learning and memorisation. Although such reservations are very reasonable and cannot be overlooked in any practical applications, they do not undermine the relative merits of glyph-based visualization, which have already been demonstrated in everyday life as well as many applications. These merits include:

- rapid semantic interpretation (e.g., visual metaphors for sound [JBMC10]),
- more scalability in dimensions for multi-field and multivariate data visualization (e.g., [Kin04, SK10]),
- suitable for both dense and sparse layout (e.g., [KW06, LKH09, LWSH04]),
- adaptable for interactive visual analysis (e.g., [SCC\*04, MKB\*12]).



The overall goal of the visualization and the size of the data are also factors which need to be considered. For instance, is the visualization intended to show specific regions in more detail? Does the visualization need to convey semantic information rapidly? Or does the visualization need to facilitate the rendering of many glyphs interactively? We find that these questions or *design requirements* are usually tailored to a specific task [LKH09] or domain [RP08, MPRSDC12], and that some may be more generalisable than others. These design requirements were beyond the scope of this survey. However, it is important to note that such design requirements should ideally be combined along with other perceptual concepts (e.g., visual semiotics) in order to achieve a more comprehensive design space of high-dimensional glyph-based visualization. One problem here is that establishing a common framework which is both meaningful for information theory and visualization technology is non-trivial.

## 2.7 Summary

In this chapter, we have presented a comprehensive survey of high-dimensional glyph-based visualizations, showcasing a variety of glyph designs, placement strategies, and rendering methods that each have their own merits and shortcomings depending on the application domain. The very wide application of glyphs across the literature is testimony to their importance and utility, and that glyphs and icons can bring cost-effective benefits for high-dimensional visualization.

During the composition of this survey, it has helped identify some major gaps in the current research of glyph-based visualization which inspired the work within this thesis. In particular, we noticed the utility of high-dimensional glyphs has received more research in some application domains than others in both scientific and information visualization (see Table 2.1). For multi-field glyphs, there has been a substantial development in areas such as tensor and flow visualization. However, one major problem as highlighted by Taylor [Tay02] is that these approaches are directly applicable only to glyph representations with a small number of fields (typically three or fewer), for example, one or two vector fields [UIL\*06]. With the introduction of more complex simulations and the demand of engineers to analyse a greater number of fields (e.g., uncertainty and sensitivity fields [WPL96]) simultaneously, we find that existing techniques do not scale particularly well for such a task. This problem motivated the work in Chapter 3 to investigate glyph-based techniques for visualizing multiple error-sensitivity fields.

In contrast to glyph-based multi-field visualization, research in multivariate visualization has mostly under investigated the use of high-dimensional glyphs, and focused more on other approaches, for example, parallel co-ordinates [Ins85, GPL\*11]. As mentioned in Section 2.3.1 and Section 2.3.2, previous studies primarily address the challenge of visualizing time-dependent data within a spatial context using glyphs such as in [TSWS05]. One common solution is to map the temporal dimension to the

z-axis (in 3D space) resulting in 3D glyphs. A drawback with such glyphs is that several attributes become occluded from view, and therefore limits the number of different dimensions displayable on the glyph. Other glyph-based approaches focus on encoding high-dimensional data (see Section 2.3.3). The major problem with such glyphs (e.g., [Che73, FCI05]) is that these encodings are often difficult to interpret (since they do not easily relate to the data), which makes identifying individual attributes on the glyph non-intuitive. In Chapter 4 and Chapter 5, we introduce glyphs that encode multiple dimensions with the fundamental difference that each attribute can be more readily perceived. We find our visual mapping can enhance the usability of glyph-based visualization and improve the performance of specific tasks, for example, information retrieval.

This chapter also provides an overview of important work in the field of visual analytics which influenced the research described in Chapter 6. We discussed in Section 2.5 some limitations of glyph-based visualization with high-dimensional data, and how multiple linked views, interaction, and analytical reasoning can be used to overcome such problems. In particular, we make use of these concepts to address the challenge of sorting multivariate events.



**Part II**

**Research Development**



---

## Designing High dimensional Glyphs for Visualizing Multiple Error-Sensitivity Fields

---

### Contents

|       |  |    |
|-------|--|----|
| 3.1   | Introduction . . . . .                                 | 51 |
| 3.2   | System Overview . . . . .                              | 54 |
| 3.3   | Camera Sensitivity and Error Derivation . . . . .      | 55 |
| 3.3.1 | Snooker Reconstruction . . . . .                       | 57 |
| 3.3.2 | Homography Sensitivity Analysis . . . . .              | 58 |
| 3.4   | Error Sensitivity Visualization . . . . .              | 59 |
| 3.4.1 | General Design Principles . . . . .                    | 60 |
| 3.4.2 | Visual Mapping of Multiple Error Sensitivity . . . . . | 61 |
| 3.4.3 | Sample points in 3D visualization . . . . .            | 63 |
| 3.4.4 | Spherical Mapping . . . . .                            | 63 |
| 3.5   | User Consultation - 2D . . . . .                       | 65 |
| 3.6   | User Consultation - 3D . . . . .                       | 70 |
| 3.7   | Discussion . . . . .                                   | 73 |
| 3.8   | Summary . . . . .                                      | 74 |

---

**I**N the previous chapter, we surveyed a collection of important glyph-based literature that addresses the challenge of high-dimensional data. A long standing problem in the field of visualization that we identified through this research, is the ability to display multiple overlaid datasets. Multiple fields (e.g., scalar, vector and tensor fields) are usually obtained from different sampling sources or computational processes. The report



**Figure 3.1:** Constraint maps of a sample snooker room wall (Left) and a construction scene (Center) with dynamic constraints (Right). The green region highlights valid camera mounting positions with invalid positions mapped to red. The construction scene images correspond to the right wall of the camera surveillance scene in Figure 3.7. The focus region must be fully in view of the camera for a position to be considered as valid.

by Taylor [Tay02] showed that existing multi-field techniques (e.g., [WEL\*00, Bok03]) are visually intuitive only up to few number of fields. Since glyph-based visualization is an effective approach for encoding multiple attributes, this motivated us to explore the use of glyphs in this particular domain.

One major topic in multi-field research is the visualization of uncertainty information and parameter sensitivity [WPL96]. Many practical applications, ranging from physical simulation [KML99] to computer vision algorithms [ZK98] rely on analysing such fields simultaneously in order to gain insight on the data. This chapter addresses the needs for visualizing error sensitivity associated in 3D scene reconstruction, which is a common modelling method in computer graphics (e.g., [RHHL02]). Error-sensitivity analysis is one approach for selecting an optimal camera position within a given scene. There are two main types of camera positioning problems. On one hand, we have the selection of virtual cameras for conveying the most information to the user, for example, for scene understanding [VFSH01], volume visualization [BS05] and image-based modelling [KBGK07, FSG09]. On the other, there is the task of positioning a real camera for optimising vision-based applications [CK88]. This work focuses on the latter. In 3D reconstruction, errors in estimating camera extrinsic parameters are the most fundamental errors, which may be caused by a variety of reasons, including errors in image processing (e.g., edge detection), feature analysis (e.g., corner recognition) and geometric correlation. This leads to multiple error sensitivity fields which need to be visualized together.

Statistical analyses on one or more error sensitivity fields is often used to analyse complex parameter spaces, for example, by computing an average error field, or identifying the camera with least error sensitivity based on magnitude. However, it is difficult for such statistics to convey detailed information such as error distribution and orientation in different fields and in different parts of a field. In many real-world applications, error analysis must also be combined with other observations and practical constraints. For example, in 3D reconstruction, the best camera position is not always determined

by the lowest error sensitivity. Additional knowledge such as feasibility of the camera position (i.e., windows, picture frames, scaffolding), mounting equipment cost, and impact on the environment (e.g., spectators, pedestrian and players) will heavily influence a user's decision as shown in Figure 3.1. Such factors are fundamental to the planning process especially when constraints are dynamic, and when a system needs to meet the specific demands of a practical framework (e.g., portable camera systems versus a permanent setup). This is often desirable since many venues, coaching rooms, and outdoor environments are multi-purpose and require a flexible solution. Therefore, we need to investigate camera placement and their associated sensitivity in a three-dimensional search space.

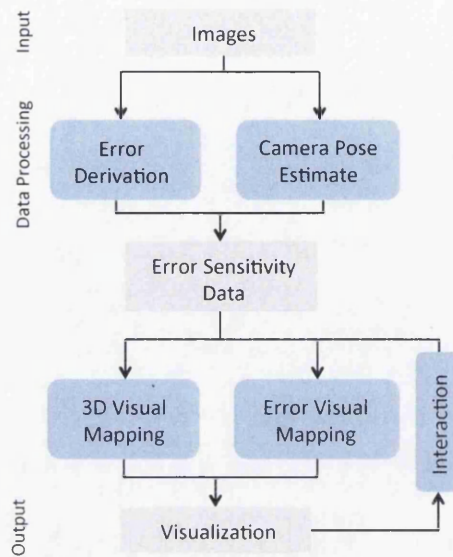
Given a set of camera positions and error sensitivity fields, a typical approach for finding an optimal solution would be to use Machine Learning [AT04, OLF09]. The process of machine learning involves modelling the problem (e.g., the requirements for camera placement) as formal parameters which are optimised. Due to the range of possible camera configurations in addition to the practical requirements of a user, encoding such semantic knowledge with attached weighting parameters into an algorithm is highly impractical due to costs in labor. This problem motivates us to explore a novel solution by introducing visualization as an effective planning tool for optimal placement of a camera. A visualization solution is desirable for informing the user of the error sensitivity in both a comparative and summative manner, while empowering the user to bring additional information and knowledge into the analysis.

We present a study using 2D and 3D visualization methods to assist in single camera positioning based on the error sensitivity of reconstruction. The goal of our visualization is to visually compare candidate camera positions through their associated error sensitivity, and to provide visual suggestions for estimating an optimal camera position. We find that visualization provides a faster, and cost-effective alternative over other viewpoint selection methods for real cameras and enables the user to make dynamic decisions that integrate trade-offs between reconstruction quality and feasibility. In particular, the main contributions of this chapter are:

- We develop a novel collection of glyph-based visualizations which depict multiple error sensitivity fields. These visual mappings can be used to evaluate prospective camera positions.
- We provide a visual summary of camera positions in a given 3D context visualization. This effectively aids the estimation of the best single camera position by enabling the user to incorporate physical, financial and other types of constraints into the decision process.
- We demonstrate the usefulness of our visualization method on two real-world applications with feedback from end-users. We note that for the application we present, financial constraints limit the user to positioning a single camera and prevent the user from incorporating sophisticated 3D scanning or sensor technology.



**Figure 3.2:** An overview of the combined visualization pipeline for depicting error sensitivity in single camera positioning. There are three main stages: Extracting the error sensitivity data from sample camera positions, generating the 2D error map and generating the 3D environment visualization.



The remainder of the chapter is organised as follows: Section 3.2 outlines the system pipeline of our visualization system. Section 3.3 briefly describes the reconstruction technique we follow, and detail our method for extracting error sensitivity from single camera. Section 3.4 gives the design process for visualizing multiple error sensitivity and the steps for generating both 2D and 3D error visualization. Section 3.5 and 3.6 gives an evaluation of our proposed visualization scheme and how this meets our requirements. Feedback from end-users and domain experts is used to evaluate our visual mappings of multiple error sensitivity and to discuss the usability of the system. Section 3.7 gives discussion on the proposed visualization and how this could be extended for future use. Finally, Section 3.8 provides a summary of this work.

## 3.2 System Overview

The system comprises of three key aspects: extracting the error sensitivity data, generating the 2D error map and generating the 3D environment visualization. An overview of the system is shown in Figure 3.2. The first stage involves taking a set of sample images from given camera positions around the scene as shown in Figure 3.3. We extract the associated error-sensitivity fields which is detailed in Section 3.3. Following this, we estimate the camera pose from each image which is necessary for mapping the camera position to the 3D environment.

The second stage maps the corresponding error sensitivity fields using visual designs we propose in Section 3.4. This aids the user in analysing the uncertainty at given positions and allows a visual comparison of multiple cameras. In the final stage, a 3D visualization is generated to summarise multiple error sensitivity associated with each



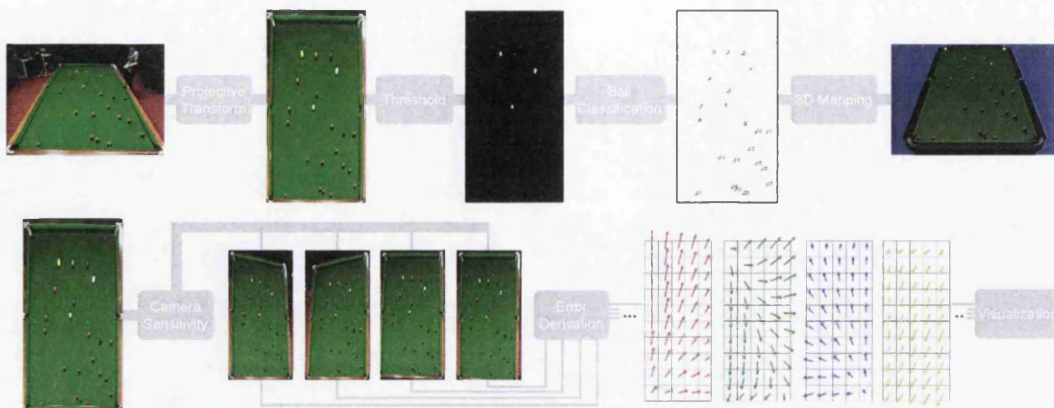
**Figure 3.3:** A 3D reconstruction of the camera environment in the snooker scene. A set of sampled camera positions are shown using grey spherical markers around the region of interest.

camera and to incorporate contextual information about the scene. Each visualization is displayed simultaneously or on a dual-screen, allowing the user to interact with the 3D visualization whilst analysing the error sensitivity in detail. Sample camera positions can be selected within the environment which update the error map visualization accordingly. In addition, users can filter cameras based on error-sensitivity to highlight potential camera suggestions.

### **3.3 Camera Sensitivity and Error Derivation**

Three-dimensional reconstruction and object tracking are highly sensitive to camera placement. Many systems (e.g., *Hawk-eye* [OHS03]) adopt multiple cameras to overcome problems such as object occlusion and sampling errors. The Hawk-eye ball tracking system is commercially used in sports such as Tennis, Snooker and Cricket to accurately reconstruct shots for television broadcasting. It is vital that the images captured from each camera contain sufficient information about the scene. There are many factors in camera sensitivity that will affect the image quality used for reconstruction:

- *Resolution* — the physical size of the image captured by the camera determines the amount of sampling error of the image data.
- *Viewing Angle* — the maximum angle in which a display can be viewed. This highly affects the availability and selection of camera poses (see below) that fully capture the entire scene.



**Figure 3.4:** (Top) Reconstruction pipeline for extracting ball positions in a snooker scene using a single camera. The 3D reconstruction is based on a 2D homography. (Bottom) Camera sensitivity analysis of the projective transform. Error sensitivity fields (or vector fields) are derived to quantify the impact of image distortion from inaccurate feature correspondence.

- *Camera Pose* — is a combination of position and orientation of the camera with respect to a static object in the scene.
- *Lighting Condition* — lighting variance can affect processing steps such as colour classification.
- *Camera Vibration* — the stability of the camera should be minimized to reduce errors in feature detection.

In our case study, we focus on using 3D reconstruction as part of a coaching tool [LPC\*11], where only an approximate estimation of the balls is required. Whilst there are key advantages to a multi-camera system, it also presents several practical drawbacks. For instance, such a system needs to be manually calibrated before use. This step can often be overwhelming and time consuming to a novice user such as snooker coaches and players. More significantly, snooker clubs and academies have yet to benefit from such technology due to the cost of installation (e.g., around £200,000 for Hawk-eye). To facilitate our target users, we propose error analysis on a more flexible system using a single camera [LPC\*11]. One desirable ability is to review a sequence of training shots [PLC\*11] to support performance analysis. In order to perform ball tracking, we use a high-speed ethernet camera capturing at 200 frames per second. Since the camera has a fixed resolution, viewing angle, and focal length, our focus is to assess the quality of an image at various camera positions that give the most reliable reconstruction.



**Figure 3.5:** Example camera positions around the (First row) snooker table scene and (Third row) security scene. Below each image is the associated inverse transformation of the camera position to obtain a projected top-down view. It can be seen that the quality of the inverse transformation is greatly influenced by the camera position.

### 3.3.1 Snooker Reconstruction

The goal of snooker reconstruction is to estimate the spatial positions of the snooker balls. As the balls lie along a planar surface, this simplifies the problem to extracting the 2D position  $(x, y)$  of the ball object, which can then be mapped onto its 3D model. Guo and Namee [GN07] were the first to introduce ball reconstruction based on a single, top-down view of the table. We follow the method presented by Legg *et al.* [LPC\*11], which extends the previous technique [GN07] to an arbitrary camera position. Figure 3.4 (top) outlines this process. The first step involves transforming the image into a top-down view using 2D homography. The next step involves applying a threshold filter to extract the specular highlight on the ball, and approximate the location of each ball. We then identify a full or partial set of balls (e.g., for training shots) using connected component analysis and colour classification in the resulting image. In the final step, the extracted balls are mapped to their corresponding position in the 3D model.

Fundamentally, the reconstruction accuracy of the balls is determined by the camera position that gives the least amount of projective error. In an ideal scenario, a camera would be placed directly top-down above the table. However, in snooker and many other

sporting facilities (e.g., table tennis and pool), constraints such as lighting fixtures, the cost of mounting the camera and the practicalities of the camera position (see Figure 3.1 for an example) means this is not possible. Therefore, we need to find alternative solutions. We determine the quality of an image by evaluating the error sensitivity of the 2D homography associated with each camera pose.

### 3.3.2 Homography Sensitivity Analysis

Homography in vision-based applications [HZ04] is used to describe the projective mapping of a set of coplanar feature points  $\mathbf{a}_i \in \mathbb{R}^2$  in the observed scene onto another set of coplanar points  $\mathbf{b}_i \in \mathbb{R}^3$  in the model. Algebraically, corresponding tuples of points are related to each other by  $\mathbf{b}_i = \mathbf{H}\mathbf{a}_i$  where the 2D homography  $\mathbf{H}$  is a 3x3 matrix. Errors in the transformation are typically introduced in the detection of feature points  $\mathbf{a}_i$ , as well as in the correspondence procedure. The impact of noise in the image, visual artifacts and even camera vibration can lead to false detection. In addition, we find that the stability of homography parameters is greatly affected depending on the camera pose (see Figure 3.5 for examples). Therefore, to investigate the quality of different camera positions, we assess the sensitivity of feature points for homography estimation. This is illustrated graphically in Figure 3.4 (bottom).

Suppose for an image  $I$ , we have a set of known ground truth positions of feature points  $\mathbf{a}_i$  that are mapped onto a set of coplanar points  $\mathbf{b}_i$  in the model for  $i = 1, \dots, N$ . The solution to  $\mathbf{H}$  will give an accurate projective mapping from one plane to the other. Now let  $\delta\mathbf{a}_i \in \mathbb{R}^2$  be a noisy feature point imposed by some fixed deviation within a sensitivity region  $\text{dist}(\mathbf{a}_i, \delta\mathbf{a}_i) \leq r$ , for  $r \in \mathbb{R}$ . Analytically, errors under the new homography mapping  $\mathbf{H}'$  can be shown using the displacement vector  $\underline{\delta\mathbf{b}} = \mathbf{H}\mathbf{a} - \mathbf{H}'\mathbf{a}$ , where  $\underline{\delta\mathbf{b}} = \{\delta\mathbf{b}_i\}$  represents the projective error when a set of points  $\mathbf{a} = \{\mathbf{a}_i\}$  is mapped onto the new plane. In image space, we describe the error in 2D homography as a set of 2D vector fields  $\mathbf{D}^{(i)} : \mathbb{R}^2 \mapsto \mathbb{R}^2$ :

$$\mathbf{D}^{(i)}(x, y) = \mathbf{H}(x, y) - \mathbf{H}^{(i)}(x, y) \quad (3.1)$$

where  $\mathbf{H}^{(i)}$  denotes the set of erroneous homographies corresponding to the sensitivity of each feature point  $\delta\mathbf{a}_1, \dots, \delta\mathbf{a}_N$ . Any inaccuracies in feature point correspondence will greatly affect the visual quality of the projective transformation. The 2D vector fields are used to effectively depict the amount of distortion as shown in Figure 3.4 (bottom). Typically, one may combine multiple error sensitivity fields to illustrate the uncertainty associated with one or several feature points. Hence, we can generalise planar error sensitivity using  $m$  2D error fields, where  $m \geq N$ . The resultant error field  $\gamma : \mathbb{R}^2 \mapsto \mathbb{R}^2$  caused by each field is one example used to provide a statistical overview. This can be computed explicitly by Eq 3.1, or implicitly using the summation:

$$\gamma(x, y) = \sum_1^N \mathbf{D}^{(i)}(x, y) \quad (3.2)$$

Due to the non-uniform distribution of errors, we find that the compositional effects of multiple error fields can lead to the negation of uncertainty. We refer to this as *vector cancellation*. This can be shown using the subadditivity property inherent in our function. Let  $\mathbf{d}_i = (\mathbf{d}_{x,i}, \mathbf{d}_{y,i})^T \in \mathbf{D}^{(i)}$  be the displacement vectors for each field and  $\lambda = (\lambda_{x,i}, \lambda_{y,i})^T \in \gamma$  denote the resultant vector at a fixed point, it holds that:

$$\|\lambda\| = \|\mathbf{d}_1 + \dots + \mathbf{d}_N\| \leq \|\mathbf{d}_1\| + \dots + \|\mathbf{d}_N\| \quad (3.3)$$

Hence, the worst case of cancellation occurs when  $\|\lambda\| = 0$  whilst  $\exists \mathbf{d}_i \in \mathbf{D}^{(i)}$  such that  $\|\mathbf{d}_i\| > 0$  for  $i = 1, 2, \dots, N$ . It is possible to take this error into account using absolute vectors or sum of vector magnitudes. However, as a result we lose other information (e.g., direction) that is critical in the analysis of planar error sensitivity. This includes identifying sensitive parameters and using the distribution of errors to guide optimisation algorithms. Hence, we find it becomes advantageous to visualize multiple error fields.

In our applications, we rely on detecting four feature points. For snooker, these points are defined by the table boundaries, where the focus is to obtain absolute ball positions for 3D scene reconstruction. In video surveillance, we use the corners of a marked rectangular region in which the position of pedestrians is of importance for vision-based applications. We develop visual methods for depicting the four error sensitivity fields as a means for assessing camera sensitivity. Adjusting the sensitivity region  $r > 0$  influences the error distribution, and therefore the size of glyphs in the resulting visualization. We set this parameter to  $r = 20$  in order to produce glyphs that are perceivable.

### 3.4 Error Sensitivity Visualization

We propose an interactive visualization system for planning the optimal positioning of a single camera based on error sensitivity and various physical and semantic constraints by allowing the user to incorporate their knowledge into the decision process. The visualization consists of two components: 1) a 2D visual map for depicting the compositional effects of multiple error sensitivity fields for each camera, and 2) a 3D visualization scene to illustrate the environment in which the camera configuration is to be arranged, adding context to the user. The 3D visualization allows the user to investigate the feasibility of camera positions based on environmental constraints and gives an overview of the error sensitivity associated with each camera. We support user exploration through an interactively linked 2D error mapping, and provide user options for filtering and displaying specific camera samples (e.g., with lowest error sensitivity) in a focus+context manner. In this Section, we outline some design considerations largely based on [Tuf83] (see Section 2.2.1) in order to deliver effective visualization. We then detail our design process for the visualization of multiple error sensitivity fields extracted from camera

sensitivity analysis (see Section 3.3), and describe a method for estimating the camera pose for mapping sample camera points to a 3D environment. Finally, we present our method for integrating error sensitivity into the 3D environment using a spherical visualization.

### 3.4.1 General Design Principles

We shall concentrate primarily on multi-field data visualization, however these design principles are applicable to other areas of visualization also. To ensure suitability of the sensitivity visualization, we outline the essential requirements that the visualization must conform to:

- **R1. Detail** — the visualization needs to clearly depict multiple error fields, each of which is a 2D vector field obtained from a single camera or from multiple cameras.
- **R2. Overview** — the visualization needs to show a summary overview that illustrates the combination of error sensitivity fields in a given contextual geometry.
- **R3. Cancellation** — the visualization needs to represent uncertainty cancellation that may be present as a result of error field composition.

In addition to this, we want to ensure that the visualizations proposed are simple and intuitive in their formation. We consider a number of design principles that aim to enhance the quality of the visualization for conveying useful information to the user.

**3.4.1.0.1 Visual Simplicity** The focus of the visualization should be to convey the contents of data and to allow for user exploration, as opposed to the visualization technique itself. For higher-dimensional scenarios this can often be conceptually difficult and hence a more complex representation is required. We present a range of visual designs with varying degrees of complexity ranging from simple colour-maps to multi-attribute glyphs. Additionally, we combine and make use of existing techniques (e.g., heat maps, vector glyphs and streamlines) that are familiar in the domain to support learnability of our visualization.

**3.4.1.0.2 Visual Comparison** In order to promote effective decision making, it is essential that visualizations can be perceptually evaluated and that comparisons can be made between two representations. By making visualization more comparative, a user should be able to visually rank two given data sets based on their visual representations. We have designed visualizations that allow the observer to compare camera positions and their associated error (e.g., Figure 3.9).

**3.4.1.0.3 Relationships Between Data Attributes** One of the main advantages of visualization is that it provides greater insight into the underlying phenomena. In the case of multivariate data, we are particularly interested in how different attributes affect one another and these relationships should be conveyed to the viewer. Our multi-attribute glyphs enable the user to examine the relationships between multiple error-fields. For example, our Bézier glyph integrates multiple vector attributes into a single shape that allows the user to perceive the distribution of error more easily.

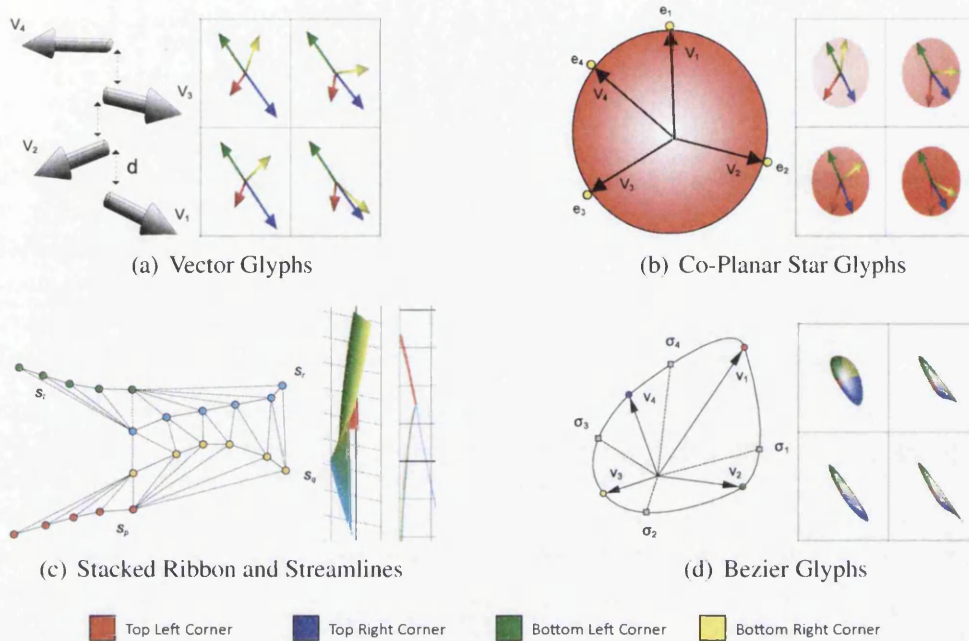
**3.4.1.0.4 Integrity** Misleading visualizations are common [GR94]. Principles tuned towards statistical graphics can provide suggestions that help limit unintentional visualization lies. For instance, clear labelling should be used to help users overcome graphical ambiguity (e.g., Figure 3.8).

The aim of multi-field visualization is the depiction of multiple fields that are co-located in the same domain for revealing complex interactions that occur between fields. Simulation data is one example where several fields (e.g., pressure and temperature) and associated uncertainties are studied together to make accurate predictions. Thus, the challenge is to make a coherent visualization that is meaningful given the high-dimensionality of the data. It is possible using statistical functions such as vector magnitude to simplify the input data and encapsulate the phenomena into a single field. However, as a result we lose information (i.e., vector direction) which may be necessary in the analysis. Therefore, we strive towards visualizing multiple fields to provide greater insight.

## **3.4.2 Visual Mapping of Multiple Error Sensitivity**

The visualization of multiple error sensitivity fields is important for making comparative assessment between different camera positions. Understanding the distribution of error is an important task to support various user-specific needs. For example, the action from a snooker training shot may typically cover a small region of the table. Therefore, camera positions that minimise the error in this area should be considered in addition to camera positions that have least, overall error sensitivity. The knowledge gained from each field can be used to minimise the reconstruction error further (e.g., as an optional post-calibration step) by optimising sensitive feature points that impact this region. It would be a huge challenge, if not an impossible one, to provide a visual design for an arbitrarily large number of fields. Here we consider a collection of visual designs for four error sensitivity fields which is minimal for solving planar homography matrix, addressing the requirements of our case studies. Figure 3.6 shows five example approaches that have been considered for the design of the visualization: Vector Glyphs, Co-Planar Star Glyphs, Stacked Ribbon and Streamlines, and Bézier Glyphs.





**Figure 3.6:** Development of the 2D error visualization using different approaches is shown. (a) presents a stacked vector glyph design, where magnitude is mapped to the length of the vector. This is extended in (b) to a Co-Planar Star glyph which normalises the vectors and uses a heat map to depict the resultant error. (c) incorporates stacked ribbons (center) and streamlines (right) into the error visualization. Streamline thickness is mapped to vector magnitude. (d) generates a closed Beziér curve based on the vector field. The glyph size is mapped to the resultant error.

**Vector Glyphs:** Arrow primitives are the most common method for depicting vector quantities. As a naive approach, we use four colour-coded arrows for representing each of the vector fields at a given point (Figure 3.6(a)). The length of the arrow is mapped according to the error magnitude with respect to each field. For visualization, the vector glyphs can be rendered either on the same plane (i.e., for  $d = 0$ ), or separated so that each individual vector field is rendered on an independent plane, resulting in four layers in 3D space. This aims to overcome overlapping issues that may arise.

**Co-Planar Star Glyphs:** Due to inevitable overlapping problems with vector glyph representations in dense sampling, the directional information can often be lost. To reduce glyph occlusion and preserve vector direction, the star glyph uses four normalised colour-coded arrows. However, rather than using arrow length to indicate vector strength we now use coloured transparent ellipses (Figure 3.6(b)). The four points on the ellipse  $e_1, e_2, e_3, e_4$  are used to map a gradient to the circle based on error magnitude for each

vector. This creates a heat map which is effective for highlighting regions of large error.

**Stacked Ribbons / Streamlines:** Streamlines are an effective and well-known technique for visualizing vector fields [MLP\*10]. Urness *et al.* [UIL\*06] present several strategies for visualising two vector fields. We adopt their streamline approach for our error visualization by mapping curve thickness to error magnitude (Figure 3.6(c)). Just as was found using vector glyphs, there are instances where occlusion can occur meaning that the vector fields can not be displayed clearly. For a more continuous representation, we extend streamlines to 3D space by rendering each vector field on a separate plane. A surface is used to connect streamlines on adjacent planes, resulting in a stacked ribbon.

**Bézier Glyphs:** Our approach considers the vectors as a series of points that form a closed Bézier curve (Figure 3.6(d)). This preserves the directional information that the vector glyphs offer, whilst giving greater visual clarity to the extreme directions of the four vector fields. The parametrized Bézier curves are divided into regions using distribution points  $\sigma_i$  centered at the midpoint of each spline, which adaptively move along the curve based on the difference in vector strength:

$$\sigma_i = \frac{1}{2} \left( 1 + \frac{\|\mathbf{v}_i\| - \|\mathbf{v}_{i+1}\|}{\max(\|\mathbf{v}_i\|, \|\mathbf{v}_{i+1}\|)} \right) \quad (3.4)$$

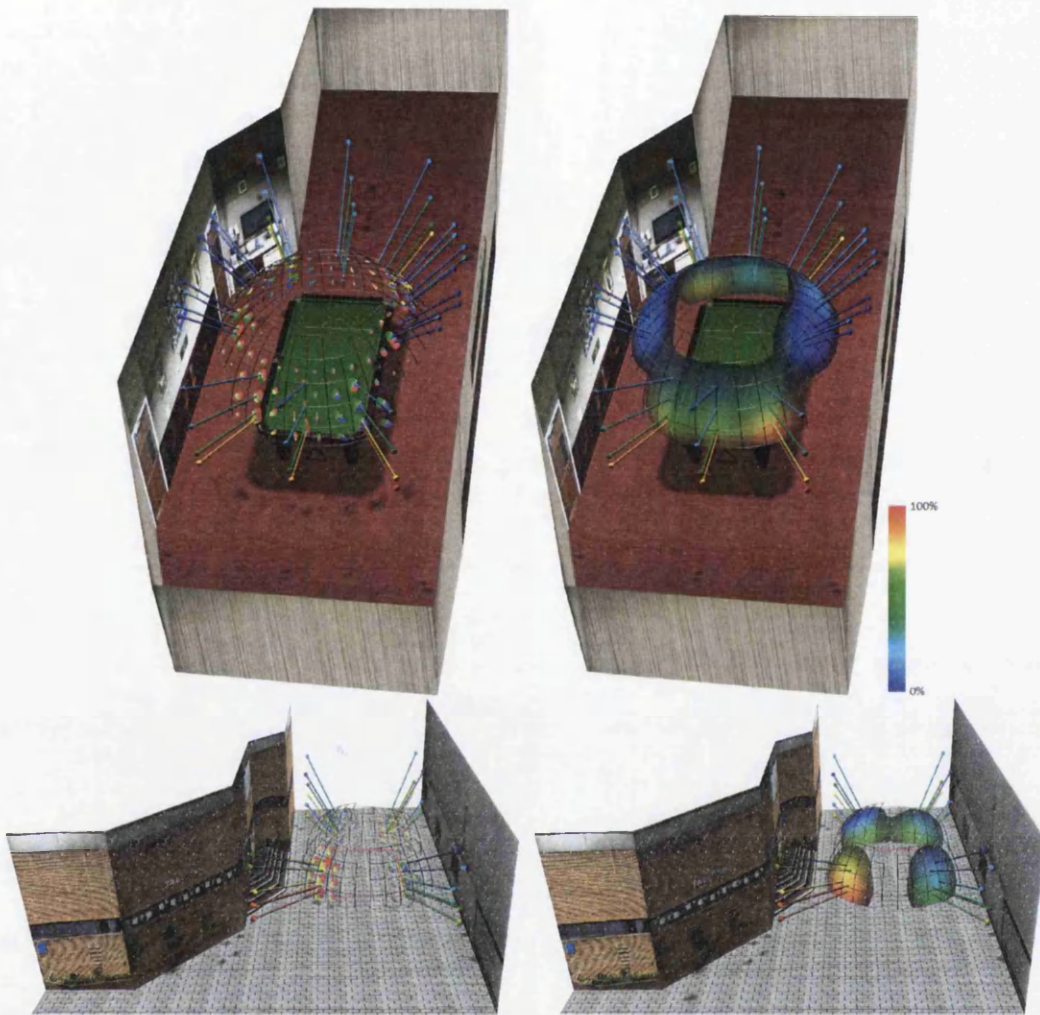
where  $\mathbf{v}_i$  and  $\mathbf{v}_{i+1}$  are two adjacent vectors. This allows the user to identify which error source (i.e., vector field) is of dominant influence to the resulting geometrical shape of the Bézier glyph.

### 3.4.3 Sample points in 3D visualization

To introduce camera positions into the 3D scene visualization, we determine the geometry of the table to obtain a camera pose estimate. Given that we have four feature points and their corresponding positions in a 3D model, it is possible to estimate the viewing angles from a single image. Here we use the four corner points of the snooker table. The basic scheme is detailed by Putz and Zagar [PZ08], where a planar homographic transformation matrix is computed and an SVD-based approach is applied to extract the rotation and incline angles. A mapping function is applied to render the cameras in 3D space using the camera pose and the measured camera distance. In addition, filtering can be applied to highlight the  $k$ -least error camera positions. We use a similarity metric  $d$  based on euclidean distance to provide  $k$  spatially different solutions to the user.

### 3.4.4 Spherical Mapping

Now that we can map our camera points to the scene, we use a spherical model to give an overview of the error sensitivity of such positions (see Figure 3.7). We visualize camera



**Figure 3.7:** Visualization of the 3D camera positioning around the snooker scene (Top row) and security scene (Bottom row). The cameras are modelled using spheres, and colour mapped to its error magnitude. The sample points are then projected onto a spherical surface centred at the focus region, giving users an overview of the statistical error. (Left) shows a glyph-based approach for depicting the average vector error and (Right) uses a colour-mapped sphere for illustrating the overall error magnitude.

positions using spherical markers and a connecting cylinder with length being mapped to the distance between the camera, and the sphere that encloses the focus region. A spherical geometry was chosen due to its uniform characteristics and its potential to be generalizable to other domains. Here, we use a partial spherical mesh to emphasise the boundary of camera positions. To quantify each camera, we propose two visual options:

multi-field glyphs and colour-coded sphere. For our glyph-based method, an average Bézier glyph representing the multiple error sensitivity fields are placed tangential to the sphere. For a colour-coded sphere, we depict the summation of the resultant error sensitivity field normalised by  $\frac{\epsilon}{\epsilon_{max}}$  using a red-to-blue colour mapping. The vectors (or error magnitude) are splatted onto the sphere using a gaussian weighted Radial Basis Function (RBF) [Che05] forming an interpolated surface that gives visual estimates of local regions. We uniformly position the glyphs along the surface of the spherical mesh. Each point on the sphere is modelled as:

$$v(q) = \sum_i^n w(\mathbf{q}, \mathbf{p}_i, r)v(\mathbf{p}_i) \quad (3.5)$$

where  $v(\mathbf{q})$  is the camera error at position  $q$ , and  $w(\mathbf{q}, \mathbf{p}_i, r)$  is the RBF weight function given by:

$$w(\mathbf{q}, \mathbf{p}_i, r) = e^{-\beta u_i^2} \quad (3.6)$$

where  $u_i = \|\mathbf{q} - \mathbf{p}_i\|/r$  is the relative distance from  $\mathbf{q}$  to  $\mathbf{p}_i$  normalized by the radius of influence  $r$ , for some  $\beta > 0$ .

Naturally, the RBF tends towards zero as the distance tends to infinity and hence a restriction is placed on the kernel based on the radius of influence. The user option  $\beta$ , is a coefficient that can be altered in order to adjust the slope of the blending function.

### 3.5 User Consultation - 2D

We have proposed 2D and 3D visualization methods to depict the error sensitivity in 3D scene reconstruction for estimating optimal camera placement. It is essential that the visualizations can effectively convey to the user the presence of error and to allow visual and comparative analysis of different camera positions. To evaluate the effectiveness of our designs, we performed a qualitative user-evaluation involving six computer scientists, three of whom are experts in computer vision. Figure 3.8 shows the collection of error-sensitivity mappings of the same camera position using the five visual designs in Section 3.4.2. Each study was carried out independently from one another, whereby participants were presented with a set of questions (see Appendix A) which we classify into three groups: *Detail*, *Overview* and *Cancellation* derived from Section 3.4.1. The remaining questions provide more general observations in order to evaluate whether our visualization approach is useful for the given task.

**R1. Detail:** It is important that multiple error-sensitivity fields can be visualized within a single image. To start with, we asked the users whether they can identify the independent vector magnitude and directions at a given point for each of the visual designs. Whilst four of the five designs succeed to perform the basic functionality of conveying detail, some designs have limitations. It is clear from the evaluation study

| Design criteria                     | Visual Designs (see Figure 3.8) |     |     |     |     |
|-------------------------------------|---------------------------------|-----|-----|-----|-----|
|                                     | (a)                             | (b) | (c) | (d) | (e) |
| <i>Independent vector direction</i> | *                               | *   | *   |     | *   |
| <i>Independent vector magnitude</i> | *                               |     |     |     | *   |
| <i>Overall error</i>                |                                 | *   |     |     | *   |
| <i>Error distribution</i>           |                                 |     |     |     | *   |
| <i>Visual separation of fields</i>  |                                 |     | *   |     | *   |
| <i>Vector cancellation</i>          |                                 |     |     |     | *   |

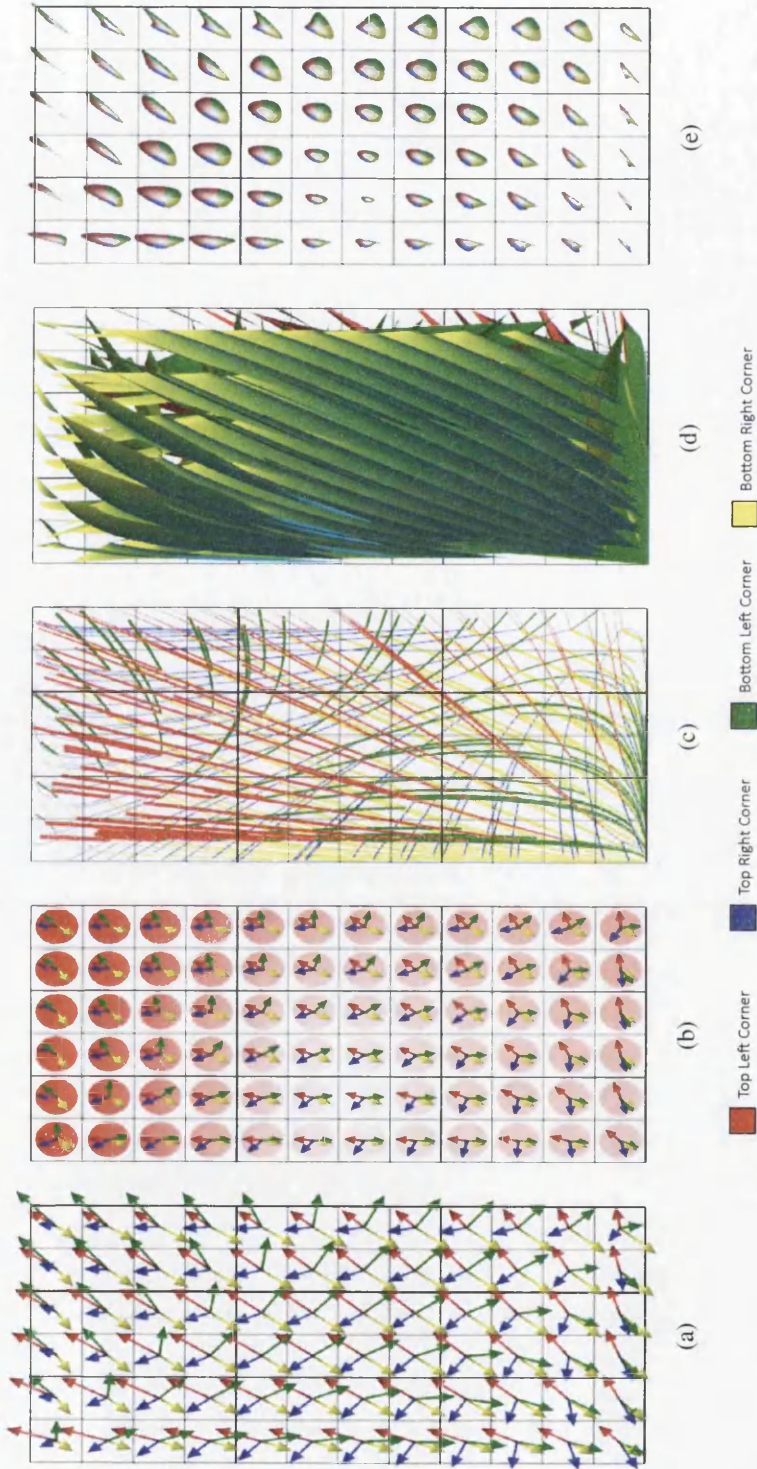
**Table 3.1:** Comparison of visual mappings shown in Figure 3.8. Each design is assessed against a number of set criteria which ideally should be achieved. An asterisk in the table indicates the design satisfies that particular criteria.

that the use of stream ribbons (Figure 3.8(d)) for depicting multiple error fields over several planes created too much visual clutter and occlusion. As a result, the users found the information to be lost. Viewpoint adjustment may overcome this, however it cannot be guaranteed. Whilst not quite so severe, we found that Figures 3.8(a) and 3.8(b) may also suffer from occlusion issues should two vectors have the same direction and magnitude. Although both magnitude and direction are visible in our streamline approach as shown in Figure 3.8(c), there were questions raised over the accuracy of comparing thicknesses between two streamlines in a quantitative manner. All the users found the Bézier glyphs (Figure 3.8(e)) to be most effective in conveying both attributes but revealed that independent vector direction became difficult to perceive for elongated glyphs (i.e., when vectors are in the same direction).

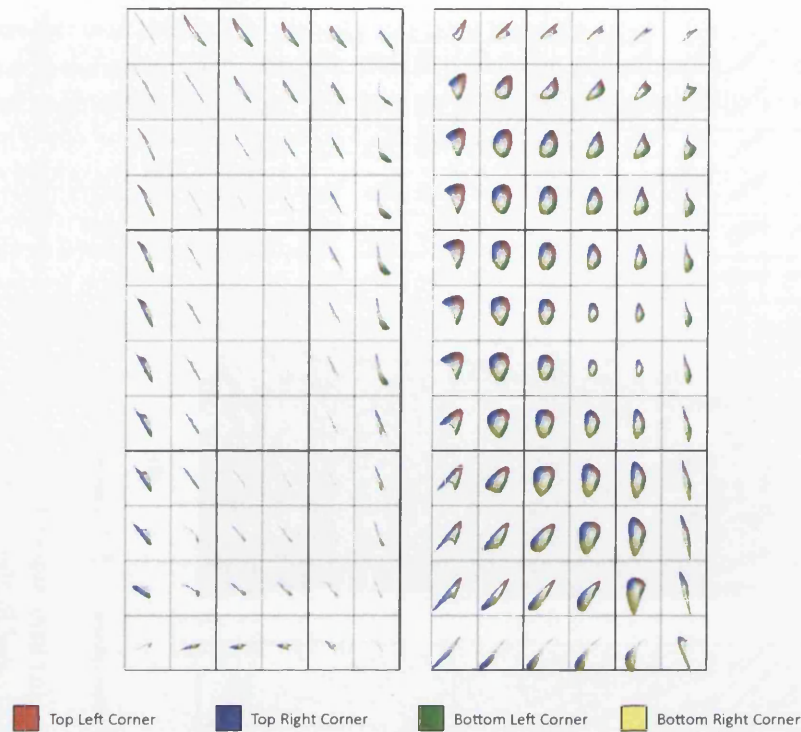
**R2. Overview:** In many focus and context visualizations, it is necessary to show the overall sensitivity for multiple fields, whether this be introduced by one or multiple cameras. The overall sensitivity can be assessed based on two uncertainty components, the overall error (resultant magnitude) and the distribution of error from each error sensitivity field. In Figure 3.8(a), although the overall error is not explicitly mapped, users were able to estimate the error given by the four vectors. However, the presence of visual clutter likewise in Figure 3.8(c) and 3.8(d) made this difficult to deduce easily. Figure 3.8(b) performed significantly better by mapping the overall error from multiple fields using intensity. The heat map behind the glyph is effective for estimating local regions of uncertainty. One limitation with the design is that visual interference was found to occur between the vector fields and the heat map. Figure 3.8(e) also shows the overall error from multiple fields, this time by size. The larger the Bézier glyph appears determines the amount of error at the location. Most of the users acknowledged this design to be the most intuitive and descriptive when displaying error, stating that the glyph shape provides a visual cue that is clearer for error analysis.

One of the goals of multi-field visualization is to be able to observe each field independently, whilst providing additional insight on how multiple fields interact. We found that vector-glyph based designs performed weakly at this task due to visual clutter, with

users stating it was difficult to visually integrate between fields. On the otherhand, the streamline visualization performed particularly well due to its continuous representation. The colour segments in the Bézier glyphs were also effective for visually separating error fields, but these became lost for highly elongated glyphs.



**Figure 3.8:** Comparative evaluation of error visualization designs. (a) uses stacked vector glyphs. (b) co-planar star glyphs. (c) weighted streamlines. (d) stacked stream ribbons and (e) colour-coded Bézier glyphs.



**Figure 3.9:** Comparison of error sensitivity between camera positions *B* (left) and position *C* (right) from Figure 3.11 using colour-coded Bézier glyphs.

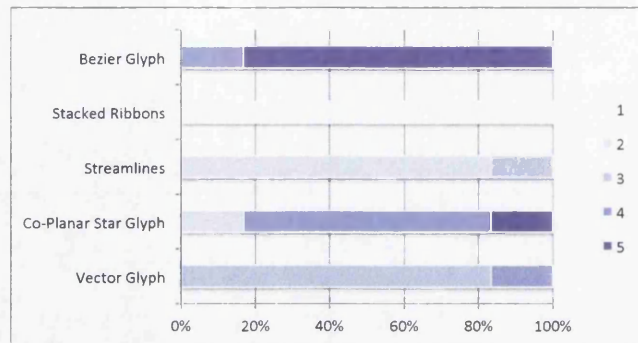
**R3. Cancellation:** Figure 3.8(e) is the only visualization to truly incorporate this requirement. This is determined based on the shape of the Bézier glyph. A circular glyph would indicate a high level of vector cancellation from multiple fields. However, any skew or elongation would represent dominant vector direction that is influencing the error for that position. It is possible to estimate cancellation from Figures 3.8(a) and 3.8(b) if two vectors are recognised to be in opposing direction, however only the Bézier design actually incorporates this. Table 3.1 provides an overview of the performance for each visual design.

In the study, we asked the participants whether the visualization approach would assist in visually quantifying a camera position based on uncertainty. The feedback was positive and the users expressed the distribution of error shown by the visualization would help attach a weighting to a particular position. One computer-vision expert in the study revealed that the depicted error distribution could be used for optimising vision-based tasks such as correcting more sensitive feature points. Another participant noted the visualization is useful for revealing camera positions with symmetric reprojection error.

Figure 3.9 gives the error mapping for two different camera positions. This provides visual comparison of the error sensitivity that is present from each camera viewpoint.



**Figure 3.10:** Graph showing the result of users ranking the visual designs from worst-to-best as a measure from 1-5.

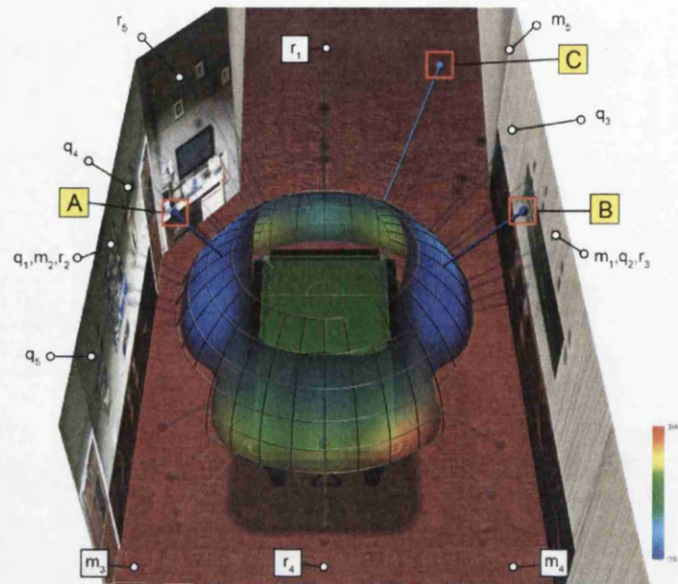


By analysing the changes between the Bézier glyph representation based on size, shape and colour, the user can determine the viewpoint that reduces the impact of error. Following the study, all users found the visualization approach significantly helped evaluate viewpoints based on error-sensitivity in a comparative manner. From this example, camera position C experiences large error that is significantly reduced in camera position B. Lastly, Figure 3.10 shows the results of the users preference by ranking the visual designs from worst-to-best. Results from the study show that users felt the Bézier design to be the most intuitive and effective in conveying error sensitivity. In the remainder of this chapter, we use the Bézier design during the user evaluation of the software which combines both 2D and 3D visualizations for finding an optimal camera position.

### 3.6 User Consultation - 3D

To evaluate our combined visualization system for selecting an optimal camera position, we conducted a study using two sets of users: three sport scientists, and three computer vision experts (one of which who also participated in the previous study in Section 3.5). We use this study to compare and contrast the decision process between end-users with minimal reconstruction knowledge using our visualization approach, and domain experts in the field of computer vision without error analysis support. Each study was conducted in isolation from other participants so to not influence their given opinions.

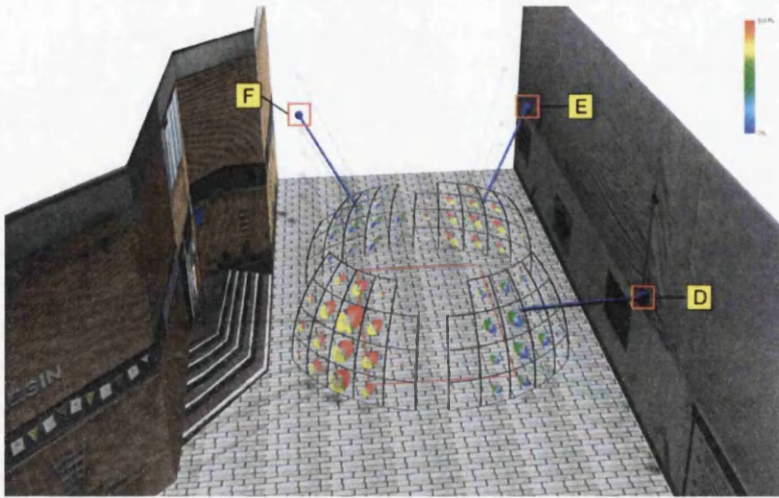
Our first study involved three sport domain experts: A snooker coach and former world champion, a snooker hardware engineer and a sports scientist. We started by explaining the motivation behind the work to each participant. It was made clear that given a single camera to configure, we wanted the position that would achieve accurate reconstruction and is most feasible for installation (i.e., taking into account physical, financial and other types of constraints). We note that the users have some prior knowledge of the scene such as structural information of the room and cost of mounting equipment which they can incorporate into the decision. Figure 3.7 was presented where they were asked to give their feedback on the usability of such a visualization. The initial reaction was very positive by all three participants. In particular, they were able to quickly identify



**Figure 3.11:** 3D visualization showing the 3 candidate camera positions labelled A, B and C, after filtering. These camera positions are highlighted using opacity.

potential camera positions, namely above the left and right hand side of the snooker table. We explained to each participant how a user can filter the number of cameras based on error sensitivity to highlight candidate positioning. Figure 3.11 shows the result of the user filtering down the data to just three prospective camera positions. This helped validate the users' understanding of the visualization as two of the three positions matched their initial observations.

The next objective was to assess how well the visualization integrates contextual geometry to influence the decision process. By navigating in the virtual environment, the feedback received suggested that the camera should be positioned to the right of the table. Participants recognised that both this and the position left of table were the two best choices. Through inspection of their error sensitivity maps, the users identified the left camera position (Camera A) to be marginally more accurate. However, due to mounting impracticalities on the left wall such as picture frames and scoreboards, the users realised that camera placement here was not a viable option. The participants found the error visualization to be clear when comparing cameras with significant error variance (see Figure 3.9). As a result, the visualization approach proved useful for clarifying the error associated with each camera position. Prior to using the visualization, the hardware engineer assumed that the best camera position would be near the bottom end of the table giving a typical TV broadcasting view. The participant was surprised by the visual results to find that the cameras either side of the snooker table were the least error prone positions, and appreciated that the visualization showed greater insight to the setup procedure for 3D scene reconstruction.



**Figure 3.12:** 3D visualization showing the 3 candidate camera positions in the surveillance scene labelled D, E and F after filtering. These camera positions are highlighted using opacity.

The second study involved the computer vision experts  $\mathbf{q}$ ,  $\mathbf{r}$  and  $\mathbf{m}$ . Initially, each participant was asked to nominate the 5 best positions for single camera reconstruction given there were no constraints. A uniform decision was observed, where the camera position directly top-down was identified as optimal. This is to be expected, however the selection is not viable since the camera position is unable to provide full coverage of the scene due to a low-ceiling. Following this, we investigate how additional knowledge on semantic constraints (e.g., low ceiling, picture frames) and financial constraints (e.g., cost of mounting) would impact their decision on camera positioning. We note that the cost of a ceiling mounted camera is more expensive due to structural issues in this case study. We asked the participants to repeat the initial task with such semantic considerations in mind. The results are shown in Figure 3.11 where camera positions marked as  $\mathbf{q}_k$ ,  $\mathbf{r}_k$  and  $\mathbf{m}_k$  are ranked from best ( $k = 1$ ) to worst ( $k = 5$ ). It can be observed that the nominated camera positions amongst the participants significantly diverges in the new task. This shows that camera positioning is not as intuitive once multiple real-world constraints are imposed. We presented the vision experts with the system, where they all recognised the mutual benefits of the visualization as it constrains the search space for optimal camera placement to support consistent positioning.

Figure 3.12 demonstrates our method for our second use-case scenario on camera surveillance, where three candidate positions have been highlighted after filtering. Here, we use multi field glyphs to provide a greater level of detail for camera error sensitivity in the 3D scene. This allows users to examine crucial information such as independent and combined error distribution and sensitivity of feature points in a global perspective, with the option to see further detail by examining the associated error sensitivity visual-

izations. Due to temporary construction works along the featured structure to the right of the region of interest, camera placement here would not be optimal. Therefore, the most suitable position would be along the wall near camera F as this provides a more temporally stable solution.

We presented a qualitative evaluation based on the feedback of two sets of users. All participants felt that the visualization helped to identify the most suitable camera positioning in a clear and simple manner. It was shown that for end-users, the visualization facilitates dynamic decisions for optimal camera placement which includes substantial trade-offs between reconstruction quality and camera feasibility without the need for extensive knowledge in reconstruction. The sporting professionals all stated that they would use this approach if they were to configure a camera set up. For computer vision experts, the visualization proved to be an excellent aid for single camera placement as a result of restricting the search space.

### **3.7 Discussion**

For this application, we have designed high-dimensional glyphs to visualize multiple error-sensitivity fields for optimal camera placement. We demonstrate this in two real-world applications, namely: snooker reconstruction and camera surveillance, which uses 2D planar homography to perform 3D reconstruction. In the context of sports, our method can be generalised to other domains that involve playing on a rectangular surface such as table tennis, badminton, and squash, where obtaining a top-down camera is often impractical. Alternate camera placements is therefore necessary, especially in applications involving projected transformations such as ball and player tracking. While sports played on larger areas such as football may be possible, the limitations of standard camera equipment means that capturing the entire scene is unlikely while also having a camera resolution that is high enough to produce accurate results. Likewise, our application can also be applied to other camera-based surveillance tasks that have a set of planar feature points which can be mapped using 2D homography.

Evaluating systems such as the one proposed in this work can be challenging because they are not designed for general public use. In addition, gathering enough domain experts to obtain meaningful evaluation data is not only expensive, but also time consuming due to their limited availability. Nevertheless, the valuable feedback from such users should not be underestimated. We acknowledge that although the feedback from the two sets of users was very positive, our system is not without its limitations. While our approach is effective for depicting the error-sensitivity of 2D homography based on four feature points, the visual mappings will become more cluttered for a larger number of fields. In addition, since there are many other possible 3D reconstruction algorithms [HZ04] that utilise a different error parameter space, our visualization approach may not necessarily be suitable for such methods.

## **3.8 Summary**

We have described 2D and 3D visualization methods to display error sensitivity fields for feasible, single camera positioning. The collection of visual mappings depict the composition of multiple error sensitivity fields. These map to a 3D visualization where the goal is to visually estimate several optimal positions for the camera. We find that the visualization can effectively aid the estimation of the best camera positioning without the need for a manual configuration through trial and error, while providing the users with sufficient flexibility to make dynamic decisions based on other facts that cannot be encoded easily in an algorithm.

The glyphs developed for this work focuses primarily on encoding multiple fields of quantitative values. As mentioned in Section 2.6, high-dimensional glyphs can take various forms, and some designs are more/less effective depending on the number of attributes and data type they encode. In the next chapter, we will discuss glyph-based designs that facilitate the mapping of data containing both quantitative and qualitative attributes.

---

# Interactive Glyph-Based Visualization for Real-Time Sports Performance Analysis

---

## Contents

---

|       |  |    |
|-------|--|----|
| 4.1   | Introduction . . . . .                         | 75 |
| 4.2   | Requirements Analysis . . . . .                | 77 |
| 4.2.1 | Rugby Union . . . . .                          | 77 |
| 4.2.2 | Rugby Performance Analysis . . . . .           | 77 |
| 4.3   | <i>MatchPad</i> Pipeline . . . . .             | 79 |
| 4.4   | Glyph-based Visual Mapping . . . . .           | 80 |
| 4.4.1 | Data Space . . . . .                           | 80 |
| 4.4.2 | Design Options . . . . .                       | 82 |
| 4.4.3 | Resultant Design for <i>MatchPad</i> . . . . . | 83 |
| 4.5   | Visualization Interaction . . . . .            | 85 |
| 4.5.1 | Interactive Visualization . . . . .            | 85 |
| 4.5.2 | Scale-Adaptive Layout . . . . .                | 86 |
| 4.6   | Case Study: Welsh Rugby Union . . . . .        | 87 |
| 4.7   | Discussion . . . . .                           | 88 |
| 4.8   | Summary . . . . .                              | 90 |

---

**S**O far, we have introduced a collection of glyph-based visual mappings that encode multiple quantitative values. This resulted in glyphs that are pre-dominantly geometric-based (i.e., they make use of two types of visual channels: *geometric*

*channels* such as size and shape, and *optical channels* such as colour and opacity) to display the data. When a multi-dimensional dataset contains mixed data types, we noticed that such glyphs do not convey information very intuitively. In fact, we observed earlier from previous works (see Chapter 2) where examples of visual designs do support multiple dimensions to be encoded, but are cognitively challenging for a user to extract certain information (i.e., identifying individual attributes) from the glyph. This work addresses the challenge of visualizing events and actions “at a glance” for real-time sports performance analysis. The analysis of sport event data poses an interesting problem to data visualization due to the large amount of categorical events, and the different levels of association (i.e., the match, team, or player) and outcomes (e.g., won/lost, score/miss, and occurrence). We note that previous work do not address this task.

Today real-time sports performance analysis is a crucial aspect of matches in many major sports. For example, in soccer and rugby, team analysts may annotate videos during the matches by tagging specific actions and events, which typically result in some summary statistics and a large spreadsheet of recorded actions and events. To a coach, the summary statistics (e.g., the percentage of ball possession) lacks sufficient details, while reading the spreadsheet is time-consuming and making decisions based on the spreadsheet in real-time is thereby impossible. One critical shortcoming in the current practice is the disconnection between the *overview* (i.e., the summary statistics) and the *details* (i.e., actual events in the match) [Shn96]. To seek details on demand, the coaching staff and match analysts have to trawl through the large collection of event records. For post-match analysis, the interaction for “visual information-seeking” is highly inefficient, while for in-match analysis, this is practically impossible. One important functional role of visualization is to facilitate efficient and effective “visual information-seeking” [Shn96]. Considering the requirements of the users and application environments, the visualization must be delivered in a comprehensible manner that is simple and intuitive to understand whilst also being informative.

In this chapter, we introduce glyph-based visualization into the process of notational analysis in sports. We considered a number of design options for the visualization, and developed a collection of glyphs that feature metaphoric visual cues for rapid recognition as well as intuitive visual channels for depicting attributes. In comparison with the tabular form of events, the visualization gives an effective overview of a match that users can interact with to obtain details on demand (Section 4.4). Since the visualization corresponds directly to the match video, key events can also be replayed to show further details. We implemented our visualization system, *MatchPad*, on a portable tablet device, which enables touch-based interaction with the visualization. We developed a scale-adaptive glyph layout algorithm to facilitate effective transition between different levels of details (Section 6.3.4). The work was carried out in close collaboration with the Wales national rugby team, and was used during the Rugby World Cup 2011. It successfully highlighted the effectiveness of visualization in sports analysis, by helping coaching staff to examine actions and events in detail whilst maintaining a clear overview of the match, and assisting in-match decision making (Section 6.4).

## 4.2 Requirements Analysis

The work described in this chapter was carried out by an interdisciplinary group composed of a sports scientist, a former international-level sportsperson, and computer scientists. I was the principal researcher concerning the different aspects of glyph-based design, and the scale-adaptive glyph layout algorithm used in the *MatchPad*. Prior to this research, we were motivated by the huge potential of using visualization in sports performance analysis during matches and in training [HB02]. For example in rugby, Duthie *et al.* [DPH03] and Nicholas *et al.* [JMJ04] confirmed the usefulness of match analysis and team performance indicators respectively. We worked closely with the Welsh Rugby Union (WRU) for over 12 months, frequently visiting their training grounds as well as inviting the chief analyst to give talks in workshops. From these close contacts, we learned the strengths and limitations of their current workflow. To fully consider the challenges involved with rugby performance analysis, we first provide a background to the game.

### 4.2.1 Rugby Union

Rugby Union is a popular team sport which consists of two teams (of 15 players) who advance an oval ball across a rectangular field (up to 144m long by 70m wide) with two H-shaped goal posts at either end. The game is played primarily by carrying the oval ball from one end of the pitch to the other. Points can be scored in several ways: A *try*, which involves grounding the ball in the opposition goal area, or through kicking the ball between the H-Shaped post from a *conversion*, *penalty kick* or *drop goal*. The ball can move from one team to another from tackles and set pieces. Each match is played in two 40-minute halves, where the objective is to score more points than the opponent.

### 4.2.2 Rugby Performance Analysis

The Welsh Rugby Union relies heavily on notational analysis [HF97], whereby a match analyst “tags” various events in the video footage of a match with semantic notations, from which a set of key performance indicators about individual teams or players are calculated. Currently there are no automated techniques on the market or in the research literature that are capable of performing such annotation reliably, and this was not the focus of this research. Personal position-tagging devices are normally disallowed in real matches for safety reasons. In practice, trained match analysts are highly skilful in video annotation. With the aid of appropriate software such as SportsCode, they are able to rapidly annotate major events as they occur within a match. Detailed annotation, which includes player identification, is normally done off the pitch. The team have three typical scenarios for analysing performance data:

- **Pitch-side** — a team of analysts will code major events during a live match or training ground, allowing them to provide constant feedback to the coaches and

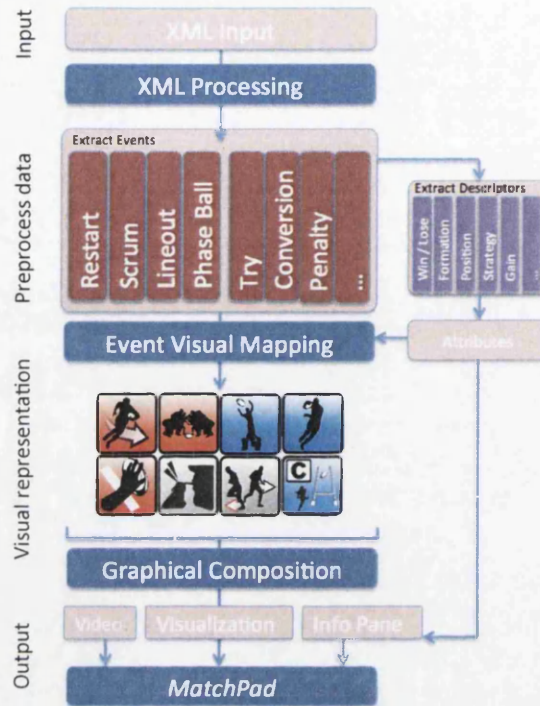


players on the pitch. This is often limited to summary statistics such as ball possession, territory percentages (i.e., where on the pitch is the ball being played), and counts of event occurrences (e.g, the number of line-outs won/loss).

- **Half-time interval** — since summary statistics is generally difficult for players to interpret and make changes to their game (as they do not capture the semantics of a match easily), the interval break is a crucial time where such information can be conveyed to the team in a more effective manner. One important job is the review of key events recorded from the match that describe, for example, opposition formations and patterns of play which the coach and analysts have identified.
- **Post-match analysis** — once a match has ended, the analysts will code specific events with more detailed descriptors. This enables a more in-depth analyses of various aspects (e.g., set-pieces, attacking and defensive strategies) that is not possible during a live match. They may also combine event data with additional data sources such as player and ball tracking information.

This chapter focuses on the challenge of analysing performance data in the first two use scenarios (pitch-side and half-time interval). Given the short amount of time available, it is critical that the analysts are able to retrieve and seek information close to real-time. As the chief match and performance analyst of the team pointed out, the primary issue is in fact “information overload” as reviewing the annotated data is a laborious task. Current software makes use of conventional plots and spreadsheets that are ineffective for conveying the overview and details of events in a match. It is necessary for visualization to address a number of requirements as follows.

- The visualization must be able to depict most, if not all, annotated events that are stored in a tabular form.
- It is necessary for the visualization to connect each event to the corresponding video footage for further analysis.
- The visualization should facilitate rapid information seeking and in-match decision making for coaching staff and analysts at different temporal granularities of a match.
- The visualization should provide coaching staff with a visual aid for post-match team and player briefings.
- The visualization must be intuitive for the target users, requiring a minimal amount of learning and memorisation. While an analyst may be willing to make effort to learn some complicated techniques, it is not reasonable to demand the same from the coaches and players.
- The visualization must be suitable for portable devices to be used during matches and training.



**Figure 4.1:** The pipeline used to compute the MatchPad visualization. There are four key stages: XML processing, event visual mapping, graphical composition, and the combined video, visualization and information pane of the MatchPad.

### 4.3 MatchPad Pipeline

Following the requirement analysis, the development of the *MatchPad* started in February 2011. Figure 4.1 shows the computational pipeline of the *MatchPad*. The pipeline consists of four key stages: XML processing, event visual mapping, graphical composition and integrated user interface that makes up the *MatchPad*.

The first stage is to process the input data. Using a wireless connection, the *MatchPad* retrieves XML data streamed from the analyst's workstation. This can be scheduled to perform at set time intervals during a match (e.g., every 15 seconds). It is therefore vital that the pipeline can be executed quickly to handle short update intervals. In the XML data, each event is recorded as an instance, of which a typical match would have in the order of hundreds. Each instance will consist of an ID number, a start time, an end time and a name (e.g., scrum). This is then followed by a series of text tags that contain descriptions such as whether the event was won or lost, the formation and strategy adopted, the position on the pitch and whether ground was gained in the play. The pipeline is designed to recognise the semantic textual codes specified in a dictionary for

a particular sport or application.

The second stage maps the series of recorded events and their attributes to a collection of glyphs. We chose to use metaphoric glyphs to provide intuitive visualization of events. Each glyph may be augmented with additional visual components and channels for different attributes. We detail our design decisions in Section 4.4.

The third stage constructs a temporally continuous visualization that arranges all event glyphs along a timeline. A scale-adaptive layout algorithm is used to accommodate different levels of detail, which is detailed in Section 6.3.4.

The final stage integrates the visualization with the accompanying video and statistical performance indicators to produce the *MatchPad* interface. While the interface allows the user to control all three previous stages, the majority of interaction is zooming and panning for rapid information seeking, forming an active feedback loop with stage 3.

## 4.4 Glyph-based Visual Mapping

In glyph-based visualization, a glyph is composed of a number of visual channels which encode specific attributes of a data entity (see Chapter 2 for details). Before creating a glyph-based visualization, it is necessary to first establish the full extent of the data space. With sufficient knowledge of the data space, one can then explore different design options and make appropriate use of different visual channels in the context of the application concerned.

### 4.4.1 Data Space

During the analysis of existing data sets, I identified the set of *event types* and the associated attributes. These include:

- *Levels of Association* — An event is usually recorded in association with different levels of interest, that is, the *match*, a specific *team*, and a specific *player or players*. In some cases an event may be associated with more than one level. During a match, analysts usually aim to record the events at the match and team level in real time, whilst much of the player-specific data is recorded post-match since this often requires repeated playback of the video footage to identify all details of the events. Because of the importance of scoring events, (e.g., try, goal kick) they are all considered as match-level events.
- *Team Identifier* — A team-specific event is accompanied by an attribute of the team identity. In our application, there are always two teams in a match, referred to as the home team and away (opposition) team respectively.

|              | Match | Team | Player | Outcome    | Values  | Metaphoric Glyph | Abstract Icon | Shape | Colour |
|--------------|-------|------|--------|------------|---------|------------------|---------------|-------|--------|
| Restart      |       | ○    |        | Occurrence |         |                  |               |       |        |
| Drop Kick    |       | ○    | ○      | Occurrence |         |                  |               |       |        |
| Scrum        |       | ○    |        | Won/Lost   |         |                  |               |       |        |
| Lineout      |       | ○    |        | Won/Lost   |         |                  |               |       |        |
| Ruck         |       | ○    |        | Won/Lost   |         |                  |               |       |        |
| Maul         |       | ○    |        | Won/Lost   |         |                  |               |       |        |
| Tackle       |       | ○    | ○      | Won/Lost   |         |                  |               |       |        |
| Pass         |       | ○    | ○      | Won/Lost   |         |                  |               |       |        |
| Try          | ○     | ○    | ○      | Occurrence |         |                  |               |       |        |
| Goal Kick    | ○     | ○    | ○      | Score/Miss | C, P, D |                  |               |       |        |
| Injury       | ○     | ○    | ○      | Occurrence |         |                  |               |       |        |
| Substitution | ○     | ○    | ○      | Occurrence |         |                  |               |       |        |
| Phase Ball   | ○     | ○    |        | Occurrence | 1-10    |                  |               |       |        |
| Territory    | ○     | ○    |        | Occurrence | A-D     |                  |               |       |        |
| Referee      | ○     |      |        | Occurrence | N, Y, R |                  |               |       |        |
| Ball in Play | ○     |      |        | Occurrence |         |                  |               |       |        |

**Table 4.1:** A range of events are to be mapped in the visualization. Each event is augmented with levels of association (i.e., the match, team or player), and additional attributes (i.e., outcome and numerical and enumerative values). We also illustrate four possible glyph designs: metaphoric pictogram, abstract icon, shape, and colour. We choose to use metaphoric pictogram to represent events in MatchPad.

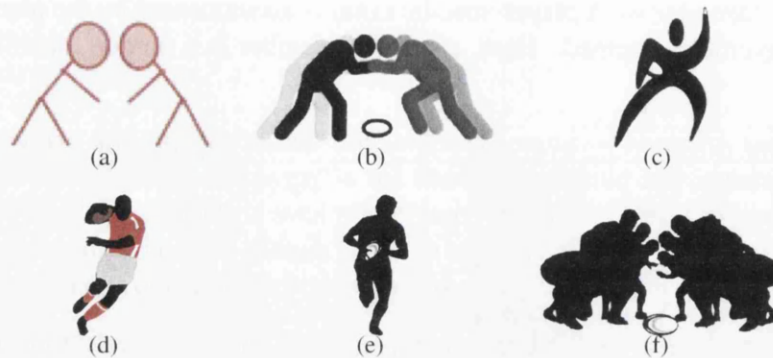
- *Player Identifier* — A player-specific event is accompanied by the identifier(s) of the player(s) concerned. Here, a player's number is a unique identifier in each team.
- *Outcome Attribute* — Some events require the recording of an explicit outcome. For instance, the outcome attribute for a “scrum” event will state whether the team won or lost. Some event types do not have an explicit outcome defined. For example, a “try” event implies the outcome that the team have successfully scored. We refer those events without an outcome attribute as *occurrence*.
- *Value Attribute* — Some events are associated with a numerical or enumerative value. For instance, a “goal kick” event can be classed as either C, P and D to define “conversion”, “penalty” and “drop goal” respectively.
- *Duration Attribute* — Most events are accompanied by an attribute indicating the duration of the event.

The first column of Table 4.1 lists most common event types, columns 2, 3, 4 indicates the levels of association, column 5 indicates the outcome attribute, and column 6 indicates the numerical and enumerative values.

#### 4.4.2 Design Options

Ward presented a number of design options in [War02], all of which were considered in this work. Columns 9 and 10 show two typical design options, namely shape and colour, for representing event types. Whilst these may be suitable for a data attribute with a smaller number of enumerative values, here we find that the number of event types would require many different shapes or colours, which would be very difficult for users to learn, remember, or guess. Considering the captured requirements mentioned in Section 6.2, we found that it was necessary to explore the design options that were more commonly used in domain-specific visualization (e.g., electronic circuit diagrams) and visualization for the masses (e.g., road signs). Such design options normally feature metaphoric pictograms that are easy to learn, remember, and guess. This led to a decision to base the visual design primarily on metaphoric glyphs.

Metaphoric glyphs can come in different forms, ranging from abstract representations to photographic icons. I ruled out the abstract representations shown in Column 8 of Table 4.1 because it would still suffer from the difficulties to learn, remember and guess. I ruled out the use of photographic icons because they would prevent the effective use of the colour channel for other attributes. Furthermore, the player or team featured in the glyph would at its best attract unnecessary attention, and at its worst would cause some confusion with the actual player and team being annotated. Once excluded both ends of the design spectrum, we considered several styles of illustration as shown in Figure 4.2. After consulting with the end users, we selected black silhouette as the graphical style of our metaphoric glyphs.



**Figure 4.2:** Some designs of metaphoric pictograms. In (a), initial stickmen designs were produced to prompt an artist. The artist produced several different designs: (b) a refined stickman design, (c) a contemporary design, (d) a posterized colour design and (e) a silhouette design. In (f) the scrum is depicted using the silhouette design (cf. (a) and (b)).

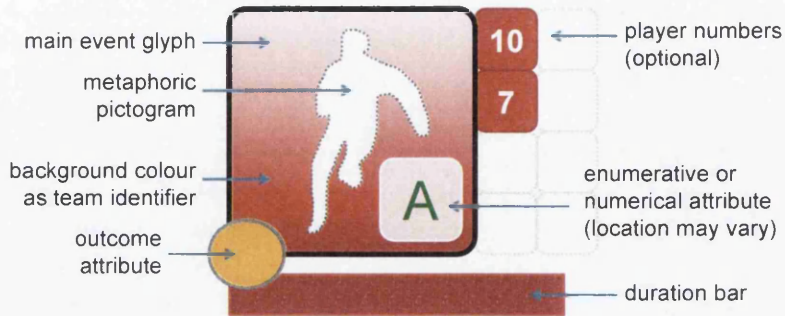
#### 4.4.3 Resultant Design for *MatchPad*

Figure 4.3 illustrates the spatial composition of glyphs designed for the *MatchPad*. The large square region is the main glyph, which contains a pictogram that represents an event type metaphorically. The set of pictograms frequently used in the *MatchPad* are shown in Column 7 of Table 4.1.

The background colour of the main glyph is used to indicate the team. The most commonly-used colour convention is red for the home team and blue for the away team. Hence all glyphs that depict events at the team level and player level are coloured-coded in either red or blue background, while all glyphs associated solely with the match-level have a grey background. To further enhance the clarity of the visualization, we also use spatial positioning to distinguish the two teams. Separating by a horizontal time line across the centre of the visualization, all home team events appear above and away team events appear below. This arrangement is designed particularly for this application. In comparison with mingling all glyphs together, the separation makes it easier for the users to identify the formation and tactics of either team, and to focus on the interaction between the two teams (rather than individual players).

As mentioned earlier, player identifiers are normally annotated by the match analysts only in post-match analysis. Hence it is optional to visualize player identifiers in conjunction with an event. If the player identifiers are available, a player's number is displayed in a small square along the right edge of the main glyph. In addition, this number is also used to distribute glyphs vertically within the team region.

As shown in Figure 4.3, the duration attribute is depicted by the length of the bar that appears below the pictogram box (in the case of the opposition team this bar appears



*Figure 4.3: Components and visual channels of the glyphs.*

above the pictogram box). When a glyph is placed in the visualization along a timeline, the bar length corresponds to the start, duration and end times in relation to the time line. An alternative approach for depicting the duration would be using a clock face [Ber83]. However, this notation would not be as easy to quantify as the duration bar.

Outcome is depicted by a coloured circle placed at the interaction between the main glyph and the duration bar (Figure 4.3). The circle is coloured in either green or amber to represent success or failure respectively. Since red is already used to represent the home team, there was a question about the multiple uses of the shade of reddish colours. However, because of the strong association between green being successful and red being unsuccessful, we decided to maintain the use of a reddish colour for unsuccessful outcome, but to alleviate the conflict by using an orange shade instead of red. This green-amber scheme allows us to make use the metaphor of traffic lights. One psychological advantage of using amber instead of red is to make an unsuccessful event as a warning rather than a failure. In addition, by overlaying a circle at the intersection between two rectangular shapes, the design offers further geometric cues for differentiation.

Some events have a visually similar form. For instance, conversion, penalty, and drop goal all involve kicking the ball at the goal. It would be difficult to design pictograms to differentiate these events through different illustrations. It is more effective to make use of textual labels, e.g., C, P and D, in conjunction with a generic pictogram for all three events that defines “goal kick”. In some other cases, there is a need for indicating additional information in numerical, textual or symbolic form, such as showing which part of the pitch an event takes place (territory A-D), different decisions by a referee (no card, yellow card, or red card), and so on. We refer to such additional information as enumerative and numerical attributes. The depiction of these attributes is placed within the boundary of the main glyph, and their locations vary according to the generic pictogram shared by each sub-group of glyphs. The attributes are usually shown in 1 or 2 numerical, textual or symbolic characters. Four colours may be used, three generic colours, black, white, and green, and one team colour, either red or blue.

The use of different colours, location and occupation styles, ensures that each sub-group that shares a common pictogram does not share the same visual representation of enumerative and numerical attributes as any other sub-groups. This extra differentiation in visual coding serves as an error detection and correction mechanism as described in [CJ10]. Note that other attributes, such as team and player identifiers and outcome, are also of an enumerative and numerical nature. Because of their frequent occurrence and semantic importance in this application, we created separate visual channels for these attributes.

Although glyph-based visualization is the main focus of this work, we are careful not to overload the glyph-based visual design. In particular, we make use of other visual designs for depicting information considered to be coarser or finer than the above-mentioned events. Since rugby can have many stoppages, we use a pale green background to indicate “Ball in Play” events (shown in Figure 4.7). This avoids the excessive use of the “Ball in Play” glyph, while providing a clearer overview of the global game pattern “at a glance”.

Rugby is a game that involves much strategic planning and tactical play. Coaching staff and match analysts have a huge interest in the progress of the game play. Analysts normally record a match in phases, each of which typically lasts for 10-15 seconds. A phase corresponds to the time intervals between tackles or similar events during an attack. For example, when a ruck or maul occurs, the previous phase ends and a new phase begins. Initially we considered using a numerical attribute to indicate phase 1, phase 2, and so forth. However, this approach would require the use of many glyphs and rely on the users’ cognitive reasoning to connect different glyphs together to establish a mental picture of phase progression. Because the relatively fine details about the phase are particularly important to the users, we make use of a step-like notation, as shown in Figure 4.7, to depict the number and progression of consecutive phases in an attack. The steps not only provide a scalable depiction of the number of phases, but also metaphorically conveys the sense of intensity of an attack. As with the event glyphs, either a green or amber circle will appear in the corner to indicate successful or unsuccessful play (e.g., whether the team have managed to push forward and gain territory on the pitch).

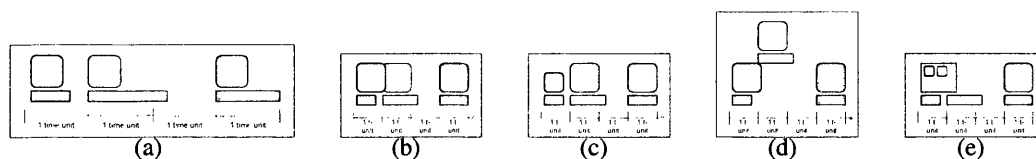
## **4.5 Visualization Interaction**

One of the requirements of the *MatchPad* is to support rapid information seeking, which involves an extensive amount of interaction for browsing and zooming, and requires a very fast layout algorithm to respond to the user’s interactions.

### **4.5.1 Interactive Visualization**

Since the *MatchPad* is designed primarily for tablet devices, we incorporate intuitive controls for touchscreen interactions. The user navigates forward and backward along





**Figure 4.4:** Scale-adaptive layout for key events. In (a), the key events are shown at a scale where no overlap occurs. As the user condenses the visualization timeline for an overview, the algorithm determines the most suited layout for each glyph. In (b), the glyphs are stacked horizontally. In (c), the glyphs are scaled based on their duration. In (d), the glyphs are stacked vertically. Finally, (e) combines two (or more) events to generate a new macro glyph that is used in place.

the timeline by sliding one finger across the screen, and can make a two finger pinch to zoom in and out of the timeline. To facilitate rapid information seeking, the user can skip by a set time period (e.g., 5 minutes) by tapping two fingers to the left or right of the display. A three finger tap will skip to the most recent event. In addition to this, the user can also expand (or condense) the timeline horizontally using a slider.

There may be occasions where many events occur within a short period of time. When the timeline is condensed, this could result in cluttering and occlusion. Therefore a glyph placement algorithm is required that can adapt the layout quickly to accommodate the new scaling factor. This is particularly important for in-match analysis, when the analyst often needs to glance back at a period of time and then to focus back on the present action.

## 4.5.2 Scale-Adaptive Layout

Each glyph is positioned primarily according to the time when the corresponding event took place. Hence in principle, its horizontal position defined by the left boundary of the main glyph box is fixed along the timeline. If player numbers are available in the annotation, we make use of a hashing function based on these numbers to distribute glyphs vertically. However, as mentioned previously, for real time annotation during a match, such information is normally not entered. The glyphs are thus, by default, placed on one of the three lines, namely home team above, match level in the middle and away team below. When a time-line condensing action is performed, the space allocated to each glyph becomes smaller, resulting in cluttering and occlusion. One naive solution is to reduce the size of glyph based purely on the zoom-factor. However, the glyphs could quickly become too small to be understandable. Hence the goal of the placement algorithm is to determine the appropriate size and position of each glyph in order to maintain clarity while preventing serious cluttering and occlusion.

Figure 4.4 illustrates a typical scenario, where the timeline is condensed to 50%

of the original length. So to preserve visual association of events, the visualization is continuously scaled between four transitional layouts (Figures 4(b-e)). Once the given threshold is reached for one layout, the algorithm will query the next layout for additional size and positioning. The four layouts are:

- *Horizontal Stacking*, which maintains the default glyph size and positioning for the current zooming factor, but can introduce occlusion of the events.
- *Size Reduction*, which resizes the glyph based on the event duration and the current scaling factor.
- *Vertical Stacking*, which adjusts the vertical position of the glyph based on the current scaling factor.
- *Macro Glyph*, which combines a set of glyphs into a macro that visually replaces the glyphs within the macro.

Figure 4.5 shows the algorithm in pseudo-code. We adopted a deterministic process as it is generally much faster than a global optimisation approach. We consider four options in the order of preference and evaluate each option based on the level of occlusion. The algorithm requires several parameters adjustable by the users. They are the minimal amount of visibility for horizontal stacking (`MINH_VISIBILITY`), scale reduction (`MINS_VISIBILITY`) and vertical stacking (`MINV_VISIBILITY`). The visibility values are in percentage of glyph area (by default, 0.5, 0.25 and 0.5 respectively).

## 4.6 Case Study: Welsh Rugby Union

We spent a year working with the performance analysts of the Welsh Rugby Union to develop the *MatchPad*. They contributed to all stages of the design and evaluated the *MatchPad* throughout its development. The primary focus was to deliver an application that would integrate with their current workflow and allow them to visually explore the huge amounts of event records. It also played an integral part during their Rugby World Cup 2011 campaign (Figure 4.6). Two annotated screen shots are given in Figure 4.7. After the tournament, the team provided us with their feedback.

*“The main thing for us is visualizing the data and visualizing it in a very easy to interpret manner. The major benefit of the MatchPad is that it gives us a good overview of how the game is going, because when you are looking at the game in such detail you lose sight of the big picture. In particular, it is a great tool for oversight when matches are very intense, and for looking at the key instances of the game and how they interact with each other. With the iPad, it is portability. We have it with us all the time so when the coach wants to know something we can see it immediately on the MatchPad.”*

**Algorithm** setScaleAdaptiveLayout(*zoom\_factor*)

---

```

1: display_glyphs_inview()
2: change = false
3: for (each glyph, g[i], in view) do
4:   compute_visibility(g[i])
5:   if (g[i].visibility < MINH_VISIBILITY) then
6:     reduce_size(g[i], zoom_factor)
7:     change = true
8:   end if
9: end for
10: if (change == true) then
11:   display_glyphs_inview()
12:   change = false
13:   for (each glyph, g[i], in view) do
14:     compute_visibility(g[i])
15:     if (g[i].visibility < MINV_VISIBILITY) then
16:       assign_yoffset(g[i], zoom_factor)
17:       change = true
18:     end if
19:   end for
20:   if (change == true) then
21:     display_glyphs_inview()
22:     change = false
23:     for (each glyph, g[i], in view) do
24:       compute_visibility(g[i])
25:       if (g[i].visibility < MINV_VISIBILITY) then
26:         generate_macro_glyph(g[i], zoom_factor)
27:       end if
28:     end for
29:   end if
30: end if

```

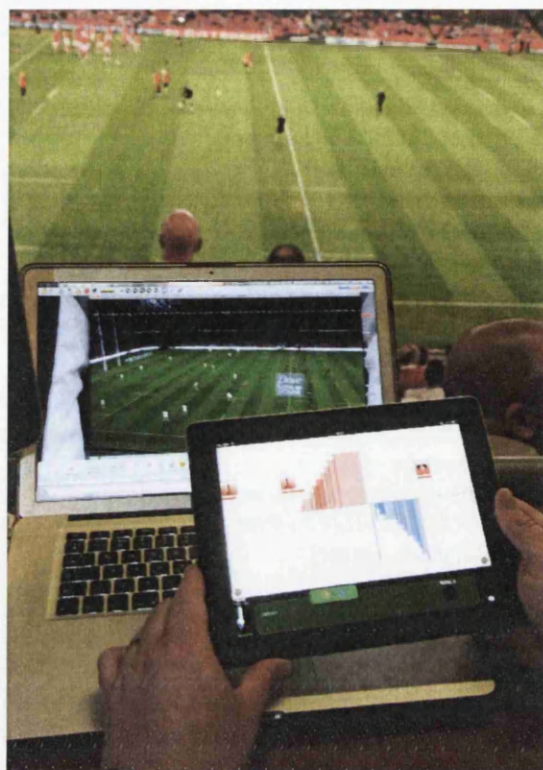
---

*Figure 4.5: Pseudo-code for the scale-adaptive layout.*

Further feedback confirms that the *MatchPad* successfully fulfils all the requirements of Section 6.2 – providing use scenarios such as in-match focus and context, half-time discussions with players (including access to video) and post match detailed analysis. Most of all, players and coaches are able to use the app with little or no training due to the metaphoric approach taken in the design and the intuitiveness of the software combined with the iPad.

## 4.7 Discussion

In this chapter, we have presented a design study on visualizing events and actions “at a glance” for real-time sports performance analysis. In particular, we investigated the use



*Figure 4.6: MatchPad being used by the Welsh Rugby Union.*

of metaphoric pictograms to represent events over other possible glyph designs such as abstract icons, shape, and colour. From this, we delivered *MatchPad*, a system that was effectively used by the Welsh Rugby Union for match analysis. Further evaluation of the system was conducted by means of a consultation meeting with a group of sports science students (5 male and 3 female) with various levels of notational analysis understanding.

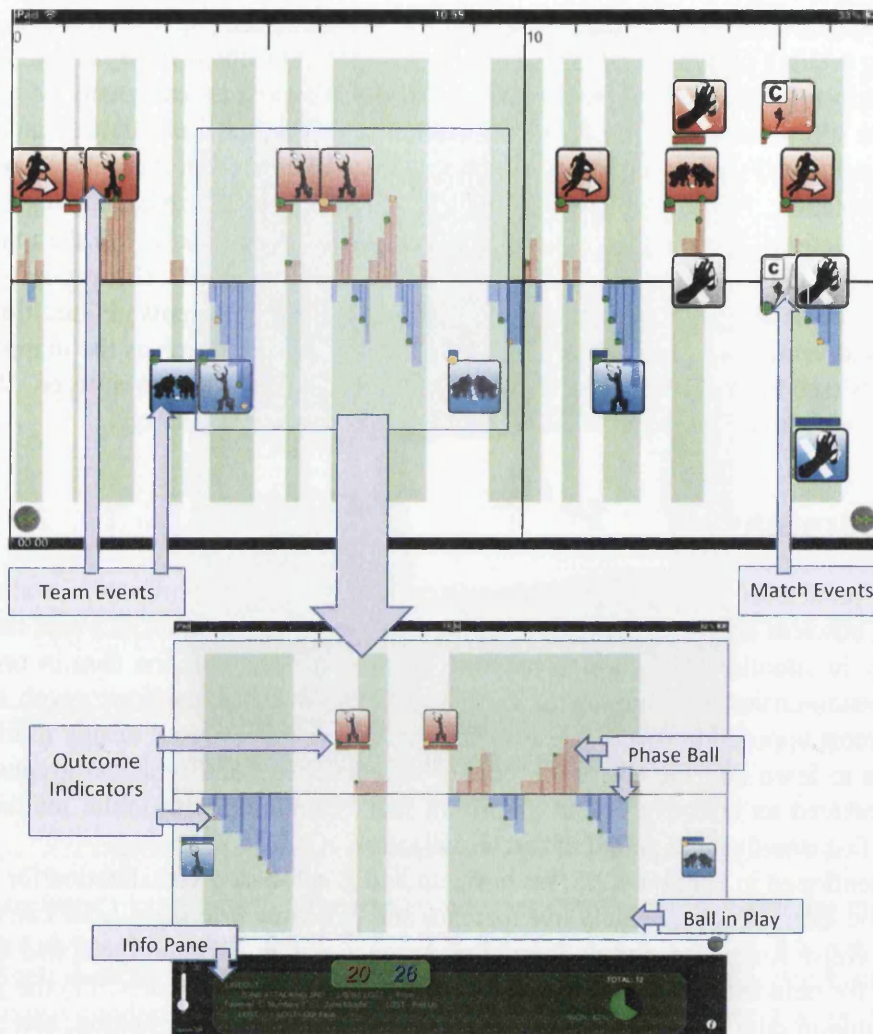
We focused on three aspects: whether the *MatchPad* improves upon existing systems, the glyph design used for notational analysis, and potential areas of improvement. All participants felt that the summary overview gave greater visual clarity than other notational analysis systems (e.g., SportsCode) and was more suitable for rapid in-match decision-making. Most participants rated it as a significant improvement over existing systems. To evaluate our glyph design for encoding events, we presented the participants with the options shown in Table 4.1. All participants agreed that metaphoric glyphs were by far the best approach for representing the events. The metaphoric glyphs were intuitive to interpret, whereas other designs (e.g., abstract icons, shape, and colour) would require significant learning, causing potential misunderstanding. For improvement, the group suggested that further statistical analysis such as live possession would be beneficial. It was also suggested that spatial information and “off-ball” positioning should be displayed (although this data is not currently collected by notational analysis). We

will look at exploring this challenge in Chapter 5. Another good suggestion was to show how many events a player has been active in, so to highlight the possibility of fatigue and need for substitution. Finally, the group felt that the *MatchPad* could easily be used in other team sports such as football, netball and hockey. The interchangeable framework of the *MatchPad* (Figure 4.1) means simply requiring a new event dictionary and icon set for adaptation. At the glyph design level, it would first involve establishing a set of events and actions, levels of association, and outcomes for the sport. We then need to create a set of intuitive metaphoric pictograms that can be mapped. This process could potentially be expensive depending on the number of different events. In addition, the glyph-based visualization may also need to be further modified such as the mapping of phase balls (see Figure 4.7) in sports that do not have an equivalent event type. We are now working with a Championship football club to adapt the *MatchPad*.

## 4.8 Summary

From the process of developing the *MatchPad* we found that glyph-based visualization offers an efficient and effective means for conveying a large amount of event records, especially in situations where users need to gain an overview of the data in order to make mission-critical decisions with very limited time. The metaphoric glyph design was the most appropriate for this particular application. This visual design minimises the needs to learn and memorise the coding scheme associated with the glyphs. We also introduced an effective layout algorithm that “combined with tablet interaction” provides fast intuitive navigation of the visualization.

As mentioned in Section 4.2.2, we have studied glyph-based visualization for a specific application in rugby, namely live matches and half-time briefings. After consulting with the Welsh Rugby Union, we found that in practice, our current glyphs had limited usability for detailed post-match analysis. There were two main issues: (1) the glyphs did not support data outside notational analysis such as spatial information, and (2) the ability to make different comparisons between events and their associated attributes directly on the glyph. This motivated the idea that glyphs need to be designed so that they can be sorted better, which we will discuss in the following chapter.



**Figure 4.7:** Screenshots of the MatchPad. **Top:** Overview of a 17 minutes period from a match using the MatchPad. Match and Team events are depicted using metaphoric pictograms that are instantly recognizable. Home team events are shown in red, above the centre line, and away team events are shown in blue below the centre line. The user can also choose whether to show critical match events such as scoring events and referee decisions on the centre line due to their high importance. **Bottom:** Zoomed-in view on a region of the visualization. Phase ball actions are shown using coloured regions sized dependent on duration and phase count. Outcome indicators for positive or negative results are shown using green and amber circles respectively when the information is available. Ball in Play events are shown by the pale green background on the timeline. The information pane at the bottom of the screen provides more in-depth detail for a particular event when selected by the user.



---

## Glyph Sorting: Interactive Visualization for Multi-dimensional Data

---

### Contents

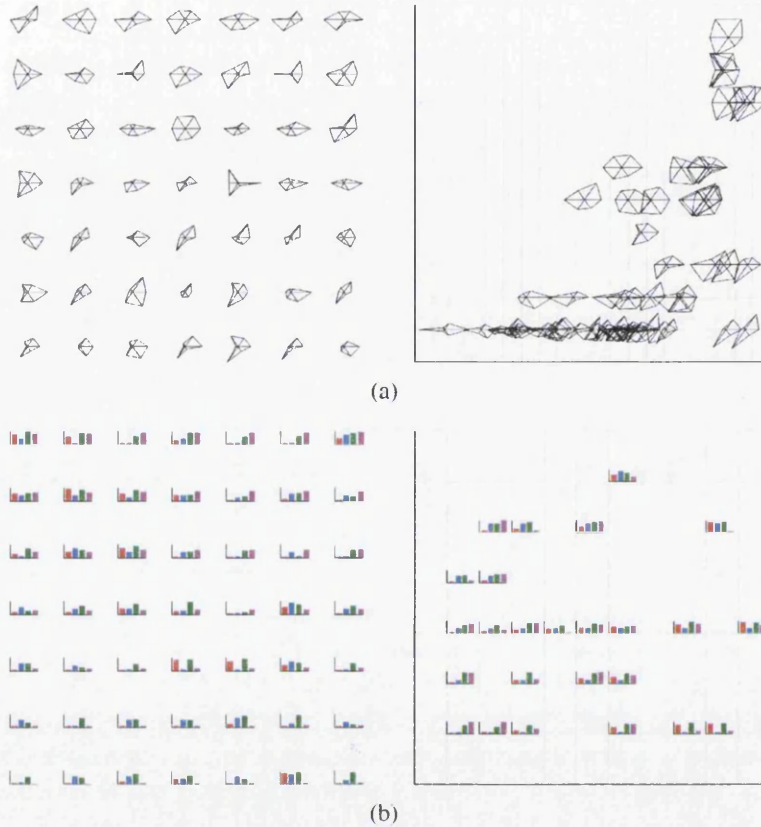
---

|       |   |     |
|-------|---|-----|
| 5.1   | Introduction . . . . .                              | 93  |
| 5.2   | Sorting: Entities and Sort Keys . . . . .           | 96  |
| 5.3   | Design Principles of Sortable Glyphs . . . . .      | 97  |
| 5.4   | Interactive Glyph-based Visual System . . . . .     | 100 |
| 5.4.1 | Focus and Context Glyph-based Interface . . . . .   | 100 |
| 5.4.2 | Interactive, Multi-dimensional Glyph Plot . . . . . | 102 |
| 5.4.3 | Hierarchical Axis Binning . . . . .                 | 102 |
| 5.5   | Case Study: Sports Event Analysis . . . . .         | 105 |
| 5.5.1 | Visual Mapping of Sort Keys . . . . .               | 105 |
| 5.5.2 | Visual Comparison of Two Matches . . . . .          | 107 |
| 5.5.3 | Domain Expert Review . . . . .                      | 111 |
| 5.6   | Discussion . . . . .                                | 112 |
| 5.7   | Summary . . . . .                                   | 113 |

---

**T**HE design of metaphoric glyphs in the previous chapter showed how glyph-based visualization can be effectively used to convey a large amount of event records. Semantic visual channels (e.g., pictograms) minimise the need of memorising and learning encodings in glyphs, and can lead to instant recognition of semantic data such as events and actions. One problem highlighted with the use of these glyphs is the ability to compare multiple values across different data records, and how the glyphs may





**Figure 5.1:** Visual representation of two example multi-dimensional glyphs, namely (a) Star glyphs and (b) Bar chart glyphs when glyphs on the left are unordered, in comparison to glyphs on the right which are ordered to two sorting parameters.

be ordered according to these attributes. Since the glyphs are arranged along a timeline, it is easy to see how they are ordered in terms of their temporal occurrence (e.g., the spatial position), but this is not so obvious if we were to focus directly on observing the visual parameters on the glyph. As sorting is one of the most common analytical tasks performed on individual attributes of a multi-dimensional dataset, this motivates the hypothesis that introducing glyph sorting would significantly enhance the usability of glyph-based visualization.

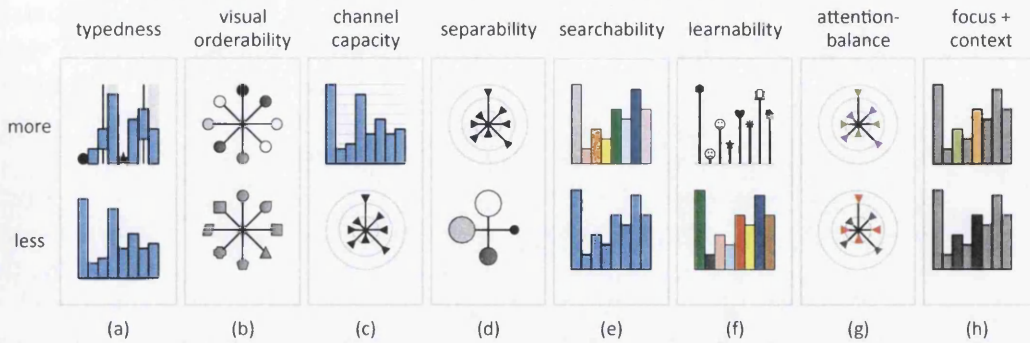
Sorting large, multi-dimensional data is a growing consensus in modern data acquisition and processes where the ordering of data is an integral part of many applications and disciplines, ranging from the analysis of scientific information (e.g., using graphs and charts), to enhancing the efficiency of algorithms. The work in this chapter investigates how we can use glyphs to support such a sorting process. Records of data are traditionally sorted analytically in a data-driven manner (e.g., via spreadsheets), where users perform sorting on individual attributes of a multi-dimensional data set. This is a

non-trivial task due to the large number of possible permutations of sorting which can greatly impact the expressiveness of high dimensional visualizations [YPWR03]. When data must be ordered using a high level of sorting, it reveals two important challenges: 1) how the data is organised, and 2) the ordering of sort keys, which can not be easily observed by viewing large tables of data.

Glyphs can be used to improve the perception of data characteristics [War02]. Chernoff Faces [Che73] and Star Glyphs [SFGF72] are some examples of multivariate glyphs where identifying glyphs with similar features is effective, but cognitively challenging when determining the ordering of glyphs. Thus, such glyphs are not visually sortable in an obvious way. This becomes a greater challenge when glyphs are unorganised. Figure 5.1 demonstrates how ordering such glyphs in a given spatial configuration is more informative in revealing multivariate trends. Glyph sorting is one approach for performing interactive sorting of multivariate data as part of a visualization process. As a data exploration mechanism, interactive sorting in visualization provides the following additional objectives: 1) making observations about data patterns (e.g., clusters and distributions) in relation to a sorted variable and stimulating hypotheses about other variables. 2) performing analytical tasks and visual evaluation of hypotheses, such as what variables may affect the ordering of a specific variable.

In this chapter, we present a novel glyph-based sorting framework to drive and facilitate interactive sorting of data in a visual and intuitive manner. We examine several technical aspects of glyph sorting and provide a set of design principles (Section 5.3) for developing effective, visually sortable glyphs. Glyphs that are visually sortable enhances the usability of glyph-based visualization for both comparative analysis of multivariate data and for supporting visual search. In Section 5.4, we present an interactive glyph-based sorting system. Novel features of the system include a focus and context glyph-based user interface (Section 5.4.1) to control high-dimensional sorting and viewing sorted results in a linked *Interactive, Multi-dimensional Glyph* (IMG) plot (Section 5.4.2). We extend traditional axis mapping using hierarchical axis binning (Section 5.4.3). This enables visual depiction of multiple sort key parameters in space, which is effective for reducing visual clutter in the IMG plot view. Following the success of our *MatchPad* system, we continued working in close collaboration with the Welsh Rugby Union throughout the development of this work. We present a real-world case study in rugby event analysis for analysing and comparing trends between matches. From using glyph sorting, the analysts report the discovery of new insight and knowledge beyond traditional match analysis. The main contributions of this work include:

- The introduction and development of high-dimensional, focus and context glyphs that are visually sortable to support sorting of multivariate data.
- A novel glyph-based, interactive system for controlling high-dimensional sorting and viewing sorted results.
- A hierarchical axis binning method for encoding multiple dimensions onto a single



**Figure 5.2:** Variations of glyph design in accordance with the design principles of sortable glyphs (a)-(h). For each principle, the top row depicts a glyph with greater emphasis and the bottom row depicts a glyph with less emphasis.

axis. This effectively reduces visual clutter by relaxing the positioning of glyphs.

- An evaluation of the effectiveness of glyph sorting in a real-world case study of sports event analysis.

## 5.2 Sorting: Entities and Sort Keys

Sorting is the most common analytical task which is used for re-organising entities consisting of single or multiple fields [Knu98]. The objectives of sorting can be classified into the following:

- *Ordering* - arranging entities of the same type, or class into some ordered sequence.
- *Categorizing* - grouping or labelling entities with similar properties through sorting.

Many sorting algorithms have been proposed, including bubble sort by Demuth [Dem85], merge sort by von Neumann [Knu98], and quick sort by Hoare [Hoa62]. Since best and worst case performance runtime can vary drastically with such algorithms, further research continues to propose new sorting techniques [BFCM06] and adaptive approaches that utilise ordered data [ECW92]. Our work is not focused on a faster sorting algorithm per se, but combining the benefits of sorting with glyph-based visualization.

A sort operation can be performed based on one or more attributes. We describe such attributes as *sort keys*. In more general form, let us consider the set of objects or entities  $E = (e_1, e_2, \dots, e_s)$ , each containing a set of attribute keys  $K = (k_1, k_2, \dots, k_n)$ .

This defines a  $n$ -dimensional attribute space which governs the sorting process. Thus,  $e_i$  is a  $n$ -tuple or contains a  $n$ -tuple (as  $e_i$  may have additional information such as a video clip). For example, a group of entities  $E$  may be classified as a pack of cards (52 entities) which is sortable by keys  $K$ , such as card type (e.g., spades, clubs, diamond, and hearts), colour (e.g., red or black) or by value (1-13).

In order theory, we can specify two types of ordering relations: a weak (non-strict) order denoted by " $\preceq$ ", or a strict ordering " $\prec$ ". These two properties characterise the mathematical concept of linear ordering [Knu98]. Given a subset of keys  $\kappa \in K$ , the goal of sorting is to arrange the entities  $e_i$  into an ordered set (a list) such that  $e_1^\kappa \prec e_2^\kappa \prec \dots \prec e_s^\kappa$ . At the level of abstraction, sort keys as attributes can not be directly compared (i.e., by arithmetic  $=$ , and  $<$ ,  $>$ ), as they are essentially concepts. Hence, we introduce the notion  $f^\kappa : E \mapsto \mathbb{R}$ , that maps the object space with context keys  $\kappa$  to a real value such that for any entity pair,  $e_i, e_j$ , the ordering relation  $e_i^\kappa \prec e_j^\kappa$  implies:

$$f^\kappa(e_i) < f^\kappa(e_j) \quad \forall i, j = 1, 2, \dots, n. \quad i \neq j$$

With additional semantics, one can define such a function  $f^\kappa$  to sort data (e.g., events) into more practical, or memorable orderings beyond common sorts (e.g., alphabetical), since  $f^\kappa$  could be an importance function consisting of several sort keys. However, this may cause data to lose its perceived ordering at the analytical level. We introduce glyph sorting as one solution for performing interactive sorting in visualization, where one goal is to use glyphs to sort the data.

### 5.3 Design Principles of Sortable Glyphs

The design of glyphs is the process of encoding attributes of a data entity to a number of *visual channels* such as size, colour, and texture that forms a small visual object. Building on previous works [Ber83, War08a, MPRSDC12], we propose the following design principles for the creation of sortable glyphs to be used in interactive sorting as part of a visualization process.

**Typedness:** Each dimension in a multivariate dataset may be of a different data type. Typically, these are classified using the theory of scales [Ste46] by: *nominal*, *ordinal*, *interval*, and *ratio*. In addition, *direction* - a 'sign' that denotes the directionality of a component (e.g., a vector arrow) should be considered as an important data type in visualization [War08b]. Although hypothetically, we can map all data types to one or a few visual channels, such as length and size, it is more appropriate to use visual mappings that intuitively convey the underlying data type. For example, in Figure 5.2(a) it is clearer to determine the underlying data types for each dimension in the glyph from the top row (that illustrates greater emphasis) than the bottom row (that illustrates less emphasis). We can visually guess the first and fourth dimension (or attribute) to be of either ordinal or nominal type more easily in the top glyph, since shape is perceived as a

discrete mapping. Similarly, the third and seventh attribute is of interval type due to its length and position. This cannot be distinguished from the bottom glyph.

**Visual Orderability:** Some visual channels (e.g., size, greyscale intensity) naturally correspond to quantitative measures that enable a viewer to order different glyphs perceptually, while some others (e.g., an arbitrary set of shapes, or textures) are much more difficult for viewers to establish a consistent rule of ordering [War08b, War04]. Figure 5.2(b) shows two example glyphs depicting 8 variables of the same data type. It is easier to visually order the 8 variables in the top glyph, than the bottom glyph. Additional semantics can be attached to a visual channel such that it becomes visually orderable. For instance, scientists often make use of the colour spectrum to determine the order of colours, which may not be natural to a child who is unfamiliar with this concept. In some cases, one may have to use a visual channel with very poor orderability such as metaphoric pictograms. The problem can be alleviated by accompanying such visual channels with an additional channel that is more visually orderable. For example, different pictograms can be associated with a background of different greyscales, or a regular polygonal boundary with different number of edges. Alternatively, one may carefully design the pictogram set to make some components of pictograms orderable. For example, Maguire *et al.* designs a set of 7 pictograms with incremental number of components to encode levels of material granularity in biology [MPRSDC12].

**Channel Capacity:** We adopt this term from information theory to indicate the number of values that may be encoded by a visual channel. It is necessary to note that such a capability value is not an absolute quality, as the number depends on the size of a glyph as well as many other perceptual factors such as just noticeable difference [BF93], interference from nearby visual objects, or from a co-channel in an integrated channel [She64, HI72]. From the glyph designs in Figure 5.2(c), we can clearly observe that the top glyph has a higher channel capacity since each bar can encode more values visually (e.g., length, size and colour) than the radial lines below in which size is not possible. It will always be desirable to use a visual channel with a higher capacity, though this is often in conflict with other requirements.

**Separability:** There have been many psychology studies on the relative merits of separable and integrated visual channels (e.g., [She64, HI72]). Maguire *et al.* discuss this requirement in the context of glyph design in [MPRSDC12]. We find that this requirement is particularly important to glyph sorting. For example, in Figure 5.2(d), the glyph below encodes 8 variables using 2 integrated channels. Each of the 4 circles encodes two variables using size and greyscale intensity. The constructive composition of integral visual channels makes it more difficult to visually separate in comparison for example, the top glyph, where each variable is mapped to radius length and position. Not only is the perception of one individual channel affected by another in an integrated encoding, but

also their ordering may demand more cognitive load in order for a viewer to detach one channel from another (e.g., intensity and size).

**Searchability:** For glyphs encoding high-dimensional multivariate data, it is necessary to help viewers to search rapidly for a specific variable among many other variables [War08b]. In Figure 5.2(e), for example, it will be much easier to search for a green *variable* than the 5th *variable*. Searchability is affected by many factors [HE12]. One dominant factor is the visual dissimilarity of individual channels. Hence searchability is closely related to *typedness* and *separability* as mentioned above. It is also related to the spatial organisation of different visual channels such as grouping and ordering, as well as design appearance of each visual channel. In many cases, one has to introduce an additional visual channel, such as colour in the top glyph in Figure 5.2(e) to help differentiate different variables. Another factor is learnability, which is to be discussed below.

**Learnability:** While legends are usually essential to glyph-based visualization systems, they cannot replace the need for careful glyph designs to help viewers learn and memorise the association between dimensions and visual channels without constantly consulting legends. It is desirable for the appearance of a visual channel to be metaphorically associated with the semantic meaning of the corresponding dimension [War08b, SJAS05]. One of the most effective metaphoric designs is to use pictograms. This design principle was demonstrated by Legg et al. [LCP\*12] through the deployment of glyph-based visualization in sports. Figure 5.2(f) shows two different levels of learnability, when for example one needs to encode the number of greeting cards in different categories. The glyph on the top row is semantically rich and is much easier to learn than that on the bottom row. However, not all glyph-based visualization can afford pictograms. These constraints can often be alleviated by making abstract metaphoric association, such as green for nature, renewable, safe, and so on.

**Attention Balance:** In multivariate visualization, one common task is to make observation of the “*behaviour*” of different attributes in relation to the attribute(s) in a sorted order. While it is helpful to make each individual attribute searchable [TCW\*95, War08b], it is also necessary to avoid unbalanced attentiveness among different channels. For example, the bottom glyph in Figure 5.2(g) features bright red indicators for some variables. When browsing different glyphs in visualization, these red triangles are dominant which may cause undesirable pop-out effects.

**Focus + Context:** In multivariate visualization, it is usually difficult, often undesirable, to pre-determine what is the focus attribute and what is the context attribute. For example, Straka *et al.* [SCC\*04] display glyphs as the foci simultaneously with the underlying bone structure (i.e., the context) in CT-angiography by varying levels of opac-

ity. We propose this can be applied to individual attributes of a multi-dimensional glyph. Naturally, in glyph sorting, a attribute that is associated with a sort key is considered as one of the foci. In some cases, the viewer may wish to consider another attribute as a focus. Hence, it is desirable for a glyph sorting system to support focus+context visualization by highlighting individual channels that are in focus. Figure 5.2(h) shows two different methods of highlighting the third and fifth bar using colour and greyscale intensity. Since colour is more visually dissimilar, it is easier to identify the attribute foci in the top glyph than the bottom glyph. This can be expensive, because in the worst case, each visual channel is accompanied with another channel as a highlighter.

**Labelling and Legends:** Axis-labelling is an essential requirement for any sorting configuration for indicating sort keys [WGK10]. It enables the viewer to understand the context (e.g., frequency vs. amplitude in sound analysis) without referring to the visualization itself. Bertin [Ber83] refers to this as external identification. Legends convey the relationships between dimensions and visual channels and its representation for a given discrete or continuous value. This is often known as internal identification [Ber83].

These design principles are general guidelines that we consider when designing glyphs to be sorted interactively in visualization. However, they should not be treated as the absolute laws. Some cases may lead to conflicting requirements when following some of these principles, or compete for limited capacity of visual channels for smaller designs.

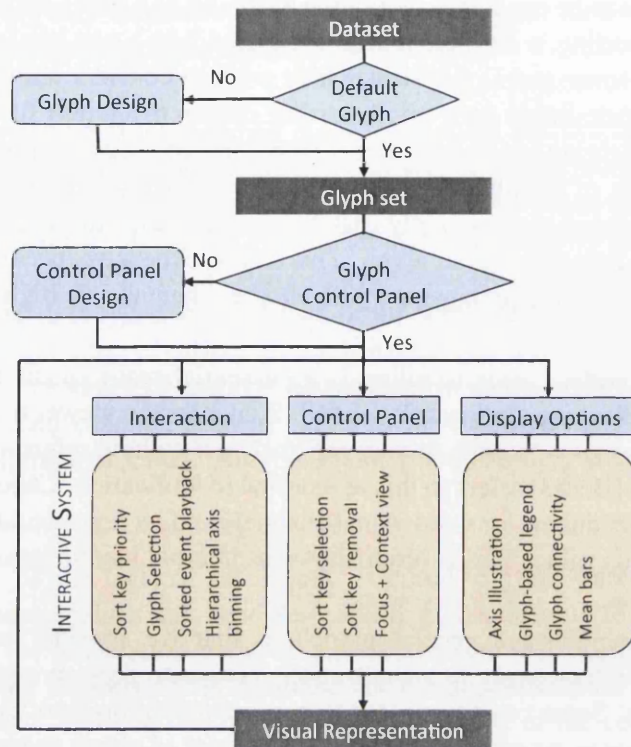
## 5.4 Interactive Glyph-based Visual System

In this section, we propose a interactive glyph-based visualization system for performing high-dimensional sorting as outlined in Figure 5.3. The system integrates two fundamental components: 1) a glyph control panel for selecting and driving the sorting process in a visual manner, and 2) an Interactive, Multi-dimensional Glyph plot for viewing sorted results.

### 5.4.1 Focus and Context Glyph-based Interface

Figure 5.4 shows a focus and context glyph-based user-interface which the system incorporates for selecting sort keys. The interface provides two main benefits. It allows users to interactively control the sorting process by populating sort keys within the linked IMG plot in a visually intuitive manner. Secondly, the focus and context glyph gives a visual reference which allows users to rapidly identify and understand the attributes that drive the sorting.

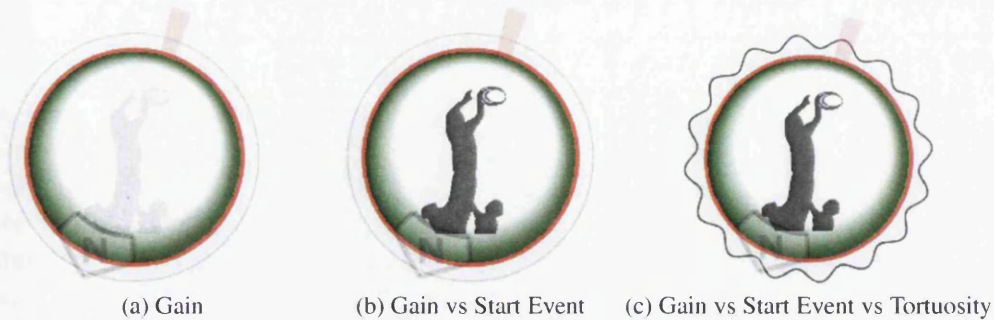
Sort keys are selected in the system by interactively clicking on a visual component of the glyph. The selected visual attribute is then rendered into focus using opacity



**Figure 5.3:** A graphical pipeline illustrating the glyph sorting framework. It consists of four key steps: 1) visual mapping of data to glyphs. We propose general design guidelines for creating visually sortable glyphs to support interactive sorting and multi-variate analysis. Alternatively, a default glyph (e.g., Star glyph) is used. 2) integrating a focus and context glyph control panel for selecting multiple sort keys, 3) constructing the glyph sorting tool which enables users to perform high-dimensional sorting and interactively adjust various display options and 4) visual representation of sorted results on an Interactive, Multi-dimensional glyph plot.

such that the data attribute is visually distinct from other attributes. This is an effective method for emphasising specific parts to the users attention in high-dimensional glyphs. Similarly, users can remove a sort key by clicking on a glyph component in focus and dragging it off the glyph to bring the attribute back into context. By linking the interface with the IMG plot, users are able to populate different sort keys in a visually intuitive manner. Furthermore, we incorporate tooltips into the interface to aid users with information on what attributes is visually encoded in each glyph component.





**Figure 5.4:** A focus and context glyph-based user interface for selecting sort keys. Clicking on a visual component of the glyph highlights that particular sort key in focus.

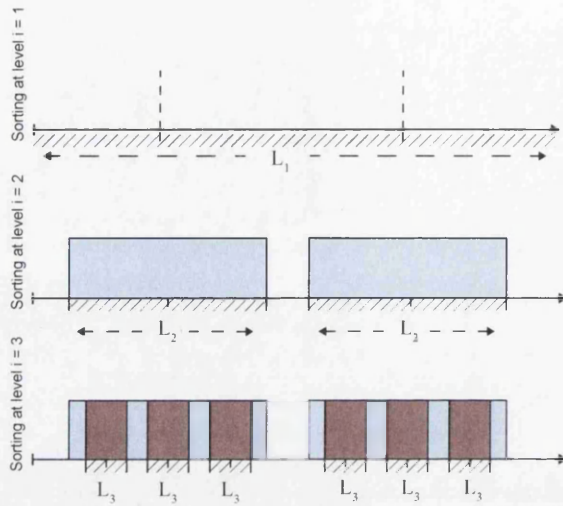
### 5.4.2 Interactive, Multi-dimensional Glyph Plot

Since ordering in a sorting plane is one of the most effective and widely recognised representations for data analysis (e.g., scatter plot), we position the glyphs along the two primary sorting axes. This forms the basis of our Interactive, Multidimensional Glyph (IMG) plot. Following the design principles in Section 5.3, populated sort keys are depicted as focus and context glyphs along each sorting axis respectively (see Figure 5.9 for example) coupled with a visual legend to illustrate how the data is ordered. The sort key priority can be changed interactively by the user via double clicking on the sort key glyph, to either promote (using the left mouse button) or demote (using the right mouse button) the ordering. We integrate a series of interactive tools to aid user exploration: sliders for adjusting axis length, brushing tools for selecting glyphs, pan-and-zoom navigation for details on demand and viewing of additional information (e.g., a video, or image) that may be associated with a glyph.

Visualizing glyphs on a 2D plane imposes additional challenges. One perceptual problem is the order in which glyphs are rendered on the IMG plot. By default, glyphs are rendered sequentially as they occur in the dataset. Depending on the sorting parameters, these will cause different levels of overlap. To alleviate this, we incorporate the ability to sort the rendering order of selected glyphs. This enables the user to emphasise glyphs of greater interest for data exploration. In addition, we provide two display preferences as a user-option. *Connectivity*, for rendering lines that connect glyphs in order of a sorting attribute, and *Mean Bars* which displays the statistical average value of a sorting axis (if applicable) as a coloured band in each hierarchical axis bin.

### 5.4.3 Hierarchical Axis Binning

In data-driven placement, sorting data by discrete variables is a typical operation one can perform. This often leads to an increase in level of overlap due to discrete positioning in the constrained sorting space. Ward [War02] describes a survey on distortion tech-



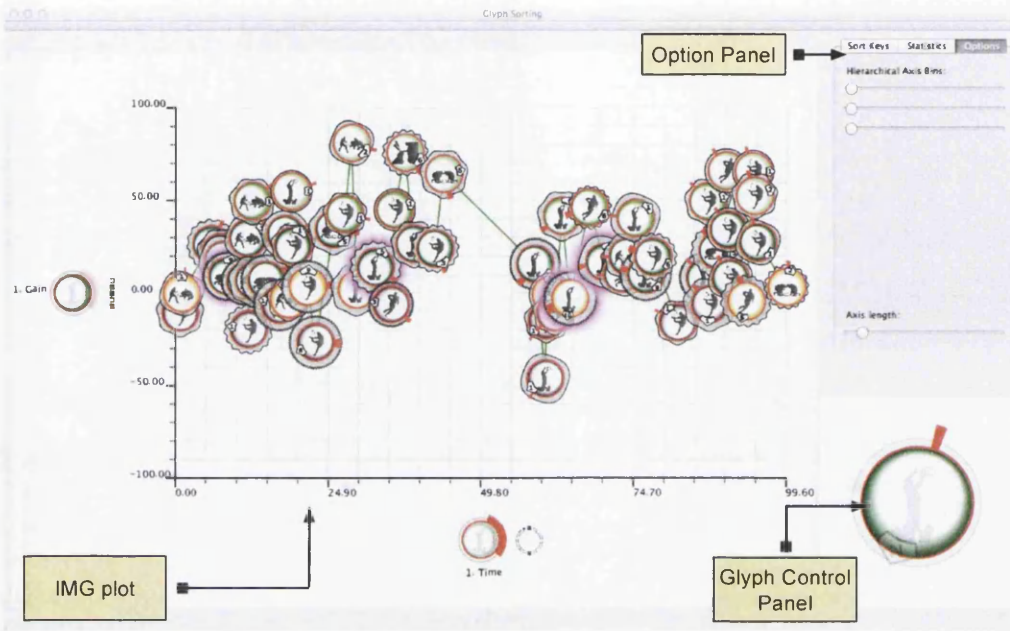
**Figure 5.5:** Diagram illustrating hierarchical axis binning along one sorting axis. Intervals (or sub-regions) at each level of sorting can be sub-divided by different attributes where additional sort functions can be mapped. We note that the axis mapping can be applied along multiple axes.

niques (e.g., random jitter [Cle93]), a post-processing step which can be used to reduce visual clutter by incorporating noise into the glyphs position. A major concern with this approach is the level of distortion introduced can significantly change the interpretation and integrity of the visualization. Another approach includes projecting data using dimension stacking [War94]. However, this does not scale well with sparse datasets.

Hierarchical axis binning is a mapping function to alleviate such a problem by representing multiple discrete variables as regions as opposed to points. Encoding multiple dimensions onto a single axis enables additional sorting functions (e.g., a continuous variable) to be mapped for relaxing the positioning of glyphs along a bounded sub-region. Figure 5.5 illustrates our generalised axis binning algorithm at different levels of sorting which we demonstrate along one axis. However, our technique can be applied over multiple sorting axes. Let  $L$  be the interval  $[L_{\min}, L_{\max}]$  and  $K = (k_1, k_2, \dots, k_n)$  be a set of sort keys we want to order the data by. We define our axis mapping function for a single key  $k$  as the following:

$$h(e, L, k) = \frac{f^k(e)}{\max f^k} ||L|| + L_{\min} \quad (5.1)$$

The linear function first normalises the attribute key and maps this to the region  $L$ , such that if  $k$  is discrete and non-numerical (e.g., name), then  $\max f^k$  is equivalent to the cardinality  $||k||$  of the sort key. For higher order sorting, we expand the region given by each discrete value hierarchically to map additional sort functions. Let us first denote the type of a key as  $k^T$ , where  $T = \{Discrete, Continuous\}$ . Now suppose  $A \in K$  is a ordered sequence of discrete and continuous sort keys. We apply the restriction  $A_i^{T_i} = \{a_1^{T_1}, \dots, a_n^{T_n}\}$  such that  $T_i \preceq T_{i+1}$  for  $i = 1, \dots, n - 1$ , where the condition  $\preceq$  is used to obtain a list where no continuous key directly precedes a discrete key for each sort key pair. With such an ordered list, we can define a hierarchical sorting function for



**Figure 5.6:** A snapshot of the glyph-based sorting system. The software consists of three main interfaces: 1) a glyph control panel for controlling sort keys in a visual manner, 2) an IMG-plot for displaying the sorted results, and 3) an option panel to support interactive exploration. Additional statistical information and a glyph-based legend is displayed through tabbed viewing panels.

mapping and relaxing points along discrete sub-regions recursively by Eq. 5.1. This is generalised to the following form:

$$H(e, L, A) = \sum_{i=1}^n h(e, L_i, a_i) \quad (5.2)$$

where  $L_i$  is the interval at each level. At the sort level  $i = 1$ , our interval is already initialised (i.e., the axis length, where  $L_1 = L$ ). Thus, it is only necessary to determine each sub-region division at successive levels of sorting. The sub-regions are defined as  $L_{i+1} \in [-\delta_{i+1}, +\delta_{i+1}]$  such that:

$$\delta_{i+1} = \frac{|L_i|}{2 \max f^k} \cdot \mu, \quad \mu \in [0, 1) \quad (5.3)$$

in which the coefficient  $\mu$  is used to adjust the maximum length of each sub region. For  $\mu = 1$ , adjacent sub regions touch (connected), while for  $\mu > 1$ , our intervals begin to overlap. Setting  $\mu$  within the interval  $[0, 0.8]$  allows axis binning to interactively expand in visualization, while leaving significant gaps such that each sub-region is visually distinct at all levels of sorting (see Figure 5.9 for example). Since our function is bijective,

it follows that each data point is unique. Hence, the complexity of ordering glyphs with multiple sort keys both analytically and visually is reduced to sorting by a dominance relation (e.g., x and y coordinate).

Given an ordered list of discrete and continuous keys, we can hierarchically build multiple axis bins to facilitate sorting of multiple functions. The user is able to interactively control the amount of spatial relaxation by adjusting two properties: the axis length and the width of axis binning. Each hierarchical axis bin size is altered by varying the sorting parameter  $\mu$  which corresponds to each level of sorting.

## 5.5 Case Study: Sports Event Analysis

We demonstrate glyph sorting on a real-world application in sports event analysis. We have worked in close collaboration with the Welsh Rugby Union (WRU) to develop a software that allows for in-depth analysis of matches (see Figure 5.6). First, we detail the process of mapping attributes to a sortable glyph. We then present a visual comparison of two matches which was conducted by analysts at the WRU. We discuss the knowledge and insight that has been derived as a result of glyph sorting and conclude the study with domain expert feedback.

### 5.5.1 Visual Mapping of Sort Keys

As described in Chapter 4, coaches and analysts heavily rely on notational analysis [HF97] to record major events in a match from which key performance statistics about teams and players can be derived. Spatial tracking data is another source of information which analysts collect (usually for post-match analysis) and study as a separate entity. However, without the semantic context of the game, such data is difficult to interpret and is often disregarded due to the deluge of data. We design new glyphs that combine both notation and spatial data, with a focus that the glyphs are visually sortable for interactive sorting and visualization. Table 5.1 gives an overview of the set of attributes in rugby event analysis which are ranked in order of data importance based on end-user feedback. The visual channel we use to map each data corresponds to the glyph design as shown in Figure 5.7. Following the design principles presented in Section 5.3, we describe the methodology of mapping rugby event data to visually sortable glyphs. A summary of our parameter space and their sortable features is illustrated in the glyph swatch chart (see Figure 5.8).

The goal of rugby is to carry a ball to the opposition try line. *Gain* is the term used for the distance gained towards the opposition try line as a result of free play. Although gain is naturally of interval type, conventions in rugby adopt an ordinal measurement (e.g., negative gain, minor variation, major gain). Thus, a discrete representation is needed. Since end-users make use of an existing ordered colour scheme, it is natural to map gain to this visual channel to support visual orderability, learnability as well as being search-

| Sort Key                 | Typedness | Visual Channel |
|--------------------------|-----------|----------------|
| Gain                     | Ordinal   | Colour         |
| Event                    | Nominal   | Pictogram      |
| Territory Start Position | Interval  | Size           |
| Tortuosity               | Ratio     | Shape          |
| Number of Phases         | Ratio     | Enumerate      |
| Direction                | Direction | Orientation    |
| Net Lateral Movement     | Ratio     | Length         |
| Time                     | Ratio     | Location       |
| Phase Duration           | Ratio     | Length         |
| Team Identifier          | Nominal   | Colour         |

**Table 5.1:** Table illustrating the set of sort keys in rugby event analysis. Each attribute is classified based on typedness, and the visual channel mapped to the glyph. Data attributes are ranked in order of importance from top to bottom.

able given the high visual priority of colour. The context in which gain is achieved is particularly important. These *start events* (e.g., from lineout, scrum, etc.) are nominal categories that classifies periods of play into more semantically meaningful groups. Here, the events are sorted by importance. We previously described in Section 5.3 the use of metaphoric pictograms for mapping such data. Pictograms can often be arbitrary, in that their shape, size, colour will vary, thus having a low visual orderability. Using different intensities to draw each pictogram is one solution to establish a visual ordering, however, this may be misleading since event is discrete and not continuous. Instead, we design and order the pictograms according to their relative greyscale pixel count which is more appropriate for our study. Typically associated with a start event, is whether that event resulted in points scored (i.e., the end event). These glyphs should be differentiable to the viewer. Therefore, we use a coloured halo effect to enhance the attention-balance of such glyphs.

In rugby, the pitch is divided into key areas known as territory, which describes the spatial property of an event. The *territory start position* gives an indication at how far an event occurs from the opposition try line. Given that visual separability of variables is a key requirement in glyph sorting, we avoid overloading a single channel (e.g., colour) by encoding this attribute using size. Using the glyph template described in [MPRSDC12], we map this to the radius of a transparent, external grey silhouette. Size is a suitable mapping for ordering quantitative variables (i.e., interval and ratio) and also yields a high searchability due to visual pop-out, making this ideal for attributes of greater importance. The additional channel capacity introduced by the silhouette enables us to encode a varying line curvature along the contour for displaying the *tortuosity* of the ball path. Semantically, the line curvature resembles the tortuosity or shape of the ball path, which makes this easier for users to infer or remember.



*Figure 5.7: Components and visual channels of the glyph.*

A single path (or ball-in-phase), consists of a series of waypoints and path segments. In rugby, these waypoints and segments correspond to the *number of phases*. A simple and effective mapping for such discrete data is to use an enumerative representation due to its natural ordering. We depict the enumerate inside an arrow head which is oriented according to the resulting ball *direction*. Since orientation has weak learnability, we incorporate metaphoric cues i.e., a compass, by positioning the arrow head along a circle to make this more memorable to the end-user. We map arrow width to *net lateral movement* which indicates the relative lateral distance travelled. Since net lateral movement and direction is co-related, it is sensible to couple both variables together.

Another data coupling is *time* and *phase duration* which describes the temporal period in which the event occurs. Because both attributes are of ratio type and continuous, it is possible to combine such data using an integrated encoding, for maximising channel capacity. We represent time using a clock visual metaphor, where time and duration is mapped to location (or orientation) and length of the time handle. The semantics of a clock is used to enhance the visual orderability property of time. In order to facilitate aspects of our sort key visual mappings, we adopt a circular-based glyph design (Figure 5.7). The final attribute we map is *team identifier* (i.e., home or opposition), which we depict by colour-coding the inner contour. We follow the general convention used in sport for distinguishing two teams by mapping red and blue to the teams respectively. This enables sporting domain experts to be more familiar with the glyph concept which improved learnability and visual search.

### 5.5.2 Visual Comparison of Two Matches

Analysts are normally tasked with watching multiple match videos to identify the occurrences of key performances. This is laborious and time-consuming, and even current techniques such as notational analysis do not allow the analysts to discover new insight but merely review what has been previously recorded. As part of our evaluation, we

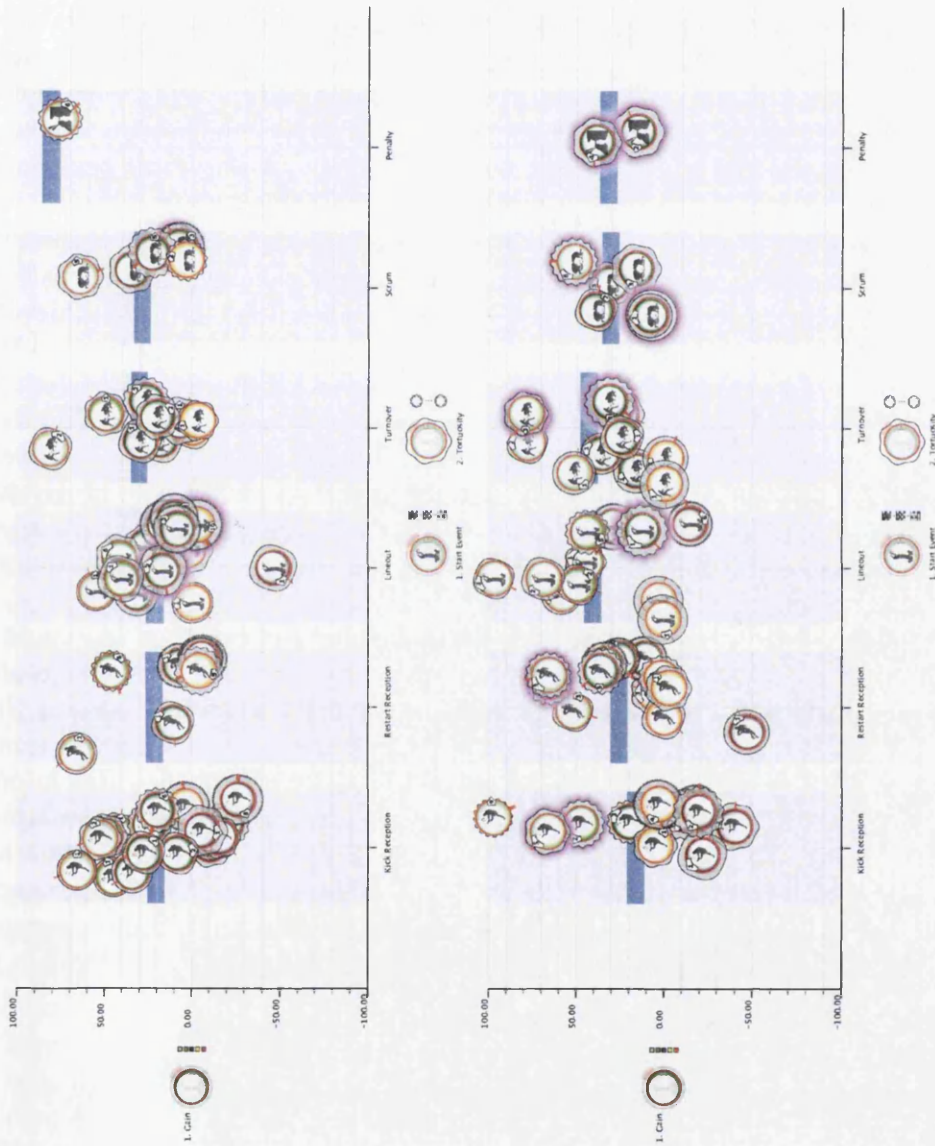
|                          |  |  |  |  |  |  |
|--------------------------|--|--|--|--|--|--|
| Gain                     |  |  |  |  |  | Major Gain<br>Negative Gain                      |
| Event                    |  |  |  |  |  | Relative Gameplay Pixel Count<br>Most<br>Least   |
| Territory Start Position |  |  |  |  |  | Attacking 3rd<br>Defensive 3rd                   |
| Tortuosity               |  |  |  |  |  | Maximum Curve length<br>Minimum Curve length     |
| Number of Phases         |  |  |  |  |  | Most<br>Least                                    |
| Direction                |  |  |  |  |  | Left<br>Right<br>Forward<br>Backward             |
| Net Lateral Movement     |  |  |  |  |  | Most<br>Least                                    |
| Time                     |  |  |  |  |  | End Start<br>Second Half First Half<br>Half Time |
| Phase Duration           |  |  |  |  |  | Event Duration                                   |

**Figure 5.8:** Swatch chart illustrating the visual sort key parameter space and legends using focus and context glyphs. Continuous attributes are indicated by (↔) and discrete attributes are labelled with their corresponding values.

compare glyph-based visual analytics for analysing the performance of a single team in two different rugby matches as shown in Figure 5.9. Match 1 (**M1**), involves two evenly matched teams, resulting in a closer point score differential. This is compared to Match 2 (**M2**) where one team proved to be more dominant. Both matches are taken from the World Cup 2011. By using visual analytics, the domain experts are interested to see how the two matches compare and for investigating why the outcome of the two matches are so different.

We presented the software to the analysts and explained the usability prior to letting the analysts explore the two datasets. One topic of interest is the relationship between gain and tortuosity, i.e., whether the strategy of working the opposition (high tortuosity) resulted in greater gain. Sorting the glyphs by the two attributes reveals a uniform gaussian distribution of glyphs in both matches. A clear observation, is the significantly lower average tortuosity in **M2**, indicated by the greater spread of glyphs and overall shift along the tortuosity sorting axis. This shows that it requires less effort to make sizeable gains in each phase and thus, attacking the opposition more directly can yield larger benefits. From a glance, the analyst identifies many different event types (i.e., pictograms) appearing within the cluster in the visualization. This directed the user to inspect how start event would affect the ordering of the glyphs via an alternative sorting strategy.





**Figure 5.9:** Visual comparison of two rugby matches using the IMG plot. Top: Match 1 (M1). Bottom: Match 2 (M2). For each match, the glyphs are ordered using three sort keys: Gain versus Start Event and Tortuosity. Mean bars are also displayed as a user-option to provide additional statistical information.

Figure 5.9 illustrates the comparison of the two matches where the user sorts the glyphs based on three attributes: gain versus start event and tortuosity. One new feature not previously observable, is the variation of start events that resulted in points scored which is depicted by glyphs highlighted in purple. It is clear in **M1**, that most points are scored from lineouts. In comparison, the other match exhibits a more uniform distribution of point scoring events. From this, we can hypothesise specific strengths and weakness of different teams. The statistical information displayed by mean bars is useful for analysing and deriving new key performance indicators. For instance, phases from turnover provide the most average gain across both matches as shown by the highest blue bands in each hierarchical axis bin. Thus, the number of turnovers is one key indicator that influences the team performance. Subsequently, scrums is the next most effective in **M1**, whereas lineouts proved more successful in **M2**.

Under the new sort operation, the analysts discover a new data trend that is present in **M1** and not the other (see Figure 5.9), where the glyphs appear within each axis bin along a linear line from top left to bottom right. This indicates that the team achieved more gain whilst attacking the opposition directly, which decreases respectively with higher tortuosity. At first, this was not what the analysts expected. By visually analysing the glyphs in the upper left cluster, we found the events to occur largely within the defensive third as shown by the shorter grey silhouette on each glyph. For a greater level of detail, the analyst studies the sorted video clips that is associated with each glyph, to find the cause of higher gain is a result to the team kicking the ball forward out of defense. Although kicking the ball results in greater gain, this comes at a cost of losing ball possession which is crucial.

The analysts found the trends to be insightful for explaining strategies against different oppositions. Tactically, the visual patterns observed in **M2** describes a more offensive game plan which is carried out each time the team regained ball possession. In comparison, **M1** shows a clear distinction between offense and defense, where the team selectively chose key moments (e.g., pitch position) to attack the opposition. The information correlates well with the analysts understanding since mistakes against stronger oppositions (i.e., **M1**) comes with higher risk which can impact the outcome of a match. One further observation visible in **M2** is shown by the ordering of glyphs in the turnover event category, in which the variable gain increases with tortuosity. Such a pattern indicates the opposition defence tiring as the home team attacked the ball, creating a prospective scoring opportunity.

### **5.5.3 Domain Expert Review**

The development of the work has been an iterative process in close collaboration with the Welsh Rugby Union (WRU), spanning over 12 months. From inception of the idea, it was clear that the analysts want to be able to interrogate their data in a more complex nature than previously available in order to gain new insight. The introduction of spatial data into visual analytics has meant that this is now achievable and has been used to

derive novel information intuitively. Rhodri Bown of the WRU performance analysis team provide valuable feedback on the usage of glyph sorting within rugby performance analysis.

*“The strongest element of the system is the ability to interactively sort vast quantities of data according to multiple attributes for revealing trends or groups of data. Your eyes are instantly drawn to those patterns. In our current practice, getting the data and generating charts (through spreadsheets) is very time consuming. Once a chart is plotted, we often get “What if we take this variable into account?”, which then requires us to go back to the raw data and process it all again. Where as with this, we can navigate the data much more effectively. The visualization is insightful for giving an overview of a match. Sorting the data gives good visual cues for pointing us in the right direction and being able to look in detail at the associated videos helps to clarify and explain what those trends are.”*

The feedback received from the WRU analysis team proved to be very encouraging. It confirms that the use of glyph sorting can significantly enhance the effectiveness of glyph-based visualization. By integrating glyphs into the sorting process and linking this with multiple video footage, the analyst is able to derive new underlying phenomena from a match. In particular, the domain experts feel that such a system is highly beneficial in their workflow for post-match analysis, where the insight obtained from sorting is useful for formulating strategies against different oppositions.

## 5.6 Discussion

For this application, we developed an interactive glyph-based visualization system to support post-match analysis of sorting rugby data. The system incorporates a focus+context glyph-based interface for selecting and driving the sorting process, and a linked IMG plot for displaying sorted results. Although the visually sortable glyphs used here (Section 5.5.1) are specific to rugby, the underlying system functionality could be adopted to other glyph-based designs. Thus, this research can be generalised to other domains that require interactive analysis of multi-dimensional data. One limitation of the results is the scalability of the IMG plot to big datasets. Since we make use of a larger glyph design, we find that this can result in a significant amount of visual clutter. To alleviate this problem, we integrate interactive tools such as axis expansion, as well as pan-and-zoom navigation. However, more sophisticated interactions could be explored to reduce the amount of occlusion.

## 5.7 Summary

In this chapter, we have proposed a glyph sorting framework for interrogating and interpreting large multivariate data. Glyph sorting combines the principles of designing visually sortable glyphs in conjunction with an interactive visual system to enhance the usability of glyph-based visualization. We found glyphs that are visually sortable is an effective means for performing comparative analysis of multiple attributes between glyphs, and to support multi-dimensional visual search. The system incorporated a novel method for encoding multiple dimensions onto a single axis to facilitate high-dimensional sorting, and also effectively reduce visual clutter in the visualization by relaxing the spatial positioning of glyphs. We have demonstrated this approach to an application of sport performance analysis. During this study, the analysts were able to derive new insight and observe trends as a result of high-dimensional sorting. It was apparent from the way the analysts interacted with the system that they would often “know” what key events they were looking for and how events should be organised (i.e., by examining the associated videos), but do not have the precise knowledge about individual sort keys. Chapter 6 extends this work by investigating the use of a knowledge-assisted visual analytic process to support such a task.

From this research, we were able to successfully encode up to nine different parameters within a glyph, where each attribute can be readily perceived and sorted in an obvious way (Figure 5.8). However, we observed that some visual encodings, for example *territory start position* using radius size, is perceptually more orderable than others, for example *time* using orientation. This led us to believe that different visual channels have a different *perceived orderedness*. As far as we know, no formal experiments evaluate such a task, and is the main motivation that inspired the study in Chapter 7.



---

## Glyph Sorting: A Visual Analytic Approach

---

### Contents

---

|       |   |     |
|-------|---|-----|
| 6.1   | Introduction . . . . .  | 115 |
| 6.2   | Problem Specification . . . . .                                 | 117 |
| 6.3   | Visual Analytics for Multivariate Sorting . . . . .             | 118 |
| 6.3.1 | System Overview . . . . .                                       | 118 |
| 6.3.2 | Knowledge-Assisted Ranking Framework . . . . .                  | 120 |
| 6.3.3 | Model Visualization . . . . .                                   | 124 |
| 6.3.4 | Glyph-based Visualization . . . . .                             | 125 |
| 6.3.5 | Sorted Event Replay . . . . .                                   | 126 |
| 6.4   | Case Study: “What is a successful strategy to score?” . . . . . | 128 |
| 6.5   | Discussion . . . . .  | 129 |
| 6.6   | Summary . . . . .   | 130 |

---

**I**N the previous chapter, we examined several technical aspects of glyph sorting and design principles for developing effective, visually sortable glyphs. Two further problems raised as a result of this work is the limitation of glyph sorting interactions to an ad hoc sorting requirement; and the perception of orderability under different visual channels. This chapter focuses on the former. One interaction of glyph sorting we introduced is the ability to encode multiple sort keys within a single axis using hierarchical axis-binning. This method allowed users to perform high-dimensional sorting interactively. However, a limitation of this approach is that a user is required to have some knowledge about the combination of sort keys to organise events in a useful manner. When such knowledge is not obvious it decreases the usability of such a tool. To

overcome this challenge, we extend previous work using a knowledge-assisted ranking framework to support the analysis and sorting of multivariate events in a flexible manner.

Event ranking (e.g., for determining relevance or prioritising actions) is an important task in visual analytics [GLG\*13, CLP\*15a]. This task becomes challenging when sorting involves several data dimensions, and the way in which each dimension influences the sorting is not well defined. Such a ranking task is commonplace in practical visual analytics, where one often encounters a request for organising data into some kind of order without a precise specification of the relevant *sort keys* and a *sorting function*. Although some analytical methods such as multidimensional scaling (MDS) [CC01] or principle component analysis (PCA) [Jol02] may help in some applications (e.g., [JZF\*09]), they focus on the discovery of the most influential attributes in the data, rather than the discovery of a *sorting function* for an ad hoc sorting task.

In this work, we propose a novel *knowledge-assisted* approach to such a visual analytics task for sorting sport event data. Our concept is inspired by the method of *card sorting* [RM97], a user-centred design that allows a user to decide how to categorise a set of items into groups or structures they are familiar with. Card sorting has been previously used to effectively classify symbols in cartography [RFB\*11], organise on-line course sites [Dou13], and cluster multivariate glyphs [BS92]. We apply a similar approach to rankings instead. In a knowledge framework [CZP\*10], we can summarise the situations as follows:

- Users have *tacit* knowledge about ranking events, but do not have the *formal* knowledge as to a sorting function. They may have *partial* knowledge about sort keys as they typically speculate a set of influential attributes.
- Although users can rank a given set of events using their tacit knowledge (because they define the ordering), this does not scale up to a large number of events. It is generally easy for users to place a few most representative events (e.g., success, neutral, failure) into order. The task becomes inefficient when the number of events increases significantly, and ineffective (i.e., less ‘accurate’) for events with a similar principle criterion (e.g., how successful), but a diverse set of conditions (left or right, earlier or later, different players involved, etc.).
- On the other hand, the system does not have any a priori knowledge about the expected ranking outcome, since the ranking requirement is not predefined. Of course, it does not have the formal knowledge about a sorting function either. If the system has a sorting function, it can perform event sorting in a scalable and consistent manner.

We thereby developed a visual analytics system that enables users to provide the system with some of their *tacit knowledge* by selecting a small set of events (typically 3-7), and ranking them in order as an example for the system. The users may also provide their *partial knowledge* about possible attributes (e.g., data dimensions) that should be

considered. This partial knowledge is not essential, but can reduce the amount of computation significantly. We use regression models to convert the input to some *formal knowledge* in the form of a sorting function and a measure of influence of different sort keys. The system then provide users with a visualization of the sorted results. The former is shown in a glyph-based sorting canvas, and the latter in a parallel coordinates plot. Users can interactively refine the sorting results through model parameters, or reactivate the knowledge discovery process by refining their initial specification of the example set or the speculated data dimensions. Satisfactory results can normally be obtained within a few iterations, and users can produce a sorted set of events (i.e., video clips) for supporting further analytical tasks such as compiling various statistical indicators, and analysing video clips in a coaching session. Our contributions of this work are:

- We introduce a novel visual analytic approach to sorting multi-dimensional events by converting users' tacit and partial knowledge to formal knowledge.
- We develop a system that supports such a process iteratively through a close integration of interaction, analysis and visualization.
- We demonstrate the efficiency and effectiveness of visual analytics for multivariate sorting through a real-world application ranking rugby events, and we evaluate our work objectively with a expert user consultations.

The remainder of the chapter is organised as follows: In Section 6.2, we outline our problem specification. Section 6.3 presents the visual analytic system, and details the variety of components (knowledge-assisted ranking framework, model visualization, glyph-based visualization, and sorted event replay) that the system incorporates. We then evaluate our work in Section 6.4 with a case study performed by analysts at the Welsh Rugby Union, and discuss the limitations of our system in Section 6.5. Finally, we summarise our work in Section 6.6.

## 6.2 Problem Specification

In modern sports, especially in high-level teams, coaches and analysts experience a deluge of data due to the introduction of various digital technologies for supporting match analysis and training. This work is motivated through the collaborative relationship with the Welsh Rugby Union (WRU). As mentioned in the previous chapter, the WRU use videos extensively for analysing performance indicators. Although quantitative analyses is helpful for getting an overview of a match, the rugby analysts consider that this alone is not enough to paint a right picture of a game.

A rugby game is coded into a series of facets known as *phase ball event*, which describes the period of play a team has possession of the ball. The rugby analysts are then tasked with the crucial role of finding key instances of such events. These events



(i.e. video clips) often have to meet a specific criteria, for example, how successful a strategy is in some conditions, and can also frequently change depending on the user's task, for example, analysing offensive or defensive play. Currently, this search process is performed manually using systems such as SportsCode to browse and select events based on a pre-defined attribute, which include:

- **start event** — the type of event in which play is started (e.g., scrum, kick reception, lineout).
- **gain** — the distance gained towards the goal area.
- **territory start position** — the spatial position on the pitch where the team received possession relative to the goals.
- **time** — the starting time of the event.
- **tortuosity** — the tortuosity of the ball path.
- **number of phases** — a count of the phases.

Given the range of requirements for different types of tasks, searching clips by some fixed criteria is time consuming, and more than often the analysts spend a considerable amount of time trawling through numerous video clips that are not relevant because the sort is not well defined. Our approach aims to alleviate this problem by enabling analysts to sort events in a flexible manner. We introduce a knowledge-assisted ranking framework that allows a user to specify their sorting requirements without depending on specific knowledge about individual sort keys to support this task.

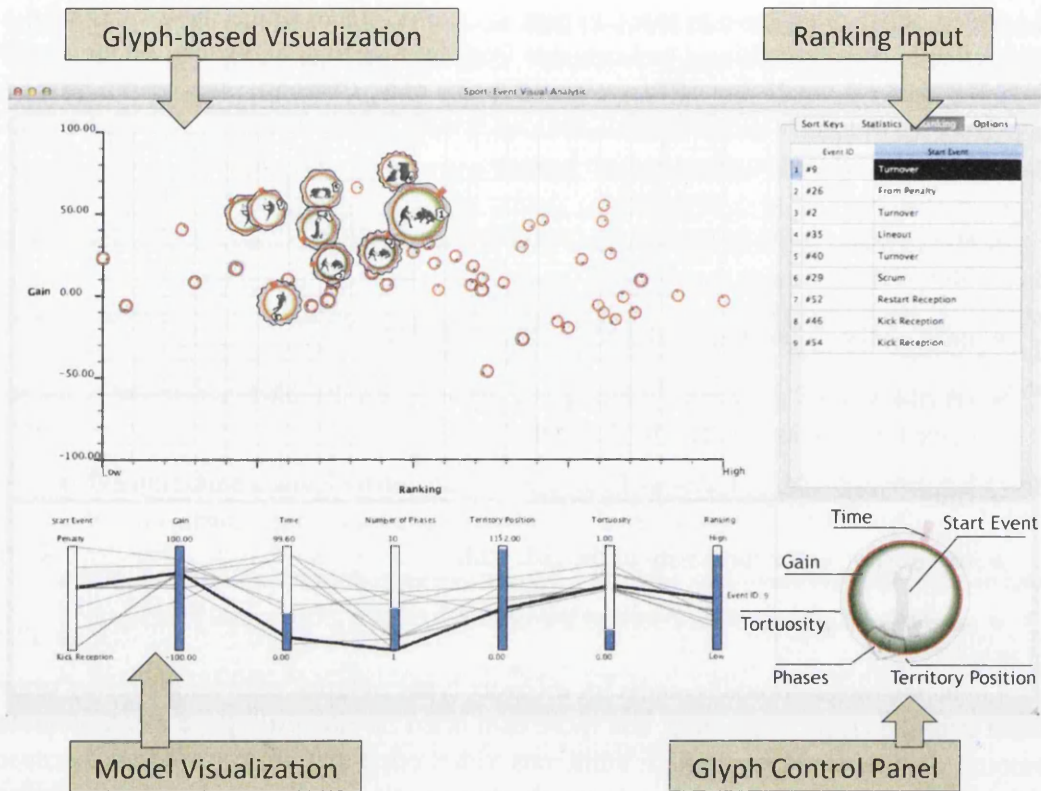
## 6.3 Visual Analytics for Multivariate Sorting

We developed a visual analytic system that closely integrates a knowledge-assisted process to enhance the exploration and sorting of sport event data. By training an analytical model with a user's knowledge on ranking, the system constructs a multivariate sort query that can be used on various matches for retrieving the desired events or associated video clips in flexible manner.

### 6.3.1 System Overview

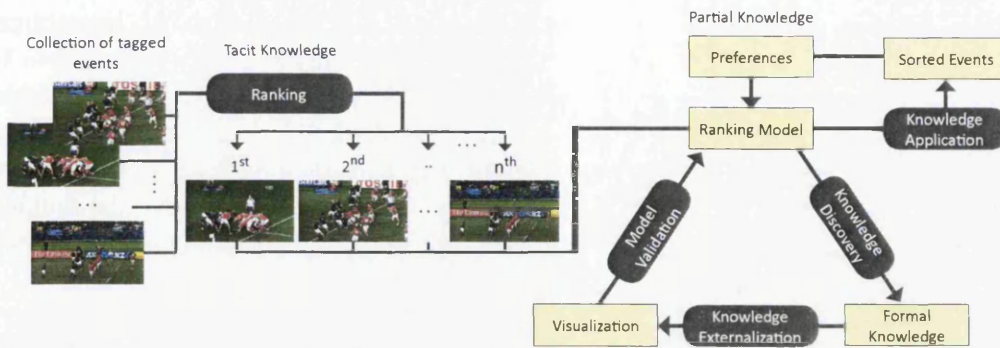
The system (Figure 6.1) contains four main views:

- **Glyph-based Visualization** — this view shows the sorted events of a match using glyphs, and is the main interface which users can select and import events into the ranking input view.



**Figure 6.1:** The user interface contains four main views. The glyph-based visualization shows the sorted events of a match, and allows a user to select and import events to the system. Once events are imported, the ranking input view is used to specify a sorting requirement. The model visualization view allows the user to analyse how the current model parameters and accuracy correspond to their ranking input. The ranking model can then be exported to one of the primary axes in the glyph-based visualization for viewing the sorted results. The axes can also be modified by clicking on a component in the glyph control panel.

- Ranking Input — this view allows the user to specify and configure their sorting requirement to the system.
- Model Visualization — this view uses parallel co-ordinates to convey how the events correspond to the individual attribute contributions and accuracy of the resulting model as defined by the ranking input.
- Glyph Control Panel — this graphical interface allows the user to interactively control the primary axes within the glyph-based canvas by clicking on the corresponding glyph attribute.



**Figure 6.2:** A knowledge-assisted ranking framework. It consists of five steps: the user's **ranking** input as an example to the system, a **knowledge discovery** process to predict a set of sortable attributes combined into a function, **knowledge externalization** to convey the analytical model through visualization, **model validation** based on ranking analysis, and finally, using the model to interactively analyse, rank and replay match videos (**knowledge application**).

Each of the views in the system are linked to support interactive exploration of the data. For example, brushing glyphs in the glyph-based view will update the corresponding polylines in the model visualization. We use a glyph-based canvas as our main interface for selecting and importing events to the system. Metaphorically, the glyphs represent the 'cards' as in our card sorting methodology. In the ranking input view, users can specify an event's rank by dragging the event to the appropriate position in the table. The selected event is then highlighted in black, both in the table and model visualization. The corresponding glyph is also highlighted by magnifying its size to help users visually navigate between each of the different views. We also provide tooltips and a statistics dashboard that displays additional information about an event. To sort events using the learned ranking function, users can export the analytical model to one of the axes in the glyph-based view using a drop-down menu. The user can then playback the video associated with each event data for detailed analyses.

### 6.3.2 Knowledge-Assisted Ranking Framework

The core framework of our visual analytics system involves converting a user's ranking (sort query) into a function that can be explicitly applied to sort the data. This process involves defining a relationship between the ranking input and the set of sort keys (i.e., data dimensions) as illustrated in the first two steps in Figure 6.2. Let  $e_1, e_2, \dots, e_n$  be a subset events, and  $e_{i,j}$  be its  $j$ -th attribute value for  $m$  attributes. By placing them into some order  $e_{s_1} < e_{s_2} < \dots < e_{s_n}$ , we can model the ranking as  $\mathbf{y} = \mathbf{E}\boldsymbol{\beta}$ , where  $\mathbf{E}$  is an  $n \times m$  matrix, and  $\boldsymbol{\beta}_j \in \mathbb{R}$ ,  $j < m$  are the weights or contribution of each sort key. The goal then is to estimate the weights  $\boldsymbol{\beta}$  such that an event's rank  $y_i$  is preserved. Typically,

a user may guess these weights during the ranking process. However, this is impractical since the criteria for sorting may frequently change depending on the user's task.

One effective approach for predicting such weights and a potential ranking function is through regression modelling, which is a common method within statistical forecasting [Act66]. In this work, we employ three different analytical models: multiple linear regression, polynomial regression, and logistic regression. We then solve the ranking system by approximating the sort key weights using a least squares fitting [Act66] which generalises to:

$$\hat{\beta} = (\mathbf{E}^T \mathbf{E})^{-1} \mathbf{E}^T \mathbf{y} \quad (6.1)$$

To ensure a solution to  $\beta$  exists, (i.e., the matrix  $\mathbf{E}^T \mathbf{E}$  is invertible), we remove any constant column vector from the model. This problem may occur since our data contains both ordinal and categorical values, for example, if the ranking input contains only a set of *scrum* events. The least square solution is applicable when the system of equations  $\mathbf{E}$  is *over-determined* (i.e., for  $n > m$ ). Conversely,  $\mathbf{E}$  is *under-determined* if there may be a lack of suitable training data. Generally, such a system may have infinitely many or no solutions. We can pick one of these solutions such that  $\hat{\beta}$  is minimised subject to the constraint  $\mathbf{y} = \mathbf{E}\beta$ . This is solved using the method of Lagrange multipliers:

$$\hat{\beta} = \mathbf{E}^T (\mathbf{E} \mathbf{E}^T)^{-1} \mathbf{y} \quad (6.2)$$

Once the ranking model has been trained, we validate and visualize the model parameters to the user as part of an analytical loop. Rather than simply presenting the model as a 'black-box', this allows the user to assess whether the sort query is reliable, and empowers the user to infer some of their own knowledge into the knowledge discovery process.

### 6.3.2.1 Regression Evaluation

Given a ranking input, the system needs to compare this against the ranks predicted by the regression model. A common approach used in statistical modelling would be to compute its Mean Squared Error (MSE) [Act66]:

$$MSE = \frac{1}{n - dof - 1} \sum_{i=1}^n (\hat{y}_i - y_i)^2 \quad (6.3)$$

where  $n$  is the number of events, *dof* is the degrees of freedom,  $\hat{y}$  is the predicted value, and  $y$  is the actual value. At this level, the computed values  $\hat{y}$  and  $y$  represent ranking scores which is used later to determine the events rank. By choosing a set of scores (e.g.,  $y_i \in [0, 1]$ ) it is easy to observe that the predicted ranks will be preserved when  $MSE = 0$ . However, this does not hold for  $MSE > 0$ . We address this by incorporating two comparison metrics to help validate different models: a ranking confidence  $\tau$ , and a Mean Ranking Error (MRE).

The ranking confidence  $\tau$  measures the accuracy of the model based on a percentage of events in which its predicted rank matches the order defined by the ranking input. Let  $f : E \mapsto \mathbb{R}$  be the trained ranking model, and  $\phi : \mathbb{R}^2 \mapsto \{0, 1\}$  be a binary mapping that returns 1 if the order between two subsequent events  $f(e_{s_i}) < f(e_{s_{i+1}})$  for all  $i = 1, \dots, n - 1$  is correct. We derive the ranking confidence as:

$$\tau = \frac{1}{n-1} \sum_{i=1}^{n-1} \phi(f(e_i), f(e_{i+1})) \quad (6.4)$$

When ranking events, for example, a set of key moments within a match, we often find that more significant events (e.g., the winning goal) can be ranked more easily and ‘accurately’ in comparison to events that are less significant (e.g., a player making a foul). This concept has been well-established within event-based detection such as video storyboarding [PLC\*11]. Since such events are more accurate in terms of their ranking, the accuracy of model should therefore take this weighting into account when being compared. We incorporate this by modulating the ranking confidence using a Gaussian function  $G(x)$  where  $x = (n - 1) - i$ . The parameter  $\sigma$  in  $G(x)$  is pre-defined, and we set  $\sigma = 2$  as default.

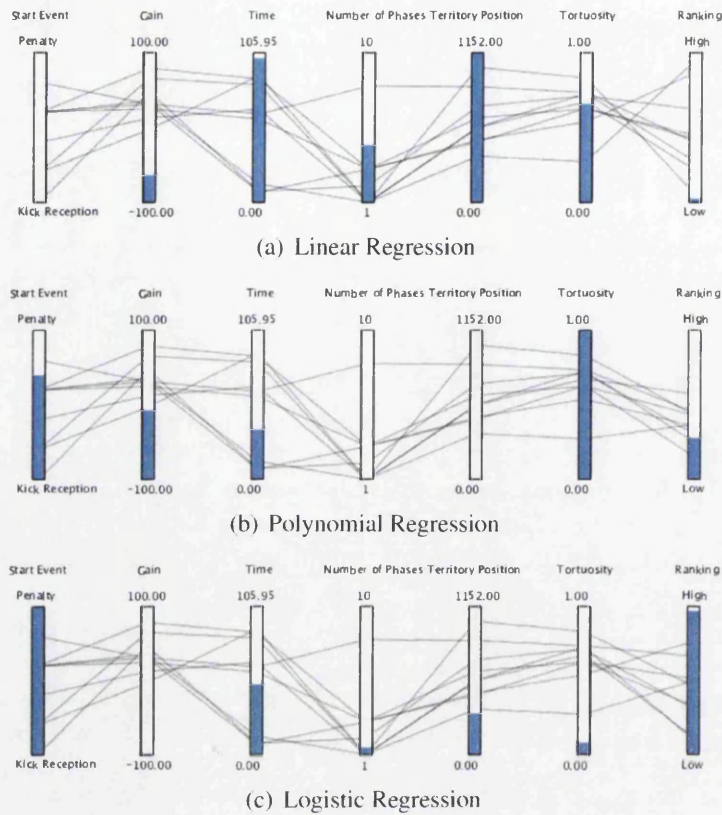
Our third comparison metric we compute for each model is the Mean Ranking Error (MRE). The MRE measures the average difference between an event’s actual rank  $s_i$  and its’ predicted rank  $t_i$  as given by:

$$MRE = \frac{1}{n} \sum_{i=1}^n ||s_i - t_i|| \quad (6.5)$$

Each of the three comparison metrics allow us to examine how the predicted ranking from different analytical models compares to the actual ranking of the training data. The next section will describe how we use these metrics to choose the optimal regression for different types of sorting requirement.

### 6.3.2.2 Model Selection

The discovery of performance indicators (sort keys) that influences the user’s ranking is particularly sensitive to the regression technique used as shown in Figure 6.3. Notice how the weight of each attribute (e.g., the blue gauges) in the model can change, and may have a significant impact to the overall accuracy. We incorporate each of the three comparison metrics into our system to validate the model using a weighted contribution. For each model, we compute its performance  $P = \lambda_1 MSE + \lambda_2(1 - \tau) + \lambda_3 MRE$ , and choose the model with the smallest value. By default, we set each weighting term to be equal (e.g.,  $\lambda_i = \frac{1}{3}$ ). However, this can be customised according to the user’s preference. The resulting model will give a predicted ranking that is most similar to the sort requirement as defined by the ranking input. We also provide the ability for a user to manually choose between different regressions. This allows the user to analyse the different sets

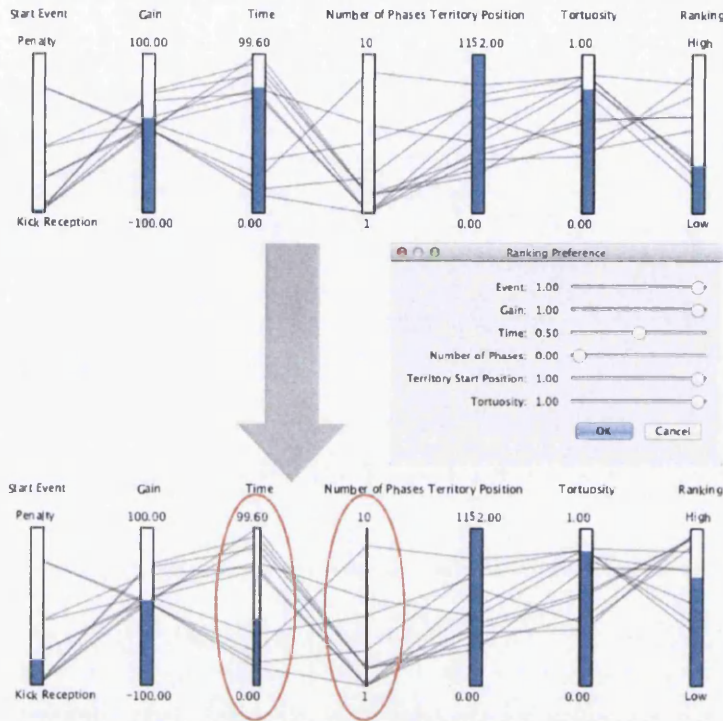


**Figure 6.3:** Visual comparison of the ranking models using (a) Linear; (b) Polynomial and (c) Logistic regression in parallel co-ordinates. The contribution of each attribute is depicted using gauges that correspond along each axis. In order to convey the model’s overall accuracy, the ranking model is plotted as an additional axis gauge which encodes the ranking confidence  $\tau$ . Note that each regression model may discover a different set of key performance indicators.

of performance indicators that may correlate better to their sort query (even though the predicted ranking may be less similar).

### 6.3.2.3 Model Interaction

When a user ranks a set of events based on some ad hoc requirement, they can often make intuitive or educated guesses on specific sort keys that may or may not affect their ranking criteria. We liken this to *partial knowledge*. Thus, we allow the user to refine the model parameters by applying additional weightings  $w_j \in [0, 1]$  to the sort key weights  $\beta$  such that the model is defined as  $y_i = f(\mathbf{w}, \beta, e_i)$ . We incorporate this into our system as a series of interactive sliders. Moving the sliders will scale the axis widths in the model

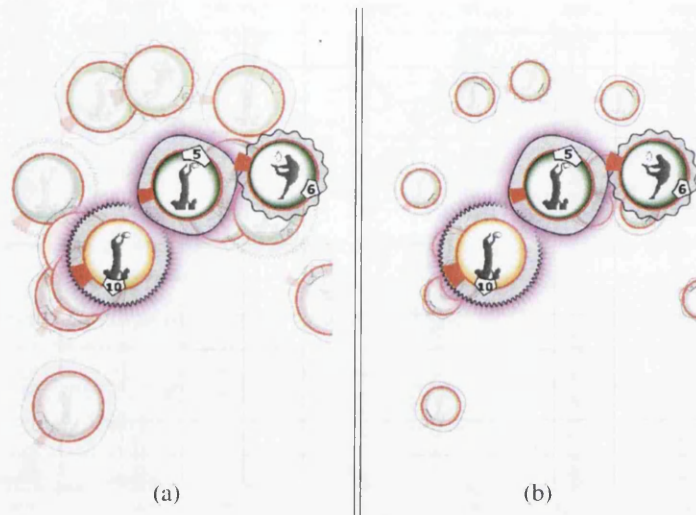


**Figure 6.4:** Refining the model parameters. Users can adjust the contribution of each attribute  $w_j$  in the ranking model by scaling the axis widths using sliders in the ranking preferences. This example shows how modifying the weights (highlighted in the red circle) can result to an improved model as shown by the larger ranking gauge (see right most axis).

visualization (see Figure 6.4). This enables a user to explore new sorting strategies and understand its impact to the predicted ranking. Optionally, users can choose to remove a sort key parameter from the model completely ( $w_j = 0$ ). Removing a sort key can significantly reduce the computational cost and parameter space, as well as potentially resulting to an improved model.

### 6.3.3 Model Visualization

Figure 6.1 shows the model visualization. In order to visualize the analytical model, we adopt the use of parallel co-ordinates which is a well-established technique in multivariate analysis [Ins85]. This provides a visual representation of the attribute weights and the overall accuracy of the trained model. Each attribute dimension is plotted as vertical gauges which are then filled according to the amount of contribution within the model. A similar approach is used by Andrienko and Andrienko [AA03] to visualize and weight multiple criteria in a decision making application context. They visualize the combined



**Figure 6.5:** Brushing glyphs in the glyph-based canvas (a) renders the glyph in focus, while non-selected glyphs are drawn as red markers to indicate their position. Non-selected glyphs can also be interactively scaled by the user (b) in order to reduce the amount of visual occlusion.

result on a separate axis. We also follow this method to convey the accuracy of the model, by plotting this as an additional axis gauge and filling the gauge according to its ranking confidence  $\tau$ . This enables the user to inspect the quality of the model and to identify which attributes contribute well for a given ranking. The user can also choose to adjust the weights manually through interaction with the visualization using sliders that adjust the axis widths for that particular attribute. For each event in the match, we render a polyline to help provide context to the model. By allowing the user to brush the polylines in the parallel co-ordinates or within a linked view (e.g., glyph-based canvas), it provides a facility to verify the model is performing as expected by observing the ranking outcome.

### 6.3.4 Glyph-based Visualization

The visual interface incorporates glyph-based visualization to depict the sorted results based on our IMG-plot in Chapter 5. Although interactive multivariate sorting is the focus of this work, we are careful not to confuse the end-user with an unfamiliar visual design. We therefore adopt the glyphs we proposed in Section 5.5.1 which we designed together with the analysts. Other visual design choices such as the number of design options presented in [War02] may be used instead depending on the application context. The glyph-based canvas is the primary interface for importing and selecting events (i.e., the glyphs) into the ranking input table, where the user can specify their ranking to the system. We found glyphs to be an intuitive mechanism for selecting and ranking





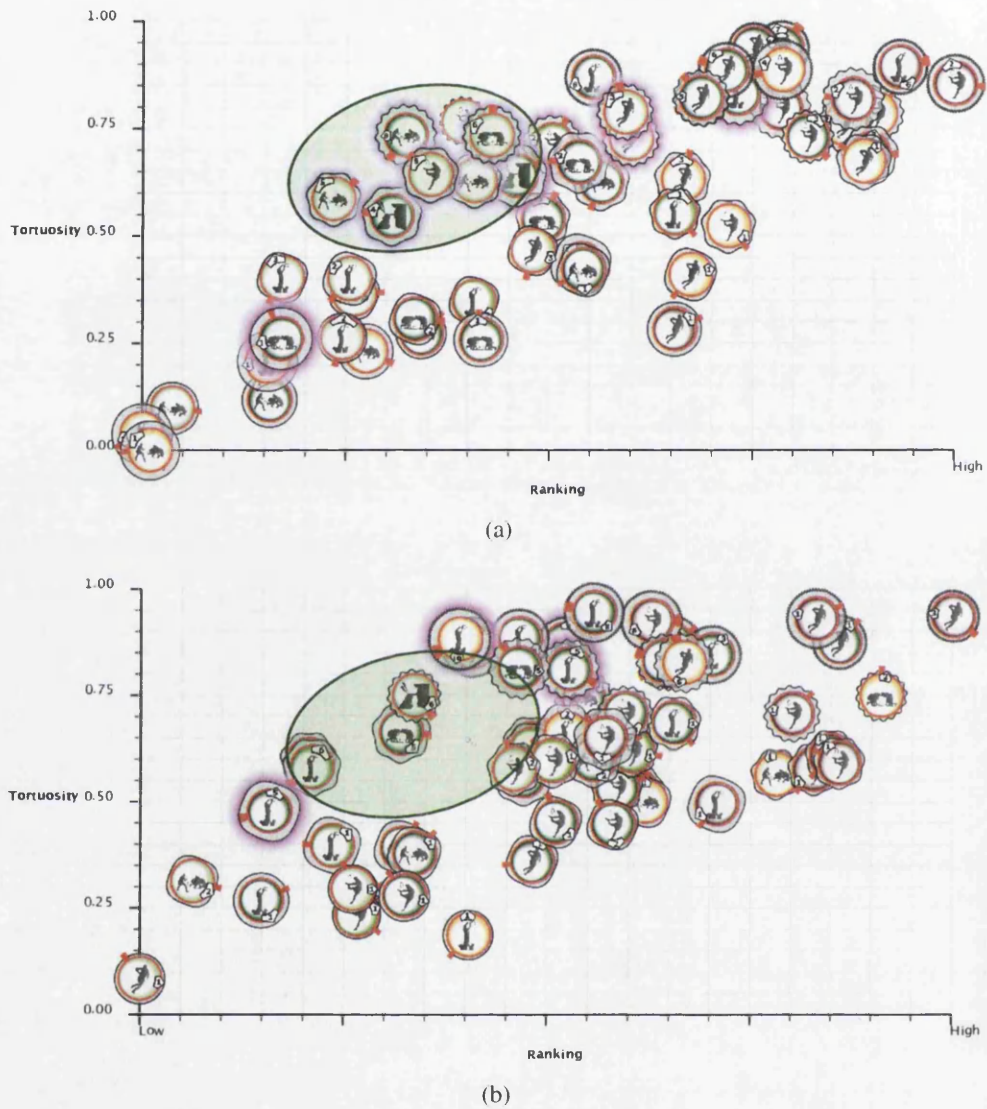
**Figure 6.6:** Video playback of sorted events. We integrate four different broadcasting feeds that recorded the event.

events. This is due to similarity with our card sorting metaphor, which is proven to be an effective approach for a sorting task [BS92].

**Interaction and Occlusion.** Due to the inherent occlusion of using glyphs [War02], we support interaction that enables the user to adjust the length of the sorting axes to help de-clutter the visualization. We also find that during the event selection process, non-selected glyphs (e.g., transparent glyphs) can sometimes interfere with this view due to their large size. In order to address this problem, users can interactively reduce the size of such glyphs so they appear as small red markers (see Figure 6.5).

### 6.3.5 Sorted Event Replay

Sporting analysts often rely on making semantic observations that can only be gained through the context of watching videos in order to determine the relevance of an event. This tool is especially important for specifying a ranking to the system. Since the data is associated with a single or multiple video clips, we incorporate a video playback user-option for viewing the sorted events (see Figure 6.6). Brushing events in the glyph-based view or parallel co-ordinates allows for smaller subsets to be replayed, which enable users to choose, view, and rank the events in a much more effective manner than the results of a typical search query.



**Figure 6.7:** Visual comparison of two matches. The events are sorted according to successful traits that resulted in points scored as defined by the model shown in Figure 6.4, and tortuosity. The analyst observed a group of events highlighted in the green circle (a) where a high percentage of points are scored, which is significantly less in the second match (b).

## 6.4 Case Study: “What is a successful strategy to score?”

Finding (and often formulating) a successful strategy against opposition teams is a critical task in professional sport. We have worked in close collaboration with the Welsh Rugby Union, where coaches and analysts perform such a task primarily by browsing video clips obtained from notational data. The limitations in current software means this is performed manually. Such a process is time consuming and does not scale well to multiple matches. This system presents a novel approach for organising match videos and event analysis. After spending time with the analysts using the system, we present a case study comparing two matches taken from the recent World Cup as part of our evaluation. Both matches present an interesting case to the user due to the huge point differential (81-7 and 16-17 respectively). The analysts would like to investigate what strategy led to such high points scored, and why this was so different to the other game. We detail the process below.

To begin with, the analysts chose a set of representative events as a training example to the system by selecting the glyphs in the glyph-based canvas. Their initial action is to layout the glyphs according to gain (a typical performance indicator) by changing the primary axes using the glyph control panel to help with this search process. While the amount of gain is important according to our analysts, a combination of other factors such as where they received the ball (territory start position) and how much they worked the opposition (tortuosity) is influential. Potential events is identified quickly based on the glyphs features. After importing these events into the ranking input, the analysts then watch each video to help determine their rank based on *how successful* the outcome is. Our domain experts are used to performing such a routine task in their usual workflow. Once the system is trained, the analysts can visually assess the quality of the resulting model in the parallel coordinate view (see Figure 6.4). During this process, they observed that phases was not a significant attribute to their ranking, and refined the attribute weights further to discover an improved model indicated by the amount of blue in the ranking axis as shown in Figure 6.4.

Figure 6.7 illustrates the sorted results according to the ranking function derived by the analysts for both matches. From ranking the events, they were able to discover a cluster of glyphs in one match (see Figure 6.7(a)) where a high percentage of points is scored depicted by the highlighted purple glyphs. What the analysts found interesting is the ability to compare and visualize the difference between entire matches in a single overview. The system reveals the second match to have fewer occurrences of events with similar features, which visually suggests why there were not as many scoring opportunities in this game. Two events can be observed within this region, however they did not result in points scored. Investigating this further through video reveals two poor kicks during play caused the possession to be turned over. Our visual analytic system helps analysts identify such events quickly and effectively. More importantly, it allows

analysts to use this to convey to players and coaches what needs to be improved, and may lead to new strategies.

**Domain Expert Feedback.** We report qualitative feedback from three domain expert users: a rugby analyst, the head coach of a university rugby team, and an international rugby player. After testing and a hands-on demonstration of our software, we held a consultation with each user.

**Analyst** *“Using the software has enabled us to discover new key performance indicators that we wouldn’t have recognised before, which ultimately helps save time as we do not need to watch as many irrelevant videos. It’s a totally different way of looking at our data. Previously, we would only look at match heuristics such as the territory that we’re in, or the gain in isolation, but being able to combine the two attributes (or more) now makes this a lot more meaningful. This is great for comparing matches. The visualization clearly identifies any differences in events, and we can then investigate those clips further and see why they’re different.”*

**Head Coach** *“Analysts have reams and reams of stats which all have to be computed and interpreted manually. The system here is a good way at grouping clips. For instance, if we’re defensively bad for a couple of games, you could press a few buttons and it’s all there for you, rather than going through manually, create a database from the first game, then add to it from the second game. Every coach will be looking at different things. For example, I might be looking at ‘Do we move forward when we catch the ball?’. Where this is useful is that it can show the best-case and worst-case, and also be able to look at examples in the middle. The flexibility of the whole model is its strength.”*

**Rugby Player** *“The software is useful as it allows you to break up the game by what you want to see. For instance, it would be irrelevant to show the Heineken cup team (which is the elite competition) all the clips with the squad involved in the LV league competition as they would be with a completely different team. Its main feature is the scalability to sort events from an archive of matches.”*

The feedback received shows the importance of organising relevant events in sports, and that our visual analysis system is a useful approach to support such a task.

## **6.5 Discussion**

Among several possibilities of modelling techniques, we used three different regression analyses to train our ranking model. Since the predicted contributions of each attribute in the model is sensitive to the type of regression (see Figure 6.3), the role of visual analytics becomes more important as it allows the user to verify whether the discovered

performance indicators correspond with their knowledge interpretation. The system may also benefit with a wider range of different models for identifying parameters with a better fit to the ranking input.

For this application, we typically train the model using a relatively small sample size (5-10 events) to generate a good ranking accuracy. However, this is not the case for all training data. A larger ranking input could result in a more robust model, but we do not know *'how much'* is enough to improve the accuracy without further testing. Ranking more events can also restrict the practicality of the system as they become more difficult to rank which is reported from our initial pilot study (see Appendix B).

The scalability of our approach in terms of the algorithm for training the model is highly generalisable, and can be easily applied to other domains and larger datasets. Extending our system to other team sports such as football, basketball, and hockey would simply require adapting the event mapping in the glyph-based design as discussed in Chapter 4. A potential issue is with the scalability of our visualization such as the glyph-based canvas. The system currently supports loading a single match, though this could be extended to multiple matches. Due to the use of large glyphs, visualizing several matches at once in this view will create more visual clutter. Likewise, higher dimensionality could also affect the visibility of the model parameters in the parallel co-ordinates view as a result of over plotting gauges.

## 6.6 Summary

We have proposed a knowledge-assisted, visual analytic process for interactive sorting of sport event data. Users provide tacit knowledge by selecting and ranking a subset of events as an example to the system. We use regression analysis to discover a set of influential sort keys, and a formal sorting function to organise events based on the user's ordering requirement. This allows users to rank events by a criteria such as importance. We find our visual analytic approach can significantly enhance the usability of multivariate sorting, and demonstrate its usefulness in rugby along with feedback from a range of domain experts.

The following chapter will now study our second research problem that we identified back in Chapter 5, relating to one important aspect of designing effective, visually sortable glyphs. This aspect is the perception of orderability. The design of effective glyphs for visualization often involves a number of different visual encodings. Since spatial position is usually already specified in advance, we must rely on other visual channels to convey additional relationships for multivariate analysis. One such relationship is the apparent order present in the data. In particular, we noticed that some visual channels (for example, size) are perceived as more ordered while for others are perceived as less ordered (for example, orientation) than the measured order present in the data. To evaluate this perceptual effect, we conduct a series of empirical studies.

---

## Glyph Sorting: Perceptual Orderability

---

### Contents

---

|       |  |     |
|-------|--|-----|
| 7.1   | Introduction . . . . .                                       | 132 |
| 7.2   | Orderability of Visual Channels . . . . .                    | 133 |
| 7.2.1 | Data generation . . . . .                                    | 134 |
| 7.2.2 | Noise Function . . . . .                                     | 134 |
| 7.2.3 | Visual Mapping of Elements . . . . .                         | 135 |
| 7.2.4 | Just Noticeable Difference . . . . .                         | 136 |
| 7.3   | Experimental Overview . . . . .                              | 138 |
| 7.3.1 | Interface . . . . .  | 139 |
| 7.3.2 | Pilot Studies . . . . .                                      | 140 |
| 7.3.3 | Crowdsource Consistency . . . . .                            | 141 |
| 7.4   | Experiment 1: How ordered is it? . . . . .                   | 142 |
| 7.4.1 | Results . . . . .  | 143 |
| 7.4.2 | Discussion . . . . .   | 145 |
| 7.5   | Experiment 2: Which is smallest? Which is largest? . . . . . | 148 |
| 7.5.1 | Results . . . . .  | 149 |
| 7.5.2 | Discussion . . . . .   | 150 |
| 7.6   | Experiment 3: How many pairs? . . . . .                      | 151 |
| 7.6.1 | Results . . . . .  | 152 |
| 7.6.2 | Discussion . . . . .   | 154 |
| 7.7   | Limitations . . . . .  | 154 |
| 7.8   | General Discussion and Summary . . . . .                     | 155 |

---

UNDERSTANDING visualization concepts and the way in which they interact with the human visual system remains a crucial aspect in developing effective data visualization; some of which are presented in Chapter 5. Semiotics provides one framework for understanding both why graphic representations work, and how to design such representations for optimal display. Important to semiotic theory and information visualization is the identification of basic *visual channels* (Section 2.2.1.1) such as size, hue, and shape that can be used to encode information. Such visual channels are known to possess a set of visual properties that determine their suitability of representing certain types of information or a task [Ber83].

This chapter investigates *ordered perception*, a fundamental concept to our framework described in Chapter 5 for designing visually sortable glyphs. When a visual channel is ordered, we can easily establish an order in which signs or objects are perceived, for example, from light → **dark**, or small → **big** (see Figure 7.1). This perceptual effect heavily reduces the reliance of legends and can result in a significant gain in performance [LFK\*13]. Given that the positioning of glyphs is often used to effectively encode spatial information [War08a], glyph designers must rely on other channels in order to convey additional orderings for multivariate analysis. It is therefore highly desirable for visualization scientists to understand how different visual channels affect the perception of order in a sequence of elements that encode different data values. As far as we know, no formal experiments exist to evaluate such a task, and this is the main motivation behind this work.

In this chapter, we present a formal study to investigate the perceptual orderability of visual channels. In order to work towards a comprehensive answer to such a big question, we focus this work on a set of commonly used visual channels and three specific research questions:

1. “*How does noise affect the perception of orderedness under different visual channels?*”
2. “*How do visual channels affect the judgment of min and max values for ordered and unordered sequences?*”
3. “*How does visual channel affect the perception of equality for ordered and unordered sequences?*”

The first research question focuses on detecting structural patterns in a visualization. Orderedness is one of such patterns, and we investigate this in a sequence of elements encoded using different visual channels. In our second research question, we explore how such sequences impact the judgement of min and max values. Such a task is typical in many visualization goals, for example, in detecting outliers. Finally, our third research question investigates how such sequences affect the perception of elements that have

equal values, which is representative of common graph-reading tasks. Our results show that the performance of each task is significantly affected depending on the choice of visual channel used.

The contributions of this chapter are: (1) we present empirical results to investigate ordered perception, and (2) we evaluate how visual orderability may impact the performance of two different types of perceptual tasks (visual search and categorical search).

We present results from three experiments that address our research questions. In the first experiment, we measure the participants' perceptual ordering of a sequence of elements under the effects of visual channel. Participants see ordered and unordered sequences with data values that are mapped to each visual channel: size, value, texture, hue, orientation, shape, and numeric. We discover a significant difference indicating that some visual channels are perceived as more ordered than others, which is consistent with previous literature [Ber83]. We also find that some visual channels are more sensitive to noise, and that noise significantly affects their perceived orderedness. The result provides insight and new considerations that a designer may wish to consider for effective visualization design.

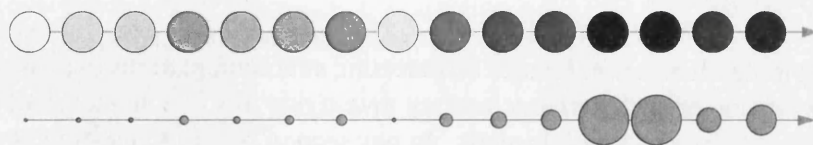
The second experiment evaluates the effects of visual channel when searching for min and max values for ordered and unordered sequences. Our results show visual orderability can significantly enhance the accuracy of such a task.

Finally, in our third experiment, we investigate how visual orderability affects the perception of pairs with equal values. For such a task, we find evidence that visual channels that are perceived less ordered (i.e., they appear more discrete), improves the accuracy of categorical search.

The remainder of the chapter is organised as follows: In Section 7.2, we describe the techniques used for creating the visual stimuli in our studies. Our experimental overview for analysing visual orderability is then outlined in Section 7.3. We present our three studies in Section 7.4, Section 7.5 and Section 7.6. Finally, we discuss our results in Section 7.8.

## 7.2 Orderability of Visual Channels

The example shown in Figure 7.1 illustrates an unordered sequence of elements using visual channels that are perceptually orderable according to Bertin [Ber83].



**Figure 7.1:** Visualizing an unordered sequence using value and size.

It is easy to see that both value (or luminance) and size impose an order that is



universal. In other words, given an element along a sequence, we can perceptually estimate its magnitude along the spectrum. We can generally observe that the sequence of grayscale elements are mostly ordered from left to right based on the changes of intensity. However, it is not *immediately* clear that both representations are actually encoding identical values. This leads us to believe that different visual channels have different perceptible levels of orderability. We now describe the process and techniques which we follow to create the visual stimuli used in our studies.

### 7.2.1 Data generation

In the data generation stage, we create synthetic datasets to model ordered and unordered sequences within a visualization. We chose the Body Mass Index (BMI) as an ideal example for its known linear model. The index is a popular measure used to assess how healthy a person's weight is for his or her height. To generate our datasets, we used a healthy or desirable index (e.g., BMI = 25) to derive a set of corresponding height and weight values. We then visualize the sequence of values by selecting a set of uniformly sampled data points, and mapping the weight values to each visual channel as shown in Figure 7.2. It is non-trivial to determine how *unordered* a sequence is, since the perception of orderability is not well-defined. For example, a collection of items can be arranged with varying degrees of *orderedness*. In signal processing theory [JJS93], we can describe such a sequence as analogue signal distortions from the result of noise. We adopt this approach to create a series of data conditions that models levels of orderedness using a noise function.

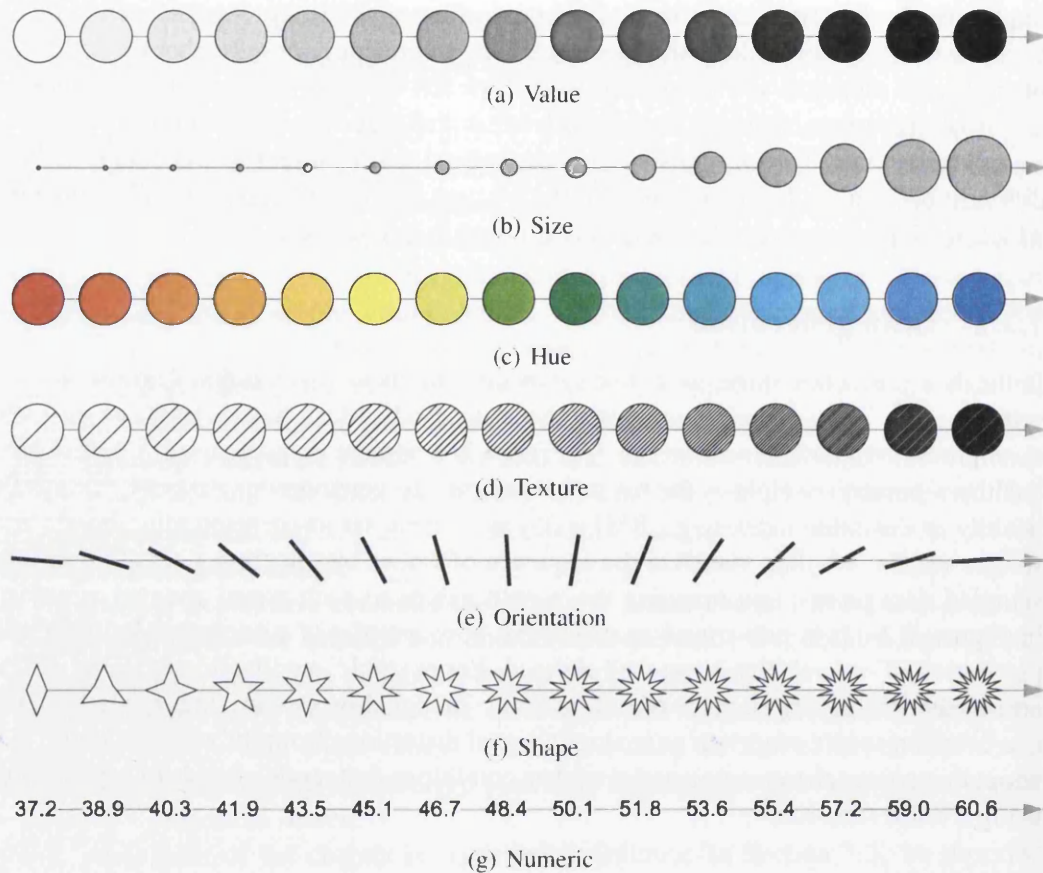
### 7.2.2 Noise Function

We introduce noise into our dataset using a swap function to create unordered sequences. Let  $x_i, x_j$  be two randomly selected data points. The swap function is defined as:

$$f(x_i, x_j, d) = \begin{cases} \text{swap}(x_i, x_j) & \text{if } ||i - j|| \leq d \\ \text{null} & \text{else} \end{cases} \quad (7.1)$$

where  $d \in \mathbb{R}$  is the distance between a pair of data points. We control the strength of the noise function using two parameters: (1) the number of swaps, and (2) the swap distance between two points. To create sequences with varying degrees of orderedness, we apply a set of noise level conditions derived by fixing the number of swaps, and increasing the swapping distance. We then measure the magnitude of orderedness by computing correlation coefficients [RN88] of the resulting dataset.

Initially, we sampled the noise levels uniformly with correlation between  $[0, 1]$ . Through observation and pilot experiments, we noticed that the perceived orderedness of such sequences was sometimes visually indistinct. As such, to avoid collecting data with no variation, we refined the noise levels manually to obtain orderings with a perceptible difference. We test a total of eight levels of orderedness:  $\eta_1 = 1.0$ ,  $\eta_2 = 0.97$ ,  $\eta_3 = 0.95$ ,



**Figure 7.2:** The visual stimuli used in our experiments. Each 1D plot is mapped using the visual channels taken from semiology of graphics [Ber83].

$\eta_4 = 0.90$ ,  $\eta_5 = 0.78$ ,  $\eta_6 = 0.71$ ,  $\eta_7 = 0.54$ , and  $\eta_8 = 0.12$ , ranging from very ordered, to very unordered.

### 7.2.3 Visual Mapping of Elements

Figure 7.2 shows the visual stimuli used in our experiments. Given that position is the most effective representation for conveying an ordering [CM84, War02], our goal is to investigate the visual channel which is next most orderable. We analyse this using 1D plot visualizations. Points (or elements) along the 1D plot are mapped using the visual channels described by Bertin [Ber83]. In addition to this, we compare their performance to raw numerical values, which is common practice when reading data within a table or spreadsheet view.

Since perceptual differences along a visual spectrum can be non-uniform [War08b], we carefully divide each visual mapping into bins equal to the number of sample points

(e.g.,  $n = 15$ ) shown in the plot. We choose the maximum number of samples to be displayed such that the just noticeable difference (JND) [Ber83] in each visual channel is respected. In the following section, we present our visual mapping methods and JND considerations to ensure each element within a sequence is visually discriminable.

## 7.2.4 Just Noticeable Difference

The literature on perceptible differences [Hei24] has been well studied over the past decade, resulting in mathematical concepts for producing uniform visual mappings [War88]. For each of our encodings, we describe the fundamental techniques we follow.

**Value** is mapped to greyscale intensity of each element (see Figure 7.2(a)). In order to realise increments of value with a perceptible difference, we follow previous work on visual discrimination of intensity [Hei24, War08b]. They show that human perception can distinguish a 0.5% change in luminance. The difference in luminance measured in our mapping is 7%, which is significantly larger than the JND.

**Size** is mapped to the radius of each element (see Figure 7.2(b)). Previous work in psychophysics demonstrates that the perception of size (e.g., area) can be effectively modelled using Weber-Fechner's Law [AR08]. In particular, the *Weber fraction* shows that the relationship between perception and size is logarithmic, which we adopt to control the difference in size. We can measure the perceived difference as:

$$p = k \ln \frac{r_i}{r_j} \quad (7.2)$$

where  $p$  is the perception between two radii  $r_i$  and  $r_j$ . We estimate the scaling parameter  $k = 0.23$  by incrementing the radius until a significantly large difference in size is perceptible. This gives a perception value of  $p = 0.048$ . Vision research show that a Weber fraction for circle radius discrimination is  $p = 0.025$  [WWH98]. As our encoding is greater than this JND, we use this to compute a set of radii that are visually discriminable.

**Hue** is mapped to the colour (from red to blue) of each element (see Figure 7.2(c)). To control for hue, we measure the colour difference between two steps of hue values in *CIE-L\*uv* colour space. The distance between two colours  $(L_1, u_1^*, v_1^*)$  and  $(L_2, u_2^*, v_2^*)$  is measured by:

$$\Delta E_{Luv}^* = \sqrt{(L_2 - L_1)^2 + (u_2^* - u_1^*)^2 + (v_2^* - v_1^*)^2} \quad (7.3)$$

where  $\Delta E_{Luv}^* = 1$  is an approximation to a JND [War08b]. We set a distance of  $\Delta E_{Luv}^* = 10$  in our encoding which is conservatively larger than a JND, and therefore ensures the colour of each element is significantly discriminable as shown in Figure 7.2(c).

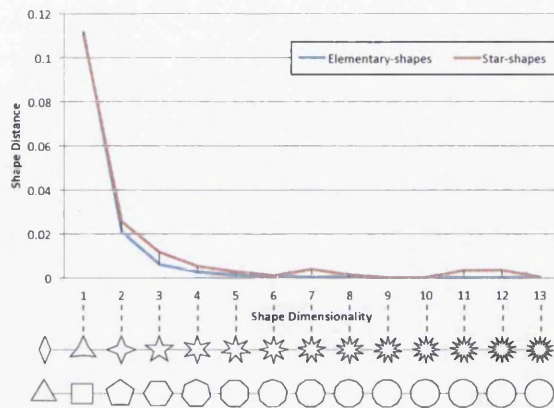
**Texture** is mapped to grain (or frequency) of the texture (see Figure 7.2(d)). At a given value, the texture is the number of separable marks contained in a unitary area. Ware and Knight [WK92] refer to this as *contrast*, and is one of the dimensions of texture along with size, and orientation. While there has been previous work on generating visually discriminable textures (e.g., [BHW05, CR68, HBW06]), they do not explicitly measure a perceptible difference. We therefore use a perceptually motivated approach to estimate the difference between two texture elements. Since texture is perceived as the ratio of white (e.g., the gap separating two marks) and black, we can use these features to determine a texture difference. First, we use connected component analysis [HZ04] to detect the amount of black  $b \in [0, -1]$ , and the amount of white  $w \in [0, +1]$  between each pattern cycle. We then calculate the difference between two textures  $t_i = (b_i, w_i)$  and  $t_j = (b_j, w_j)$  as:

$$|t_i - t_j| = |(b_j + w_j) - (b_i + w_i)| \quad (7.4)$$

To investigate the texture difference which corresponds to a JND, we performed a pilot test with five participants. We showed each participant two randomly selected texture elements side-by-side on a fifteen inch laptop display, and asked whether they were equal, or not equal. Participants could only respond using the keyboard to eliminate movement delays, and we recorded their error rate and response time. During pilot testing, we found a distance  $|t_i - t_j| > 0.01$  is an approximate value of a perceptible difference.

**Orientation** is mapped to line orientation (see Figure 7.2(e)). We mapped orientation to a unique range of angles  $[5^\circ, 175^\circ]$  to avoid any ambiguity. A number of psychology experiments indicate that line orientation discrimination ranges between  $1.06^\circ - 6.44^\circ$  as a factor of line length [VVO86]. Our vision is particularly sensitive to changes from a vertical and horizontal orientation where a JND is reported as little as  $0.71^\circ$  [OVV84, VO85]. Since the orientation difference here in our visualization (e.g.,  $11.3^\circ$ ) is significantly greater than this JND, we find that the difference between elements can be accurately perceived.

**Shape** is mapped to the number of *spikes* of a star-shaped glyph (see Figure 7.2(f)). For our studies, it is important that viewers are able to extract an underlying relationship between the set of shape values. The discrete nature of shape makes such an encoding challenging [Ber83, Mac86]. From a restricted set of shapes, we considered two visual designs: (1) elementary shapes, and (2) star shape glyphs as shown in Figure 7.3. The elementary shape maps the value to the number of edges.



**Figure 7.3:** Comparing shape similarity between a given shape, and its predecessor, to measure the distinctiveness as the number of spikes (star-shape) and edges (elementary-shape) increases.

Computer vision offers many techniques to measure the distance between two shapes [HZ04], and we use one of these to choose the visual design that is most discriminable. To measure a shape difference, we utilise image moment statistics [Hu62]. Figure 7.3 compares the similarity of the two set of shapes as the number of dimensions increases. The elementary shape (blue line) converges to a difference where sequential shapes are no longer dissimilar quicker than the star-shape glyph (red line). Since we cannot be sure whether this distance correlates with their perceived difference, we perform another pilot study similar to the one we analysed for texture. We did not find any clear differences in performance, however, participants were slightly more accurate with star-shaped glyphs (Error = 11.11%) compared to elementary shapes (Error = 12.04%). Based on these findings, we chose star-shaped glyphs as our encoding.

### 7.3 Experimental Overview

In order to compare the perceptual orderability of visual channels, we performed a within subject experiment design to analyse orderability based on three criteria:

- **How ordered is it?** — we measure the perceived orderedness in a sequence of elements from 1 (unordered) to 5 (ordered).
- **Which is smallest? Which is largest?** — we assess the ability to identify whether a target element has the smallest value, largest value, or neither. Their accuracy and response time is measured.
- **How many pairs?** — we assess the ability of counting pairs of elements which have the same value. Similarly, their accuracy and response time is measured.

This led us to develop three experiments which we conducted using Amazon's Mechanical Turk, an online crowdsourcing platform [KZ10]. Online crowdsourcing experiments present an attractive option for evaluating the perceptual challenges in visualization design due to its low cost and increased scalability [HB10, KZ10]. A number of successful studies include semantic colouring [HS12, LFK\*13, Mor03], designing effective treemaps [LHH\*12] and visual tasks for human computation algorithms [GSCO12]. Heer and Bostock [HB10] demonstrate the validity of using such a platform for graphical perception experiments by replicating previous controlled laboratory studies on Amazon's Mechanical Turk. With an expected larger variance, their crowdsourced results are consistent with previous findings. The cause of this variance is reported to be a range of factors such as display size, colour calibration, viewing distance and lighting, which may reflect more accurately the working environment of real users.

We follow previous crowdsourcing studies to help design our experiments. In Experiment 1, the aim is to understand how different visual channels affect the perception of orderedness within a sequence, where one goal is to analyse the relationship between perceived orderedness versus measured orderedness. We considered several experimental designs for this task such as Two-Alternative Forced Choice (2AFC) [Fec60]. While this approach would enable us to analyse a user's perception on whether a sequence is more or less ordered than another, it does not allow us quantify perceived orderedness and fulfil the requirement of our analyses. We also considered a ranking approach whereby users would rank a set of sequences based on their perceived order. The amount of user interaction required for this approach made this unsuitable for our crowdsourcing environment, where it is expected that tasks should be very quick to answer (less than one minute). We therefore find a rating approach as described in Section 7.4 to be the most appropriate design for this particular task. For Experiment 2 and Experiment 3, we opted for a multiple choice question approach with three possible answers (see Section 7.5 and Section 7.6 for details). This design was chosen in order to reduce the possibility of bias in the results from unfaithful workers. We also apply additional consistency checks to detect such contributors from our data (Section 7.3.3).

Each study followed a similar experimental procedure. Before users participated in the study, we first demonstrate the interface to the participants through a video tutorial which was embedded on the web page. These demonstrations allowed participants to gain familiarity with the interface prior the experiment, and to understand the required task. For each experiment, we recorded the following details: gender, age group, whether they were colour blind, and the device they were using. After the study, each participant completed a qualitative survey regarding the experiment (see Table 7.1). We also provide an optional feedback form for participants to give additional comments.

### **7.3.1 Interface**

We developed the web-based interface using HTML, Javascript and PHP. The experiment interface consists of a single view of the visual stimuli, and the question at the

| Question  | Answer               |
|---|----------------------|
| When the sequence of elements are <b>ordered</b> , how difficult did you find the task?   | (Easy) 1 - 5 (Hard)  |
| When the sequence of elements are <b>unordered</b> , how difficult did you find the task? | (Easy) 1 - 5 (Hard)  |
| <b>Rank the visual channels</b> in order of their perceived difficulty.                   | (Least) 1 - 7 (Most) |

*Table 7.1: Qualitative survey participants filled after each experiment.*

top of the screen as shown in Figure 7.4. A series of radio buttons appears at the bottom of the interface indicating the possible answers. Based on the feedback from our experimental pilot (see Section 7.3.2), we improved the size of the button by drawing a clickable box around each radio button. Once a radio button is selected, participants then confirm their response by clicking on the large button at the bottom of the screen, and the next stimuli is presented in the view. Another feature which participants requested from our pilot results is a progress bar observed in the top right corner of the screen. Due to the repetitive nature of the task, they found such a visual cue would help monitor their progress, and reduce the risk of a participant rushing to complete the study.

### 7.3.2 Pilot Studies

Before deploying our experiments on Amazon’s Mechanical Turk, we conducted both lab-based and crowdsource-based pilot studies.

**Experimental Pilot.** We first conducted an initial pilot study using 5 participants for each experiment. Our focus here is to investigate the following: (1) the usability of the interface, (2) estimate the time for completion, and (3) evaluate the experimental design. For Experiment 1 and 2, there were 168 trials of each condition: 7 visual channels  $\times$  8 noise levels  $\times$  3 repetitions. The repetitions in Experiment 2 correspond to the three question types asked. In the third experiment (see Section 7.6 for details), we reduced the number of noise levels to 3 and repeated the condition for each answer, making a total of 189 trials. This reduction was so that the number of stimuli for the three experiments is of similar length. Each of these trials is randomised per participant. To help overcome any learning effects, the block of trials is preceded by a practice block of sample questions, selected randomly from a training dataset, with each condition being asked at least twice. After each experiment, we held a consultation with each participant individually and report their feedback.

Most participants found the interface intuitive to use. However, some mentioned that the radio buttons were too small which we address by enlarging the hit box in the final interface (see Figure 7.4 for example). Since we cannot control the environment of

online contributors (e.g., preventing workers from taking long breaks), we designed our experiments with a strong emphasis to objective (2) to minimise fatigue, and encourage workers to complete the study. During pilot testing, participants felt Experiment 1 (~45 minutes) and Experiment 3 (~50 minutes) was too long. On the other hand, participants felt comfortable in Experiment 2 (~15 minutes). Based on this experience, we find an approximate guideline to an experimental length should not exceed 15-20 minutes in order for participants to complete our study without breaks. We therefore modified the conditions in Experiment 1 by reducing the levels of noise from 8 ( $\eta_1, \dots, \eta_8$ )  $\rightarrow$  5 ( $N_1, \dots, N_5$ ) and by removing only those where the variation is not significant as found in our pilot results. In addition, we decreased the number of repetitions to two for Experiment 3. This reduces the total number of tasks a participant sees such that the experimental completion time is consistent with our second study.

**Mechanical Turk Pilot.** In order to verify the experimental updates derived from our previous pilot, as well as gauge the behaviour of online contributors, we ran a second pilot of 20 participants using Mechanical Turk. This data is not included in our overall analyses.

Many online platforms such as Mechanical Turk provide an option to target your job to skilled contributors only as an approach to improve the quality of the crowdsourced data. We apply this feature in our studies. Each participant can only perform the study once. The maximum time allowed for each session is one hour. We found that all participants finished within time and no further issues are reported.

### 7.3.3 Crowdsourcing Consistency

Apart from restricting the job to a set of skilled contributors, we have no way of ensuring whether a worker does a good job, and we therefore have to be careful filtering bad data. In fact, even with this option, we observed some cases in our pilot where contributors were not invested in the experiment, for example, selecting the same answer for all stimuli. Previous crowd-sourced user studies by Cole *et al.* [CSD\*09] and McCrae *et al.* [MMS13] propose the use of consistency checks to address this. Using the same principles, we devised a set of consistency checks based on the results we found in our Mechanical Turk pilot:

- **C1.** Close to chance - users for whom the error is close to chance (e.g.,  $\mu > 0.66$ ) we reject from the analysis.
- **C2.** Standard deviation of answers - we reject contributors whose distribution of answers in an experimental task is close to zero ( $\sigma < 0.2$ ). This identifies participants who are mostly choosing just one answer throughout their experiment.
- **C3.** Variance of answers for ordered sequences - since we are asking information about interpretation in Experiment 1, there are no definitively wrong answers,



especially when a sequence of elements is unordered. We therefore perform a check based on how reliable a user's answer is for a known data condition (e.g., an ordered sequence for each visual channel), by looking at their variance. For Experiment 1, we reject contributors whose variance is significantly large (e.g.,  $\sigma^2 > 2$ ). This is one approach to identify potential users who are answering randomly.

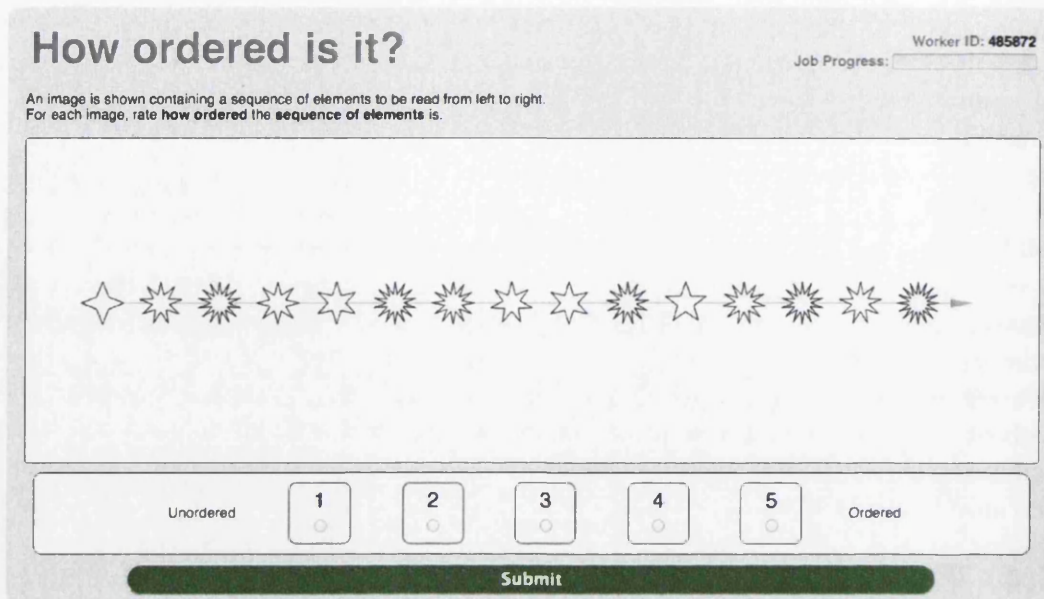
C1 cannot be used in *How ordered is it?*, as we have no ground truth to compare. We therefore use checks C2 and C3. For *Which is smallest? Which is largest?* and *How many pairs?*, we use C1 and C2 since we can measure for correctness by calculating an error. With our consistency checks we are able to remove severely negligent workers without removing many trustworthy workers. In all, approximately 95% of the data gathered passes our criteria and is included in our dataset.

## 7.4 Experiment 1: How ordered is it?

The goal of our first experiment is to investigate whether different visual channels affect the perceptual order of a sequence of elements. In addition, we hypothesise that the perceived order of different visual channels are more/less sensitive to noise than others. Such a property can be desirable to improve the performance of various analytical tasks [Mac86]. For example, users may often seek an encoding that is sensitive to noise for detecting outliers (e.g., temperature maps). Whereas a less sensitive mapping is also desirable, for example, in extracting trends in multi-dimensional analysis. Choosing the most appropriate visual encoding for the task is an important step in effective data visualization. We test this hypothesis through an experiment conducted on Amazon Mechanical Turk. Participants were asked to rate how ordered a sequence of elements is using 1D plot graphs. Each 1D plot showed 15 data samples which we mapped using each visual channel as described in Section 7.2.3.

**Participants.** 115 contributors on Mechanical Turk participated in the experiment. Two participants reported they were colour-blind, and their data was discarded. Another three participants failed our consistency checks, and were also removed. Therefore, 110 participants (62 male and 48 female) were included in our final analysis. The devices used were: 49 desktop, 54 laptop, 6 tablet, and 1 phone. Participants were paid \$1.00.

**Experimental Design.** The experiment followed a within subject design and consisted of seven visual channels, five different noise levels, and three repetitions (105 trials). At the start of the experiment, participants completed a training block of 14 sample questions showing an ordered and unordered sequence for each visual channel (see Appendix C.1), making a total of 119 trials. To limit any confounding effects of fatigue and



**Figure 7.4:** A screenshot of the visual interface for Experiment 1: *How ordered is it?* Shape is tested in this example.

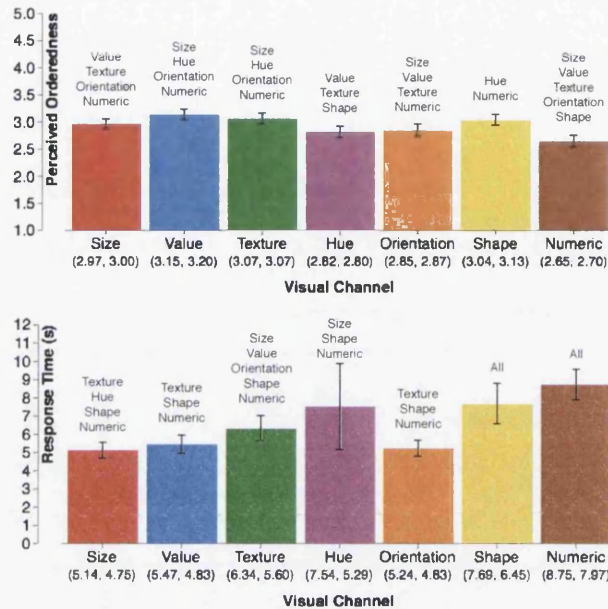
learning, the two blocks of trials were randomised per participant. To counteract memory, the dataset used for each repetition of a noise level was generated independently with equal correlation coefficients to two significant figures. The correlation measured at each noise level is:  $N_1 = 1.0$ ,  $N_2 = 0.97$ ,  $N_3 = 0.90$ ,  $N_4 = 0.71$ , and  $N_5 = 0.12$ .

For a single trial, we showed participants a 1D plot and asked them to rate *how ordered* the elements are using a 5-point Likert scale that corresponds to 1 (unordered) through to 5 (ordered) respectively (see Figure 7.4). After observing the sequence of elements, participants provided their rating by clicking on one of the radio buttons below the image followed by the submit button. We measured both answer and response time after each trial, before the next stimulus was automatically displayed. In order to overcome change blindness, we used an Inter-Stimulus-Interval (ISI) [BBK09] in between each stimuli. A simple loading screen is displayed for two seconds between trials which was chosen through pilot experiments and determined as a comfortable length. This served for two purposes: 1) to indicate that the stimulus has actually changed, and 2) to ‘reset’ the visual system and remove any possibilities of a previous stimuli influencing the following one.

### 7.4.1 Results

We perform our analysis in two stages. First, we consider the effect of perceptual orderability based on visual channel overall, as this is our primary research question. We

**Figure 7.5:** Comparing the effects of visual channel against perceived orderedness (top) and response time (bottom) in Experiment 1. Significant differences are listed above each bar, with (mean, median) values indicated below. Error bars show 95% confidence intervals. Bars are colour-coded using ColorBrewer [HB11].



find that the data is not always normally distributed, and therefore use a non-parametric Friedman's test with standard statistical level  $\alpha = 0.05$  to determine the statistical significance between conditions.

We then analyse how visual channel affects the perceptual orderability under the condition of noise level. When dividing the data by noise level, we apply a Bonferroni correction, reducing the significance level to  $\alpha = 0.01$  for this second second-level analysis. Post-hoc analysis was conducted using the Nemenyi-Damico-Wolfe-Dunn test [HW99] for testing multiple pair-wise comparison. We report our results below.

#### 7.4.1.1 Orderability of Visual Channel Overall

Figure 7.5 shows the mean orderability and response time results. We find a significant difference in both perceived orderedness ( $\chi^2(6) = 149.05$ ,  $p \ll 0.05$ ) and response time ( $\chi^2(6) = 289.61$ ,  $p \ll 0.05$ ) depending on the visual channel participants see.

##### • Mean orderability:

- Value (3.15) and texture (3.07) is perceived significantly more ordered than size (2.97), orientation (2.85), hue (2.82), and numeric (2.65) ( $p \ll 0.05$ ).
- Shape (3.04) is perceived more ordered than hue (2.82) and numeric (2.65) ( $p \ll 0.05$ ).
- Size (2.97) is perceived more ordered than orientation (2.85) and numeric (2.65), but less ordered than value (3.15) and texture (3.07) ( $p \ll 0.05$ ).

- Orientation (2.85) is perceived more ordered than numeric (2.65), but less ordered than value (3.15), texture (3.07) and shape (3.04) ( $p \ll 0.05$ ).
- Hue (2.82) is perceived less ordered than value (3.15), texture (3.07), and shape (3.04) ( $p \ll 0.05$ ).
- Numeric (2.65) is perceived less ordered than size (2.97), value (3.15), texture (3.07), shape (3.04), and orientation (2.85) ( $p \ll 0.05$ ).

- **Response time:**

- Size (5.14s) is significantly faster than texture (6.34s), hue (7.54s), shape (7.69s), and numeric (8.75s) ( $p \ll 0.05$ ).
- Orientation (5.24s) and value (5.47s) are faster than texture (6.34s), shape (7.69s), and numeric (8.75s) ( $p \ll 0.05$ ).
- Texture (6.34s) is faster than shape (7.69s) and numeric (8.75s), but slower than size (5.14s), orientation (5.24s), and value (5.47s) ( $p \ll 0.05$ ).
- Hue (7.54s) is faster than shape (7.69s) and numeric (8.75s), but slower than size (5.14s) ( $p \ll 0.05$ ).
- Shape (7.69s) is faster than numeric (8.75s), but slower than all other visual channels ( $p \ll 0.05$ ).
- Numeric (8.75s) is significantly the slowest compared to all other visual channels ( $p \ll 0.05$ ).

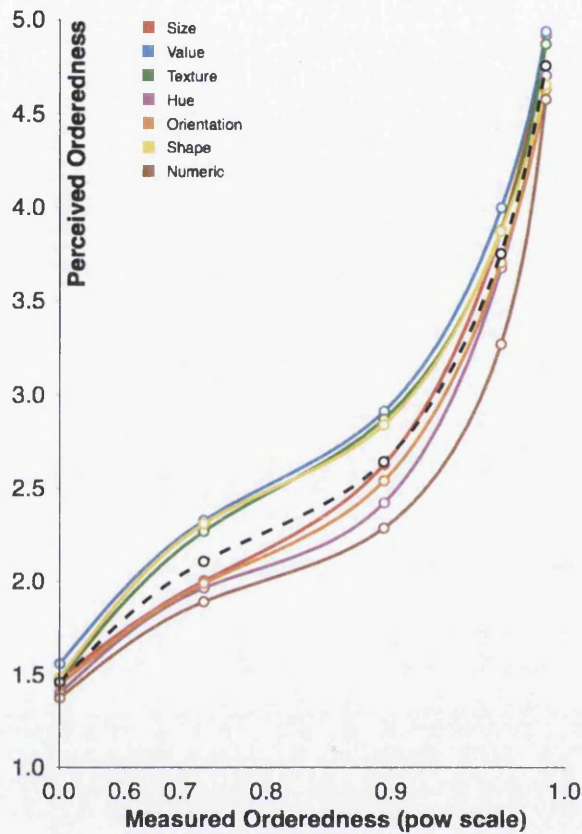
#### **7.4.1.2 Noise Sensitivity of Visual Channels**

Figure 7.6 compares the effects of noise level (i.e., measured orderedness) to the perceived orderedness under different visual channels. Our results show that noise level has a significant effect on the perceived order ( $p \ll 0.01$ ). The significant differences are shown in Table 7.2.

## **7.4.2 Discussion**

**Overall.** Our results show significant evidence that different visual channels affect the perception of orderedness in sequences. For example, participants tend to rate a sequence as being more ordered using value, while other visual channels (e.g., hue) are often judged as being less ordered. This suggests that if a visualization task involves detecting ordered or unordered patterns, mappings to different visual channels will lead to different judgements.

Overall, value and texture lead to higher degree of perceived orderedness. Given the encoding for texture we used, this makes sense as both channels can be viewed as a form of grayscale. Surprisingly, we also find shape to be orderable. However, using shape led to increased response time overall by 1.23s compared to value and texture. Looking at



**Figure 7.6:** Comparison of measured orderedness (or correlation coefficient) versus perceived orderedness. Points depict the perceived orderedness for each visual channel, organised by power scale of measured orderedness. The average is plotted (dashed line) against visual channels (coloured lines) using a line of best fit.

our results based on medians, we also observe size has a perceived orderedness of 3.0 on average, which indicates that size may produce similar judgements of orderedness as to value, texture, and shape.

If the goal is to detect an ordered pattern, participants reacted faster with visual channels that have a higher degree of perceived orderedness (e.g., value, texture, and size). This allowed time savings of up to three seconds or more (e.g., versus hue and numeric) per task. However, if the task is to detect an unordered pattern, participants respond faster using orientation. Since visualization viewers often engage in many trend extracting tasks both within and across charts, this may improve both performance (e.g., detecting an ordering), and reduce cognitive load depending on the choice of visual channel used.

| Pair-wise test        | Noise level |      |      |      |      |
|-----------------------|-------------|------|------|------|------|
|                       | N5          | N4   | N3   | N2   | N1   |
| Value - Shape         | 0.86        | 0.97 | 0.53 | 0.99 | 0.00 |
| Value - Texture       | 0.76        | 0.83 | 0.96 | 0.49 | 0.77 |
| Value - Size          | 0.98        | 0.00 | 0.00 | 0.84 | 0.98 |
| Value - Orientation   | 0.40        | 0.00 | 0.00 | 0.05 | 0.00 |
| Value - Hue           | 0.07        | 0.00 | 0.00 | 0.00 | 0.00 |
| Value - Numeric       | 0.00        | 0.00 | 0.00 | 0.00 | 0.00 |
| Shape - Texture       | 1.00        | 0.99 | 0.97 | 0.89 | 0.00 |
| Shape - Size          | 0.99        | 0.00 | 0.30 | 0.99 | 0.00 |
| Shape - Orientation   | 0.98        | 0.00 | 0.03 | 0.26 | 0.35 |
| Shape - Hue           | 0.73        | 0.00 | 0.00 | 0.02 | 0.40 |
| Shape - Numeric       | 0.25        | 0.00 | 0.00 | 0.00 | 1.00 |
| Texture - Size        | 0.99        | 0.00 | 0.03 | 0.99 | 0.99 |
| Texture - Orientation | 0.99        | 0.00 | 0.00 | 0.94 | 0.30 |
| Texture - Hue         | 0.84        | 0.00 | 0.00 | 0.45 | 0.26 |
| Texture - Numeric     | 0.36        | 0.00 | 0.00 | 0.00 | 0.00 |
| Size - Orientation    | 0.90        | 0.98 | 0.97 | 0.67 | 0.06 |
| Size - Hue            | 0.45        | 0.99 | 0.00 | 0.16 | 0.05 |
| Size - Numeric        | 0.09        | 0.35 | 0.00 | 0.00 | 0.00 |
| Orientation - Hue     | 0.98        | 0.99 | 0.06 | 0.97 | 1.00 |
| Orientation - Numeric | 0.72        | 0.84 | 0.08 | 0.00 | 0.38 |
| Hue - Numeric         | 0.98        | 0.59 | 1.00 | 0.00 | 0.43 |

**Table 7.2:** Experiment 1 results. Reporting *p*-values of post-hoc results analysing the effects of noise level on perceived orderedness under different visual channels. Significant differences are highlighted in red using a Bonferroni corrected  $\alpha = 0.01$ .

**Sensitivity to noise.** Looking at the effect sizes of noise level (see Figure 7.6), we observe that the perceived orderedness of different visual channels decreases at different rates. This behaviour is consistent across all visual channels tested, and that the relationship between measured orderedness (i.e., noise level), and perceived orderedness is non-linear. There is a common trend in the middle where the perceived orderedness dips between the measured orderedness  $N_2 = 0.97$  and  $N_4 = 0.71$  illustrated by the slope of the curves. For example, shape decreased in perceived orderedness by 1.55 in this range. Comparing this to a visual channel such as hue, we see a greater difference of 1.74. This difference indicates that some visual channels (e.g., shape) are less sensitive to noise such that viewers may perceive an ordered pattern that does not exist in the data. Similarly, other visual channels (e.g., hue) are more sensitive to noise such that viewers are less likely to see an ordered pattern.

We present further comparative analyses by plotting visual channels against an average curve (dashed line) as shown in Figure 7.6. There are two observable clusters above and below the curve. Our results show that value, texture, and shape seem to lead to participants to estimate a higher degree of orderedness than orientation, size, hue, and numeric. We also find that this gap is significant as shown in Table 7.2. Notice that

for  $N_4$ , the visual channels that lie above the average (e.g., value, shape and texture) are significantly different to those below (e.g., size, orientation, hue and numeric) indicated by the  $p$ -values highlighted in red. The same differences can mostly be seen in  $N_3$ . At this condition, size and orientation perform closer to the average, and thus we find this gap becomes less distinct. One interesting observation is that size starts and finishes above and below the average as measured orderedness increases. This means that the orderability of size is less sensitive to low frequency noise, but more sensitive to high frequency noise, which makes size a good visual channel for detecting both ordered and unordered patterns.

For very ordered and very unordered sequences (e.g.,  $N_5$  and  $N_1$ ), different visual channels lead to almost the same judgement. Participants mostly rate the order of such sequences to be 1 (unordered) and 5 (ordered) respectively, independent of the visual channel used. We therefore found fewer significant differences. At such levels of measured orderedness, the decision becomes a binary process (e.g., ordered, or not ordered). Hence, we expected such results to appear in our data. Based on our findings, we conclude that human's judgement of orderedness is sensitive to the choice of visual channel. The amount of difference depends on the level of orderedness. We look at how this may affect the performance of visual search in Experiment 2.

## 7.5 Experiment 2: Which is smallest? Which is largest?

The goal of our second experiment investigates how the perceptual orderability of different visual channels affects the performance of a visual search task. For such a task, we adopt the test proposed by Bertin [Ber83] to analyse a viewer's ability to perceptually determine whether an element is less than or greater than a target element. We test this using a set of 1D plots as described in Section 7.2.3. The experiment follows a similar design to Experiment 1. We describe the differences below.

**Participants.** 88 contributors on Mechanical Turk participated in the experiment. No participants reported they were colour-blind. One participant failed our consistency checks and was removed. Therefore, 87 participants (42 male and 45 female) were included in our final analysis. The devices used were: 40 desktop, 42 laptop and 5 tablet. Participants were paid \$1.00.

**Experimental Design.** The experiment followed a within subject design. The visual stimuli consisted of seven visual channels and eight different noise levels (see Appendix C.2). We tested the eight noise levels  $\eta_1, \dots, \eta_8$  as described in Section 7.2.2. Participants saw a series of 1D plots containing a sequence of elements with one target element highlighted in a red bounding box as shown in Figure 7.7. For each trial, we asked participants to identify whether the highlighted element has: (1) the **smallest** value, (2) the **largest** value, or (3) **neither**. The experimental procedure required

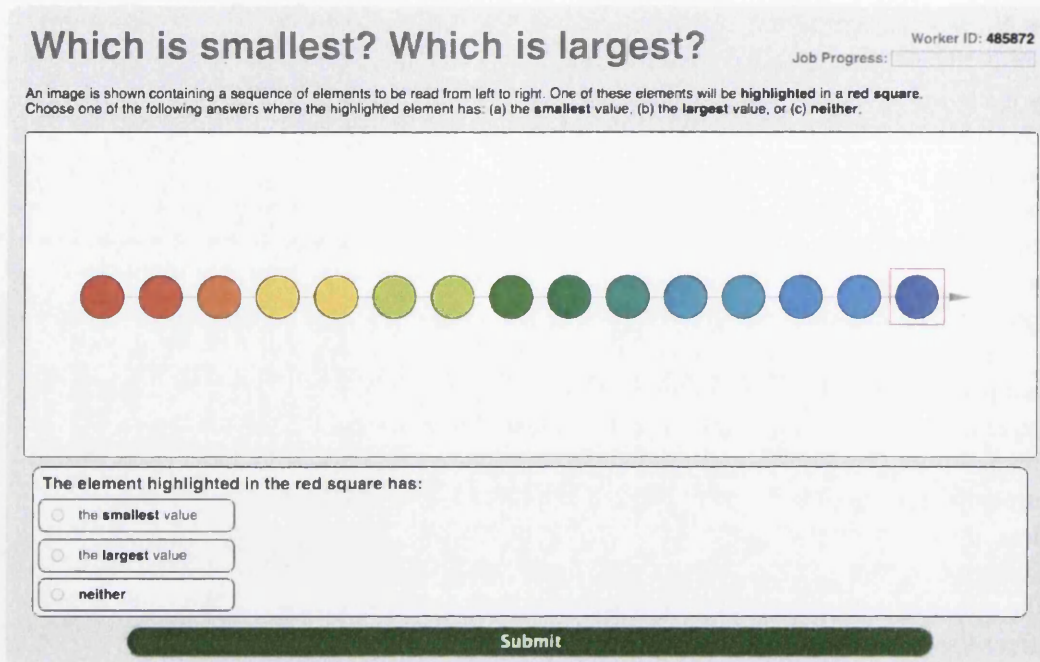


Figure 7.7: A screenshot of the visual interface for Experiment 2: Which is smallest? Which is largest?

participants to answer all question types under each condition (168 trials). Similar to Experiment 1, we first showed a training block of 16 sample questions unrelated to later trials. Each participant therefore completed a total of 184 trials which were randomised in both blocks. We used the same interface as in Experiment 1, with a list of answers presented below the stimuli. Participants respond by selecting one of these answers. The keywords of each question type is highlighted in bold text to enable easy identification. We measured both error rate and response time.

### 7.5.1 Results

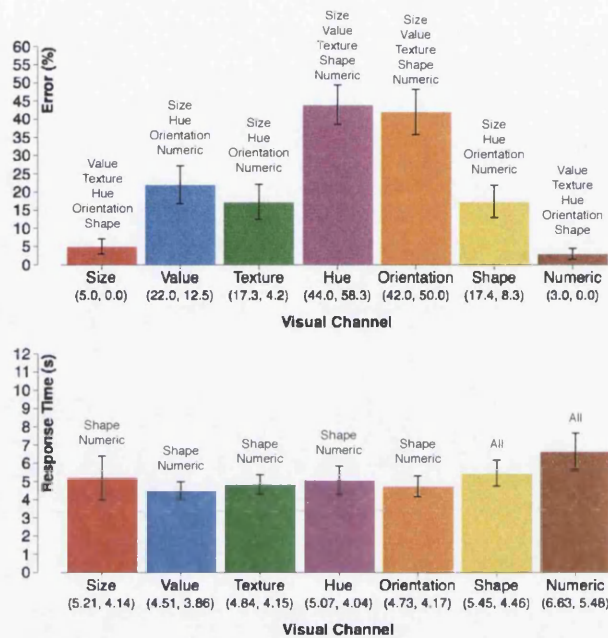
Figure 7.8 shows the mean error and response time results in this experiment. Since the data we collected is not normally distributed, we once again apply non-parametric statistics. A Friedman's test shows significant differences in error rate ( $\chi^2(6) = 276.15$ ,  $p \ll 0.05$ ) and response time ( $\chi^2(6) = 121.46$ ,  $p \ll 0.05$ ) under the effects of visual channel. We report results following the same approach used in Experiment 1.

- **Error rate:**

- Numeric (3.0%) and size (5.0%) produced significantly fewer errors than texture (17.3%), shape (17.4%), value (22.0%), orientation (42.0%), and hue (44.0%) ( $p \ll 0.05$ ).



**Figure 7.8:** Comparing the effects of visual channel against error rate (top) and response time (bottom) in Experiment 2. Significant differences are listed above each bar, with (mean, median) values indicated below. Error bars show 95% confidence intervals.



- Texture (17.3%), shape (17.4%), and value (22.0%) produced fewer errors than orientation (42.0%) and hue (44.0%), but more errors than size (5.0%) and numeric (3.0%) ( $p \ll 0.05$ ).
- Orientation (42.0%) and hue (44.0%) produced more errors than numeric (3.0%), size (5.0%), texture (17.3%), shape (17.4%), and value (22.0%) ( $p \ll 0.05$ ).

- **Response time:**

- There were no significant differences in response time between value (4.51s), orientation (4.73s), texture (4.84s), hue (5.07s), and size (5.21s).
- Shape (5.45s) is significantly faster than numeric (6.63s), but slower than all other visual channels ( $p \ll 0.05$ ).
- Numeric (6.63s) is significantly the slowest compared to all other visual channels ( $p \ll 0.05$ ).

## 7.5.2 Discussion

**Overall.** Given a sequence of elements, we find that different visual channels have a significant effect on the error rate of min-max judgements. Participants produced fewest errors with numeric. This is what we expected, since the value is explicitly given and the number of samples shown is relatively small. Despite the numerical values observed being not very complex (e.g., 3 digits) which meant that the cognitive load on short

term memory is relatively low, we find participants spent a significant amount of time scanning the numbers as shown in their response data (see Figure 7.8(bottom)). Thus visual encodings seem to help in this task.

Judgements using size also produced fewer errors which cannot be explained in our data. To investigate potential reasons, we refer back to Bertin's classification of visual properties and find that size is the only channel which is quantitative [Ber83]. A quantitative variable means we can perceive the numerical ratio between two sizes, for example, this circle is twice the size of that circle. This may explain why size performed so well in our tests. However, further experimentation is needed to fully understand the exact causes.

Conversely, error rate significantly increased when using hue and orientation. It is easy to see that such encodings can be misleading (e.g., they do not impose a universal perceived order) and would therefore produce more errors in such a task. This is consistent with previous claims, for example, the error-prone use of rainbow colour-mapping within the visualization community [BT07].

We find few significant effects in our response time data. However, shape and numeric were once again the slowest as found in Experiment 1, which supports that both encodings are cognitively demanding, and thus, increases response times.

## 7.6 Experiment 3: How many pairs?

In our third experiment, we investigate how different visual channels affect categorical perception for ordered and unordered sequences. This study focuses on the perception of equality, by identifying the number of pairs of elements which have the same value. Such a question is representative of common graph-reading tasks (e.g., "how many countries have an average life expectancy of 75 or above"). The experiment follows a design similar to Experiment 2. We outline the differences below.

**Participants.** 136 contributors on Mechanical Turk participated in the experiment. Three participants reported they were colour-blind, and their data was discarded. Another five participants failed our consistency checks, and were also removed. Therefore, 128 participants (61 male and 67 female) were included in our final analysis. The devices used were: 51 computer, 70 laptop, 5 tablet, and 2 phone. We raised the reward to \$1.50 to accommodate the increased average task completion time over our previous experiments.

**Experimental Design.** The experiment followed a within subject design and consisted of seven visual channels, three different noise levels, and two repetitions (see Appendix C.3). Each participant a series of 1D plots and we asked them how many pairs of elements have the same value? Participants responded with either: (1) **0 pairs** (each element has a different value to others), (2) **1 pair** (only one pair of elements have

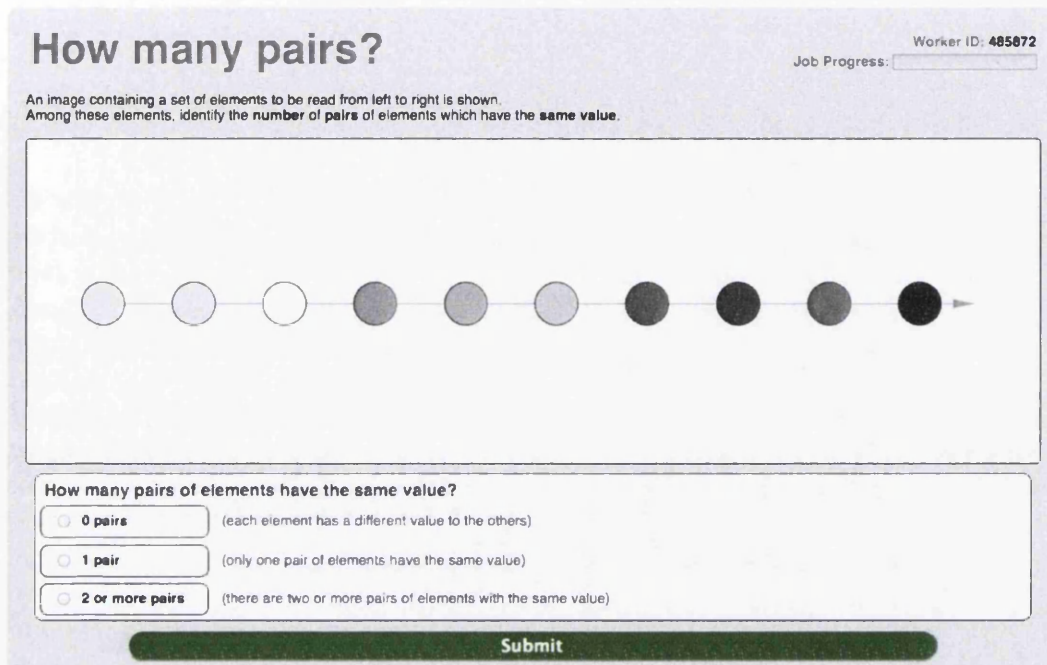


Figure 7.9: A screenshot of the visual interface for Experiment 3: How many pairs?

the same value), or (3) **2 or more pairs** (there are two or more pairs of elements with the same value). Each participant was required to answer all question types under each condition twice (126 trials). Like our previous studies, participants first completed a training block of 15 sample questions before they were able to answer later trials. Each participant would therefore complete a total of 141 trials.

We used the same interface as before. In each trial, participants observed a 1D plot as shown in Figure 7.9. From piloting (see Section 7.3.2), we modified our experimental design according to feedback from participants finding the task difficult. We also decreased the number of trials a participant sees through a reduction of noise levels ( $5 \rightarrow 2$ ) and repetitions ( $3 \rightarrow 2$ ). The correlation of each dataset used were:  $N_1 = 1.0$ ,  $N_2 = 0.90$ ,  $N_3 = 0.12$ . Prior to encoding, datasets are discretised to integer values.

### 7.6.1 Results

The mean error and response time results for this experiment is shown in Figure 7.10. Our data was not normally distributed, hence, we applied the same analysis approach as in Experiment 2. There was a statistical significant difference in both error rate ( $\chi^2(6) = 488.44$ ,  $p \ll 0.05$ ) and response time ( $\chi^2(6) = 393.87$ ,  $p \ll 0.05$ ) under the effects of visual channel. We report our post-hoc analysis below.

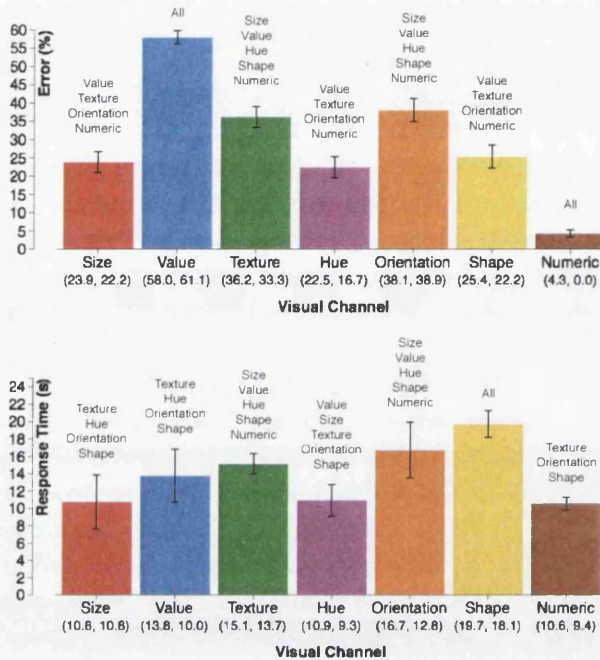


Figure 7.10: Comparing the effects of visual channel against error rate (top) and response time (bottom) in Experiment 3. Significant differences are listed above each bar; with (mean, median) values indicated below. Error bars show 95% confidence intervals.

• Error rate:

- Numeric (4.3%) produced significantly fewer errors compared to all other visual channels ( $p \ll 0.05$ ).
- Hue (22.5%), size (23.9%), and shape (25.4%) produced fewer errors than value (58%), texture (36.2%), and orientation (38.1%), but more errors than numeric (4.3%) ( $p \ll 0.05$ ).
- Texture (36.2%) and orientation (38.1%) produced fewer errors than value (58%), but more errors than hue (22.5%), size (23.9%), and shape (25.4%) ( $p \ll 0.05$ ).
- Value (58%) produced more errors compared to all other visual channels ( $p \ll 0.05$ ).

• Response time:

- Numeric (10.6s) is significantly faster than texture (15.1s), orientation (16.7s), and shape (19.7s) ( $p \ll 0.05$ ).
- Size (10.8s) is significantly faster than hue (10.9s), texture (15.1s), orientation (16.7s), and shape (19.7s) ( $p \ll 0.05$ ).
- Hue (10.9s) is significantly faster than texture (15.1s), orientation (16.7s), and shape (19.7s), but slower than size (10.8s) ( $p \ll 0.05$ ).

- Value (13.8s) is significantly faster than texture (15.1s), orientation (16.7s), and shape (19.7s) ( $p \ll 0.05$ ), but slower than hue (10.9s) ( $p \ll 0.05$ ).
- Texture (15.1s) and orientation (16.7s) is significantly faster than shape (19.7s), but slower than numeric (10.6s), size (10.8s), hue (10.9s), and value (13.8s) ( $p \ll 0.05$ ).
- Shape (19.7s) is significantly the slowest compared to all other visual channels ( $p \ll 0.05$ ).

## 7.6.2 Discussion

**Overall.** In general, we found that categorical perception significantly improved when using discrete encodings such as hue and shape. On the other hand, participants performed worse using grayscale (value), making on average 20% or more errors. It is possible that the continuous mapping of value made discriminating pairings, in particular within the middle range of the spectrum, more challenging. With that respect, size performed particularly well in our experiments but with no explanation. Moreover, we find no significance favouring size over other top performers such as hue in terms of accuracy.

Our current experiment shows a significant increase in speed when using hue and numeric for ordered and unordered sequences. This is shown by the median response times in Figure 7.10. Similarly to Experiment 2, it is unsurprising that participants performed significantly better using numeric. These results may be particular to the small number of sampled points displayed in each plot, and hence the performance might degrade for longer sequences.

## 7.7 Limitations

All three experiments are limited by their parameters, and the empirical results are generalisable only within the scope of those parameters. We used synthetic datasets to generate ordered and unordered sequences that is appropriate for our task, and hence, the application to a real dataset may give different results. Our definition of *orderedness* for a sequence of data items is also restricted to the definition used in signal processing theory [JJS93]. From this concept, we created sequences with eight varying levels of noise (i.e., measured orderedness). These noise levels was chosen through pilot testing such that each sequence is visually distinct. Although this study is the first of its kind to look at perceptual orderability of visual channels, we acknowledge that different results may be produced depending on other definitions of orderedness, and how orderedness is measured.

In Experiment 1, we studied the perceptual orderability of six basic visual channels, namely Bertin's retinal variables [Ber83] as well as no visual encoding (i.e., numeric). Each visual mapping was reflective of the work presented by Bertin so that our results

could be directly compared. One fundamental difference is the use of shapes. We enforced a restricted set of shapes in order for a viewer to be able to extract an underlying relationship between the set of shape values. While this was necessary for our task, this may not be equivalent to the shapes originally tested; and thus leading to different conclusions. It is important to note that Bertin presented only three different shapes (square, triangle, and circle) and hence this would not have been enough to encode the number of different values in our sequence.

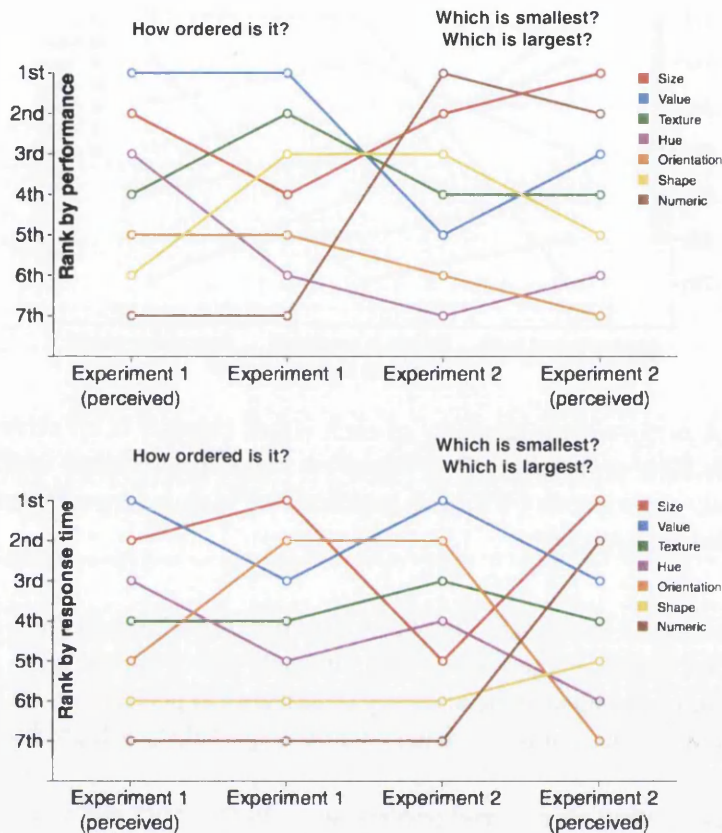
For Experiment 2 and Experiment 3, we chose two specific tasks appropriate for reading ordered and unordered sequences, and analysed our data separately according to these tasks. Our results therefore cannot be easily generalised to tasks of a different nature. Overall, while the basic visual channels studied in this research is important to glyph-based visual design, they do not fully extend to the richer set of visual channels identified in Chapter 2, indicating that further research is still needed for a more comprehensive study on ordered perception.

## 7.8 General Discussion and Summary

We now provide a summary of the work in this chapter which contains our most recent research on glyph-based visualization. The analysis described here focuses primarily on the results from Experiment 1 and 2 which we have studied in greater detail. However, we also include some of our initial findings gained from Experiment 3.

**Perceptual orderability and visual search.** Overall, we noticed that visual channels that are perceived as ordered in Experiment 1, perform well in Experiment 2. A summary of this combined performance is shown by the two middle axes in Figure 7.11(top). With the exception of numeric, the ranking is fairly consistent across both experiments. Scaling our tests to a larger number of samples may provide a more accurate ranking that reflects our results, since we predict that numeric will be greatly affected due to its high cognitive demand (see response time). We find value performs worse in our visual search task comparatively, which is surprising considering that participants perceived it as most orderable. However, it is still significantly better than less orderable channels such as hue and orientation. Our results suggest that in practice, visual orderability can improve the accuracy of visual tasks such as the one presented in our study.

**Measured vs. Perceived difficulty.** The following remarks describe the observations we made between Experiment 1 and Experiment 2. At the end of each experiment, we collected survey data as outlined in Table 7.1 to understand what participants felt was least and most difficult about the task. Most participants found both experiments to be easier when the sequence of elements are ordered, compared to unordered. In addition, we asked participants to rank the visual channels in terms of their perceived difficulty. Figure 7.11 compares this feedback against their measured rankings based on average

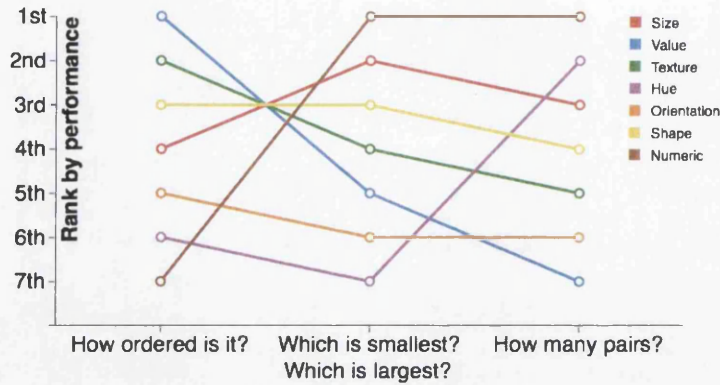


**Figure 7.11:** Visual channel ranking for Experiment 1 and Experiment 2 based on performance (top) and response time (bottom). We also compare this to participants' perceived ranking collected from our qualitative survey data. The ranking is from worst (7th) to best (1st).

performance and response time. There were no clear overall trends between perceived and actual performance (see Figure 7.11(top)). However, one observation is there is a negative correlation between hue's performance, and its perceived difficulty. This tells us that participants tend to perceive hue to be less difficult than their actual results. Similarly, shape performed better than what they expected, but not in response time.

Across both studies, we find that the perceived ranking is generally well correlated to participants' response times. For example, the ranking of shape, texture, and value remain relatively constant (straight line) as shown in Figure 7.11(bottom). It suggests that the higher the preference of a visual channel, the faster their response for that task.

**Perceptual orderability and categorical search.** Figure 7.12 summarises the performance of each visual channel under the three experiments. At the macroscopic level,



**Figure 7.12:** A performance summary of each visual channel in all three experiments. The ranking in **How ordered is it?** is based on mean orderedness, while the ranking in the other two experiments (**Which is smallest? Which is largest?** and **How many pairs?**) is based on mean error.

we noticed an inverse relationship between Experiment 1 (left axis) and Experiment 3 (right axis). Our results suggest that visual channels which appear more discrete (e.g., numeric and hue) can improve the accuracy of categorical perception. The opposite can also be said in that a more ordered visual channel (e.g., value) will produce more errors.

**Bertin’s categorisation on ordered perception.** In this work, we investigated the perceptual orderability of different visual channels for ordered and unordered sequences. The original concept described by Bertin show that shape, hue, and orientation are not ordered. However, our crowd-sourced results indicate that shape can be orderable. Of course, any arbitrary encoding of shapes will not be orderable as argued by Bertin [Ber83]. The reason behind our results is that our shapes can be considered as using two types of channels. While shape itself is not ordered, we find that counting (e.g., the number of spikes or edges) is. This raises another interesting research question: “How does the combination of visual channels affect the perceived order?”. For example, in Experiment 2, by combining value (fastest response time) with numeric (most accurate), do we gain the performance advantage from both in the resulting composition? Further experiments might therefore explore the trade-offs between such combinations.





---

## Conclusion

---

### Contents

---

|                           |     |
|---------------------------|-----|
| 8.1 Future Work . . . . . | 163 |
|---------------------------|-----|

---

**M**ULTI-DIMENSIONAL data is fast becoming the norm in many areas of practical data analysis including sports and engineering. In particular, data collected today commonly possess spatial and temporal properties, as well as containing a large number of attribute dimensions that is difficult to visualize using classical methods such as bar charts, pie charts, and line graphs. For the past several years, multi-dimensional techniques such as parallel coordinates and scatter plot matrices has been at the forefront of multivariate analysis [HJ05, Tel07]. However, with the former being less suited at conveying the spatial relationship inherent in the data; and the latter only showing bivariate relationships (when it is known there are interactions between three or more attributes), the need for alternative methods is necessary. Glyph-based visualization is one approach for realising this. We have since seen an increase in research activity towards glyph-based approaches primarily due to the fact that previous techniques are less effective with current datasets [War08a]. The goal of this thesis is to explore the potential of glyph-based visualization for high-dimensional data.

The work in Chapter 2 provides us some insight towards this goal through reviewing the most recent developments in high-dimensional glyph-based visualization. This state-of-the-art survey gave a foundation for our glyph-based visualization research. In particular, we were able to identify major gaps and limitations of current glyph-based techniques. Such an area is the visualization of multiple fields [Tay02], which led to the research described in Chapter 3. Given the constraints of glyphs such as their size and their very limited capacity of encoding individual channels, this challenge is non-trivial. Our contribution towards this specific aspect is through the development of 2D and 3D visual mappings to visualize multiple error-sensitivity fields for single camera

positioning. A focus of the work is to visualize the compositional effects from different fields. For this, we used glyph-based visualization to evaluate prospective camera positions based on 2D homography sensitivity. These map to a 3D context visualization where the goal is to visually estimate several optimal positions for the camera. The combined visualization enabled users to make dynamic decisions on best camera positioning which incorporates financial, physical, and other types of constraints that cannot be easily encoded into an algorithm.

Whilst there are several other glyph-based techniques which support the mapping of high-dimensional data such as star glyphs [SFGF72] and parallel glyphs [FCI05], they may not be suitable to every application. In theory, such techniques allow up to  $n$ -dimensions to be visualized. However, in practice, this number is a lot less, since beyond a certain number of dimensions, additional values can no longer be accurately perceived due to the limited display resolution of glyphs and the way each dimension is mapped. Although such glyphs is effective at providing an overview of the data, a 'good' glyph design should also be able to convey the information which the user wants to see in detail. For instance, some tasks may require rapid recognition of certain information. In order to convey such aspects of data faster and effectively, more 'ink' or pixel space within the visualization is needed to emphasise certain visual features of the glyph, which generally goes against Tufte's principles on efficient visualization design [Tuf90]. For instance, Chapter 4 described the use of metaphoric glyphs for visualizing actions and events "*at a glance*". We demonstrated this successfully to an application of real-time sports performance analysis. A design study was conducted to compare metaphoric glyphs to other types of visual designs such as colour, shape, and abstract shape for visualizing a large number of categorical events. Our results showed that by mapping data to more expensive visual channels (e.g., pictograms - because they require more physical display space), the effectiveness of glyph-based visualization can be significantly enhanced, especially in situations where users need to gain an overview of the data in order to make critical decisions with very limited time. It was very rewarding to see how positively our *MatchPad* system was effectively used by the Welsh Rugby Union at the 2012 rugby world cup.

One problem we noticed during the design of glyphs in previous works, is the perceptual difficulty at comparing multiple values directly between different glyphs. The ability to compare glyphs in an accurate manner and determine their ordering is an important task in multivariate analysis, for example to identify trends and patterns in data. Since sorting is one of the most common analytical tasks performed on individual attributes of a multi-dimensional data set, this motivated the concept behind our glyph-based sorting framework, introduced in Chapter 5 to enhance the usability of glyph-based visualization. In this framework, we examined several technical aspects of glyph sorting and describe design principles for developing effective, visually sortable glyphs. Glyphs that are visually sortable provides two key benefits: 1) performing comparative analysis of multiple attributes between glyphs, and 2) to support multi-dimensional visual search. We demonstrate this using a system that incorporates high-dimensional focus

and context glyphs to control, view, and perform high-dimensional sorting for interactive analysis. A real-world case-study is presented on analysing rugby events for team and player performance. Our framework enabled analysts to derive new insight from high-dimensional sorting that was previously not observable with existing techniques.

In Chapter 6, we proposed a novel visual analytic extension for sorting multivariate events. The visual analytic system closely integrated a variety of components, including a knowledge-assisted ranking framework for converting a user's tacit and partial knowledge on rankings, a model visualization for displaying the discovered sorting function, a glyph-based visualization for viewing sorted results, and a tool for reviewing sorted video clips that may be associated with each event. This approach allowed users to organise events under some ad hoc sorting requirement (e.g., by importance) without depending on precise specification of multiple sort keys and a sorting function. To evaluate the system, we demonstrated its usefulness in an application of sorting rugby events.

As described in Section 2.2.1, the design of effective glyphs for visualization usually involves a number of different visual channels such as size, colour, and shape. In order to evaluate our glyph-based sorting framework, we conducted three crowdsourcing empirical studies that focus on the perceptual evaluation of orderability for such visual channels. The discovery of ordered perception for visual channels was first studied by Bertin [Ber83], but it was never evaluated on *how* the perception of order is affected using different visual channels. Through this work, we found that certain visual channels (for example, value) is perceived more ordered than other visual channels (for example, hue) than the actual order measured in the data. As a result, different visual channels are more/less sensitive to noise. We found evidence that this has a significant impact to two specific visualization tasks, namely: visual search and categorical perception. In particular, we find that visual channels that have a higher degree of orderedness, improves the accuracy of making min and max judgements within a visualization. On the other hand, visual channels that are perceived to be less ordered, improves the accuracy of identifying the number of element pairs.

To conclude this thesis, we provide a set of generalisable recommendations for designing high-dimensional glyphs in the context of different use scenarios explored in this research:

- **DR1. Composition effect of multiple fields** — when a data set consists of multiple co-located fields (e.g., a vector field) that need to be examined together, then one should consider using a geometric-based approach such as the glyphs presented in Chapter 3. Geometric glyphs primarily use visual channels such as size, colour, and shape to encode the data which are effective for displaying quantitative values. A user may also be interested in observing the compositional effect of several fields, such as the distribution or orientation in different fields. For such tasks, we encourage the use of shape as it highlights the relationship of multiple data attributes in an overall glyph (e.g., the Bézier glyphs in Chapter 3).
- **DR2. Categorical events at a glance** — the visual mapping of categorical events

and actions is challenging to depict due to the semantic information that is often associated with such data. Conventional glyph-based encoding strategies such as using colour or a set of shapes can often be non-intuitive to the user as a result of the poor coupling between data and visualization. One effective approach is to use semantic visual channels (e.g., pictograms, icons, and text) to map this type of data within a glyph. While some semantic visual channels (e.g., pictograms) can be visually expensive as they require more physical display space, they also provide cost-effective benefits such as minimising the need for memorising and learning the coding scheme within a glyph. This leads to rapid recognition of event types, and is scalable to a large number of event records.

- **DR3. Perceptual orderability** — when spatial positioning is already pre-defined, one must rely on other visual encodings to display additional relationships in glyphs for multivariate analysis. One such pattern is the order present in the data. For such tasks, we recommend using visual channels that have a high perceptual orderability such as value (i.e., grayscale), size (e.g., radius length), and texture (e.g., frequency). Such visual channels are less sensitive to noise, meaning linear relationships are more likely to be perceived if present in the data. On the other hand, visual channels such as hue and orientation are perceived to be less ordered, and therefore may be considered instead if the focus is to visually detect data anomalies and outliers.
- **DR4. Min/Max judgements** — a common visual search task is the ability to find min and max values in visualization. Glyphs can support this process by taking advantage of previous design recommendation **DR3.** on perceptually orderable channels to reduce the reliance on legends. These visual encodings (for example, size) impose a universally perceived order which can significantly improve the accuracy of min and max judgements.
- **DR5. Categorical search** — another common task performed in visualization is categorical search. In the context of design recommendation **DR3.** and unordered sequences, glyphs that incorporate hue or shape (i.e., visual channels that tend to be perceived less ordered) enhance categorical perception, making this ideal in tasks that involves, for example, finding one or more relevant data points that have equal values.
- **DR6. Visually sortable glyphs** — when a glyph needs to be designed so that they can be sorted in visualization, several glyph-based aspects need to be considered as described in Chapter 5. Firstly, each data attribute should be prioritised in order of data importance. This prioritisation determines what visual channel is most suitable to represent the data. It is desirable to map more important attributes to visual channels that have a higher level of pop-out (pre-attentive search) and visual orderability. Grayscale intensity or size are good candidates to use. Colour

can also be very effective due to its high pop-out effect. However, it also has a low perceptual orderability, and hence colour should only be used if, for example, the domain has an existing colour mapping which is orderable. Furthermore, glyphs need to be carefully constructed to prevent overuse of a single visual channel and violating the separability design principle. One can improve the perception of certain features on a glyph by incorporating focus+context interactions to highlight specific attributes.

This thesis has investigated and addressed the challenges of designing high-dimensional glyphs to two specific applications; namely, for visualizing multiple error-sensitivity fields in single camera positioning and encoding large event records for real-time sports analysis, and also provides a flexible sorting framework for interactive analysis and sorting of multivariate data, which is fully extensible into other applications and domains. In pursuit of our research goal: “*How many variables can we effectively encode using a glyph*”, we have shown excellent examples of glyph-based visual mappings that encode up to nine different parameters simultaneously using a variety of different methods such that each attribute on the glyph can be readily perceived, and effectively sorted in a visual manner.

## 8.1 Future Work

Although the use of glyphs and icons is historically well-established as a form of visual communication, the development of high-dimensional glyphs as a visualization tool is still relatively new. It is clear from the recent work in this thesis and within the literature that the potential of glyph-based visualization is still far from being fully explored. We outline some potential directions below:

- **Advances in multi-field visualization.** With the advent of simulations becoming more complex (and so to as their data sets), the need for visualization techniques to cope with the increasing number of fields is necessary. In this thesis, we have presented results of depicting multiple error-sensitivity fields simultaneously using glyph-based visualization for single camera positioning. One possible extension to this work would be to visualize the error sensitivity for multiple cameras. Many computer vision algorithm often use a multi-camera setup such as 3D pose estimation [HZ04], and therefore understanding the interactions between multiple camera error sensitivity fields is extremely relevant to this research topic. However, the combined number of error sensitivity fields associated at each camera will be a challenging task to visualize.
- **Collaboration with domain experts.** The inception of many of our ideas have come through close collaboration with domain experts. We have mainly demonstrated the application of glyphs in the area of sports visualization which has led

to the development of several successful systems that have made an impact to the work flow of real users. An aspect of future work would be to collaborate with other domain scientists in which glyph-based visualization can be of benefit. For example, it would be interesting to see how the systems we developed could be of help to other sports such as football, tennis, and golf.

- **Scalability to big data.** The growing mass of concurrent data presents several unaddressed challenges to data visualization research. In particular, when datasets involve several thousands or sometimes millions of high-dimensional data entities, many visualization techniques do not scale very well. Glyph-based visualization is especially challenging due to the large number of glyphs that need to be rendered, and the perceptual problems this approach will cause such as visual occlusion. Some examples of work (e.g., [RE05, PPvA\*09]) have shown it is possible to adopt glyphs to big physical simulation data. Visual occlusion in such a case is less of a problem as the scientists are focused only on looking at global structural patterns. The focus of our work differs in that users need to be able observe details of the glyph clearly. We have demonstrated some glyph-based techniques that is effective for visualizing a relatively small number of entities. Future work would therefore be to develop and evaluate the scalability of such glyphs to larger datasets.
- **Semantic zooming.** To facilitate the rapidly growing dimensionality of data that need to be visualized in modern applications, larger and more complex glyph designs are often required. This is visually expensive in terms of screen space and limits the number of records displayable to the user. One method to overcome this is through zooming out, which provides an overview to the user. However, this often leads to deficiencies in glyph representation, since certain visual features is lost due to sampling size. For example, a 'square' would eventually look like a 'circle' once the visualization is zoomed out beyond a threshold distance. Thus, the semantic information of glyph-based visualization is inconsistent at different zoom levels. Semantic zooming is the ability to maintain the visual information of glyphs during interactive zooming.

There are several major steps that need to be addressed. Of course, since it is almost impossible to retain all the information within a complex glyph when viewing at a great distances, one may simply choose to remove attributes from the glyph to make other visual features more clear. However, selecting the appropriate attribute to be removed, in addition to at which point (i.e., zoom level) they are removed is non-trivial. Alternatively, one may come up with different glyph-based visual designs depending on the level of zoom. This creates a different type of challenge such as how to smoothly transition between different designs in order to maintain visual coherency. No previous work currently address these issues, making this an interesting research direction for glyph-based visualization.

- **Perceptual experiments on high-dimensional glyphs.** While existing perception studies on visual channels and icons have provided a concrete foundation for glyph-based visualization, most findings are directly applicable only to glyph representations in three or fewer dimensions. An area of future work would therefore be to perform more empirical studies on high-dimensional glyph representations. For example, in Chapter 7, we evaluate the perceptual orderability of visual channels and their impact to two different visualization tasks. One extension to this work would be to investigate how combinations of different visual channels affect will this performance.





---

## Bibliography

---

- [AA03] ANDRIENKO N., ANDRIENKO G.: Coordinated views for informed spatial decision making. In *International Conference on Coordinated and Multiple Views in Exploratory Visualization* (July 2003), pp. 44–54.
- [ABK98] ANKERST M., BERCHTOLD S., KEIM D.: Similarity clustering of dimensions for an enhanced visualization of multidimensional data. In *Proc. IEEE Visualization Conf. (Vis '98)* (oct 1998), pp. 52–60, 153.
- [Act66] ACTON F. S.: *Analysis of Straight-line data*. Wiley, 1966.
- [AR08] AUGUSTIN T., ROSCHER T.: Empirical evaluation of the near-miss-to-weber's law: a visual discrimination experiment. *Psychology Science Quarterly* 50, 4 (2008), 469–488.
- [AT04] AGARWAL A., TRIGGS B.: 3d human pose from silhouettes by relevance vector regression. In *IEEE Conference on Computer Vision and Pattern Recognition (CVPR 2004)* (2004), pp. 882–888.
- [AWB01] ANDERSON J. E., WATSON P., BOS P. J.: Comparisons of the vector method and tensor method for simulating liquid crystal devices. *Liquid Crystals* 28 (2001), 109–115.
- [Bar81] BARR A. H.: Superquadrics and angle-preserving transformations. *IEEE Computer Graphics and Applications* 1, 1 (1981), 11–23.
- [BBK09] BUONOMANO D. V., BRAMEN J., KHODADADIFAR M.: Influence of the interstimulus interval on temporal processing and learning: testing the state-dependent network model. *Philosophical Transactions of The Royal Society B* 365 (2009), 1865–1873.
- [BBS\*08] BOTCHEN R. P., BACHTHALER S., SCHICK F., CHEN M., MORI G., WEISKOPF D., ERTL T.: Action-based multifield video visualization. *IEEE Transactions on Visualization and Computer Graphics* 14, 4 (2008), 885–899.
- [Ber83] BERTIN J.: *Semiology of graphics*. University of Wisconsin Press, 1983.

- [BF93] BOOTH D. A., FREEMAN R. P. J.: Discriminative measurement of feature integration in object recognition. *Acta Psychologica* 84 (1993), 1–16.
- [BFCM06] BENDER M. A., FARACH-COLTON M., MOSTEIRO M.: Insertion sort is  $O(n \log n)$ . *Theory of Computing Systems* 39, 3 (2006), 391–397.
- [BHW05] BAIR A., HOUSE D., WARE C.: Perceptually optimizing textures for layered surfaces. In *Proceedings of the 2nd Symposium on Applied Perception in Graphics and Visualization* (2005), APGV '05, ACM, pp. 67–74.
- [BKC\*13] BORGIO R., KEHRER J., CHUNG D. H., MAGUIRE E., LARAMEE R. S., HAUSER H., WARD M., CHEN M.: Glyph-based visualization: Foundations, design guidelines, techniques and applications. In *Eurographics State of the Art Reports* (2013), Eurographics Association.
- [Bly82] BLY S.: Presenting information in sound. In *Proceedings of the 1982 conference on Human factors in computing systems* (1982), CHI '82, ACM, pp. 371–375.
- [Bok03] BOKINSKY A. A.: *Multivariate Data Visualization with Data-Driven Spots*. PhD thesis, 2003.
- [BS92] BORG I., STAUFENBIEL T.: Performance of snow flakes, suns, and factorial suns in the graphical representation of multivariate data. *Multivariate Behavioral Research* 27, 1 (1992), 43–55.
- [BS05] BORDOLOI U., SHEN H.-W.: View selection for volume rendering. In *Proc. IEEE Visualization Conf. (Vis 2005)* (2005), pp. 487–494.
- [BSG89] BLATTNER M. M., SUMIKAWA D. A., GREENBERG R. M.: Earcons and icons: Their structure and common design principles. *Human-Computer Interaction* 4, 1 (1989), 11–44.
- [BT07] BORLAND D., TAYLOR R. M.: Rainbow color map (still) considered harmful. *IEEE Computer Graphics and Applications* 27, 2 (2007), 14–17.
- [CA91] CRAWFIS R., ALLISON M. J.: A scientific visualization synthesizer. In *Proceedings IEEE Visualization '91* (1991), pp. 262–267.
- [CAB\*14] CHUNG D. H. S., ARCHAMBAULT D., BORGIO R., EDWARDS D. J., LARAMEE R. S., CHEN M.: *How Ordered is it? On Perceptual Orderability of Visual Channels*. Tech. rep., The Visual and Interactive Computing Group, Computer Science Department, Swansea University, Wales, UK, 2014.
- [CC01] COX T., COX M.: *Multidimensional Scaling*. Chapman and Hall, 2001.
- [CF13] CHEN M., FLORIDI L.: An analysis of information visualisation. *Synthese* 190, 16 (2013), 3421–3438.
- [Che73] CHERNOFF H.: Using faces to represent points in  $k$ -dimensional space graphically. *Journal of the American Statistical Association* 68 (1973), 361–368.

- [Che05] CHEN M.: Combining point clouds and volume objects in volume scene graphs. In *Fourth International Workshop on Volume Graphics (2005)*, pp. 127–235.
- [Chi06] CHITTARO L.: Visualizing information on mobile devices. *Computer* 39, 3 (2006), 40–45.
- [CJ10] CHEN M., JÄNICKE H.: An information-theoretic framework for visualization. *IEEE Transactions on Visualization and Computer Graphics* 16, 6 (2010), 1206–1215.
- [CK88] COWAN C. K., KOVESI P. D.: Automatic sensor placement from vision task requirements. *IEEE Transactions on Pattern Analysis and Machine Intelligence* 10, 3 (may 1988), 407–416.
- [CKB09] COCKBURN A., KARLSON A., BEDERSON B. B.: A review of overview+detail, zooming, and focus+context interfaces. *ACM Computing Surveys* 41 (2009), 1–31.
- [Cle93] CLEVELAND W. S.: *Visualizing Data*. Hobart Press: Summit, 1993.
- [CLP\*15a] CHUNG D. H. S., LEGG P. A., PARRY M. L., BOWN R., GRIFFITHS I. W., LARAMEE R. S., CHEN M.: Glyph sorting: Interactive visualization for multi-dimensional data. *Information Visualization* 1, 1 (2015), 76–90.
- [CLP\*15b] CHUNG D. H. S., LEGG P. A., PARRY M. L., BOWN R., GRIFFITHS I. W., LARAMEE R. S., CHEN M.: Knowledge-assisted ranking: A visual analytic application for sport event data. *IEEE Computer Graphics and Applications forthcoming* (2015).
- [CM84] CLEVELAND W. S., MCGILL R.: Graphical perception: theory, experimentation and application to the development of graphical methods. *Journal of the American Statistical Association* 79, 387 (1984), 531–554.
- [CM92] CRAWFIS R., MAX N.: Direct volume visualization of three-dimensional vector fields. In *Proceedings of the Workshop on Volume Visualization (1992)*, ACM Press, pp. 55–60.
- [CM93] CRAWFIS R., MAX N.: Texture splats for 3d scalar and vector field visualization. In *IEEE Visualization* (oct 1993), pp. 261–266.
- [CPL\*11] CHEN G., PALKE D., LIN Z., YEH H., VINCENT P., LARAMEE R. S., ZHANG E.: Asymmetric tensor field visualization for surfaces. *IEEE Transactions on Visualization and Computer Graphics* 17, 6 (2011).
- [CPL\*12] CHUNG D. H. S., PARRY M. L., LEGG P. A., GRIFFITHS I. W., LARAMEE R. S., CHEN M.: Visualizing multiple error-sensitivity fields for single camera positioning. *Computing and Visualization in Science* 15, 6 (2012), 303–317.
- [CR68] CAMPBELL F. W., ROBSON J. G.: Application of fourier analysis to the visibility of gratings. *Journal of Physiol* 197, 3 (1968), 551–566.

- [CR00] CEDILNIK A., RHEINGANS P.: Procedural annotation of uncertain information. In *Proc. IEEE Visualization Conf. (Vis 2000)* (2000), pp. 77–83.
- [CSD\*09] COLE F., SANIK K., DECARLO D., FINKELSTEIN A., FUNKHOUSER T., RUSINKIEWICZ S., SINGH M.: How well do line drawings depict shape? *ACM Transactions on Graphics* 28, 3 (2009), 28:1–28:9.
- [CWD\*02] CERQUEIRA M. D., WEISSMAN N. J., DILSIZIAN V., ET AL.: Standardized myocardial segmentation and nomenclature for tomographic imaging of the heart. *Circulation* 105, 4 (2002), 539–542.
- [CZP\*10] CHANG R., ZIEMKIEWICZ C., PYZH R., KIELMAN J., RIBARSKY W.: Learning-based evaluation of visual analytic systems. In *Proceedings of the 3rd BELIV'10 Workshop: BEyond time and errors: novel evaluation methods for Information Visualization* (2010), BELIV '10, pp. 29–34.
- [DEK\*12] DILL J., EARNSHAW R., KASIK D., VINCE J., WONG P. C.: *Expanding the Frontiers of Visual Analytics and Visualization*. Springer (2012 Edition), 2012.
- [Dem85] DEMUTH H. B.: Electronic data sorting. *IEEE Transactions on Computing* 34, 4 (1985), 296–310.
- [DH93] DELMARCELLE T., HESSELINK L.: Visualization of second order tensor fields with hyperstreamlines. *IEEE Computer Graphics and Applications* 13, 4 (1993), 25–33.
- [dLvW93] DE LEEUW W. C., VAN WIJK J. J.: A probe for local flow field visualization. In *Proceedings IEEE Visualization '93* (1993), pp. 39–45.
- [Dou13] DOUBLEDAY A.: Use of card sorting for online course site organization within an integrated science curriculum. *Journal of Usability Studies* 8, 2 (2013), 41–54.
- [DPH03] DUTHIE G., PYNE D., HOOPER S.: Applied physiology and game analysis of rugby union. *Sports Medicine* 33, 13 (2003), 973–991.
- [DYW\*13] DOU W., YU L., WANG X., MA Z., RIBARSKY W.: Hierarchical topics: Visually exploring large text collections using topic hierarchies. *IEEE Transactions on Visualization and Computer Graphics* 19, 12 (Dec 2013), 2002–2011.
- [E\*00] EBERT D. S., ET AL.: Procedural shape generation for multi-dimensional data visualization. *Computers & Graphics* 24, 3 (2000), 375–384.
- [ECW92] ESTIVILL-CASTRO V., WOOD D.: A survey of adaptive sorting algorithms. *ACM Computing Surveys* 24, 4 (1992), 441–476.
- [EM91] ELIADE M., MAIRET P.: *Images and symbols: studies in religious symbolism*. Mythos: The Princeton/Bollingen Series in World Mythology. Princeton University Press, 1991.

- [ES01] EBERT D. S., SHAW C. D.: Minimally immersive flow visualization. *IEEE Transactions on Visualization and Computer Graphics* 7, 4 (2001), 343–350.
- [ESZM96] EBERT D. S., SHAW C., ZWA A., MILLER E. L.: Minimally-immersive interactive volumetric information visualization. In *Proc. IEEE Symp. Information Visualization (InfoVis '96)* (1996), pp. 66–67.
- [FCI05] FANEA E., CARPENDALE S., ISENBERG T.: An interactive 3d integration of parallel coordinates and star glyphs. In *Proc. IEEE Symp. Information Visualization (InfoVis 2005)* (Washington, DC, USA, 2005), INFOVIS '05, IEEE Computer Society, pp. 20–.
- [Fec60] FECHNER T. G.: *Elemente der Psychophysik*, 2 ed. No. Volume 2 in *Elemente der Psychophysik*. Breitkopf & Härtel, Leipzig, 1860.
- [FH09] FUCHS R., HAUSER H.: Visualization of multi-variate scientific data. *Computer Graphics Forum* 28, 6 (2009), 1670–1690.
- [FK03] FRIENDLY M., KWAN E.: Effect ordering for data displays. *Comput. Stat. Data Anal.* 43, 4 (Aug. 2003), 509–539.
- [FLKI09] FENG D., LEE Y., KWOCK L., II R. M. T.: Evaluation of glyph-based multi-variate scalar volume visualization techniques. In *Proceedings of the 6th Symposium on Applied Perception in Graphics and Visualization, APGV 2009* (2009), Mania K., Riecke B. E., Spencer S. N., Bodenheimer B., O'Sullivan C., (Eds.), ACM, pp. 61–68.
- [Fod02] FODOR I. K.: *A Survey of Dimension Reduction Techniques*. Tech. rep., Center for Applied Scientific Computing, Livermore National Laboratory, Livermore, 2002.
- [FS04] FUCHS G., SCHUMANN H.: Visualizing abstract data on maps. In *Proc. IEEE Symp. Information Visualization (InfoVis 2004)* (July 2004), pp. 139–144.
- [FSG09] FEIXAS M., SBERT M., GONZÁLEZ F.: A unified information-theoretic framework for viewpoint selection and mesh saliency. *ACM Transactions on Application Perception* 6, 1 (2009), 1–23.
- [FW10] FORLINES C., WITTENBURG K.: Wakame: Sense making of multi-dimensional spatial-temporal data. In *Proceedings of the International Conference on Advanced Visual Interfaces* (2010), AVI '10, pp. 33–40.
- [FWZ01] FOREST M. G., WANG Q., ZHOU H.: Methods for the exact construction of mesoscale spatial structures in liquid crystal polymers. *Physica D* 152-153 (2001), 288–309.
- [Gay89] GAYER W. W.: The sonicfinder: An interface that uses auditory icons (abstract only). *SIGCHI Bull.* 21 (August 1989).

- [Gew96] GEWIRTZ P.: On "i know it when i see it". *Yale Law Journal* 105 (1996), 1023–1047.
- [GLG\*13] GRATZL S., LEX A., GEHLENBORG N., PFISTER H., STREIT M.: Lineup: Visual analysis of multi-attribute rankings. *IEEE Transactions on Visualization and Computer Graphics* 19, 12 (2013), 2277–2286.
- [GN07] GUO H., NAMEE B. M.: Using computer vision to create a 3D representation of a snooker table for televised competition broadcasting. In *Proceedings of the 18th Irish Conference on Artificial Intelligence and Cognitive Science* (2007), pp. 220–229.
- [GPL\*11] GENG Z., PENG Z., LARAMEE R., ROBERTS J., WALKER R.: Angular histograms: Frequency-based visualizations for large, high dimensional data. *IEEE Transactions on Visualization and Computer Graphics* 17, 12 (Dec 2011), 2572–2580.
- [GR94] GLOBUS A., RAIBLE E.: Fourteen ways to say nothing with scientific visualization. *IEEE Computer* 27, 7 (1994), 86–88.
- [GRE09] GROTTTEL S., REINA G., ERTL T.: Optimized data transfer for time-dependent, gpu-based glyphs. In *Proceedings of IEEE Pacific Visualization Symposium 2009* (april 2009), pp. 65–72.
- [GSCO12] GINGOLD Y., SHAMIR A., COHEN-OR D.: Micro perceptual human computation for visual tasks. *ACM Transactions on Graphics* 31, 5 (2012), 119:1–119:12.
- [H89] HÄGERSTRAND T.: "what about people in regional science?". *Papers in Regional Science* 66, 1 (1989), 1–6.
- [Hab90] HABER R. B.: Visualization techniques for engineering mechanics. *Computing Systems in Engineering* 1, 1 (1990), 37–50.
- [HB02] HUGHES M. D., BARTLETT R. M.: The use of performance indicators in performance analysis. *Journal of Sports Science* 20, 10 (2002), 739–754.
- [HB10] HEER J., BOSTOCK M.: Crowdsourcing graphical perception: using mechanical turk to assess visualization design. In *Proceedings of the SIGCHI Conference on Human Factors in Computing Systems* (2010), pp. 203–212.
- [HB11] HARROWER M., BREWER C. A.: *ColorBrewer.org: An Online Tool for Selecting Colour Schemes for Maps*, in *The Map Reader: Theories of Mapping Practice and Cartographic Representation*. Wiley-Blackwell, 2011.
- [HBW06] HOUSE D. H., BAIR A. S., WARE C.: An approach to the perceptual optimization of complex visualizations. *IEEE Transactions on Visualization and Computer Graphics* 12, 4 (2006), 509–521.

- [HE99] HEALEY C. G., ENNS J. T.: Large datasets at a glance: Combining textures and colors in scientific visualization. *IEEE Transactions on Visualization and Computer Graphics* 5, 2 (1999), 145–167.
- [HE12] HEALEY C., ENNS J.: Attention and visual memory in visualization and computer graphics. *IEEE Transactions on Visualization and Computer Graphics* 18, 7 (2012), 1170–1188.
- [Hei24] HEICHT S.: The visual discrimination of intensity and the weber-fechner law. *The Journal of General Physiology* 7, 2 (1924), 235–267.
- [HF97] HUGHES M. D., FRANKS I. M.: *Notational analysis of sport*. London: E. & F.N. Spon., 1997.
- [HI72] HANDEL S., IMAI S.: The free classification of analyzable and unanalyzable stimuli. *Perception and Psychophysics* 12 (1972), 108–116.
- [HJ05] HANSEN C. D., JOHNSON C. R.: *The Visualization Handbook*. Academic Press, 2005.
- [HLNW11] HLAWATSCH M., LEUBE P., NOWAK W., WEISKOPF D.: Flow radar glyphs - static visualization of unsteady flow with uncertainty. *IEEE Transactions on Visualization and Computer Graphics* 17, 12 (2011), 1949–1958.
- [HNNH\*12] HOFERLIN B., NETZEL R., HOFERLIN M., WEISKOPF D., HEIDEMANN G.: Inter-active learning of ad-hoc classifiers for video visual analytics. In *IEEE Conference on Visual Analytics Science and Technology (VAST)* (2012), pp. 23–32.
- [Hoa62] HOARE C. A. R.: Quicksort. *The Computer Journal* 5, 1 (1962), 10–16.
- [HS12] HEER J., STONE M.: Color naming models for color selection, image editing and palette design. In *Proceedings of the SIGCHI Conference on Human Factors in Computing Systems* (2012), pp. 1007–1016.
- [HSH07] HLAWITSCHKA M., SCHEUERMANN G., HAMANN B.: Interactive glyph placement for tensor fields. In *Advances in Visual Computing* (2007), pp. 331–340.
- [Hu62] HU M.-K.: Visual pattern recognition by moment invariants. *IRE Transactions on Information Theory* 8, 2 (1962), 179–187.
- [HW99] HOLLANDER M., WOLFE D. A.: *Nonparametric Statistical Methods*, 2nd ed. Wiley-Interscience, 1999.
- [HYW03] HASHASH Y. M. A., YAO J. I.-C., WOTRING D. C.: Glyph and hyperstreamline representation of stress and strain tensors and material constitutive response. *International Journal for Numerical and Analytical Methods in Geomechanics* 27, 7 (2003), 603–626.



- [HZ04] HARTLEY R. I., ZISSERMAN A.: *Multiple View Geometry in Computer Vision*, second ed. Cambridge University Press, 2004.
- [Ins85] INSELBERG A.: The plane with parallel coordinates. *The Visual Computer 1* (1985), 69–91.
- [JBMC10] JÄNICKE H., BORGIO R., MASON J. S. D., CHEN M.: Soundriver: Semantically-rich sound illustration. *Computer Graphics Forum 29*, 2 (2010), 357–366.
- [JJS93] JAYANT N., JOHNSTON J., SAFRANEK R.: Signal compression based on models of human perception. *Proceedings of the IEEE 81*, 10 (1993), 1385–1422.
- [JKLS10] JANKUN-KELLY T., LANKA Y., SWAN J.: An evaluation of glyph perception for real symmetric traceless tensor properties. *Computer Graphics Forum 29*, 3 (2010), 1133–1142.
- [JKM06] JANKUN-KELLY T. J., MEHTA K.: Superellipsoid-based, real symmetric traceless tensor glyphs motivated by nematic liquid crystal alignment visualization. *IEEE Transactions on Visualization and Computer Graphics 12*, 5 (September 2006), 1197–1204.
- [JMJ04] JONES N. M. P., MELLALIEU S. D., JAMES N.: Team performance indicators as a function of winning and losing in rugby union. *International Journal of Performance Analysis in Sport 4*, 1 (2004), 61–71.
- [Jol02] JOLLIFFE I. T.: *Principal Component Analysis*, second ed. Springer, 2002.
- [JZF\*09] JEONG D. H., ZIEMKIEWICZ C., FISHER B., RIBARSKY W., CHANG R.: ipca: an interactive system for pca-based visual analytics. In *IEEE VGTC conference on Visualization* (2009), pp. 767–774.
- [KAF\*08] KEIM D., ANDRIENKO G., FEKETE J.-D., GÖRG C., KOHLHAMMER J., MELANÇON G.: Visual analytics: Definition, process, and challenges. In *Information Visualization*, Kerren A., Stasko J., Fekete J.-D., North C., (Eds.), vol. 4950 of *Lecture Notes in Computer Science*. Springer Berlin Heidelberg, 2008, pp. 154–175.
- [KBGK07] KOHLMANN P., BRUCKNER S., GROLLER E. M., KANITSAR A.: Livesync: Deformed viewing spheres for knowledge-based navigation. *IEEE Transactions on Visualization and Computer Graphics 13*, 6 (2007), 1544–1551.
- [KE01] KRAUS M., ERTL T.: Interactive data exploration with customized glyphs. In *WSCG (Posters)* (2001), pp. 20–23.
- [Kin04] KINDLMANN G.: Superquadric tensor glyphs. In *Proc. Eurographics/IEEE-TCVG Symp. on Visualization (VisSym 2004)* (2004), Eurographics Association, pp. 147–154.

- [KMDH11] KEHRER J., MUIGG P., DOLEISCH H., HAUSER H.: Interactive visual analysis of heterogeneous scientific data across an interface. *IEEE Transactions on Visualization and Computer Graphics* 17, 7 (2011), 934–946.
- [KMH03] KONYHA Z., MATKOVIC K., HAUSER H.: Interactive 3d visualization of rigid body systems. In *Proc. IEEE Visualization Conf. (Vis 2003)* (2003), IEEE Computer Society, pp. 71–.
- [KML99] KIRBY R. M., MARMANIS H., LAIDLAW D. H.: Visualizing multivalued data from 2D incompressible flows using concepts from painting. In *Proceedings IEEE Visualization '99* (1999), pp. 333–340.
- [Knu98] KNUTH D. E.: *The Art of Computer Programming, Vol. 3: Sorting and Searching, Second Edition*. Addison-Wesley, Reading, Mass., 1998.
- [KW06] KINDLMANN G., WESTIN C.-F.: Diffusion tensor visualization with glyph packing. *IEEE Transactions on Visualization and Computer Graphics* 12, 5 (2006), 1329–1336.
- [KYHR05] KRIZ R. D., YAMAN M., HARTING M., RAY A. A.: Visualization of Zeroth, Second, Fourth, Higher Order Tensors, and Invariance of Tensor Equations. *Computers & Graphics* 21, 6 (2005), 1–13.
- [KZ10] KOSARA R., ZIEMKIEWICZ C.: Do mechanical turks dream of square pie charts? In *Proceedings of the 3rd BELIV'10 Workshop: BEyond time and errors: novel evaluation methods for Information Visualization* (2010), ACM, pp. 63–70.
- [LAK\*98] LAIDLAW D. H., AHRENS E. T., KREMERS D., AVALOS M. J., JACOBS R. E., READHEAD C.: Visualizing diffusion tensor images of the mouse spinal cord. In *Proc. IEEE Visualization Conf. (Vis '98)* (1998), pp. 127–134.
- [LBR03] LEE M. D., BUTAVICIUS M. A., REILLY R. E.: Visualizations of binary data: A comparative evaluation. *International Journal of Human-Computer Studies* 59, 5 (2003), 569–602.
- [LCP\*12] LEGG P. A., CHUNG D. H. S., PARRY M. L., JONES M. W., LONG R., GRIFFITHS I. W., CHEN M.: Matchpad: Interactive glyph-based visualization for real-time sports performance analysis. *Computer Graphics Forum* 31, 3pt4 (2012), 1255–1264.
- [LFK\*13] LIN S., FORTUNA J., KULKARNI C., STONE M., HEER J.: Selecting semantically-resonant colors for data visualization. *Computer Graphics Forum (Proc EuroVis)* (2013).
- [LHH\*12] LIANG J., HUA J., HUANG M. L., NGUYEN Q. V., SIMOFF S.: Rectangle orientation in area judgment task for treemap design. In *Proceedings of the 24th Australian Computer-Human Interaction Conference* (2012), OzCHI '12, ACM, pp. 349–352.

- [Liu11] LIU Y.: Multivariate data visualization: A review from the perception aspect. In *Human Interface and the Management of Information. Interacting with Information*, Smith M., Salvendy G., (Eds.), vol. 6771 of *Lecture Notes in Computer Science*. Springer Berlin Heidelberg, 2011, pp. 221–230.
- [LKH09] LIE A. E., KEHRER J., HAUSER H.: Critical design and realization aspects of glyph-based 3d data visualization. In *Proceedings of the 2009 Spring Conference on Computer Graphics* (2009), SCCG '09, ACM, pp. 19–26.
- [LLCD11] LIPSA D., LARAMEE R. S., COX S., DAVIES T.: Foamvis: Visualization of 2d foam simulation data. *IEEE Transactions on Visualization and Computer Graphics* 17, 12 (2011), 2096–2105.
- [LPC\*11] LEGG P. A., PARRY M. L., CHUNG D. H. S., JIANG M. R., MORRIS A., GRIFFITHS I. W., MARSHALL D., CHEN M.: Intelligent filtering by semantic importance for single-view 3d reconstruction from snooker video. In *IEEE International Conference on Image Processing* (2011), pp. 2433–2436.
- [LPSW96] LODHA S. K., PANG A., SHEEHAN R. E., WITTENBRINK C. M.: UFLOW: Visualizing uncertainty in fluid flow. In *Proceedings IEEE Visualization '96* (1996), pp. 249–254.
- [LWSH04] LARAMEE R., WEISKOPF D., SCHNEIDER J., HAUSER H.: Investigating Swirl and Tumble Flow with a Comparison of Visualization Techniques. In *Proceedings IEEE Visualization 2004* (2004), pp. 51–58.
- [Mac86] MACKINLAY J.: Automating the design of graphical presentations of relational information. *ACM Transactions on Graphics* 5, 2 (1986), 110–141.
- [Mac92] MACEACHREN A. M.: Visualizing uncertain information. *Cartographic Perspective*, 13 (1992), 10–19.
- [Mac95] MACEACHREN A. M.: *How maps work: representation, visualization, and design*. New York: Guildford Press, 1995.
- [Mar03] MARCUS A.: Icons, symbols, and signs: visible languages to facilitate communication. *Interactions* 10 (May 2003), 37–43.
- [MBP98] MACEACHREN A. M., BREWER C. A., PICKLE L. W.: Visualizing georeferenced data: Representing reliability of health statistics. *Environment and Planning A* (1998), 1547–1561.
- [MgDN06] MARTIN C., GROSSE DETERS H., NATTKEMPER T. W.: Fusing biomedical multi-modal data for exploratory data analysis. In *Proceedings of the 16th International Conference on Artificial Neural Networks - Volume Part II* (2006), ICANN'06, Springer-Verlag, pp. 798–807.
- [MKB\*12] MISTELBAUER G., KOCHL A., BOUZARI H., BRUCKNER S., SCHERNTHANER R., SRAMEK M., BACLIJA I., GROLLER M. E.: Smart super views:

- A knowledge-assisted interface for medical visualization. In *IEEE Conference on Visual Analytics Science and Technology (VAST)* (2012), pp. 163–172.
- [MLP\*10] MCLOUGHLIN T., LARAMEE R., PEIKERT R., POST F. H., CHEN M.: Over Two Decades of Integration-Based, Geometric Flow Visualization. *Computer Graphics Forum* 29, 6 (2010), 1807–1829.
- [MMS13] MCCRAE J., MITRA N. J., SINGH K.: Surface perception of planar abstractions. *ACM Transactions on Applied Perception* 10, 3 (2013), 14:1–14:20.
- [Mor74] MORRISON J. L.: A theoretical framework for cartographic generalization with the emphasis on the process of symbolization. *International Yearbook of Cartography* 14 (1974), 115–127.
- [Mor03] MORONEY N.: Unconstrained web-based color naming experiment. *Proceedings of SPIE 5008* (2003), 36–46.
- [MPRSDC12] MAGUIRE E., P. ROCCA-SERRA S.-A. S., DAVIES J., CHEN M.: Taxonomy-based glyph design: with a case study on visualizing workflows of biological experiments. *IEEE Transactions on Visualization and Computer Graphics* 18, 12 (2012), 2603–2612.
- [MRO\*12] MACEACHREN A. M., ROTH R. E., O'BRIEN J., LI B., SWINGLEY D., GAHEGAN M.: Visual semiotics & uncertainty visualization: An empirical study. *IEEE Transactions on Visualization and Computer Graphics* 18, 12 (2012), 2496–2505.
- [MSM\*08] MARTIN J. P., SWAN E. J., MOORHEAD R. J., LIU Z., CAI S.: Results of a user study on 2D hurricane visualization. *Computer Graphics Forum* 27, 3 (2008), 991–998.
- [MSS12] MOHAMMAD S H., SHIRKHODAIE A.: A survey of visual analytics for knowledge discovery and content analysis. In *Proceedings of SPIE* (2012), vol. 8392, pp. 83920T–83920T–11.
- [MSSD\*08] MEYER-SPRADOW J., STEGGER L., DÖRING C., ROPINSKI T., HINRICHS K.: Glyph-based SPECT visualization for the diagnosis of coronary artery disease. *IEEE Transactions on Visualization and Computer Graphics* 14, 6 (2008), 1499–1506.
- [NAS] NASA: Pioneer f plaque symbology. <http://grin.hq.nasa.gov/ABSTRACTS/GPN-2000-001623.html>. Accessed: 2014-06-01.
- [OHG\*08] OELTZE S., HENNEMUTH A., GLASSER S., KÜHNEL C., PREIM B.: Glyph-based visualization of myocardial perfusion data and enhancement with contractility and viability information. In *Proceedings of the First Eurographics conference on Visual Computing for Biomedicine* (2008), EG VCBM'08, pp. 11–20.

- [OHS03] OWENS N., HARRIS C., STENNETT C.: Hawk-eye tennis system. In *International Conference on Visual Information Engineering* (2003), pp. 182–185.
- [OLF09] OZUYSAL M., LEPETIT V., FUA P.: Pose estimation for category specific multiview object localization. In *IEEE Conference on Computer Vision and Pattern Recognition (CVPR 2009)* (june 2009), pp. 778–785.
- [OVV84] ORBAN G. A., VANDENBUSSCHE E., VOGELS R.: Human orientation discrimination tested with long stimuli. *Vision Research* 24, 2 (1984), 121–128.
- [Pan01] PANG A.: Visualizing uncertainty in geo-spatial data. In *In Proceedings of the Workshop on the Intersections between Geospatial Information and Information Technology* (2001).
- [PGL\*12] PENG Z., GRUNDY E., LARAMEE R., CHEN G., CROFT N.: Mesh-driven vector field clustering and visualization: An image-based approach. *IEEE Transactions on Visualization and Computer Graphics* 18, 5 (2012), 283–298.
- [PL09] PENG Z., LARAMEE R. S.: Higher dimensional vector field visualization: A survey. In *Theory and Practice of Computer Graphics* (2009), pp. 149–163.
- [PLC\*11] PARRY M. L., LEGG P. A., CHUNG D. H. S., GRIFFITHS I. W., CHEN M.: Hierarchical event selection for video storyboards with a case study on snooker video visualization. *IEEE Transactions on Visualization and Computer Graphics* 17, 12 (dec 2011), 1747–1756.
- [PNE02] POST F. H., NIELSON G., (EDS.) G.-P. B.: *Data Visualization: The State of the Art*. Springer, 2002.
- [PPvA\*09] PEETERS T. H. J. M., PRCKOVSKA V., VAN ALMSICK M. A., BARTROLI A. V., TER HAAR ROMENY B. M.: Fast and sleek glyph rendering for interactive hardi data exploration. In *IEEE Pacific Visualization Symposium* (2009), pp. 153–160.
- [PR08] PEARLMAN J., RHEINGANS P.: Visualizing network security events using compound glyphs from a service-oriented perspective. In *VizSEC 2007*, Goodall J. R., Conti G., Ma K.-L., Farin G., Hege H.-C., Hoffman D., Johnson C. R., Polthier K., (Eds.), *Mathematics and Visualization*. Springer Berlin Heidelberg, 2008, pp. 131–146.
- [PRdJ07] PEARLMAN J., RHEINGANS P., DES JARDINS M.: Visualizing diversity and depth over a set of objects. *IEEE Computer Graphics and Applications* 27 (2007), 35–45.
- [PSBS12] PILEGGI H., STOLPER C. D., BOYLE J. M., STASKO J. T.: Snapshot: Visualization to propel ice hockey analytics. *IEEE Transactions on Visualization and Computer Graphics* 18, 12 (2012), 2819–2828.

- [PVF13] PERIN C., VUILLEMOT R., FEKETE J. D.: Soccerstories: A kick-off for visual soccer analysis. *IEEE Transactions on Visualization and Computer Graphics* 19, 12 (Dec 2013), 2506–2515.
- [PWL96] PANG A. T., WITTENBRINK C. M., LODH S. K.: Approaches to uncertainty visualization. *The Visual Computer* 13 (1996), 370–390.
- [PWR04] PENG W., WARD M. O., RUNDENSTEINER E. A.: Clutter reduction in multi-dimensional data visualization using dimension reordering. In *Proc. IEEE Symp. Information Visualization (InfoVis 2004)* (2004), pp. 89–96.
- [PZ08] PUTZ V., ZAGAR B. G.: Single-Shot estimation of Camera Position and Orientation using SVD. In *Proc. IEEE Conf. Instrumentation and Measurement Technology* (2008), pp. 1914–1919.
- [QH87] QUINLAN P., HUMPHREYS G.: Visual search for targets defined by combinations of color, shape, and size: an examination of the task constraints on feature and conjunction searches. *Perception & psychophysics* 41, 5 (1987), 455–527.
- [RE05] REINA G., ERTL T.: Hardware-accelerated glyphs for mono- and dipoles in molecular dynamics visualization. In *EuroVis* (2005), Eurographics Association, pp. 177–182.
- [RFB\*11] ROTH R. E., FINCH B. G., BLANFORD J. I., KLIPPEL A., ROBINSON A. C., MACEACHREN A. M.: Card sorting for cartographic research and practice. *Cartography and Geographic Information Science* 38, 2 (2011), 89–99.
- [RHHL02] RUSINKIEWICZ S., HALL-HOLT O., LEVOY M.: Real-time 3D model acquisition. In *SIGGRAPH 2002 Conference Proceedings* (2002), Annual Conference Series, ACM Press/ACM SIGGRAPH, pp. 438–446.
- [RM97] RUGG G., MCGEORGE P.: The sorting techniques: a tutorial paper on card sorts, picture sorts and item sorts. *Expert Systems* 14, 2 (1997), 80–93.
- [RN88] RODGERS J. L., NICEWANDER A. W.: Thirteen ways to look at the correlation coefficient. *The American Statistician* 42, 1 (1988), 59–66.
- [ROP11] ROPINSKI T., OELTZE S., PREIM B.: Survey of glyph-based visualization techniques for spatial multivariate medical data. *Computers & Graphics* 35 (2011), 392–401.
- [RP08] ROPINSKI T., PREIM B.: Taxonomy and usage guidelines for glyph-based medical visualization. In *Proc. Simulation and Visualization (SimVis 2008)* (2008), pp. 121–138.
- [RSMS\*07] ROPINSKI T., SPECHT M., MEYER-SPRADOW J., HINRICHS K., PREIM B.: Surface glyphs for visualizing multimodal volume data. In *Proc. Vision, Modeling, and Visualization (VMV 2007)* (2007), pp. 3–12.

- [RWG\*12] RIBICIC H., WASER J., GURBAT R., SADRANSKY B., GROLLER M. E.: Sketching uncertainty into simulations. *IEEE Transactions on Visualization and Computer Graphics* 18, 12 (2012), 2255–2264.
- [SCC\*04] STRAKA M., CERVENANSKY M., CRUZ A. L., KOCHL A., SRAMEK M., GROLLER E., FLEISCHMANN D.: The vesselglyph: Focus & context visualization in ct-angiography. In *Proc. IEEE Visualization Conf. (Vis 2004)* (2004), pp. 385–392.
- [SEK\*98] SHAW C., EBERT D., KUKLA J., ZWA A., SOBOROFF I., ROBERTS D.: Data visualization using automatic, perceptually-motivated shapes. In *Visual Data Exploration and Analysis* (1998), SPIE.
- [SFGF72] SIEGEL J., FARRELL E., GOLDWYN R., FRIEDMAN H.: The surgical implication of physiologic patterns in myocardial infarction shock. *Surgery* 72 (1972), 27–35.
- [SHB\*99] SHAW C. D., HALL J. A., BLAHUT C., EBERT D. S., ROBERTS D. A.: Using shape to visualize multivariate data. In *In Proceedings of the Workshop on New Paradigms in Information Visualization and Manipulation (NPIVM '99)* (1999), ACM Press, pp. 17–20.
- [She64] SHEPARD R.: Attention and the metric structure of the stimulus space. *Journal of Mathematical Psychology* 1 (1964), 54–87.
- [Shn96] SHNEIDERMAN B.: The eyes have it: a task by data type taxonomy for information visualizations. In *IEEE Symposium on Visual Languages* (1996), pp. 336–343.
- [SJAS05] SAYIM B., JAMESON K. A., ALVARADO N., SZESZEL M. K.: Semantic and perceptual representations of color: Evidence of a shared color-naming function. *The Journal of Cognition and Culture* 5, 3-4 (2005), 427–486.
- [SK10] SCHULTZ T., KINDLMANN G. L.: Superquadric glyphs for symmetric second-order tensors. *IEEE Transactions on Visualization and Computer Graphics* 16, 6 (2010), 1595–1604.
- [SKH95] SONNET A., KILIAN A., HESS S.: Alignment tensor versus director: Description of defects in nematic liquid crystals. *Physical Review E* 52 (July 1995), 718–722.
- [SSOG08] SUNTINGER M., SCHIEFER J., OBWEGER H., GROLLER M. E.: The event tunnel: Interactive visualization of complex event streams for business process pattern analysis. In *Proc. IEEE Pacific Visualization Symp. (PacificVis 2008)* (March 2008), pp. 111–118.
- [Ste46] STEVENS S. S.: On the theory of scales of measurement. *Science* 103, 2684 (1946), 677–680.

- [SZD\*10] SANYAL J., ZHANG S., DYER J., MERCER A., AMBURN P., MOORHEAD R.: Noodles: A tool for visualization of numerical weather model ensemble uncertainty. *IEEE Transactions on Visualization and Computer Graphics* 16, 6 (2010), 1421–1430.
- [Tay02] TAYLOR R.: Visualizing multiple fields on the same surface. *IEEE Computer Graphics and Applications* 22, 3 (2002), 6–10.
- [TB96] TURK G., BANKS D.: Image-guided streamline placement. In *Proceedings of the 23rd Annual Conference on Computer Graphics and Interactive Techniques* (New York, NY, USA, 1996), SIGGRAPH '96, ACM, pp. 453–460.
- [TC05] THOMAS J. J., COOK K. A.: *Illuminating the Path: The Research and Development Agenda for Visual Analytics*. IEEE Computer Society, Los Alamitos, CA, 2005.
- [TCW\*95] TSOTSOS J. K., CULHANE S. M., WINKY W. Y. K., LAI Y., DAVIS N., NUFLO F.: Modeling visual attention via selective tuning. *Artificial Intelligence* 78, 1-2 (1995), 507–545.
- [Tel07] TELEA A.: *Data Visualization: Principles and practice*. A. K. Peters, Ltd., 2007.
- [Tre00] TREINISH L.: Visual data fusion for applications of high-resolution numerical weather prediction. In *Proc. IEEE Visualization Conf. (Vis 2000)* (2000), pp. 477–480.
- [TSWS05] TOMINSKI C., SCHULZE-WOLLGAST P., SCHUMANN H.: 3D information visualization for time-dependent data on maps. In *Proc. Int'l. Conf. Information Visualization (IV '05)* (2005), pp. 175–181.
- [Tuf83] TUFTE E. R.: *The visual display of quantitative information*. Graphics Press, 1983.
- [Tuf90] TUFTE E. R.: *Envisioning Information*. Graphics Press, 1990.
- [TWBW99] TUCH D. S., WEISSKOFF R. M., BELLIVEAU J. W., WEDEEN V. J.: High angular resolution diffusion imaging of the human brain. In *Proceedings of the 7th Annual Meeting of ISMRM* (1999), Springer, p. 321.
- [UIL\*06] URNESS T., INTERRANTE V., LONGMIRE E., MARUSIC I., O'NEILL S., JONES T. W.: Strategies for the visualization of multiple 2d vector fields. *IEEE Computer Graphics and Applications* 26, 4 (2006), 74–82.
- [VFSH01] VÁZQUEZ P.-P., FEIXAS M., SBERT M., HEIDRICH W.: Viewpoint selection using viewpoint entropy. In *Proc. Vision, Modeling, and Visualization (VMV 2001)* (2001), pp. 273–280.



- [VMCJ10] VIAU C., MCGUFFIN M. J., CHIRICOTA Y., JURISICA I.: The flowvizmenu and parallel scatterplot matrix: Hybrid multidimensional visualizations for network exploration. *IEEE Transactions on Visualization and Computer Graphics* 16, 6 (Nov 2010), 1100–1108.
- [VO85] VOGELS R., ORBAN G. A.: The effect of practice on the oblique effect in line orientation judgements. *Vision Research* 25, 11 (1985), 1679–1687.
- [VVO86] VANDENBUSSCHE E., VOGELS R., ORBAN G. A.: Human orientation discrimination: Change with eccentricity in normal and amblyopic vision. *Investigative Ophthalmology & Visual Science* 27, 2 (1986), 237–245.
- [War88] WARE C.: Color sequences for univariate maps: theory, experiments and principles. *IEEE Computer Graphics and Applications* 8, 5 (Sept 1988), 41–49.
- [War94] WARD M. O.: Xmdvtool: Integrating multiple methods for visualizing multivariate data. In *Proceedings IEEE Visualization '94* (1994), pp. 326–333.
- [War02] WARD M. O.: A taxonomy of glyph placement strategies for multidimensional data visualization. *Information Visualization* 1, 3-4 (2002), 194–210.
- [War04] WARE C.: *Information Visualization, Second Edition: Perception for Design (Interactive Technologies)*. Morgan Kaufmann Publishers Inc., 2004.
- [War08a] WARD M. O.: Multivariate data glyphs: Principles and practice. In *Handbook of Data Visualization* (2008), Springer Handbooks Comp. Statistics. Springer, pp. 179–198.
- [War08b] WARE C.: *Visual Thinking: for Design*. Morgan Kaufmann Publishers Inc., 2008.
- [WB97a] WONG P. C., BERGERON R. D.: 30 years of multidimensional multivariate visualization. In *Scientific Visualization, Overviews, Methodologies, and Techniques* (1997), IEEE Computer Society, pp. 3–33.
- [WB97b] WONG P. C., BERGERON R. D.: Multivariate visualization using metric scaling. In *Proc. IEEE Visualization Conf. (Vis '97)* (1997), pp. 111–118.
- [WEL\*00] WEIGLE C., EMIGH W. G., LIU G., TAYLOR R. M., ENNS J. T., HEALEY C. G.: Oriented sliver textures: A technique for local value estimation of multiple scalar fields. In *Graphics Interface* (2000), Canadian Human-Computer Communications Society, pp. 163–170.
- [Wes90] WESTOVER L.: Footprint evaluation for volume rendering. *SIGGRAPH Computer Graphics* 24 (1990), 367–376.
- [WG11] WARD M., GUO Z.: Visual exploration of time-series data with shape space projections. *Computer Graphics Forum* 30, 3 (2011), 701–710.

- [WGK10] WARD M. O., GRINSTEIN G., KEIM D.: *Interactive Data Visualization: Foundations, Techniques and Applications*. A K Peters/CRC Press, 2010.
- [Wil67] WILLIAMS L.: The effects of target specification on objects fixated during visual search. *Acta psychologica* 27 (1967), 355–415.
- [WK92] WARE C., KNIGHT W.: Orderable dimensions of visual texture for data display: Orientation, size and contrast. In *Proceedings of the SIGCHI Conference on Human Factors in Computing Systems* (1992), CHI '92, ACM, pp. 203–209.
- [WMM\*02] WESTIN C. F., MAIER S. E., MAMATA H., NABAVI A., JOLESZ F. A., KIKINIS R.: Processing and visualization for diffusion tensor MRI. *Medical Image Analysis* 6, 2 (2002), 93–108.
- [WPL95] WITTENBRINK C., PANG A., LODHA S.: *Verity Visualization: Visual Mappings*. Tech. rep., University of California at Santa Cruz, Santa Cruz, CA, USA, 1995.
- [WPL96] WITTENBRINK C. M., PANG A. T., LODHA S. K.: Glyphs for visualizing uncertainty in vector fields. *IEEE Transactions on Visualization and Computer Graphics* 2, 3 (1996), 266–279.
- [WWH98] WILKINSON F., WILSON H. R., HABAK C.: Detection and recognition of radial frequency patterns. *Vision Research* 38, 22 (1998), 3555–3568.
- [YHW\*07] YANG J., HUBBALL D., WARD M. O., RUNDENSTEINER E. A., RIBARSKY W.: Value and relation display: Interactive visual exploration of large data sets with hundreds of dimension. *IEEE Transactions on Visualization and Computer Graphics* 13, 3 (2007), 1077–2626.
- [YKSJ07] YI J. S., KANG Y. A., STASKO J. T., JACKO J. A.: Toward a deeper understanding of the role of interaction in information visualization. *IEEE Transactions on Visualization and Computer Graphics* 13, 6 (2007), 1224–1231.
- [YPWR03] YANG J., PENG W., WARD M. O., RUNDENSTEINER E. A.: Interactive hierarchical dimension ordering, spacing and filtering for exploration of high dimensional datasets. In *Proc. IEEE Symp. Information Visualization (InfoVis 2003)* (2003), IEEE Computer Society.
- [ZK98] ZHANG Z., KANADE T.: Determining the epipolar geometry and its uncertainty: A review. *International Journal of Computer Vision* 27 (1998), 161–195.
- [ZSAcL08] ZUDILOVA-SEINSTRAL E., ADRIAANSEN T., CAN LIERE R.: *Trends in Interactive Visualization: State-of-the-Art Survey*, 1 ed. Springer Publishing Company, Incorporated, 2008.



---

# Designing High-dimensional Glyphs for Visualizing Multiple Error-Sensitivity Fields

---

This appendix provides supplementary material for the user consultation described in Chapter 3.

## A.1 User Consultation: Questionnaire

1. Given each visual design, can you identify the independent direction error?
2. Given each visual design, can you identify the independent error magnitude?
3. Does the visualization methods help illustrate the overall error from a given camera position?
4. Does the visualization help illustrate the overall distribution from a given camera position?
5. Given each visualization technique, can you identify regions where potential vector cancellation may occur? Which visual design shows this best and briefly explain why?
6. Would the visualization be of help towards selecting an optimal camera position? If yes, give a brief description on why?
7. Does the visualization method help identify which feature point is more sensitive?
8. Given two camera positions and their associated error-sensitivity fields, is the visualization technique useful for deciding which camera is better?
9. Is each error-field observable in the visualization methods?
10. Can you rank the glyph visualizations, worst-to-best, with respect to how well they convey error?



---

## Glyph Sorting: A Visual Analytic Approach

---

This appendix provides supplementary material for evaluating the work in Chapter 6.

### B.1 Empirical Study on Formal Rankings

To supplement the motivation of this chapter, we performed an empirical study using 5 participants (3 computer scientists and 2 sport scientists) to investigate the difficulty of formalising a ranking for an ad hoc task in the context of rugby. Each participant had knowledge in both rugby and visualization.

**Experiment design.** We tasked the participants with identifying, and ranking a set of events that highlight the *most important positive outcomes* of a match. We consider positive outcomes in rugby when a team gains an advantage either through scoring, or winning a set piece such as penalties and free kicks. The study is designed such that importance is the tacit knowledge we are trying to formalise. During each session, we presented the same match containing 12 of such events using a basic system with two views as in Figure 6.1(b) and (c). This system represents a similar environment, albeit more advanced, to current notational software for selecting events, and playing back video clips. To help us analyse the confidence of a participant's result, the users provide an additional meta-answer: (a) I am reasonably confident about my answer, (b) I am unsure about my answer and (c) I do not know how to do this, with each task outlined in Figure B.1.

**Results.** For task 1 and 2, we compare the difficulty of ranking a small set of events (e.g., five), to a relatively larger sample (e.g., ten). Figure B.1 illustrates our results, where the events are ranked from worst-to-best with 1-5, and 1-10 respectively. We notice that the majority of participants were fairly confident with their results in task 1. In contrast, they became unsure of their ranking for task 2. We observed during the process that users were able to establish the rank of important events more easily based on some clear objective feature (e.g., the most gain),

| Task  | (optional)<br>meta-answer | Result  |                |                |                |                |                |                |                |                |                 |                 |                 |
|---|---------------------------|---|----------------|----------------|----------------|----------------|----------------|----------------|----------------|----------------|-----------------|-----------------|-----------------|
|   |                           | e <sub>1</sub>  | e <sub>2</sub> | e <sub>3</sub> | e <sub>4</sub> | e <sub>5</sub> | e <sub>6</sub> | e <sub>7</sub> | e <sub>8</sub> | e <sub>9</sub> | e <sub>10</sub> | e <sub>11</sub> | e <sub>12</sub> |
| 1. Identify and rank 5 events from best-to-worst            | (a)                       | 3   |                | 1              |                |                |                |                | 5              | 4              | 2               |                 |                 |
|   | (a)                       |   | 4              | 5              |                | 2              |                | 3              | 1              |                |                 |                 |                 |
|   | (b)                       |   | 2              |                |                |                |                | 4              | 3              | 1              |                 |                 | 5               |
|   | (a)                       |   | 3              |                |                |                |                | 1              | 5              | 2              |                 |                 | 3               |
|   | (b)                       |   |                | 1              |                |                |                |                | 5              | 3              |                 | 4               | 2               |
|   | (b)                       |   |                |                |                |                |                |                |                |                |                 |                 |                 |
| 2. Identify and rank 10 events from best-to-worst           | (a)                       | 4   | 8              | 2              |                | 1              |                | 7              | 10             | 9              | 3               | 6               | 5               |
|   | (b)                       | 10  | 7              | 8              |                | 5              | 4              | 6              | 1              | 2              | 9               | 3               |                 |
|   | (b)                       | 2   | 7              | 8              |                | 10             | 1              | 4              | 9              | 3              | 5               | 6               | 8               |
|   | (b)                       | 7   | 8              | 2              | 3              |                |                | 4              | 10             | 5              | 1               | 9               | 6               |
|   | (b)                       | 2   |                | 3              | 6              | 4              | 8              |                | 10             | 5              | 1               | 9               | 7               |
|   | (b)                       |   |                |                |                |                |                |                |                |                |                 |                 |                 |
| 3. Identify a set of attributes that may affect the ranking | (a)                       | Gain (high), Tortuosity (low), Number of Phases (low)   |                |                |                |                |                |                |                |                |                 |                 |                 |
|   | (b)                       | (Tortuosity + Number of Phases), (Gain + Territory Position)  |                |                |                |                |                |                |                |                |                 |                 |                 |
|   | (b)                       | Tortuosity, Number of Phases, Start Event   |                |                |                |                |                |                |                |                |                 |                 |                 |
|   | (a)                       | Gain, Start Event, Number of Phases   |                |                |                |                |                |                |                |                |                 |                 |                 |
|   | (a)                       | Gain, Number of Phases  |                |                |                |                |                |                |                |                |                 |                 |                 |
| 4. Formulate a ranking based on the set of attributes       | (c)                       | N/A   |                |                |                |                |                |                |                |                |                 |                 |                 |
|   | (c)                       | N/A   |                |                |                |                |                |                |                |                |                 |                 |                 |
|   | (c)                       | N/A   |                |                |                |                |                |                |                |                |                 |                 |                 |
|   | (a)                       | Combination of high gain, low tortuosity and a weighted start event (e.g., turnover is more important than scrum) |                |                |                |                |                |                |                |                |                 |                 |                 |
|   | (b)                       | Sequences containing high gain or high number of phases from various start events                                 |                |                |                |                |                |                |                |                |                 |                 |                 |
|   | (b)                       |   |                |                |                |                |                |                |                |                |                 |                 |                 |

**Figure B.1:** Table showing the empirical study results for sorting rugby events. Each sub-row within a task corresponds to five participants along with their optional meta-answer (see Appendix for details). For task 1 and 2, their ranking is shown from the 12 possible events  $e_i$ , and are ranked from worst-to-best with 1-5 and 1-10 respectively. A colour-map is applied to emphasise the worst and best events.

than events of less importance. This would suggest, and support the use of a moderated ranking confidence  $\tau$  which we incorporate in our system.

In task 3, we asked the users to identify a set of influential attributes that affected their ranking. Since they define the sorting outcome, the participants could speculate a set of performance indicators confidently which determined their ranking. However, it was clear from task 4 that combining each attribute and formally specifying their ranking proved to be challenging. Whilst a typical participant could perhaps describe such a formalisation in an abstract manner, they acknowledged that this would be too difficult to define into an analytical form which can then be used for event organisation. Finally, we demonstrated our visual analytic system to the users by importing their rankings into the model. We found the discovered sort keys to be consistent with the participant's ranking. All the participants were impressed with the system, and believed that such a tool would be useful for sorting event data in a more effective and efficient manner.






---

## Glyph Sorting: Perceptual Orderability

---






This appendix provides supplementary material for the three empirical studies described in Chapter 7.

### C.1 Experimental Stimuli: How ordered is it?






| Noise Level  | Experiment 1: Value Stimulus   |
|--------------|--|
| $N_1 = 1.0$  |  |
| $N_2 = 0.97$ |  |
| $N_3 = 0.90$ |  |
| $N_4 = 0.71$ |  |
| $N_5 = 0.12$ |  |

**Table C.1:** The visual stimuli for value (visual channel) under five different noise levels (measured orderedness) used in Experiment 1: How ordered is it?








| Noise Level  | Experiment 1: Size Stimulus  |
|--------------|--|
| $N_1 = 1.0$  |  |
| $N_2 = 0.97$ |  |
| $N_3 = 0.90$ |  |
| $N_4 = 0.71$ |  |
| $N_5 = 0.12$ |  |

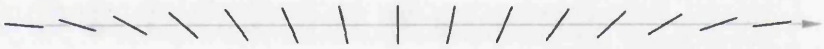
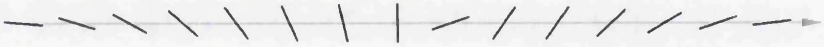



**Table C.2:** The visual stimuli for size (visual channel) under five different noise levels (measured orderedness) used in Experiment 1: How ordered is it?

| Noise Level  | Experiment 1: Hue Stimulus   |
|--------------|--|
| $N_1 = 1.0$  |  |
| $N_2 = 0.97$ |  |
| $N_3 = 0.90$ |  |
| $N_4 = 0.71$ |  |
| $N_5 = 0.12$ |  |

**Table C.3:** The visual stimuli for hue (visual channel) under five different noise levels (measured orderedness) used in Experiment 1: How ordered is it?

| Noise Level  | Experiment 1: Texture Stimulus   |
|--------------|--|
| $N_1 = 1.0$  |  |
| $N_2 = 0.97$ |  |
| $N_3 = 0.90$ |  |
| $N_4 = 0.71$ |  |
| $N_5 = 0.12$ |  |

**Table C.4:** The visual stimuli for texture (visual channel) under five different noise levels (measured orderedness) used in Experiment 1: How ordered is it?

| Noise Level  | Experiment 1: Orientation Stimulus   |
|--------------|--|
| $N_1 = 1.0$  |  |
| $N_2 = 0.97$ |  |
| $N_3 = 0.90$ |  |
| $N_4 = 0.71$ |  |
| $N_5 = 0.12$ |  |

**Table C.5:** The visual stimuli for orientation (visual channel) under five different noise levels (measured orderedness) used in Experiment 1: How ordered is it?













| Noise Level  | Experiment 1: Shape Stimulus |
|--------------|------------------------------|
| $N_1 = 1.0$  |                              |
| $N_2 = 0.97$ |                              |
| $N_3 = 0.90$ |                              |
| $N_4 = 0.71$ |                              |
| $N_5 = 0.12$ |                              |

**Table C.6:** The visual stimuli for shape (visual channel) under five different noise levels (measured orderedness) used in Experiment 1: How ordered is it?

| Noise Level  | Experiment 1: Numeric Stimulus   |
|--------------|--|
| $N_1 = 1.0$  | 37.2 — 38.6 — 40.2 — 41.7 — 43.3 — 44.9 — 46.5 — 48.2 — 49.9 — 51.5 — 53.3 — 55.1 — 56.9 — 58.7 — 60.6 — ► |
| $N_2 = 0.97$ | 37.2 — 38.6 — 40.2 — 41.7 — 43.1 — 44.9 — 46.5 — 48.2 — 58.2 — 54.4 — 53.3 — 55.0 — 56.9 — 58.7 — 60.6 — ► |
| $N_3 = 0.90$ | 37.2 — 41.6 — 40.2 — 44.6 — 46.1 — 46.0 — 46.5 — 48.2 — 48.9 — 52.7 — 43.8 — 55.1 — 56.9 — 58.7 — 56.2 — ► |
| $N_4 = 0.71$ | 40.2 — 40.4 — 39.2 — 46.0 — 43.3 — 39.5 — 52.1 — 48.2 — 49.9 — 56.7 — 53.3 — 45.5 — 56.9 — 58.7 — 60.6 — ► |
| $N_5 = 0.12$ | 53.5 — 53.3 — 41.0 — 41.7 — 43.3 — 56.2 — 39.9 — 60.2 — 46.9 — 51.2 — 59.8 — 58.2 — 47.2 — 38.0 — 60.6 — ► |

**Table C.7:** The visual stimuli for numeric (visual channel) under five different noise levels (measured orderedness) used in Experiment 1: How ordered is it?

## C.2 Experimental Stimuli: Which is smallest? Which is largest?

| Noise Level  | Target  | Experiment 2: Value Stimulus   |
|--------------|---------|--|
| $N_1 = 1.0$  | Min     |    |
|              | Max     |    |
|              | Neither |    |
| $N_2 = 0.97$ | Min     |    |
|              | Max     |    |
|              | Neither |    |
| $N_3 = 0.95$ | Min     |   |
|              | Max     |  |
|              | Neither |  |
| $N_4 = 0.90$ | Min     |  |
|              | Max     |  |
|              | Neither |  |

**Table C.8:** The visual stimuli for value (visual channel) under noise levels  $N_1, N_2, N_3,$  and  $N_4$  (measured orderedness) used in Experiment 2: Which is smallest? Which is largest?

| Noise Level  | Target  | Experiment 2: Value Stimulus (cont.) |
|--------------|---------|--------------------------------------|
| $N_5 = 0.78$ | Min     |                                      |
|              | Max     |                                      |
|              | Neither |                                      |
| $N_6 = 0.71$ | Min     |                                      |
|              | Max     |                                      |
|              | Neither |                                      |
| $N_7 = 0.54$ | Min     |                                      |
|              | Max     |                                      |
|              | Neither |                                      |
| $N_8 = 0.12$ | Min     |                                      |
|              | Max     |                                      |
|              | Neither |                                      |











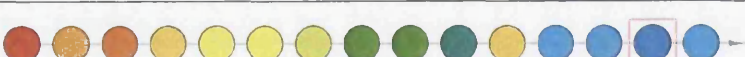
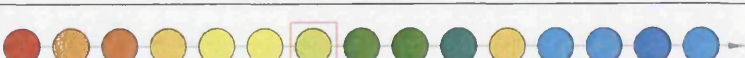
**Table C.9:** The visual stimuli for value (visual channel) under noise levels  $N_5, N_6, N_7,$  and  $N_8$  (measured orderedness) used in Experiment 2: Which is smallest? Which is largest?

| Noise Level  | Target  | Experiment 2: Size Stimulus |
|--------------|---------|-----------------------------|
| $N_1 = 1.0$  | Min     |                             |
|              | Max     |                             |
|              | Neither |                             |
| $N_2 = 0.97$ | Min     |                             |
|              | Max     |                             |
|              | Neither |                             |
| $N_3 = 0.95$ | Min     |                             |
|              | Max     |                             |
|              | Neither |                             |
| $N_4 = 0.90$ | Min     |                             |
|              | Max     |                             |
|              | Neither |                             |

**Table C.10:** The visual stimuli for size (visual channel) under noise levels  $N_1, N_2, N_3,$  and  $N_4$  (measured orderedness) used in Experiment 2: Which is smallest? Which is largest?







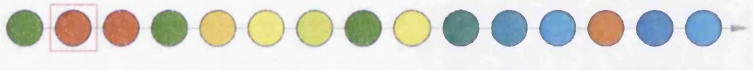
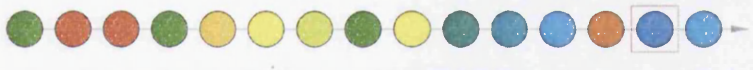




| Noise Level  | Target  | Experiment 2: Size Stimulus (cont.) |
|--------------|---------|-------------------------------------|
| $N_5 = 0.78$ | Min     |                                     |
|              | Max     |                                     |
|              | Neither |                                     |
| $N_6 = 0.71$ | Min     |                                     |
|              | Max     |                                     |
|              | Neither |                                     |
| $N_7 = 0.54$ | Min     |                                     |
|              | Max     |                                     |
|              | Neither |                                     |
| $N_8 = 0.12$ | Min     |                                     |
|              | Max     |                                     |
|              | Neither |                                     |

**Table C.11:** The visual stimuli for size (visual channel) under noise levels  $N_5, N_6, N_7,$  and  $N_8$  (measured orderedness) used in Experiment 2: Which is smallest? Which is largest?













| Noise Level  | Target  | Experiment 2: Hue Stimulus   |
|--------------|---------|--|
| $N_1 = 1.0$  | Min     |    |
|              | Max     |    |
|              | Neither |    |
| $N_2 = 0.97$ | Min     |    |
|              | Max     |    |
|              | Neither |    |
| $N_3 = 0.95$ | Min     |   |
|              | Max     |  |
|              | Neither |  |
| $N_4 = 0.90$ | Min     |  |
|              | Max     |  |
|              | Neither |  |

**Table C.12:** The visual stimuli for hue (visual channel) under noise levels  $N_1, N_2, N_3,$  and  $N_4$  (measured orderedness) used in Experiment 2: Which is smallest? Which is largest?



| Noise Level  | Target  | Experiment 2: Hue Stimulus (cont.)   |
|--------------|---------|--|
| $N_5 = 0.78$ | Min     |    |
|              | Max     |    |
|              | Neither |    |
| $N_6 = 0.71$ | Min     |    |
|              | Max     |    |
|              | Neither |    |
| $N_7 = 0.54$ | Min     |   |
|              | Max     |  |
|              | Neither |  |
| $N_8 = 0.12$ | Min     |  |
|              | Max     |  |
|              | Neither |  |

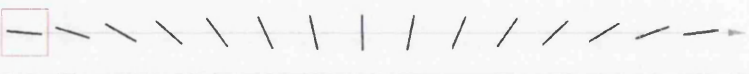
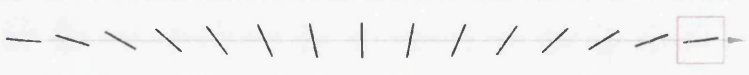
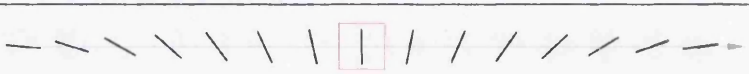
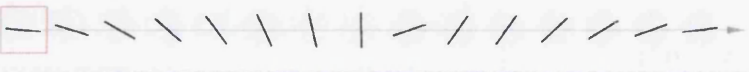
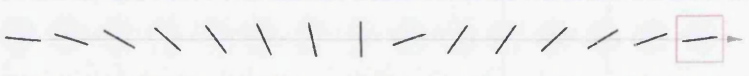
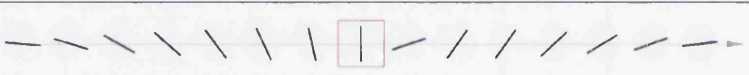
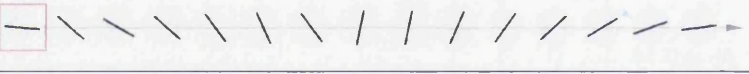
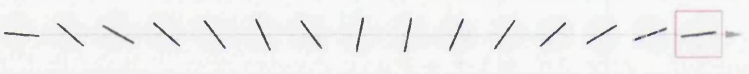
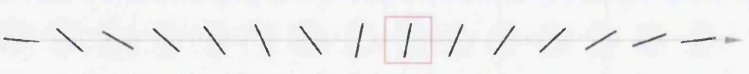
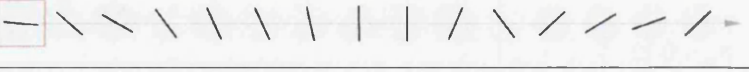
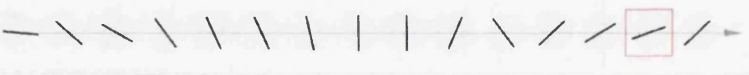
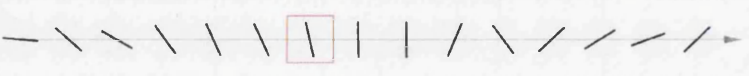
**Table C.13:** The visual stimuli for hue (visual channel) under noise levels  $N_5, N_6, N_7,$  and  $N_8$  (measured orderedness) used in Experiment 2: Which is smallest? Which is largest?

| Noise Level  | Target  | Experiment 2: Texture Stimulus   |
|--------------|---------|--|
| $N_1 = 1.0$  | Min     |    |
|              | Max     |    |
|              | Neither |    |
| $N_2 = 0.97$ | Min     |    |
|              | Max     |    |
|              | Neither |    |
| $N_3 = 0.95$ | Min     |  |
|              | Max     |  |
|              | Neither |  |
| $N_4 = 0.90$ | Min     |  |
|              | Max     |  |
|              | Neither |  |

**Table C.14:** The visual stimuli for texture (visual channel) under noise levels  $N_1, N_2, N_3,$  and  $N_4$  (measured orderedness) used in Experiment 2: Which is smallest? Which is largest?

| Noise Level  | Target  | Experiment 2: Texture Stimulus (cont.) |
|--------------|---------|--|
| $N_5 = 0.78$ | Min     |  |
|              | Max     |  |
|              | Neither |  |
| $N_6 = 0.71$ | Min     |  |
|              | Max     |  |
|              | Neither |  |
| $N_7 = 0.54$ | Min     |  |
|              | Max     |  |
|              | Neither |  |
| $N_8 = 0.12$ | Min     |  |
|              | Max     |  |
|              | Neither |  |






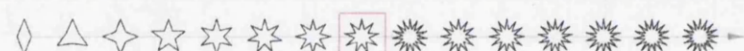
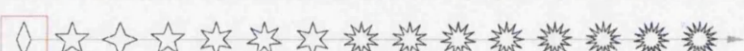
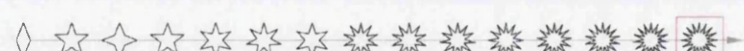
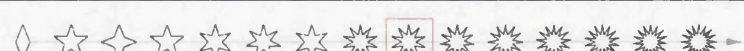
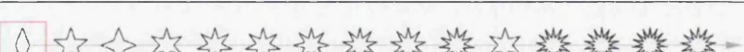
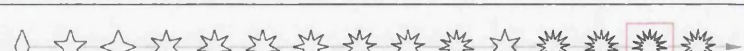
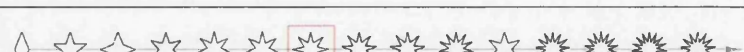
**Table C.15:** The visual stimuli for texture (visual channel) under noise levels  $N_5, N_6, N_7,$  and  $N_8$  (measured orderedness) used in Experiment 2: Which is smallest? Which is largest?

| Noise Level  | Target  | Experiment 2: Orientation Stimulus   |
|--------------|---------|--|
| $N_1 = 1.0$  | Min     |    |
|              | Max     |    |
|              | Neither |    |
| $N_2 = 0.97$ | Min     |    |
|              | Max     |    |
|              | Neither |    |
| $N_3 = 0.95$ | Min     |   |
|              | Max     |  |
|              | Neither |  |
| $N_4 = 0.90$ | Min     |  |
|              | Max     |  |
|              | Neither |  |



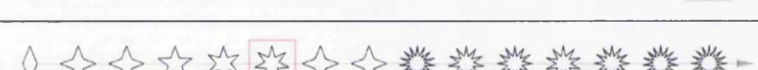
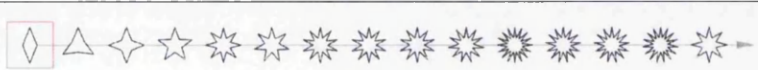
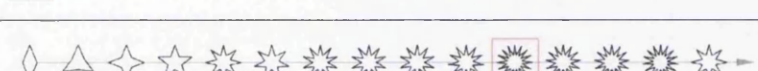
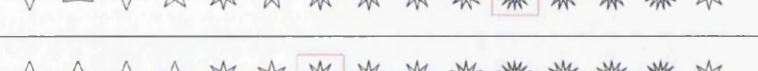
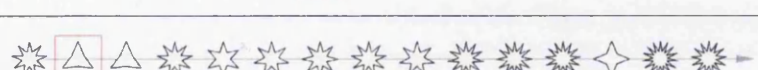
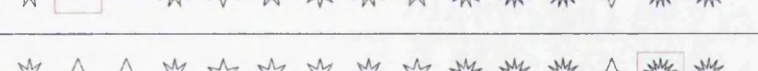
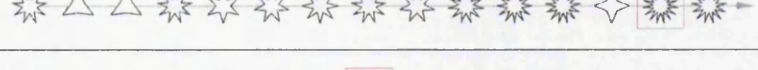
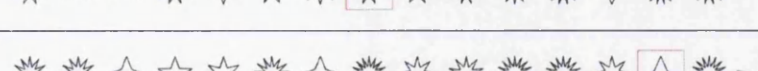
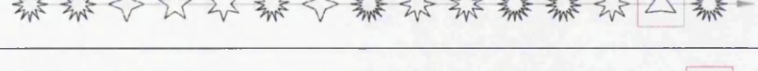
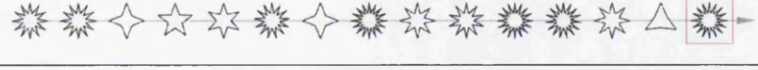
**Table C.16:** The visual stimuli for orientation (visual channel) under noise levels  $N_1, N_2, N_3$ , and  $N_4$  (measured orderedness) used in Experiment 2: Which is smallest? Which is largest?

| Noise Level  | Target  | Experiment 2: Orientation Stimulus (cont.) |
|--------------|---------|--|
| $N_5 = 0.78$ | Min     |  |
|              | Max     |  |
|              | Neither |  |
| $N_6 = 0.71$ | Min     |  |
|              | Max     |  |
|              | Neither |  |
| $N_7 = 0.54$ | Min     |  |
|              | Max     |  |
|              | Neither |  |
| $N_8 = 0.12$ | Min     |  |
|              | Max     |  |
|              | Neither |  |

**Table C.17:** The visual stimuli for orientation (visual channel) under noise levels  $N_5, N_6, N_7,$  and  $N_8$  (measured orderedness) used in Experiment 2: Which is smallest? Which is largest?

| Noise Level  | Target  | Experiment 2: Shape Stimulus   |
|--------------|---------|--|
| $N_1 = 1.0$  | Min     |    |
|              | Max     |    |
|              | Neither |    |
| $N_2 = 0.97$ | Min     |    |
|              | Max     |    |
|              | Neither |    |
| $N_3 = 0.95$ | Min     |   |
|              | Max     |  |
|              | Neither |  |
| $N_4 = 0.90$ | Min     |  |
|              | Max     |  |
|              | Neither |  |

**Table C.18:** The visual stimuli for shape (visual channel) under noise levels  $N_1, N_2, N_3$ , and  $N_4$  (measured orderedness) used in Experiment 2: Which is smallest? Which is largest?

| Noise Level  | Target  | Experiment 2: Shape Stimulus (cont.)   |
|--------------|---------|--|
| $N_5 = 0.78$ | Min     |    |
|              | Max     |    |
|              | Neither |    |
| $N_6 = 0.71$ | Min     |    |
|              | Max     |    |
|              | Neither |    |
| $N_7 = 0.54$ | Min     |   |
|              | Max     |  |
|              | Neither |  |
| $N_8 = 0.12$ | Min     |  |
|              | Max     |  |
|              | Neither |  |

**Table C.19:** The visual stimuli for shape (visual channel) under noise levels  $N_5, N_6, N_7,$  and  $N_8$  (measured orderedness) used in Experiment 2: Which is smallest? Which is largest?

| Noise Level  | Target  | Experiment 2: Numeric Stimulus   |
|--------------|---------|--|
| $N_1 = 1.0$  | Min     | 37.2 38.6 40.2 41.7 43.3 44.9 46.5 48.2 49.9 51.5 53.3 55.1 56.9 58.7 60.6 ▶ |
|              | Max     | 37.2 38.6 40.2 41.7 43.3 44.9 46.5 48.2 49.9 51.5 53.3 55.1 56.9 58.7 60.6 ▶ |
|              | Neither | 37.2 38.6 40.2 41.7 43.3 44.9 46.5 48.2 49.9 51.5 53.3 55.1 56.9 58.7 60.6 ▶ |
| $N_2 = 0.97$ | Min     | 37.2 38.6 40.2 41.7 43.1 44.9 46.5 48.2 58.2 54.4 53.3 55.0 56.9 58.7 60.6 ▶ |
|              | Max     | 37.2 38.6 40.2 41.7 43.1 44.9 46.5 48.2 58.2 54.4 53.3 55.0 56.9 58.7 60.6 ▶ |
|              | Neither | 37.2 38.6 40.2 41.7 43.1 44.9 46.5 48.2 58.2 54.4 53.3 55.0 56.9 58.7 60.6 ▶ |
| $N_3 = 0.95$ | Min     | 37.2 42.3 40.2 41.7 43.3 44.9 44.3 50.0 49.9 51.5 53.3 55.1 56.9 58.7 60.5 ▶ |
|              | Max     | 37.2 42.3 40.2 41.7 43.3 44.9 44.3 50.0 49.9 51.5 53.3 55.1 56.9 58.7 60.5 ▶ |
|              | Neither | 37.2 42.3 40.2 41.7 43.3 44.9 44.3 50.0 49.9 51.5 53.3 55.1 56.9 58.7 60.5 ▶ |
| $N_4 = 0.90$ | Min     | 37.2 41.6 40.2 44.6 46.1 46.0 46.5 48.2 48.9 52.7 43.8 55.1 56.9 58.7 56.2 ▶ |
|              | Max     | 37.2 41.6 40.2 44.6 46.1 46.0 46.5 48.2 48.9 52.7 43.8 55.1 56.9 58.7 56.2 ▶ |
|              | Neither | 37.2 41.6 40.2 44.6 46.1 46.0 46.5 48.2 48.9 52.7 43.8 55.1 56.9 58.7 56.2 ▶ |

**Table C.20:** The visual stimuli for numeric (visual channel) under noise levels  $N_1, N_2, N_3,$  and  $N_4$  (measured orderedness) used in Experiment 2: Which is smallest? Which is largest?



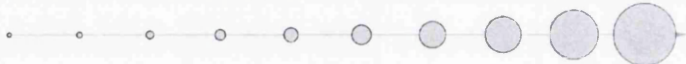




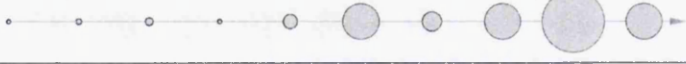
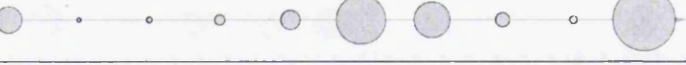
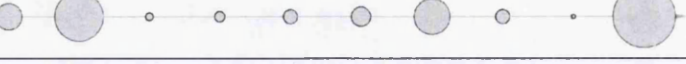
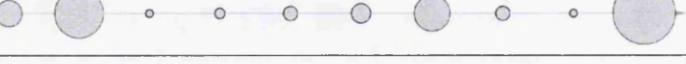
| Noise Level  | Target  | Experiment 2: Numeric Stimulus (cont.)                                       |
|--------------|---------|--|
| $N_5 = 0.78$ | Min     | 37.2 40.2 40.2 41.7 43.3 44.9 41.4 40.1 58.2 51.5 53.3 50.5 53.6 58.7 60.6 ▶ |
|              | Max     | 37.2 40.2 40.2 41.7 43.3 44.9 41.4 40.1 58.2 51.5 53.3 50.5 53.6 58.7 60.6 ▶ |
|              | Neither | 37.2 40.2 40.2 41.7 43.3 44.9 41.4 40.1 58.2 51.5 53.3 50.5 53.6 58.7 60.6 ▶ |
| $N_6 = 0.71$ | Min     | 37.2 38.6 40.2 41.7 47.4 45.1 49.8 51.4 49.9 51.5 59.9 55.1 55.7 58.7 47.6 ▶ |
|              | Max     | 37.2 38.6 40.2 41.7 47.4 45.1 49.8 51.4 49.9 51.5 59.9 55.1 55.7 58.7 47.6 ▶ |
|              | Neither | 37.2 38.6 40.2 41.7 47.4 45.1 49.8 51.4 49.9 51.5 59.9 55.1 55.7 58.7 47.6 ▶ |
| $N_7 = 0.54$ | Min     | 49.1 38.6 39.3 49.2 43.3 44.9 46.5 48.4 45.2 51.5 53.3 55.1 40.3 58.7 54.8 ▶ |
|              | Max     | 49.1 38.6 39.3 49.2 43.3 44.9 46.5 48.4 45.2 51.5 53.3 55.1 40.3 58.7 54.8 ▶ |
|              | Neither | 49.1 38.6 39.3 49.2 43.3 44.9 46.5 48.4 45.2 51.5 53.3 55.1 40.3 58.7 54.8 ▶ |
| $N_8 = 0.12$ | Min     | 53.5 53.3 41.0 41.7 43.3 56.2 39.9 60.2 46.9 51.2 59.8 58.2 47.2 38.0 60.6 ▶ |
|              | Max     | 53.5 53.3 41.0 41.7 43.3 56.2 39.9 60.2 46.9 51.2 59.8 58.2 47.2 38.0 60.6 ▶ |
|              | Neither | 53.5 53.3 41.0 41.7 43.3 56.2 39.9 60.2 46.9 51.2 59.8 58.2 47.2 38.0 60.6 ▶ |

**Table C.21:** The visual stimuli for numeric (visual channel) under noise levels  $N_5, N_6, N_7$ , and  $N_8$  (measured orderedness) used in Experiment 2: Which is smallest? Which is largest?

### C.3 Experimental Stimuli: How many pairs?

| Noise Level  | No. Pairs   | Experiment 3: Value Stimulus |
|--------------|-------------|------------------------------|
| $N_1 = 1.0$  | None        |                              |
|              | One         |                              |
|              | Two or more |                              |
| $N_2 = 0.90$ | None        |                              |
|              | One         |                              |
|              | Two or more |                              |
| $N_3 = 0.12$ | None        |                              |
|              | One         |                              |
|              | Two or more |                              |






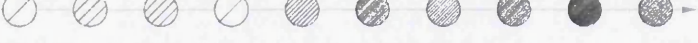
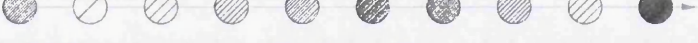

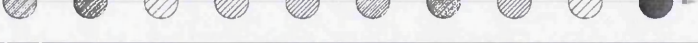
**Table C.22:** The visual stimuli for value (visual channel) under three different noise levels (measured orderedness) used in Experiment 3: How many pairs?

| Noise Level  | No. Pairs   | Experiment 3: Size Stimulus  |
|--------------|-------------|--|
| $N_1 = 1.0$  | None        |    |
|              | One         |    |
|              | Two or more |    |
| $N_2 = 0.90$ | None        |    |
|              | One         |   |
|              | Two or more |  |
| $N_3 = 0.12$ | None        |  |
|              | One         |  |
|              | Two or more |  |

**Table C.23:** The visual stimuli for size (visual channel) under three different noise levels (measured orderedness) used in Experiment 3: How many pairs?

| Noise Level  | No. Pairs   | Experiment 3: Hue Stimulus |
|--------------|-------------|----------------------------|
| $N_1 = 1.0$  | None        |                            |
|              | One         |                            |
|              | Two or more |                            |
| $N_2 = 0.90$ | None        |                            |
|              | One         |                            |
|              | Two or more |                            |
| $N_3 = 0.12$ | None        |                            |
|              | One         |                            |
|              | Two or more |                            |





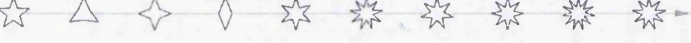
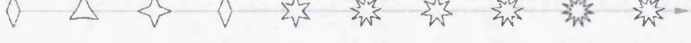
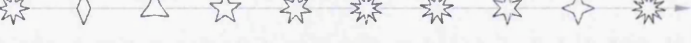
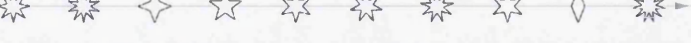
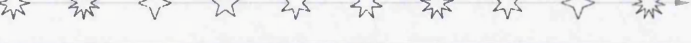
**Table C.24:** The visual stimuli for hue (visual channel) under three different noise levels (measured orderedness) used in Experiment 3: How many pairs?

| Noise Level  | No. Pairs   | Experiment 3: Texture Stimulus   |
|--------------|-------------|--|
| $N_1 = 1.0$  | None        |    |
|              | One         |    |
|              | Two or more |    |
| $N_2 = 0.90$ | None        |    |
|              | One         |   |
|              | Two or more |  |
| $N_3 = 0.12$ | None        |  |
|              | One         |  |
|              | Two or more |  |

**Table C.25:** The visual stimuli for texture (visual channel) under three different noise levels (measured orderedness) used in Experiment 3: How many pairs?

| Noise Level  | No. Pairs   | Experiment 3: Orientation Stimulus |
|--------------|-------------|------------------------------------|
| $N_1 = 1.0$  | None        |                                    |
|              | One         |                                    |
|              | Two or more |                                    |
| $N_2 = 0.90$ | None        |                                    |
|              | One         |                                    |
|              | Two or more |                                    |
| $N_3 = 0.12$ | None        |                                    |
|              | One         |                                    |
|              | Two or more |                                    |

**Table C.26:** The visual stimuli for orientation (visual channel) under three different noise levels (measured orderedness) used in Experiment 3: How many pairs?

| Noise Level  | No. Pairs   | Experiment 3: Shape Stimulus   |
|--------------|-------------|--|
| $N_1 = 1.0$  | None        |    |
|              | One         |    |
|              | Two or more |    |
| $N_2 = 0.90$ | None        |    |
|              | One         |   |
|              | Two or more |  |
| $N_3 = 0.12$ | None        |  |
|              | One         |  |
|              | Two or more |  |

**Table C.27:** The visual stimuli for shape (visual channel) under three different noise levels (measured orderedness) used in Experiment 3: How many pairs?

| Noise Level  | No. Pairs   | Experiment 3: Numeric Stimulus   |
|--------------|-------------|--|
| $N_1 = 1.0$  | None        | 1.00 — 2.00 — 3.00 — 4.00 — 5.00 — 6.00 — 7.00 — 8.00 — 9.00 — 10.00 ▶ |
|              | One         | 2.00 — 2.00 — 3.00 — 4.00 — 5.00 — 6.00 — 7.00 — 8.00 — 9.00 — 10.00 ▶ |
|              | Two or more | 1.00 — 1.00 — 3.00 — 4.00 — 5.00 — 6.00 — 7.00 — 8.00 — 8.00 — 10.00 ▶ |
| $N_2 = 0.90$ | None        | 1.00 — 2.00 — 3.00 — 4.00 — 5.00 — 9.00 — 6.00 — 8.00 — 10.00 — 7.00 ▶ |
|              | One         | 4.00 — 2.00 — 3.00 — 1.00 — 5.00 — 8.00 — 6.00 — 7.00 — 10.00 — 8.00 ▶ |
|              | Two or more | 1.00 — 2.00 — 3.00 — 1.00 — 5.00 — 8.00 — 6.00 — 8.00 — 10.00 — 8.00 ▶ |
| $N_3 = 0.12$ | None        | 7.00 — 1.00 — 2.00 — 4.00 — 6.00 — 9.00 — 8.00 — 5.00 — 3.00 — 10.00 ▶ |
|              | One         | 7.00 — 9.00 — 3.00 — 4.00 — 5.00 — 6.00 — 8.00 — 5.00 — 1.00 — 10.00 ▶ |
|              | Two or more | 7.00 — 9.00 — 3.00 — 4.00 — 5.00 — 6.00 — 8.00 — 5.00 — 3.00 — 10.00 ▶ |

**Table C.28:** The visual stimuli for value (visual channel) under three different noise levels (measured orderedness) used in Experiment 3: How many pairs?